UNIVERSITÀ DI BOLOGNA

Dipartimento di Scienze della Terra e Geologico-Ambientali

DOTTORATO IN SCIENZE DELLA TERRA
XXIII CICLO
Coordinatore: Prof. Roberto Barbieri

Settore scientifico-disciplinare di appartenenza
GEO/08

Tesi di Dottorato

PETROLOGY AND GEOCHEMISTRY OF LIPARI ISLAND (AEOLIAN ARCHIPELAGO): CONSTRAINTS ON MAGMA GENESIS AND EVOLUTION

Presentata da:
Dott. Francesca Forni

Relatore
Prof. C.A. Tranne

Correlatori
Prof. F. Lucchi

Prof. A. Peccerillo

Esame finale anno 2011

Ai miei genitori

Science, my lad, is made up of mistakes,

but they are mistakes, which it is useful to make,

because they lead little by little to the truth.

Jules Verne

Table of Contents

Abstract

A full set of geochemical and Sr, Nd and Pb isotope data both on bulk-rock and mineral samples is provided for volcanic rocks representative of the whole stratigraphic succession of Lipari Island in the Aeolian archipelago. These data, together with petrographic observations and melt/fluid inclusion investigations from the literature, give outlines on the petrogenesis and evolution of magmas through the magmatic and eruptive history of Lipari. This is the result of nine successive Eruptive Epochs developing between 271 ka and historical times, as derived from recentmost volcanological and stratigraphic studies, combined with available radiometric ages and correlation of tephra layers and marine terrace deposits. These Eruptive Epochs are characterized by distinctive vents partly overlapping in space and time, mostly under control of the main regional tectonic trends (NNW-SSE, N-S and minor E-W). A large variety of lava flows, scoriaceous deposits, lava domes, coulees and pyroclastics are emplaced, ranging in composition through time from calcalkaline (CA) and high-K (HKCA) basaltic andesites to rhyolites. CA and HKCA basaltic andesitic to dacitic magmas were erupted between 271 and 81 ka (Eruptive Epochs 1-6) from volcanic edifices located along the western coast of the island (and subordinately the eastern Monterosa) and the M.Chirica and M.S.Angelo stratocones. These mafic to intermediate magmas mainly evolved through AFC and RAFC processes, involving fractionation of mafic phases, assimilation of wall rocks and mixing with newly injected mafic magmas. Following a 40 ka-long period of volcanic quiescence, the rhyolitic magmas were lately erupted from eruptive vents located in the southern and north-eastern sectors of Lipari between 40 ka and historical times (Eruptive Epochs 7-9). They are suggested to derive from the previous mafic to intermediate melts through AFC processes. During the early phases of rhyolitic magmatism (Eruptive Epochs 7-8), enclaves-rich rocks and banded pumices, ranging in composition from HKCA dacites to low-SiO2 rhyolites were erupted, representing the products of magma mixing between fresh mafic magmas and the fractionated rhyolitic melts.

The interaction of mantle-derived magmas with the crust represents an essential process during the whole magmatic hystory of Lipari, and is responsible for the wide range of observed geochemical and isotopic variations. The crustal contribution was particularly important during the intermediate phases of activity of Lipari when the cordierite-bearing lavas were erupted from the M. S.Angelo volcano (Eruptive Epoch 5, 105 ka). These lavas are interpreted as the result of mixing and subsequent hybridization of mantle-derived magmas, akin to the ones characterizing the older phases of activity of Lipari (Eruptive Epochs 1-4), and crustal anatectic melts derived

from dehydration-melting reactions of metapelites in the lower crust.

A comparison between the adjacent islands of Lipari and Vulcano outlines that their mafic to intermediate magmas seem to be genetically connected and derive from a similar mantle source affected by different degrees of partial melting (and variable extent of crustal assimilation) producing either the CA magmas of Lipari (higher degrees) or the HKCA to SHO magmas of Vulcano (lower degrees). On a regional scale, the most primitive rocks (SiO2<56%, MgO>3.5%) of Lipari, Vulcano, Salina and Filicudi are suggested to derive from a similar MORB-like source, variably metasomatized by aqueous fluids coming from the slab and subordinately by the additions of sediments.

Riassunto

Importanti informazioni riguardo la petrogenesi e l'evoluzione dei magmi che caratterizzano la storia eruttiva dell'isola di Lipari (Arcipelago Eoliano), fra 271 ka e l'attuale, vengono fornite dall'utilizzo congiunto di un set completo di dati geochimici e isotopici (Sr, Nd e Pb) su campioni di roccia e minerali rappresentativi di tutta la successione stratigrafica affiorante e dall'insieme di osservazioni petrografiche e dati di inclusioni fluide e vetrose di letteratura. Sulla base dei più recenti studi stratigrafici e vulcanologici, combinati alle età radiometriche disponibili e a correlazioni basate sull'utilizzo di livelli di tefra noti e terrazzi marini, la storia eruttiva di Lipari è stata definita come il risultato di nove Epoche Eruttive, durante le quali distinti centri vulcanici, controllati dai più importanti lineamenti tettonici regionali (NNW-SSE, N-S e in minor misura E-W), si sovrappongono parzialmente nello spazio e nel tempo. L'attività di questi centri si esplica attraverso la messa in posto di colate laviche, depositi piroclastici, duomi lavici e coulée che variano composizionalmente nel tempo da andesiti basaltiche calcalcaline (CA) e calcalcaline alte in potassio (HKCA) a rioliti. I prodotti da CA e HKCA andesitico-basaltici a HKCA dacitici sono riferiti ad una serie di edifici vulcanici localizzati lungo la costa ovest di Lipari (e subordinatamente nel settore orientale), e agli stratoconi di M.Chirica e M. S.Angelo, attivi nell'insieme a partire da 271 ka fino a 81 ka (Epoche Eruttive 1-6). L'evoluzione di questi magmi da mafici a intermedi avviene principalmente attraverso processi di AFC e RAFC che prevedono il frazionamento delle fasi mafiche in profondità, l'assimilazione delle rocce crostali e il mixing dei magmi residenti con nuovi magmi mafici di provenienza mantellica che entrano in camera magmatica. Nell'isola, successivamente a un periodo di quiescenza dell'attività vulcanica della durata di circa 40 ka, si realizza uno spostamento dell'attività vulcanica, inizialmente nel settore sud (Epoche Eruttive 7 e 8) e successivamente nel

settore nord-est di Lipari (Epoca Eruttiva 9). Durante queste epoche eruttive (da 40 ka fino all'attuale) si ha la messa in posto di grandi volumi di magmi riolitici derivanti dai magmi mafici ed intermedi (simili a quelli eruttati durante le Epoche Eruttive 1-6) attraverso processi di AFC. Particolarmente significativa risulta anche la presenza di enclaves mafici (HKCA andesitici, tachitici e latitici) e pomici bandate in alcuni prodotti riferiti alle Epoche Eruttive 7 e 8, che indica chiaramente la presenza di fenomeni di magma mixing/mingling fra i magmi riolitici (AFC-derivati) e nuovi magmi mafici.

Il processo d'interazione fra magmi di derivazione mantellica e la crosta ha un ruolo essenziale durante tutta la storia magmatica di Lipari ed è ritenuto il principale responsabile delle ampie variazioni geochimiche ed isotopiche osservate nelle vulcaniti oggetto di questo studio. Tale interazione culmina con l'effusione delle lave a cordierite, riferite all'attività eruttiva dello stratocono del M. S.Angelo durante l'Epoca Eruttiva 5 (105 ka) e interpretate come il risultato di mixing e ibridizzazione di magmi di derivazione mantellica (simili a quelli che caratterizzano le Epoche Eruttive 1-4) con magmi anatettico-crostali derivanti da reazioni di dehydration-melting di rocce metapelitiche nella bassa crosta.

Una comparazione fra le adiacenti isole di Lipari e Vulcano evidenzia che le rocce da mafiche ad intermedie a diverso contenuto in K_2O, che caratterizzano due periodi di attività distinti nelle due isole (270-116 ka a Lipari e 120-30 ka Vulcano) potrebbero derivare da sorgenti mantelliche simili affette da un diverso grado di fusione parziale (e vario contributo dell'assimilazione crostale). Un basso grado di fusione parziale è suggerito per i magmi da HKCA a shoshonitici (SHO) di Vulcano, mentre un più alto grado di fusione parziale potrebbe aver dato origine ai magmi CA di Lipari. Inoltre, a scala regionale, le rocce più primitive (SiO_2 <56%, MgO >3.5%) di Lipari, Vulcano, Salina e Filicudi potrebbero derivare da una sorgente magmatica simile (sorgente MORB-like), variabilmente metasomatizzata da fluidi provenienti dallo slab, e in minor misura dalla addizione di sedimenti.

Structure and aim of the thesis

The aim of this PhD thesis is to supply a complete petrogenetic model of the magmatic evolution of Lipari Island on the basis of a petrological, geochemical and isotopic study in the light of recentmost volcanological and stratigraphic reconstructions.

The manuscript is structured as a collection of two papers (Chapters 1 and 3) and a geological map (cf. attached CD) submitted to international journals and accepted for publication, two thematic chapters (Chapters 2 and 4) and the final conclusions (Chapter 5).

In Chapter 1 (Forni F., Lucchi F., Peccerillo A., Tranne C.A., Rossi P.L., Di Martino C., Frezzotti M.L. & Ayuso R.A. Lipari. In: Lucchi, F., Peccerillo A., Keller J., Tranne C.A. & Rossi P.L. (Eds.), Geology of the Aeolian Islands (Italy). Geological Society of London, Memoirs, accepted for publication) the authors provide a complete outline of the stratigraphic evolution of Lipari and a new geological map of the island (Lucchi F., Tranne C.A., Forni, F. & Rossi, P.L. Geological map of Lipari Island, scale 1:10,000 (Aeolian archipelago), in: Lucchi F., Peccerillo A., Keller J., Tranne C.A. & Rossi P.L. (Eds.), Geology of the Aeolian Islands (Italy), Geological Society of London, Memoirs, accepted for publication; cf. enclosed CD). Moreover, they present a full set of original major and trace element data covering the whole stratigraphic succession of Lipari. Combined with isotopic analyses and melt and fluid inclusions data from the literature, the resulting data-set provide an up-to-date review about the petrogenesis of the magmatic rocks of Lipari and the structure and evolution of its plumbing system.

Chapter 2 is the advanced proof of a paper in preparation and is focused on the petrogenesis of the mafic to intermediate rocks referred to the older to intermediate phases of activity of Lipari (270-80 ka). The role of mantle sources and evolutionary processes at Lipari, and the relationships with the nearby island of Vulcano and with the other islands of the Aeolian archipelago are discussed on the basis of new geochemical, isotope (Sr, Nd and Pb) and mineral chemistry data representative of the stratigraphic interval of interest.

Chapter 3 (Di Martino C., Forni F., Frezzotti M.L., Palmeri R., Webster J.D., Ayuso R.A., Lucchi F. & Tranne C.A. Anatexis and magma-hybridization in the lower-crust: petrogenesis of cordierite-bearing lavas from Lipari, Aeolian Arc, Italy. Contribution to Mineralogy and Petrology, accepted for publication) is focused on the petrogenesis of the cordierite-bearing lavas erupted from the M. S.Angelo volcano during the intermediate activity of Lipari (105 ka). The eruption of these peculiar lavas, characterized by the coexistence of typical igneous minerals along with cordierite, garnet and a huge amount of magmatic and metamorphic xenoliths, marks a turning

point in the magmatic evolution of Lipari. Therefore, a detailed study of these rocks represents a fundamental step in the reconstruction of the magmatic evolution of Lipari. The study is based on petrography, glass and mineral chemistry data, together with the substantial contribution of Sr and Nd isotope data obtained both on whole-rock and mineral samples.

Chapter 4 is aimed at unravelling the petrogenesis of rhyolitic rocks referred to the youngest activity of Lipari (40 ka-historical times). A new set of geochemical, isotope (Sr, Nd and Pb) and mineral chemistry data is presented and discussed in order to examine the evolutionary processes leading to the genesis of the sialic melts and their relationships with the older magmatism of Lipari (cf. Chapter 2). The origin of sialic melts at Lipari (but also at Vulcano, Salina and Panarea) represents one of the most interesting petrogenetic problems concerning the magmatic evolution of the single islands and of the entire Aeolian archipelago. Thus, this subject hints at further investigations.

Chapter 5 contains a summary of the main results.

CHAPTER 1

Forni F., Lucchi F., Peccerillo A., Tranne C.A., Rossi P.L., Di Martino C., Frezzotti M.L. & Ayuso R.A. Lipari. In: Lucchi, F., Peccerillo A., Keller J., Tranne C.A. & Rossi P.L. (Eds.), Geology of the Aeolian Islands (Italy). Geological Society of London, Memoirs, accepted for publication

LIPARI

FORNI F. ([1]), LUCCHI F. ([1]), PECCERILLO A. ([2]), TRANNE C.A. ([1]), ROSSI P.L. ([1]), DI MARTINO C. ([1]), FREZZOTTI M.L. ([3]), AYUSO R.A. ([4])

([1]) Department of Earth and Geological-Environmental Sciences, University of Bologna, Piazza Porta S.Donato 1, 40126 Bologna, Italy.
([2]) Department of Earth Sciences, University of Perugia, Piazza Università 1, 06100 Perugia, Italy.
([3]) Department of Earth Sciences, University of Siena, Via Laterina 8, 53100 Siena, Italy.
([4]) U.S. Geological Survey, Mail Stop 954, National Center Reston, 20192 Virginia, USA.

Abstract

The Lipari volcano, situated in the central Aeolian sector, is constructed between 271 ka and historical times through the emplacement of various lava flows, scoriaceous deposits, lava domes (coulees) and pyroclastics related to hydromagmatic and strombolian activities. The eruptive history of Lipari is described by nine successive Eruptive Epochs interrupted by dormant periods, volcano-tectonic phases and episodes of terrace formation during the last interglacial. Several (partially overlapping) volcanic edifices are active through time mostly under control of the NNW-SSE and N-S (minor E-W) regional tectonic trends. The latest eruptive events at M. Pilato and Rocche Rosse occurred in *AD* 776 to 1230.

Lipari rocks widely range in composition from calcalkaline and high-K basaltic andesites and andesites (from 271 to 81 ka) to rhyolites (<42 ka), with minor dacites. There is a clear increase of K_2O and incompatible elements through time, with distinct trends for mafic-intermediate and sialic rocks. Sr, Nd, and Pb isotopes are highly variable and cover almost the whole range of isotopic compositions of the Aeolian archipelago. Petrographic and geochemical data suggest AFC and mixing evolution processes, with a localized important influence of crustal anatexis, in the context of a polybaric feeding system.

Key words

Lipari, Marine terraces, Unconformity-bounded Units, Eruptive history, Petrogenesis

Introduction

Lipari is the largest of the Aeolian Islands, located in a strategic position in the central sector of the archipelago along the Tindari-Letojanni structural system. It developed entirely during the late Quaternary between 270 ka BP and hystorical times, and presently behaves in a quiescent stage of activity with a few low temperature fumaroles (along the western and central-southern sectors) and hot springs (in the western sector, at Bagni termali di San Calogero and Bagno Secco). Geological fieldwork and stratigraphic analysis carried out during the nineties, combined with previous data and radiometric ages from the literature (Bigazzi and Bonadonna, 1973; Pichler, 1980; Crisci et al., 1981, 1983; Gillot, 1987; Losito, 1989; Crisci et al., 1991; De Rosa et al., 2003b; Tanguy et al., 2003; Lucchi et al., 2004a), have resulted in a geological map of Lipari elaborated by primarily following the unconformity-bounded criteria (Tranne et al., 2002; Lucchi et al., 2004b; Lucchi et al., 2010). What we present here is an updated 1:10,000 scale version of Lipari's map based on recent radiometric ages (Leocat et al., 2009; Leocat et al., 2010) and new stratigraphic investigation performed in the course of ongoing geological mapping of sheet Nos. 577 bis – "Isole di Stromboli e Panarea", 580 bis – "Isole di Alicudi e Filicudi", and 581/586 – "Isole di Salina, Lipari e Vulcano" as part of the Geological Mapping of Italy - 1:50.000 project (CARG Project). The main purpose of this paper is to provide an accurate description of stratigraphical, morphologic, structural and petrochemical features of volcanic rocks building up the articulated stratigraphic succession of Lipari Island, which consists of lava flows, scoriaceous deposits, lava domes and widespread hydromagmatic pyroclastic products, originated from several eruptive vents partly overlapping in space (and time) under control of major tectonic trends. Note that Lipari is the site of explosive eruptions with the highest intensity and magnitude across the entire Aeolian archipelago (*i.e.,* M.Guardia, Vallone del Gabellotto, M.Pilato pyroclastic products).

For the great variety of rock types and the complexity of its stratigraphy, the late-Quaternary Lipari Island represents a useful case study for the application of a stratigraphic methodology to fieldwork and mapping in volcanic areas based on the adoption of unconformity-bounded units (UBUs), together with more descriptive lithosomes and lithostratigraphic units (see Lucchi and Tranne, 2011). We aim to show that UBUs can provide effective tools of correlation and a practical and clear approach to stratigraphic analysis at Lipari, by subdividing the volcanic succession through unconformities with a clear field evidence on a large scale and a strong relative chronostratigraphic significance. Particular attention is given to the late-Quaternary terraced marine deposits diffusely reported along the western coastal slopes of Lipari Island, resulting from the interaction between recurrent sea-level fluctuations during the last interglacial and continuous crustal uplifting. Together with major tephra layers, the terrace deposits are used as powerful

stratigraphic means of correlation and relative dating at Lipari as well as fundamental stratigraphic constraints for the geological evolution of the entire Aeolian archipelago. This approach is able to provide an effective stratigraphic synthesis of the geological evolution and eruptive history of Lipari, as the result of volcanic activity of local and external provenance, sea-level fluctuations and tectonics. In particular, the compilation of stratigraphic, volcanological and structural data provides a detailed stratigraphic outline of Lipari and a accurate perspective on the relations between volcanism, regional tectonic trends and volcano-tectonic structures through time. This has a fundamental outcome towards the evaluation of volcanic hazard of active or recent volcanoes, which is the case of Lipari where latest eruptive events are dated back at *AD* 776-1238.

Moreover, this paper makes available a set of new petrological, geochemical and melt-inclusion data, which, combined with isotopical data from the literature (Crisci *et al*., 1991; Esperanca *et al*., 1992; Gioncada *et al*., 2003; Gioncada *et al*., 2005), can provide an up-to-date petrogenetic model of Lipari's magmatism according to the most recent volcanological and stratigraphical reconstruction. On this subject, it is to be noticed that Lipari is characterized by a wide compositional range of erupted products from calcalkaline (CA) basaltic andesites to high-K rhyolites, with a steep increase in K_2O through time from mafic to silicic rocks (which is common to most of the Aeolian islands), a notable gap in the field of dacites, and late appearance of rhyolite products after a prolonged period of quiescence. These are long-debated aspects of Lipari's magmatism and have been related either to heterogeneities in the mantle source, the effect of different magmatic differentiation processes or the influence of regional tectonic trends. Our aim here is to give a contribution towards the reconstruction of the magmatic history of Lipari prior to eruption, particulary regarding the nature of magma sources and the role of magma differentiation processes.

Site and morphostructural setting

The Lipari Island (38 km^2 - 602 meters *asl* at M. Chirica) is the subaerial portion of a broad volcanic edifice rising ~1000 m from the sea floor in the central portion of a largely submerged volcanic belt that includes also Vulcano and Salina volcanoes (Fig. 1). This volcanic belt transversely intersects the arc-shaped structure of the Aeolian archipelago striking along the NNW-SSE direction of the major Tindari-Letojanni fault system (Mazzuoli et al., 1995; Continiso et al., 1997; Lanzafame and Bousquet, 1997; Ventura, 2011). Both subaerial and submerged portion of Lipari volcano are directly controlled by the Tindari-Letojanni fault system, which is responsible for alignment of active eruptive centres, changes of eruptive styles, and, in general, magma genesis and evolution. The Tindari-Letojanni fault system is primarily demonstrated by the occurrence of NNW-SSE strike-slip to transtensional faults with metric to decametric dip-slip along the south-western coast of Lipari (Fig. 2). Major

fault scarps give rise to 100-m-high subvertical cliffs and triangular to trapezoidal facets along the south-western coastline nearby Scogliera sotto il Monte (Mazzuoli et al., 1995). Minor N-S to NE-SW trending normal faults are also reported in distinct sectors of the island (Mazzuoli et al., 1995; Ventura et al., 1999). Mazzuoli et al. (1995) suggest that these extensional fractures are more likely kinematically compatible with the major NNW-SSE shear zone, splaying out from the major strike-slip structures. The influence of regional fault systems is moreover outlined by the intense hydrotermalization of volcanic rocks in correspondence of a wide strip affected by NNW-SSE to N-S tectonic lineaments along the western coast of Lipari from Timpone Carrubbo, to the south, to Pietrovito, to the north (Decrée et al., 2005). The NNW-SSE and N-S striking faults are supposed to have conditioned ponding and ascent of magmas responsible of Lipari's volcanism (De Astis et al., 2003), which is particularly shown by the alignment of eruptive vents in N-S to NNW-SSE directions through the entire geological history of Lipari. A minor E-W-oriented extensional tectonic trend is demonstrated by the aligned scoria cones of Monterosa, along the eastern coast of Lipari.

Accurate morphostratigraphic investigation has allowed identification of distinct volcano-tectonic structures outlined by subvertical escarpments with curved geometry (Fig. 2), which are invariably marked by the high-angle discordance relations between pre-collapse and collapse-filling volcanic products. Overall, major caldera-type volcano-tectonic collapses on Lipari are represented by (in stratigraphic order):

- vc1) 700-m-large collapse structure reconstructed in the area of Quattropani-Pietrovito, northern Lipari;
- vc2) 1.3 km-large, elliptical N-S-elongated morphologic depression rim outlined by evident morphological slope breaks under the cover of younger volcanic products between the M. S.Angelo and M. Chirica topographic reliefs. This apparently demonstrates the occurrence of a buried caldera-type collapse structure. A similar structure is also possibly documented along the western coastal sector of Lipari, nearby Timpone Ricotta.
- vc3) semi-circular collapse rim exposed nearby Quattrocchi, at the northern border of the large dome field occupying the southern sector of Lipari Island. Based on structural and geophysical data, Ventura et al. (1999) suggest that this collapse structure is the northern counterpart of the older stages of development of La Fossa caldera structure on Vulcano Island, both bounding a wide basin-like structure. This is apparently confirmed by our structural and stratigraphic analysis showing that collapse vc3 on Lipari and the older collapse rims of the multi-stage La Fossa caldera structure on Vulcano both developed at around 100 ka BP.

- vc4) semi-circular collapse rims observed in the southern sector of Lipari, nearby Falcone-Capistello.

Mazzuoli et al. (1995) suggest that regional N-S to NE-SW trending extensional structures had a primary influence on the development of major collapse structures. Conversely, our morphostratigraphic analysis demonstrates that collpase structures have an evident curved geometry that apparently indicates a volcano-tectonic or volcano-related origin. The possibility that major volcano-tectonic collapses on Lipari are the surficial expression of caldera-type structures cannot thus be discounted. If this is the case, similarly to what assumed for Vulcano Island, collapse structures may result from recurrent subsidence processes induced by the extraction of magma from shallow magma reservoirs, which is compatible with the observed absence of caldera-forming pyroclastic products.

Terraced marine deposits and a few marine notches, together with numerous carbonate buildups, are reported along the entire western of Lipari Island, and in a few places along the eastern coast, at elevations ranging between 45 m and a few metres above sea level (*asl*). (Fig. 3A, B). Due to diffuse cover of younger continental detrital deposits and volcanics, marine features are best exposed along the steep coastal cliffs, repeatedly interbedded with successive volcanic products related to the western volcanoes. Terraced deposits correspond to paleoshorelines I (43-45 m *asl*), II (23-27 m *asl*), III (~12 m *asl*), which are attributed to the interglacial sea-level peaks of MIS 5e (124 ka), MIS 5c (100 ka) and MIS 5a (81 ka), respectively, on the basis of cross-cutting relations, stratigraphic constraints and radiometric ages of volcanic products (Fig. 3C; Calanchi et al., 2002, Lucchi et al., 2004a). This relative chronological attribution is confirmed by the U/Th age of *Cladocora caespitosa* corals related to paleoshoreline I (119±6 ka; Calanchi et al., 2002). The staircase of paleoshorelines has not a complete outcrop exposure in any part of the island owing to subsequent erosional processes or located tectonic instability, but their correlation is founded on their sub-horizontal distribution and widespread dispersion of paleoshoreline II terraces. Paleoshorelines I, II and III are invariably arranged in a downstepping stacking pattern with older terraces placed at higher elevations (Fig. 3B; Lucchi, 2009). This setting accounts for the long-term effect of continuous crustal uplift (mean rate of ~0.34 m/ka from the last interglacial; Calanchi et al., 2002; Lucchi et al., 2004a) superposed to recurrent glacio-eustatic sea-level fluctuations.

Geology and mapping

Literature review

- Dolomieu (1783), Cortese and Sabatini (1892), Bergeat (1899), Keller (1967), Pichler (1968), Barberi et al. (1974) gave general information about the Lipari Island, which has long known for to its exceptional variety of lithological and petrochemical rock types and its strategic position in the middle of the Aeolian archipelago.
- The first systematic geological map at a 1:10.000 scale was drawn by Pichler (1976; 1980), who performed a subdivision of Lipari's volcanic activity in four successive periods ranging in time from the early Tyrrhenian to the Late Roman age, on the basis of Pleistocene eustatic coast-lines, and age determinations using ^{14}C and fission track methods. The Pichler's map provided a generic lithological and volcanological characterization of rocks with a thorough field description and interpretation mostly limited to their petrochemical attitude, which ranges from quartz-andesites to alkali feldspar rhyolites belonging to a typical calcalkaline series.
- Largely based on Pichler's stratigraphy, Crisci et al. (1991) developed, as a tool for their petrochemical studies, a chrono-stratigraphic framework subdivided into ten cycles of volcanic activity separated by chronological gaps, stratigraphic unconformities and compositional changes.
- Several petrological and volcanological studies (Crisci et al., 1981, 1983; De Rosa and Sheridan, 1983; Cortese et al., 1986; Sheridan et al., 1987; Esperanca et al., 1992; Gioncada et al., 2003, 2005: Davì et al., 2008, 2009), mostly based on the were the map and stratigraphy of Pichler (1976; 1980) and its implementation by Crisci et al. (1991), have been performed with the aim of investigating the magmatic and eruptive history of Lipari, particularly regarding its most recent volcanic rocks.

Chronostratigraphic framework

The age of Lipari's volcanic rocks is shown to range from 270 ka BP to historical times, as derived by geological fieldwork and stratigraphic analysis combined with several radiometric age determinations obtained with K/Ar (Gillot, 1987; Crisci et al., 1991; De Rosa et al., 2003b; Leocat et al., 2009), Ar/Ar (Lucchi, 2000; Lucchi et al., 2004a), ^{14}C (Crisci et al., 1981, 1983; Losito, 1989; Pichler, 1980), fission track (Bigazzi and Bonadonna, 1973) and archeomagnetic (Tanguy et al., 2003) methods. Further relative age assignments are provided by the correlation of terraced marine deposits formed during the interglacial sea-level peaks of MIS 5e (124 ka), MIS 5c (100 ka) and MIS 5a (81 ka). These marine deposits are repeatedly interlayered with volcanic rocks mostly along the western coast of Lipari (Calanchi et al., 2002; Lucchi et al., 2004a), and act as fundamental time-stratigraphic markers for the reconstruction of its geological evolution. Moreover, numerous chronostratigraphic attributions are established by means of accurate tephrostratigraphy. The stratigraphic record of Lipari is in fact characterized by the occurrence of several prominent

tephra layers represented by large-scale, primary air-fall deposits of inter-island and external provenance (Lucchi et al., 2008; Lucchi et al., 2011). The Campanian tephra layers are represented by the Ischia Tephra (56 ka) and by the probable occurrence of the deep-sea marine Y-5 tephra layer (39 ka) correlated with the Campanian Ignimbrite (Lucchi et al., 2011). The inter-island tephra layers are instead originated by explosive eruptions of Aeolian volcanoes. They include the Grey Porri Tuffs (67-70 ka) and Lower Pollara Tuffs (~23 ka) from Salina Island and the Lower (<70-56 ka), Intermediate (56-22 ka) and Upper Brown Tuffs (21-7 ka) from Vulcano Island, these latter representing the most prominent pyroclastic succession over the entire Aeolian archipelago (Lucchi et al., 2008). Main characters of recognized tephra layers are summarized in Table 1.

Unconformity-bounded stratigraphic succession

The stratigraphic framework of Lipari Island is described in terms of 21 unconformity-bounded units (UBUs) and the informal Paleo-Lipari unit, which are bounded by several unconformities with variable duration and distribution (Fig. 4; Table 2). Major rank discontinuities are the the large-scale allogenic unconformities U_I and U_{II} (Fig. 4), which stratotype has been defined on Lipari (Lucchi, 2009; Lucchi et al., 2011). Unconformity U_I is the surface of marine ravinement bounding at base MIS 5 marine deposits and formed during sea-level rise at the onset of MIS 5e. Instead, unconformity U_{II} is found at top of MIS 5 marine deposits and corresponds to the subaerial unconformity developed during sea-level fall and lowstand and the end of MIS 5a. Unconformity U_{II} is notably covered along its whole lateral extension by the Brown Tuffs pyroclastics originated from Vulcano Island (Lucchi et al., 2008; Lucchi et al., 2011). Based on widespread recognition of Brown Tuffs and MIS 5 terraced marine deposits, unconformities U_I and U_{II} are correlated across most of the Aeolian archipelago, thus assuming a first-order rank (Lucchi, 2009). They allow designation of two major UBUs, namely the Cala Fico and Punta le Grotticelle Supersynthems, which were first introduced on Lipari (Tranne et al., 2002) and then extended to the rest of the archipelago. The Cala Fico Supersynthem includes alternating terraced marine deposits and volcanic products emplaced during the time interval corresponding to the last interglacial (=MIS 5, between 124 and 81 ka). The Punta le Grotticelle Supersynthem is entirely composed of volcanics formed during the long time interval spanning from the end of MIS 5a (<81 ka) to historical times, together with coeval pyroclastics of external provenance. By means of introduction of second-order unconformities L_1-L_5 and third-order unconformity I_a-I_g, the Cala Fico and Punta le Grotticelle Supersynthems are furtherly subdivided into seven synthems (Piano Grande, Sc.° le Torricelle, Bruca, Fontanelle, Scogliera sotto il Monte, V. Muria, Vallone Fiume Bianco), twelve subsynthems and the Paleo-Lipari informal unit, the latter including volcanic rocks which bottom unconformity does not occur (Fig. 4). These minor-

rank unconformities are represented either by allogenic unconformities developed during recurrent sea-level oscillations in the course of MIS 5 (*i.e.,* L_3, l_c, l_d), or by autogenic unconformities formed during major quiescent stages (*i.e.,* L_1, L_2, L_4, L_5, l_a, l_b, l_e, l_f, l_g). The latter are represented by surfaces of subaerial erosion, angular discordance and/or paleosols, and are frequently associated with volcano-tectonic collapse events, shifting of eruptive vents and remarkable change of conposition of erupted products. Description and intepretation of bounding unconformities are summarized in Table 2, with areal distribution of main UBUs shown in Fig. 5. The UBUs build up an overall synthetic stratigraphic framework of classification and correlation on a scale from local to regional, which includes several lithosomes, formations and members for descriptive purposes (Fig. 6). A series of volcanic lithosomes are introduced to define 22 main eruptive vents on Lipari, which correspond either to large stratocones (*i.e.,* Timpone Carrubbo, Monte Mazzacaruso, Monte Chirica, Chiesa Vecchia, Monterosa, Monte S.Angelo lithosomes) or to monogenetic scoria cones or tuff cones and related lava flows or domes (*i.e.,* Timpone Croci, Pietrovito, Monte Chirica-Costa d'Agosto, Vallone del Gabellotto-Monte Pilato, Forgia Vecchia and M. Pilato lithosomes), aligned spatter cones or domes (i.e., Timpone Ospedale, P. del Perciato, Falcone, M.Guardia-M.Giardina, P. S.Giuseppe, Castello, V.ne Canneto dentro, Capo Rosso). Moreover, a few external volcanic source areas have been identified on Vulcano (*i.e.,* Varesana and La Fossa di Vulcano lirthosomes) and Salina islands (*i.e.,* Monte dei Porri lithosome). Non-volcanic lithosomes are introduced to identify the marine terraces formed during MIS 5 (*i.e.*, Palmeto lithosome). The lithostratigraphic units, adopted in integration with lithosomes (Lucchi and Tranne, 2011), give a description of main lithological properties and petrochemical features of Lipari's rocks, which are summarized in Table 3. Eruption types and emplacement mechanisms are inferred by interpreting the lithostratigraphic units in terms of distinct eruption units (*sensu* Fisher and Schmincke, 1984; cf. Lucchi et al., 2011, for a review).

Eruptive history

Based on the reconstructed unconformity-bounded stratigraphy, the eruptive history of Lipari Island developing between 270 ka BP and historical times is the result of nine successive Eruptive Epochs (furtherly subdivided into distinct eruptions), separated by inter-eruption intervals of quiescence of varying duration and character (see Fisher and Schmincke, 1984; Lucchi and Tranne, 2011 for a review of the adopted methodology). Eruptive Epochs (and Eruptions) and inter-eruption periods are hereafter listed according to the corresponding UBUs (Fig. 5 and 6). They are described in terms of active eruptive vents (using lithosomes) and physical characteristics of erupted products (using lithostratigraphic units). In fact, eruptive activity through time is characterized by distinctive localization and

type of eruptive vents, chemical composition of erupted products and eruption types. The periods between eruptions are characterized by variable degrees of subaerial erosion of the volcanic reliefs, and are associated with development of several volcano-tectonic collapses (namely vc1, vc2, vc3, vc4). Erosion and reworking of volcanic reliefs were mostly driven by the sea-level oscillations occurred during MIS 5, which lead to development of successive marine terraces.

Eruptive Epoch 1: older volcanoes *(i.e., Paleo-Lipari informal unit)*

The oldest exposed Paleo-Lipari volcanic products are represented by lava flows and pyroclastics (minor scoriae) building up a series of isolated volcanoes along the west coast of Lipari (Pietrovito, Timpone Carrubbo, M. Mazzacaruso; Fig. 5) and very subordinately in its central sector (Timpone Croci). Volcanism was of central-type, generally with initial hydromagmatic explosive phases of activity driving the generation of multiple dilute pyroclastic density currents (PDC) followed by the effusion (prevalent) of lava flows and minor strombolian fallout processes. This pattern reflects the interaction between magmas and external sea-water in very shallow water conditions and the progressive transition from hydromagmatic to magmatic (strombolian and effusive) phases of activity during the progressive building of a volcanic island (cf. Schmidt and Schmincke, 2000).

The remnants of Pietrovito volcano are presently found on the sides of caldera-type collapse vc1, in the area of Quattropani (NW Lipari), which is interpreted to have dissected its summit. Yellowish to grey, plane-parallel stratified, hydromagmatic lapilli-tuffs crop out at an oblique angle to the slope of Quattropani-Costa d'Agosto (*i.e.,* Costa d'Agosto formation), representing the eastern flank of a tuff cone structure. Massive and blocky lava flows (*i.e.,* Quattropani formation) are instead exposed on the western side of collapse vc1, accounting for the effusive phases of activity of the Pietrovito volcano.

The lower (and main) portion of the Timpone Carrubbo volcano is represented by a ~180m high stratocone made up of massive and blocky lava flows and interbedded strombolian fallout scoriaceous deposits (*i.e.,* Sc.^{o} Bianco formation, sb_1 member), exposed in the SW coastal sector between Spiaggia Valle Muria and Punta delle Fontanelle (Figs. 5 and 7A). Yellowish planar- to cross-stratified pyroclastics are interbedded (sb_2 member), reflecting the occurrence of intense hydromagmatic phases of activity giving rise to a series of dilute PDC eruption units. The inner part of this volcano with several subvertical feeding dykes is presently exposed near to P. le Grotticelle due to prolonged marine erosion and cliff retreat.

The M. Mazzacaruso compound volcano, in the central-western sector of Lipari, is largely constructed during Eruptive Epoch 1. The initial hydromagmatic (and minor strombolian) explosive phases of activity lead to development of a 70m high and 200m large tuff ring-type

structure (V.ne dei Lacci formation, vla_1 member), which was lately filled and covered by several massive and blocky lava flows (vla_2 member) that determined the growth of the volcano up to elevations of ~300 metres.

Overall, these products are homogeneously CA basaltic andesites, which represent the most primitive rock types on Lipari. They are diffusely characterized by very intense hydrotermalization and are largely dismantled, which frequently leads to the development of brecciated, kaolin-rich deposits with only a few remnants of the original volcanic lithotypes (*e.g.*, at Timpone Carrubbo, Bagno Secco). For example, the strongly hydrotermalized lavas constituting the Timpone Croci relief nearby the Lipari village (*i.e.,* Timpone Croci formation) are only generically suggested to represent the remnants of a lava cone, mostly due to morphological features. Moreover, the Fossa di Faurdo formation includes volcanic products that are pervasively hydrotermalized and altered, thus not being certainly attributable to any precise source area. The intense alteration of products and the paucity of direct stratigraphic contacts (between the distinct volcanoes) prevent the reconstruction of a continuous stratigraphic succession for the Paleo-Lipari products, which are grouped together mostly on the basis of similar compositional features and general stratigraphic relationships. This requires the introduction of several ranges of stratigraphic variability (Fig. 6A). The chronological assessment of Eruptive Epoch 1 is still defective.

Eruptive Epoch 2: Western coast volcanoes (271-188 ka) *(i.e., Piano Grande Synthem, Bagno Secco Subsynthem)*

Renewal of volcanic activity between ~271 and 188 ka BP occurred in correspondence of scattered volcanoes both of central-type (M. Mazzacaruso, Timpone Carrubbo and Chiesa Vecchia) and fissural-type (M. Chirica, Fuori del Pertuso and Timpone Ospedale), mostly distributed along N-S alignments. They are mostly represented by lava flows and strombolian/hawaiian scoriaceous products (with minor hydromagmatic pyroclastics) with homogeneous CA (to very subordinate high-K) basaltic andesite to andesite compositions. Our preferred interpretation is that volcanic activity during Eruptive Epochs 1 to 2 occurred in shallow marine to subaerial environments, which is in accordance with sea level generally much lower than present during the 271-188 ka time interval, corresponding to MIS 6 and 7 (cf. Chappell and Shackleton, 1986; Waelbroeck et al., 2002).

The active eruptive vents are hereafter described according to the reconstructed stratigraphic succession of products (Fig. 6A), although it must be noted that several ranges of stratigraphic variability are necessary due to lacking radiometric ages and stratigraphic contacts between some of the distinct units.

M. Mazzacaruso volcano (upper portion)

Renewal of M. Mazzacaruso volcanic activity occurred from an eruptive vent located above the north-western rim of the older crater structure (cf. Eruptive Epoch 1). Repeated hawaiian-strombolian explosive eruptions gave rise to the emplacement of fallout eruption units amalgamated in thick, chaotic and coarse-grained, matrix-supported pyroclastic-breccias (*i.e.,* M. Mazzacaruso formation). These products are composed of both moderately vesicular clasts and scoriae, which may be the result of magma ponding in (and around) the vent leading to simultaneous eruptions of gas-rich magmas together with already degassed magmas (cf. Vespermann and Schmincke, 2000). Thin and discontinuous lava flows are frequently interbedded, and, together with a few thick massive lava flows (*i.e.,* maz_1 member), account for effusive activity contemporaneous with hawaiian fountaining. A few hydromagmatic pulses occurred giving rise to very discontinuous, dilute PDC eruption units. Note that the M. Mazzacaruso deposits include numerous sub-rounded clasts together with high amounts of fine sand grains constituting the matrix that englobes the breccia lava clasts. This more likely accounts for transportation along steep volcanic slopes leading to progressive abrasion, rounding, breakage and comminution of loose lava and scoriaceous fragments.

Following a period of quiescence, an eruptive vent was active above the eastern rim of the M. Mazzacaruso crater structure, near to Timpone Ricotta, giving rise to its recentmost products (*i.e.,* Bagni Termali S.Calogero formation). They are welded to loose scoriaceous products (bt_1 member) and massive lava flows (bt_2 member) accounting for contemporaneous effusive phases of activity and strombolian-hawaiian fallout processes, with very subordinate hydromagmatic pulses driving the generation of a few thinly bedded dilute PDC eruption units.

Timpone Ospedale spatter cones (271 ka)

The N-S aligned spatter cones of Timpone Pataso (334 m), Timpone Ospedale (352 m) and Valle di Pero (333 m) are the result of strombolian-hawaiian phases of activity of an eruptive fissure located to the north of M. Mazzacaruso volcano (Figs. 5 and 7B). They are constructed by volcanic products (*i.e.,* Timpone Ospedale formation) with lithological, textural and sedimentological features similar to those of M. Mazzacaruso formation (see above), thus outlining a comparable eruptive scenario with prevailing strombolian-hawaiian explosive eruptions, minor hydromagmatic pulses and effusion of lava flows at base of the lava fountain (*i.e.,* to_1 member). Consistently, the reconstructed stratigraphic relationships reveal that the Timpone Ospedale eruptive fissure was more likely active (almost) contemporaneously with the phases of activity of M. Mazzacaruso volcano during Eruptive Epoch 2. Note that the lava flow cropping out at Sc. Le Torricelle (*i.e.,* to_1 member) has been

403 recently dated at 271 ka (Leocat et al., 2009; see Tab. 3), which is the oldermost age
404 constraint for volcanic rocks on Lipari.
405
406 *Timpone Carrubbo volcano (upper portion)*
407 Renewed volcanism of Timpone Carrubbo occurred from a vent located near to Belvedere
408 which erupted volcanic products distributed along the south-eastern flank of the volcano in
409 the direction of Spiaggia Valle Muria (*i.e.,* Belvedere formation). The activity was
410 characterized by an hydromagmatic onset and crater opening, associated with development
411 of dilute PDC eruption units, which gradually developed to dominant strombolian explosive
412 phases of activity and welded scoriaceous fallout eruption units (*i.e.,* bel_1 member). A
413 massive lava flow with blocky carapaces accounts for the latest effusive activity of Timpone
414 Carrubbo (*i.e.,* bel_2 member). Both lava and scoriae are CA andesite (among the more
415 evolved compositions of Eruptive Epoch 2) and contain millimetric amphibole phenocrysts.
416
417 *M. Chirica stratocone (lower portion - 256 ka)*
418 The lower portion of the M. Chirica stratocone (up to elevations of ~350 m), N Lipari (Fig.
419 5), is constructed by alternating lava flows and strombolian-hawaiian scoriaceous products
420 (*i.e.,* Vallone Malopasso formation) reflecting persistent fissural-type strombolian-hawaiian
421 (and effusive) phases of activity. An eccentric spatter cone along the N flank of the M. Chirica
422 volcano is recorded by welded strombolian scoriae and lava flows cropping out near to P. del
423 Legno Nero. Moreover, three roughly N-S-aligned spatter cones (average diameter of 350
424 metres) were constructed by lava flows and strombolian scoriaceous products (*i.e.,* Fuori del
425 Pertuso formation) emitted from an eruptive fissure more likely contemporaneous with the M.
426 Chirica activity.
427 The M. Chirica products have been recently dated at 256 ka (Leocat et al., 2009; see Tab.
428 3), thus being among the oldermost volcanic rocks on Lipari. This is approximately consistent
429 with the age of 223 ka provided by Crisci et al. (1991), which is attributable to volcanic rocks
430 in the northern sector of Lipari near to Acquacalda (R. De Rosa, personal communication),
431 although this attribution is not unequivocal.
432
433 *Chiesa Vecchia volcano (188 ka)*
434 The main portion of Chiesa Vecchia volcano, in the north-western corner of Lipari Island
435 (Fig. 5), was constructed by CA to high-K CA andesite, massive and blocky lava flows
436 outpoured from a large crater rim in the area of Quattropani (*i.e.,* Bonanno and Puddino
437 formations; Fig. 7C). These lava flows flowed down the slopes of Lipari and reached the sea
438 in the sector between Le Puntazze (to the north) and Fuori del Pertuso (to the south), where
439 they frequently reveal strong brecciation probably induced by autoclastic fracturing along

steep slopes (cf. Borgia et al., 1983). The recurrent effusive phases of activity of Chiesa Vecchia volcano were punctuated by hydromagmatic explosive pulses driving the generation of thinly-bedded dilute PDC eruption units.

During its latest stages, volcanic activity focused in an eruptive vent located near Chiesa Vecchia (Fig. 5). Initial phases of activity were hydromagmatic and gave rise to several dilute PDC eruption units recorded by planar yellowish lapilli tuffs (*i.e.,* Bertaccia formation, ber_1 member). The crater opening phase and reaming out of the conduit is witnessed by the occurrence of lithic-rich pyroclastic breccias. The activity of Chiesa Vecchia eruptive vent was characterized by the transition to strombolian-hawaiian eruptions driving the emplacement of scoriaceous fallout deposits. Increased accumulation rates (and higher temperature of emplaced clasts; cf. Wolff and Sumner, 2000) during these phases of activity favored the emplacement of fountain-fed clastogenic lava flows (ber_2 member). Both scoriae and clastogenic lavas are CA andesite, among the more evolved compositions during Eruptive Epoch 2. Volcanic products attributable to the recentmost phases of activity of Chiesa Vecchia volcano are dated at 188 ka (De Rosa et al., 2003b; see Tab. 3).

Eruptive Epoch 3: M. Chirica volcano (150 ka) *(i.e., Piano Grande Synthem, Le Puntazze Subsynthem)*

The upper portion of M. Chirica volcano up to present height of 602 m (diameter of 1,5 km, average slope gradient of 25°) was constructed during Eruptive Epoch 3 by volcanic products of the $V.^{ne}$ di Bezzotti formation (Figs. 5 and 6A). These mostly consist of grey to black massive to cross-stratified scoriaceous lapilli-tuffs and tuffs (*i.e.,* vb_1 member), accounting for recurrent hydromagmatic (to subordinate magmatic) explosive phases of activity driving the emplacement of alternating fallout and dilute PDC eruption units. Lithic-rich deposits are exposed at the base of the unit and in near-vent areas (strongly hydrotermalized) accounting for the crater opening phases at the onset of activity. Inverse-graded deposits are frequently reported as a consequence of grain flow movements of loose clasts along steep slopes immediately following their primary deposition („fall-and-roll“ processes). Thick massive lava flows (*i.e.,* vb_2 member*)* were erupted from the summit crater during the latest phases of activity of M. Chirica volcano. These products are dated at 150 ka (Gillot, 1987).

Inter-eruption period: MIS 5e terraces (124 ka) *(i.e., Sc. le Torricelle Synthem)*

Marine ingression at the onset of last interglacial (=MIS 5) is recorded on Lipari by paleoshoreline I marine terraces with inner margins at 43-45 m *asl.* (P. Palmeto lithosome - Sc.^{o} dell'Immeruta formation; Fig. 6A), developing during the 124ka old interglacial sea-level peak of MIS 5e (Calanchi et al., 2002; Lucchi et al., 2004a). These terraces are mostly

represented by conglomerate horizons cropping out along the western coastal cliffs from Bruca (to the south) to P. del Legno Nero (to the north). Due to the thick cover of more recent deposits, the field evidence of terraces is frequently given by morphological slope breaks at the foot of the older volcanic reliefs of Eruptive Epochs 1 and 2 (Fig. 7B-C). Paleoshoreline I terraces are notably absent along the entire central-southern sector of Lipari (south of Bruca) due to localized tectonic displacement along a series of normal faults, which followed their formation (Lucchi, 2009). *Cladocora caespitosa* corals contained within isolated carbonate buildups above the terraces have been dated at ~119 ka (Calanchi et al., 2002; Lucchi, 2009; see Tab. 3), which is fully consistent with the relative age attribution of paleoshoreline I based on morphostratigraphy.

Eruptive Epoch 4: M. S.Angelo stratocone (lower portion) and Monterosa scoria cones (119-116 ka) *(i.e., Sc.^{o} le Torricelle Synthem)*

Eruptive Epoch 4 developed during early MIS 5 and lead to construction of the basal portion of M. S.Angelo stratocone and the Monterosa scoria cones. This outlines a significant shifting of eruptive vent location towards the central (eastern) sector of Lipari Island (Fig. 5), associated with the change of active stress fields (with the activation of the secondary E-W tectonic trend), and the progressive differentiation of erupted products (with the prevalence of high-K CA andesites).

Monterosa scoria cones (119-116 ka)

The cape of Monterosa is made up of the twin scoria cones of Pietra Campana and U Mazzuni developed along a E-W aligned eruptive fissure with recurrent strombolian-hawaiian and effusive phases of activity. The polygenetic nature of the Monterosa scoria cones is outlined by the occurrence of deep erosional unconformities of local significance (Fig. 8A), which allow subdivision of the stratigraphic architecture into the Sciarra di Monterosa, Pignataro di Fuori and U Mazzuni formations (Figs. 6A and 8A). Overall, the erupted products are CA (to high-K) basaltic andesite to andesite.

The oldermost Monterosa products (*i.e.,* Sciarra di Monterosa formation) are exposed along the coastal cliff on the eastern side of U Mazzuni relief, near to Sciarra di Monterosa (Fig. 5). They gave rise to construction of a 60m high scoria cone representing the basal portion of the U Mazzuni volcano (Fig. 8A). The onset of activity is hydromagmatic with the generation of thinly bedded dilute PDC eruption units that built up a tuff ring-type structure with shallow dipping rim beds (sci_1 member). Subsequently, the gradual reduction of sea water influence on eruptive conditions lead to the development of strombolian phases of activity and emplacement of fallout welded to loose scoriaceous deposits that constructed a steeper sided scoria cone (sci_1 member; Fig. 8A). This is the typical growth pattern of scoria

cones developed in shallow water conditions (cf. Vespermann and Schmincke, 2000). Thick lava flows were issued during latest stages of activity and filled the crater depression (sci_2 member).

The main portion of the U Mazzuni and Pietra Campana twin scoria cones (up to elevations of 100 m) is constructed by welded reddish scoriaceous products representing multiple fallout eruption units emplaced during prolonged strombolian-hawaiian explosive phases of activity (*i.e.,* Pignataro di Fuori formation; Fig. 8A). Some discontinuous thinly bedded dilute PDC eruption units were generated during minor, episodic hydromagmatic pulses. Several discontinuous thin lava flows were erupted at the base of the fountain, together with a few massive lava flows exposed along the southern and south-western sides of the Pietra Campana scoria cone (*i.e.,* pf_1 member) and a squat lava dome along its western side (pf_2 member).

The Monterosa scoria cones were built up to their present elevation of ~200 m by volcanic products of the U Mazzuni formation (Fig. 8A). They consist of black/yellow scoriaceous deposits (*i.e.,* ma_1 member) accounting for prevailing strombolian fallout processes, with the crater opening phases revealed by lithic-rich tuff-breccias exposed in the morphologic depression between the reliefs of Pietra Campana and U Mazzuni. The onset of activity was triggered by the interaction between magma and external water leading to deposition of thinly bedded, varicoloured dilute wet-type PDC eruption units at base of the unit. A series of massive lava flows was erupted from the northern sides of the Pietra Campana and U Mazzuni scoria cones during their latest phases of activity.

Lava flows attributed to the U Mazzuni formation have been recently dated at 119 ka (Leocat et al., 2009; see Tab. 3), which is consistent with our stratigraphic investigation showing that the Monterosa volcanoes were more probably active contemporaneously with the oldest phases of activity of M. S.Angelo volcano (dated at ~116 ka; see below). Note that the age of 102 ka obtained for the older Pignataro di Fuori lava flows by De Rosa et al. (2003) unfortunately does not fit this chronological framework. Based on the 119-116 ka age constraints, the Monterosa volcanoes are assumed to have been active mostly in the course of early MIS 5. This is far more precise than previous attribution to the Paleo-Lipari unit based uniquely on comparable petrochemical features and eruption types (Pichler, 1980; Crisci et al., 1991; Tranne et al., 2002; Lucchi et al., 2010).

M. S.Angelo stratocone (lower portion - 116 ka)

The large M. S.Angelo stratocone is the dominant morphostructural feature in the central sector of Lipari Island (Fig. 5). Its early phases of activity developed during Eruptive Epoch 4 with the emplacement of the Timpone Ricotta pyroclastic products (Fig. 6A). They are thick yellowish to grey planar bedded lapilli tuffs accounting for prolonged hydromagmatic

551 explosive phases of activity giving rise to recurrent dilute, dry-type PDC eruption units, with
552 lithic-rich deposits at the base being the result of the crater opening phases. These
553 pyroclastic products are widely distributed along the flanks of M. S.Angelo volcano (Fig. 8B)
554 and are suggested to have constructed a large tuff cone-type structure (with estimated
555 diameter of about 2 km), which is presently almost completely buried by more recent
556 deposits. The currents from M. S.Angelo are interpreted to have reached the coastal sector
557 of Marina di Porto Salvo (E Lipari) where the presence of lithic-rich tuffaceous breccias with
558 diffuse rip-up structures and plastic deformation of strata provides evidence of syn-
559 depositional marine reworking occurred as primary PDCs entered the sea. A series of thick,
560 lobate lava flows (*i.e.,* Timpone del Corvo Formation) were erupted from the southern crater
561 rims of the M. S.Angelo tuff cone during its latest effusive phases of activity.
562 These early M. S.Angelo lava flows have provided contrasting K/Ar age attributions of 127
563 ka (Crisci et al., 1991), 116 ka (Leocat et al., 2010) and 84 ka (De Rosa et al., 2003b). This
564 puts in evidence the limited reliability of these dating methods on low-K_2O volcanic rocks. No
565 further relative age constraints are provided by marine terraces because direct stratigraphic
566 contacts with early M. S.Angelo products are lacking. Our preferred chronological attribution
567 among the various possibilities is that the early M. S.Angelo activity has developed at ~116
568 ka, consistently with the field evidence of contemporaneous activity of the Monterosa scoria
569 cones at 119 ka (see above). In fact, in an outcrop site near to Marina di Porto Salvo, we
570 found several impact sags (up to 40 cm large) within the M. S.Angelo pyroclastics (*i.e.,*
571 Timpone Ricotta formation) showing a E-to-W (N90°E) direction of provenance, which is
572 remarkably opposite respect to the M. S.Angelo source area and fully consistent with the
573 location of Monterosa scoria cones (Fig. 8C). This likely indicates that the early phases of M.
574 S.Angelo activity were contemporaneous with ballistic fallout from the adjacent Monterosa
575 scoria cones. Moreover, discontinuous layers of coarse-grained, lithic-rich scoriaceous tuff-
576 breccias and bomb-sags originated from the eastern quadrangles are reported within the M.
577 S.Angelo pyroclastics also in an outcrop site near to Timpone Croci, which apparently
578 indicates that minor eruptive vents located in E Lipari (in addition to the Monterosa cones)
579 were active during the early stages of development of the M. S.Angelo volcano. The same
580 information is given by the occurrence of fountain-fed clastogenic lavas within the M.
581 S.Angelo pyroclastic products (tr_a member) in a few outcrops at Marina di Porto Salvo.
582
583 **Eruptive Epoch 5: M. S.Angelo stratocone (intermediate portion - 105 ka)**
584 *(i.e., Bruca Synthem)*
585 After a major period of volcanic inactivity mostly developed at the end of MIS 5e (*i.e.,*
586 erosional unconformity L_2), renewal of volcanic activity lead to construction of the
587 intermediate (and main) portion of the M. S.Angelo stratocone. This is represented by a

588 400m high tuff cone-type structure (with estimated diametre of the crater rim of 800 metres)
589 built up by widespread high-K CA andesite pyroclastic products and lava flows emitted during
590 two distinct and successive stages of activity (Eruptions 5.1 and 5.2).
591
592 ***Eruption 5.1*** *(i.e., Timpone del Grado Subsynthem)*
593 This is an intense and prolonged hydromagmatic phase of activity giving rise to recurrent
594 dilute (mostly dry-type) PDC eruption units represented by a thick succession of thinly to
595 medium bedded, grey to pink lapilli-tuffs (*i.e.,* Timpone Pataso formation; Fig. 9A), with
596 interbedded scoriaceous lapilli-tuff layers accounting for minor strombolian fallout processes.
597 These primary pyroclastics diffusely crop out uniquely in near-vent areas (e.g. near Serra
598 Pirrera), constituting the framework of the M. S.Angelo cone. Towards distal areas, they are
599 gradually substituted by widespread, sheet-like horizons of massive grey-green lapilli-tuffs
600 (Fig. 9A), which are known as „leaf-bearing pyroclastics“ due to the high content of unburned
601 fossil plant relicts (Ricci Lucchi et al., 1988). Based on this feature, together with absence of
602 traction structures, valley ponding thickness variations and substrate erosion, they have been
603 interpreted by Ricci Lucchi et al. (1988) as lahar deposits generated from the interaction
604 between primary pyroclastics (frequently cropping out as relics) and an external water
605 source. This may have been represented by a lacustrine basin filling the morphologic
606 depression related to caldera-type collapse vc2 in the area between the M. S.Angelo and M.
607 Chirica reliefs (Fig. 2). The emplacement from lahar-type processes is confirmed by the
608 occurrence and flat attitude of plant-leaf relics at the top of distinct lahar depositional unit,
609 which more likely indicates that transportation occurred afloat watery laminar flows more than
610 in turbulent suspensions (Ricci Lucchi et al., 1988). These lahar-fed deposits have a wide
611 distribution along the flanks of the M. S.Angelo cone.
612 In the area of Timpone Pataso, they are suggested to have progressively filled a small
613 lacustrine basin formed as a consequence of tectonic displacement along N-S faults (Fig.
614 9B). This is recorded by a regularly stratified lentiform body (tp_a member - up to 100 m thick,
615 400 m large) composed of alternating leaf-bearing pyroclastics and varicoloured aphanitic
616 chert. Lacustrine depositional conditions are suggested by the faint varve-like lamination of
617 these deposits, together with the occurrence of numerous load and drag casts indicative of
618 high content of liquid water. In this context, the chert layers do not contain traces of fossils
619 and are thus interpreted to reflect syngenetic chemical precipitation (rather than diagenetic
620 replacement) induced by the saturation in silica of water when PDCs entered the lake (Ricci
621 Lucchi et al., 1988).
622
623 ***Eruption 5.2 (~105 ka)*** *(i.e., Fossa della Valle Subsynthem)*

Eruption 5.2 followed a period of volcanic inactivity witnessed by a widespread red paleosol developed above the early leaf-bearing pyroclastic products of Timpone Pataso formation (see above in the text; Fig. 9A). The initial explosive phases of activity lead to the emplacement of the leaf-bearing pyroclastic products of Serra Pirrera formation, which have lithological, sedimentological and structural features similar to those of Timpone Pataso formation (Fig. 9A). This outlines a fully comparable eruptive scenario with recurrent hydromagmatic explosive eruptions giving rise to multiple dilute PDC eruptions units (and minor strombolian fallout deposits), followed by the deposition of lahar deposits driven by the interaction between PDCs and the caldera-filling lacustrine basin. Both these leaf-bearing horizons (*i.e.,* Timpone Pataso and Serra Pirrera formations) have a wide areal distribution over most of Lipari Island (Fig. 10), from the area of Chiesa Vecchia (to the north) to Monterosa (to the east). They are moreover reported along a few coastal areas (Fig. 11A), in places revealing evidence of the interaction between primary pyroclastic products and sea water (i.e., Punta del Cugno Lungo formation, cl_a member).

A series of high aspect ratio, blocky lava flows, known as cordierite-bearing lavas for their high content of megacrysts of cordierite and garnet (Bergeat, 1910; Maccarone, 1963; Honnorez and Keller, 1968; Klerx et al., 1974; Pichler, 1980; Barker, 1987; Crisci et al., 1991; Esperanca et al., 1992; Di Martino, 2010), were erupted during the latest phases of activity of Eruption 5.2. These lava flows were emitted from the southern (and subordinately eastern) crater rims of the M. S.Angelo tuff cone, spreading along its flanks for a total length of up to 3 kms and branching out in different lobes till invading the coastal sector between Bruca and Punta delle Fontanelle (Fig. 11B). Whole-rock composition of these lavas is high-K CA andesite, tipically with sub-millimetric to millimetric (up to 2 cm) abundant xenoliths (up to 50% in volume) set in a dacite to rhyolite groundmass (see below in the text). Due to their wide areal distribution and unequivocal field recognizability, the cordierite-bearing lavas (and leaf-bearing pyroclastics) are fundamental key-beds for stratigraphic correlations on Lipari (Fig. 10). They are dated at 104-105 ka (Crisci et al., 1991; Lucchi, 2000; Lucchi et al., 2004a; see Tab. 3).

Inter-eruption period: MIS 5c terraces (100 ka) *(i.e., Fontanelle Synthem, Cala Sciabeca Subsynthem)*

The 100ka old interglacial sea-level peak of MIS 5c is recorded on Lipari by paleoshoreline II marine terraces, with inner margins are 23-27 m *asl.* (P. Palmeto lithosome – Punta del Cugno Lungo formation; Fig. 6A). These terraces are scattered along the entire western coast of Lipari from P. del Legno Nero (to the north) to P. le Grotticelle (to the south), overcutting most of the Paleo-Lipari volcanic products together with cordierite-bearing lavas and leaf-bearing pyroclastics, and the older MIS 5e terraces (Fig. 11A-B). Small and

narrow terraces are preserved at P. del Cugno Lungo and Cala Sciabeca, although paleoshoreline II is usually covered by more recent deposits and represented by conglomeratic horizons along the steep coastal cliffs. Finer-grained deposits made up of granules and sands are visible in places, particularly along the steep coastal cliff of Cala Sciabeca where they constitute a 20m thick and 600m large lentiform body (cl_a member; Fig. 11C). These deposits reveal large-scale cross-stratification gradually upward passing to planar and low-angle cross stratification, with clast composition reflecting that of Serra Pirrera leaf-bearing pyroclastics. As such, they are interpreted to record a prograding submerged beach sand body deposited in upper shoreface to foreshore environments under the abundant influx of fine-grained pyroclastic products (Lucchi, 2009).

Eruptive Epoch 6: M. S.Angelo and M. Chirica volcanoes (92-81 ka)

(i.e., Fontanelle Synthem, Lo Inzolfato Subsynthem)

Eruptive Epoch 6 was characterized by the reactivation of M. S.Angelo and M. Chirica volcanoes after a substantial period of quiescence, with no significant changes of eruptive vent location, eruption types and chemical composition of erupted products (high-K CA andesites).

The construction of M. S.Angelo stratovolcano up to present elevation of 593 metres *asl* (with crater diameter of 500 m) was completed through emplacement of the Chiappe Lisce volcanic products. The upper flanks of the cone (average slope gradient of 30-35°) are composed of massive pyroclastic-breccias with numerous bread-crust bombs laterally passing to thinly bedded, planar- and cross-stratified lapilli-tuffs (ch_1 member). These deposits account for the emplacement of several low-energy dilute PDC eruption units *plus* ballistic fallout during recurrent vulcanian-type explosive eruptions. These were followed by the effusion of two blocky lava flows (ch_2 member) that overflowed the southern and western crater rims for a total length of only 250 metres. Successively, a series of lahar depositional units (*i.e.,* ch_3 member) were generated by rainfall reworking of loose pyroclastic deposits and lava blocks along the steep south-western flanks of the M. S.Angelo cone. The summit lava flows are dated at 92 ka (Crisci et al., 1991) and signed the interruption of volcanic activity of M. S.Angelo. Note that the same lava flows have yielded a contrasting age of 55 ka (De Rosa et al., 2003b), which is not consistent with the occurrence of Lower Brown Tuffs (70-56 ka) and Grey Porri Tuffs (67-70 ka) on the top of M. S.Angelo cone (see below in the text), thus being considered uncertain.

The latest phases of activity of M. Chirica volcano were characterized by the emission of a series of thick lava flows from the western side of the summit crater rim, near to Costa d'Agosto (Fig. 5). These lava flows spread from the source area flowing down the western flanks of M. Chirica and progressively filled the morphologic depression of caldera-type

collapse vc1 in the area of Pietrovito, subsequently overflowing its western side (forming a spectacular fossil lava fall) and fanwise opening and invading the coast between Lo Inzolfato and Cala Sciabeca (Fig. 11C). Along this coastal sector, a 1.5km large lava front constituted by the superposition of three successive lava flows is exposed, paraconformably overlying the MIS 5c marine deposits (*i.e.,* P. del Cugno Lungo formation; Fig. 11C). A squat massive lava dome was likely effused from an eccentric dyke near P. del Legno Nero, N Lipari (ch_1 member). These recentmost M. Chirica lava flows are dated at 92-81 ka (De Rosa et al., 2003b), more likely indicating that they were almost contemporaneous with latest phases of activity of M. S.Angelo volcano.

Inter-eruption period: MIS 5a terraces (81 ka)*(i.e., Fontanelle Synthem, Fossa di Faurdo Subsynthem)*

Marine ingression during the MIS 5c interglacial sea-level peak (81 ka) determined the formation of paleoshoreline III marine terraces, with inner margins at 12 m *asl* (P. Palmeto lithosome – Punta delle Fontanelle formation; Fig. 6A). These terraces are discontinuously recorded in the coastal sector between Fossa di Faurdo and Punta le Grotticelle, invariably crosscutting the older paleoshoreline II terraces (Lucchi, 2009). Moreover, marine conglomerates attributed to paleoshoreline III are reported in two small outcrops on the northern side of the Monterosa cape, E Lipari (fo_a member).

Inter-eruption period: younger than MIS 5 (81-22 ka)*(i.e., Scogliera sotto il Monte Synthem)*

Starting from the end of MIS 5 (<81 ka), the Lipari volcanic complex was characterized by a prolonged period of volcanic inactivity, which was interrupted by early rhyolite eruptions in the southern sector of the island (~42 ka; see below). The 81-22 ka time interval mostly corresponds to a relative lowstand segment of the sea-level curve (MIS 4 to 2), which triggered intense subaerial reworking, mass-wasting and relief smoothing of volcanic slopes (and marine terraces) leading to the emplacement of thick epiclastic deposits at the foot of coastal reliefs (particularly along the western coast). Moreover, recurrent explosive activity from external source areas during the past 70 ka is recorded on Lipari by the emplacement of widespread pyroclastic products originated from Aeolian volcanoes or the Campanian Province. In particular, the massive brownish ash-rich deposits known as Brown Tuffs are prominently demonstrated in most of the stratigraphic profiles across Lipari Island (Fig. 10), invariably overlying the marine terraces along the west coast (Fig. 11). They were deposited from fallout processes and dilute PDCs (the latter in southern Lipari) related to high-energy hydromagmatic eruptions of an eruptive vent located within the La Fossa caldera on Vulcano (Lucchi et al., 2008; Lucchi et al., 2011). Based on the interbedding of the Ischia Tephra (56

735 ka) from the Campanian Province, they are subdivided into the Lower (70-56 ka) and
736 Intermediate (56-22 ka) Brown Tuff units, which may be correlated on a regional scale
737 (Lucchi et al., 2008). These are both included in the Pianoconte formation (Fig. 6B). A few
738 other tephra layers are interbedded within this Brown Tuff succession. In stratigraphic order,
739 they are the l_1 tephra layer and the 67-70ka old Grey Porri Tuffs. These are a pumiceous-
740 scoriaceous pyroclastic succession related to the initial high-energy explosive eruptions of
741 the Monte dei Porri stratocone on Salina, dated at 67-70 ka (Monte dei Porri lithosome,
742 Rocce di Barcone formation; Lucchi et al., 2011; Keller et al., 2011). Their more distal portion
743 is diffusely represented in the northern and central-western sectors of Lipari (Fig. 11A-B) by
744 pumiceous-scoriaceous pyroclastics with comparable textural and petrochemical features,
745 which are intercalated within the Lower Brown Tuffs (see Tab. 3). These pyroclastic products
746 irregularly mantle the pre-depositional topography with a general rapid W-to-E thickness
747 decreas (from a maximum of 15 m along the western coast to a few dms along the eastern
748 one), and are mostly interpreted as fallout products, with a few dilute PDC eruption units.
749
750 **Eruptive Epoch 7: Southern dome field (~42 ka)***(i.e., Scogliera sotto il Monte*
751 *Synthem)*
752 Renewal of volcanism on Lipari was characterized by the remarkable onset of rhyolite
753 magmatism in this volcanic system. Active eruptive vents were located to the south of
754 volcano-tectonic collapse vc3 affecting the flanks of the M. S.Angelo and Timpone Carrubbo
755 stratocones (Figs. 5 and 12A), and determined the progressive construction of the southern
756 sector of Lipari through the emplacement of thick pumiceous successions and viscous
757 endogenous lava domes, alternating with external pyroclastics (Figs. 6B and 12B). Eruptive
758 Epoch 7 developed around 42-40 ka and was arranged into two distinct eruptions leading to
759 the effusion of the P. di Perciato (Eruption 6.1) and Falcone domes and pyroclastics
760 (Eruption 6.2). Both Eruptions 6.1 and 6.2 were controlled by the main NNW-SSE tectonic
761 trend and characterized by the emission of slightly porphyritic, high-K rhyolite products.
762
763 ***Eruption 7.1 (>42 ka)*** *(i.e., P. del Perciato lithosome)*
764 The oldermost products in the southern sector of Lipari are represented by the remnants
765 of two endogenous, NNW-SSE aligned lava domes cropping out along the coastal cliff of
766 Scogliera sotto il Monte (*i.e.,* Punta del Perciato formation, pe_1 member; Fig. 12B), including
767 the isolated rocks of le Formiche, Pietralunga and Pietra Menalda. They account for the early
768 stages of development of the southern dome field of Lipari. These domes were characterized
769 by the latest explosive eruption of whitish pumiceous pyroclastics exposed in the southern-
770 central Lipari (pe_2 member; see Tab. 3), interbedded within the Intermediate Brown Tuffs.
771 They are the result of decelerating dilute and turbulent PDC eruption units moving from south

to north Lipari, which were generated during exogenic explosive eruptions mostly driven by magmatic volatile-driven fragmentation mechanisms (cf. Fink and Anderson, 2000), as indicated by the occurrence of dominantly well vesiculated pumiceous clasts. These explosive eruptions likely caused the partial destruction of the P. del Perciato domes, as inferred by the abundance of dome-type lava blocks within the proximal pyroclastic breccias.

Eruption 6.1 can not be precisely dated, but our stratigraphic analysis allows definition of a restricted time-interval of emplacement ranging between 56 ka (age of underlying Ischia Tephra) and 40-42 ka (age of younger Falcone domes).

Eruption 7.2 (42-40 ka) *(i.e., Falcone lithosome)*

The eruption of Falcone pyroclastic products and domes (*i.e.,* Falcone formation; see Tab. 3) is representative of the intermediate stages of development of the southern dome field of Lipari. The initial high-energy explosive phases of activity from a source area located in the area of Capparo-Falcone gave rise to multiple northward-spreading, dilute and turbulent PDC eruption units, which are represented by thick, massive to cross-laminated whitish pumiceous pyroclastics (fa_1 member; Fig. 12B), found interbedded within the Intermediate Brown Tuffs. Pumices are mostly well vesiculated accounting for magmatic fragmentation mechanisms. These products are assumed to have constructed a large tuff ring-type structure which is at present almost entirely covered by more recents deposits. The endogenous lava domes at Falcone, Capparo and Capistello (fa_2 member) were lately erupted, and possibly filled the tuff ring structure. These domes are deeply eroded and weathered, and are displaced by intense tectonic activity along NNW-SSE-aligned normal faults (along the cliff of Scogliera sotto il Monte) and by volcano-tectonic collapse vc4 (Fig. 5). A small black lava dome (fa_3 member) crops out near Punta della Crapazza, cutting the Falcone domes (Fig. 12C) and likely rising along the trace of a N-S normal fault (Fig. 5). This dome is high-K dacite (the Falcone domes are homogeneously high-K rhyolite) and very rich in xenocrysts, which seems to provide the field evidence of mingling/mixing processes occurred between rhyolite and more mafic magmas, already suggested by Gioncada et al. (2003, 2005) on the basis of latite enclaves reported within the Falcone domes (see below in the text). The Falcone domes are dated at 42-40 ka (Crisci et al., 1991; Gillot, 1987).

Eruptive Epoch 8 (22-8 ka)*(i.e., V. Muria Synthem)*

Renewal of volcanic activity in southern Lipari occurred between 22 ka and ~8 ka and followed a prolonged period of quiescence after the eruption of the Falcone domes (42-40 ka). During this period of dormancy, the younger units of the Intermediate Brown Tuffs from Vulcano are deposited, together with the 39ka old Y-5 tephra layer representing the distal equivalent of the Campanian Ignimbrite (Fig. 12B) and the 23ka old Lower Pollara Tuffs from

Salina (see Tab. 1; Lucchi et al., 2011), which act as fundamental time-stratigraphic key beds.

Eruptive Epoch 8 developed through two distinct eruptions (namely, Eruptions 8.1 and 8.2), subdivided by a minor period of inactivity.

Eruption 8.1: Southern dome field-M. Guardia (22-21 ka)*(i.e., Urnazzo Subsynthem)*

The eruption of the M. Guardia-M. Giardina domes and pyroclastics, together with the P. S.Giuseppe domes, signed the latest stages of development of the southern dome field of Lipari, under control of NNW-SSE tectonic lineaments. This occurred in a short time-interval between 22 and 21 ka (Fig. 6B), as shown by the age of Brown Tuff units at base and top of the corresponding products (Lucchi et al., 2008; Lucchi et al., 2011).

The initial high-energy, subplinian explosive eruptions are originated from an eruptive vent in the area of M. Guardia-M. Giardina, within the morphologic depression formed by volcano-tectonic collapse vc4 affecting the older Falcone domes (Fig. 5). These eruptions gave rise to the widespread M. Guardia pumiceous pyroclastics (*i.e.,* M. Guardia formation; see Tab. 3), which correspond to the reknown „Monte Guardia sequence“ (Crisci et al., 1983; De Rosa and Sheridan, 1983; Colella and Hiscott, 1997; De Rosa et al., 2003a). These pyroclastic products are correlated throughout the entire Lipari Island (Fig. 10) and on most of the Aeolian archipelago, thus representing a major stratigraphic key-bed (Lucchi et al., 2011). They are characterized by remarkable proximal-to-distal (and vertical) facies variations from coarse-grained, lithic-rich, disorganized tuff-breccias in near-vent areas, passing to thinly to medium bedded lapilli-tuffs and tuffs with planar to cross-stratification towards distal areas (Colella and Hiscott, 1997)(Fig. 12B). These facies variations are typical of decelerating and waning, dilute and turbulent, dry-type (subordinately wet-type) PDC eruption units spreading mostly to the north of the eruptive vent (Colella and Hiscott, 1997). Fine-grained tuff layers and the laterally persistent salmon-coloured key-beds (adopted by Colella and Hiscott, 1997, for the correlation of distinct eruption unit) account for fallout processes from the fully dilute, low-concentration tails of these PDCs. These layers contain abundant accretionary lapilli, which is indicative of high moisture content of the currents, due to high atmospheric humidity or hydromagmatic explosive fragmentation at source (Crisci et al., 1981; Colella and Hiscott, 1997). On this subject, note that the M. Guardia activity was mostly driven by magmatic volatile fragmentation mechanisms, as indicated by the prevalence of white, highly vesiculated rhyolite pumices (together with minor mildly vesicular, latite to high-K dacite pumices and banded pumices; De Rosa et al., 2003a), with only a subordinate role for impulsive magma-water interaction (Crisci et al., 1981; Colella and Hiscott, 1997). The distal ash beds found on Vulcano, Panarea and Salina (Lucchi et al., 2011) reflect the fallout emplacement from an associated eruption plume, the occurrence of which is outlined on

Lipari by subordinate coarse-grained, fines-depleted pumiceous lapilli-tuff layers (Colella and Hiscott, 1997). Eruptive activity was likely triggered by a fresh latite magma batch entering into a shallow rhyolite chamber, as suggested by De Rosa and Sheridan (1983), Crisci et al. (1991) and De Rosa et al. (2003a) on the basis of evidence of mingling/mixing processes (*i.e.,* latite enclaves, two distinct pumice compositions, banded pumices, disequilibrium crystal assemblages). This is consistent with the observed vertical zonation of M. Guardia pyroclastics with denser mixed magmas (*i.e.,* banded pumices) emitted in the initial phases of the eruption followed by the dominant discharge of low density rhyolite magmas (*i.e.,* white pumices).

Eruptive activity late shifted from explosive to effusive, thus generating the NNW-SSE aligned, endogenous obsidian-rich lava domes of S.Lazzaro, M. Guardia, and M. Giardina (M. Giardina formation; Fig. 12A-B), named in the order of progressive effusion from south to north. These high-K rhyolite domes are glassy, highly vesicular and porphyritic, with the same mineral assemblage (K-feldspar, clinopyroxene, amphibole, zircon) of the white M. Guardia pumices and no evidence of disequilibrium, which indicates a comparable pre-eruptive water content and a continuous undisturbed transition from explosive to effusive activity (De Rosa et al., 2003a).

Poorly sorted massive tuff-breccias made up of obsidian and rhyolite angular clasts (similar to the underlying domes) and minor pumices built up a crater structure at top of the M. Giardina dome (gi_1 member). These products likely account for fallout processes and subordinate dilute PDCs emitted during latest explosive eruptions disrupting the dome surface, possibly driven by high anomalies of water content developing within the inner dome. Conversely, based on the paucity of new juvenile material, we can not exclude that explosive activity was triggered by the interaction between the hot dome interior and groundwater entering the fractures on the dome surface (*i.e.,* phreatic activity).

Three NNW-SSE aligned, endogenous lava domes (*i.e.,* P. S.Giuseppe formation) were effused in the sector of P. S.Giuseppe (Fig. 5) contemporaneously with the M. Giardina domes (22-21 ka). The southernmost (and bigger) dome is affected by a sub-circular steep-walled collapse structure (furtherly displaced by a NNW-SSE fault), which is partially filled by a small resurgent dome cropping out near P. di Costa (Fig. 5). Noteworthy, the high-K rhyolite P. S.Giuseppe domes contain clinopyroxene-rich magmatic enclaves and xenocrysts, differently from the M. Giardina domes that are characterized by plagioclase- and pyroxene-rich enclaves. Moreover, the P. S.Giuseppe domes are substantially aphyric (the M. Giardina domes are porphyritic) and show a distinctive trace element composition for a given SiO_2 content (Gioncada et al., 2003; Gioncada et al., 2005). Given these features, Gioncada et al. (2005) suggest that the P. S.Giuseppe and M. Giardina domes derive from

different magma batches, consistently with their emplacement along two different and parallel tectonic fractures (Fig. 5).

Inter-eruption period: Upper Brown Tuffs (21-16 ka)*(i.e., Quattrocchi Subsynthem)*

The Upper Brown Tuffs are massive brownish ash-rich deposits originated from high-energy hydromagmatic eruptions sourced in the area of La Fossa caldera at Vulcano (*i.e.,* Piano Grotte dei Rossi formation; De Astis et al., 2011). They are defined above the M. Guardia pyroclastics (22-21 ka) and correlated on a regional scale on most of the Aeolian archipelago and at Capo Milazzo, northern Sicily (Lucchi et al., 2008; Lucchi et al., 2011). The Upper Brown Tuffs deposited on Lipari reflect the emplacement of northwards-spreading dilute and turbulent PDCs (south Lipari) and associated fallout processes. They are mostly related to the time-interval between 21 and 16 ka (see Tab. 3), during which the Lipari volcano was substantially quiescent.

Eruption 8.2: N-S aligned domes (between 16 and 8 ka)*(i.e., Vallonaccio Subsynthem)*

A series of N-S aligned, endogenous lava domes (Castello, V.^{ne} Canneto dentro, Capo Rosso; Figs. 5) were erupted in distinct sectors of the eastern coast of Lipari during the time-interval between 16 (age of underlying Upper Brown Tuffs) and 8 ka (age of the overlying Vallone del Gabellotto pyroclastics). These domes are high-K rhyolite, with aphyric texture and cpx-rich porphyritic latite enclaves (similarly to the P. S.Giuseppe domes; Gioncada et al., 2003). The effusion of V.^{ne} canneto dentro dome, in the central sector of Lipari, was preceded by low-energy explosive eruptions giving rise to obsidian-rich, pumiceous PDC eruption units with a limited dispersal area (cd_1 member; see Tab. 3). The Capo Rosso endogenous domes, in the north-eastern area of Lipari (Fig. 13A), anticipated the progressive shifting to the north of active eruptive vents (and the compositional change) that became effective during later stages of volcanic activity at Lipari (*i.e.,* Eruptive Epoch 9; see below).

Eruptive Epoch 9: North-eastern dome field (8 ka-*AD* 1230)*(i.e., Vallone Fiume Bianco Synthem)*

Ranging from ~8 ka to historical times, Eruptive Epoch 9 determined the construction of the north-eastern sector of Lipari through the emplacement of high-K rhyolite pumiceous pyroclastics and viscous lava coulees. Volcanic activity was strongly controlled by the main NNW-SSE strike-slip system (and associated N-S and NE-SW extensional lineaments) and developed during three successive eruptions (Eruptions 9.1, 9.2, 9.3) characterized by the same eruptive pattern with initial strombolian or subplinian explosive eruptions followed by late effusive phases of activity.

Eruption 9.1: Vallone del Gabellotto-M. Pilato (~8 ka)

The early phases of activity during Eruptive Epoch 9 determined the emplacement of widespread pyroclastic products and a lava coulee representing the basal portion of the large Vallone del Gabellotto-M. Pilato composite volcano. The initial high-energy explosive phases of activity gave rise to widespread whitish pumiceous pyroclastics (*i.e.,* Vallone del Gabellotto formation; see Tab. 3), which diffusely crop out in the entire central-northern sector of Lipari (Figs. 10 and 13A), with distal tephra layers found on Panarea and Vulcano islands (Lucchi et al., 2008). They are massive lithic-rich pumiceous tuff breccias (near-vent areas) laterally passing to planar and cross-stratified lapilli tuffs with large-scale wavy bedforms (towards distal areas), which mostly derived from the emplacement of dilute, dry-type PDC eruption units. These are interbedded with well sorted, pumiceous fallout eruption units. Based on thickness and grain-size variations, these pyroclastic products are assumed to have been originated from a source area in the vicinity of Vallone del Gabellotto gorge (Fig. 5), in agreement with Cortese et al. (1986). They more likely constructed an asymmetric tuff cone (with estimated diameter of more than 1 km), which is presently largely eroded and almost completely covered by more recent deposits. Explosive activity was conditioned by both end-member fragmentation processes as shown by the coexistence of moderately vesicular, blocky and equant pumiceous clasts (typical of hydromagmatic fragmentation) and highly vesicular pumices (indicative of exsolution of magmatic gases). The large obsidian-rich Pomiciazzo lava coulee (*i.e.,* Pomiciazzo formation) erupted from the eastern crater rim of the Vallone del Gabellotto tuff cone and reached the coastal sector forming three lava lobes. The submarine continuation of these coulee lobes is documented by Gamberi and Marani (1997) in the corresponding offshore sector. The Pomiciazzo coulee is dated at 11-8 ka (Bigazzi and Bonadonna, 1973; see Tab. 3). This is approximately consistent with the age of 8.2 ka recently obtained for the Vallone del Gabellotto pyroclastic products based on the correlation with the marine E-1 tephra layer in Adriatic and Tyrrhenian deep-sea cores (Zanchetta et al., 2010). Notably, an obsidian clast within the Vallone del Gabellotto pyroclastics near Acquacalda gave an age of 21 ka (Bigazzi and Bonadonna, 1973), which apparently predates the onset of rhyolite magmatism in the north-eastern sector of Lipari Island. Unfortunately, this obsidian clast can not be attributed with certainty to any stratigraphic units cropping out in the area.

Eruption 9.2: Forgia Vecchia and M. Pilato (1.6 ka-AD 776)

Renewal of volcanic activity during Eruptive Epoch 9 followed a period of volcanic quiescence during which a widespread red paleosol was formed above the Vallone del Gabellotto pyroclastics (Fig. 13A). This period of dormancy developed between ~8 ka and

historical times and was characterized by the deposition of the most recent Upper Brown Tuff units on Lipari (*e.g.,* in the Vallone Fiume Bianco pumice quarry and along the NE coastal cliff nearby Capo Rosso).

Two distinct eruptive vents (Forgia Vecchia and M. Pilato), following a rough NNW-SSE alignment (Fig. 5), were active during Eruption 9.2.

Forgia Vecchia coulee (~1.6 ka)

The tongue-like, obsidian-rich lava coulee of Forgia Vecchia (*i.e.,* Forgia Vecchia formation, fv_2 member) was outpoured from an eruptive vent in the area of Pirrera, and flowed down forming two lava lobes standing at the back of the Canneto village (Fig. 5). Its eruption was preceded by low-energy explosive phases of activity giving rise to lithic-rich pumiceous near-vent fallout eruption units (and a few PDCs) with a limited ~1 km^2 dispersal (fv_1 member; see tab. 3). The explosive activity was mostly driven by magmatic fragmentation mechanisms as indicated by the dominance of highly vesicular pumices. The Forgia Vecchia coulee is dated at 1.6 ka (Bigazzi and Bonadonna, 1973), whereas Cortese et al. (1986) suggest that the Forgia Vecchia activity was contemporaneous with that of M. Pilato cone (*AD 776*; see below) based on the interbedding of the corresponding pyroclastic products.

M. Pilato pumice cone (AD 776)

The M. Pilato pumice cone, developing on top of the Pomiciazzo coulee, was constructed by thick whitish pumiceous pyroclastic products (*i.e.,* Sciarra dell'Arena formation, sa_1 member; see Tab. 3). They are best exposed on the sub-vertical walls of the pumice quarries near Campo Bianca and Acquacalda (Fig. 5), and widely crop out in the north-eastern sector of Lipari, mantling the topography and overlying the lateral persistent red paleosol developed above the Vallone del Gabellotto pyroclastics (Fig. 13A). Based on the facies analysis of Dellino and La Volpe (1995), the M. Pilato pyroclastics are mostly composed of well-sorted, normal graded pumiceous lapilli-tuffs (*i.e.,* lithofacies 1) representing strombolian-type fallout eruption units related to a sustained eruption column. The tephra layers found on Vulcano, Stromboli and Panarea (Lucchi et al., 2008; Lucchi et al., 2011) more likely represent the distal component of these fallout processes. High-concentration (*i.e.,* poorly sorted, matrix-supported pumiceous lithofacies 2) and dilute PDC eruption units (*i.e.,* planar laminated lithofacies 3) are discontinuously interbedded within the pyroclastic succession in near-vent areas. Planar laminated tuffs with abundant accretionary lapilli (*i.e.,* lithofacies 4) become gradually prevalent towards the top of the succession (and with distance from the vent), accounting for prevalent wet-type dilute PDC eruption units during the latest stages of activity. Massive fine ash layers found in the more distant sectors of Lipari derive from the

993 fallout-dominated distal portion of these currents (Dellino and La Volpe, 1995). Based on the
994 coexistence of highly vesiculated pumices and poorly vesiculated, blocky and equant fine
995 ash particles, Dellino and La Volpe (1995) suggest that both end-member fragmentation
996 mechanisms were active during the M. Pilato activity, with initial prevailing magmatic
997 fragmentation followed by magma-water interaction. Some eruptive pulses were
998 characterized by coexisting magmatic and hydromagmatic fragmentation mechanisms, as a
999 consequence of inhomogeneous gas exholution distribution with magma-water interaction
1000 being effective only in the outer portions of the conduit (Dellino and La Volpe, 1995; Dellino
1001 et al., 2001). Obsidian-rich lava coulees (sa_2 member), presently limitedly exposed from
1002 below the homogeneous cover of more recent deposits, were erupted from the northern side
1003 of the M. Pilato cone.
1004 The M. Pilato pyroclastic products cover Greco-Roman ruins found in the archeological
1005 site of Contrada Diana near the village of Lipari, and are accordingly attributed to a Late
1006 Roman age (*i.e.,* 4^{th}-5^{th} century *AD*; Keller, 1970). Historical reports notice that St. Willibald
1007 observed explosive activity in the M. Pilato-Rocche Rosse area in 729 *AD* („Vitae Willibaldis";
1008 Bernabò-Brea and Krönig, 1978), although they might also indicate eruptive activity on the
1009 neighboring Vulcano Island (Keller J., personal communication). These relative chronological
1010 constraints should be reconsidered on the basis of latest, high-precision ^{14}C age of 776 *AD*
1011 provided by Keller (2002) for short-lived carbonized plant fragments contained within the
1012 basal portion of M. Pilato pyroclastics. Keller (2002) moreover suggests that a report of monk
1013 Gregorius, travelling through Lipari in 787 *AD*, may be interpreted as the description of still
1014 ongoing explosive eruptions of M. Pilato.
1015
1016 *Lami eruptive vent*
1017 Obsidian-rich, coarse-grained pumiceous pyroclastic products with a few bread-crust
1018 bombs limitedly crop out near Lami village (*i.e.,* Lami formation), at the foot of the northern
1019 flanks of M. Pilato cone. These products are morphologically independent, being separated
1020 from the M. Pilato flanks by a sharp slope break. Based on this feature, together with the
1021 average coarser grain size and different componentry with respect to M. Pilato products (see
1022 above), we suggest that the Lami deposits account for vulcanian-type, near-vent fallout (and
1023 minor PDC) eruption units originated from a small, eccentric eruptive vent. The occurrence of
1024 a secondary eruptive vent in this area is in agreement with Pichler (1976), Cortese et al.
1025 (1986) and Dellino (1991). Welded and flattened pumiceous deposits are reported at top of
1026 the unit (*i.e.,* pipernoid pumices; Pichler, 1976) reflecting the emplacement of fallout eruption
1027 units during a latest phase of hawaiian-type fountaining.
1028 Considering that the Lami products are not covered by the widespread M. Pilato
1029 pyroclastics, we believe that the Lami eruptive vent is more likely younger than the M. Pilato

activity. This is in agreement with Dellino (1991) who point out the lithological and textural similarity between the Lami deposits and the Fossa delle Rocche Rosse pyroclastics (see below). Differently, Cortese et al. (1986) suggest that the Lami activity was contemporaneous with that of M. Pilato cone based on the interbedding between the corresponding products.

Eruption 9.3: Rocche Rosse coulee (AD 1230)

After a relatively short period of quiescence marked by a localized erosional unconformity in inner crater areas (Dellino and La Volpe, 1995), volcanic activity of M. Pilato renewed from an eruptive vent located within the older crater area at Fossa delle Rocche Rosse (fig. 5). Small-scale explosive phases of activity gave rise to obsidian lithic-rich pumiceous fallout eruption units and minor PDC deposits (*i.e.,* Fossa delle Rocche Rosse formation, frr_1 member; see Tab. 3). Hydrotermalized dense lava lithics are more abundant in the basal portion of the succession reflecting the crater opening phase. Explosive activity was driven by magmatic volatile-derived fragmentation mechanisms, as shown by the prevalence of highly vesiculated pumices (Dellino and La Volpe, 1995). These pyroclastic products built up a 30m high and 400m large crater rim open to the north-east that is coalescent with the older M. Pilato crater (Fig. 5). The Fossa delle Rocche Rosse tongue-like, obsidian-rich coulee (frr_2 member) overflowed the north-eastern rim of this crater and flowed down along the M. Pilato slopes till reaching the sea in the NEmost coastal sector between Porticello and Acquacalda (Fig. 13B), for a total length of 1.5 km (up to 4 km with its submarine continuation). This is a spectacular, worldwide known example of rhyolite lava flow („Rocche Rosse obsidian coulée"; Cas and Wright, 1987, and references therein). Its surface (best exposed along the coast road from Porticello to Acquacalda) is blocky and rough, with concentric curved cracks, whereas the internal structure (exposed along the northern coastal cliff of Lipari) is typically characterized by ramp structures that curve down to sub-horizontal flow foliation, consisting of dense interbanding of obsidian (frequently spherulitic or partly perlitised) and lithic rhyolite layers and frequently folded. The high-K rhyolite Rocche Rosse coulee is substantially aphyric to subaphyric (with a few mafic enclaves) which accounts for water-undersaturated conditions of magma ascent (Davì et al., 2009). A very high temperature of emission is suggested by its anomalously low viscosity and increased mobility (Cas and Wright, 1987, and references therein). A mafic input is indicated to have been a major trigger for the eruption of Rocche Rosse coulee (Davì et al., 2009), as already illustrated for older rhyolite domes on Lipari and for the historical eruptions on Vulcano (Gioncada et al., 2003; 2005; Peccerillo et al., 2006).

The Rocche Rosse coulee has been dated at 1.4 ka (Keller, 1970; Bigazzi and Bonadonna, 1973; see Tab. 3), which is approximately consistent with the age of 524-562 *AD* indicated by various legends and historical reports (see Pichler, 1980). Instead, Tanguy

et al. (2003) obtained a younger archeomagnetic age of *AD* 1230, which is more consistent with our stratigraphic reconstruction showing that effusion of the Rocche Rosse coulee followed a period of quiescence after the M. Pilato main activity (*AD 776*, see above in the text). Whatever the case, the Rocche Rosse coulee accounts for the most recent phases of activity on Lipari.

Summary of eruptive history

The eruptive history of Lipari is described by nine successive Eruptive Epochs (and related Eruptions) developing between more than 271 ka and historical times (Figs. 14-15). The location of active eruptive vent through time is directly controlled by regional tectonic trends (N-S, NNW-SSE), mostly associated with the major NNW-SSE-oriented Tindari-Letojanni fault system (and minor E-W trend), together with recurrent volcano-tectonic collapse events (Fig. 15).

The western sector of Lipari is constructed by a series of scattered eruptive vents both of central-type (from north to south, M. Chirica, Chiesa Vecchia, Pietrovito, M. Mazzacaruso and Timpone Carrubbo volcanoes) and fissural-type (Fuori del Pertuso and Timpone Ospedale spatter cones), characterized by hydromagmatic to strombolian volcanic activity occurred in a shallow marine to subaerial environments. They are active during the 271-150 ka time-interval and mostly distributed along NNW-SSE to N-S lineaments (*i.e.,* Eruptive Epochs 1-2; Fig. 15a, b, c).

The Monterosa twin strombolian scoria cones developed in the eastern sector of Lipari along the minor E-W tectonic trend during early MIS 5 (~119 ka; Eruptive Epoch 4; Fig. 15d), almost contemporaneously with the early stages of activity of the M. S.Angelo volcano. This is a large, long-lived, central-type stratocone that was constructed between ~120 and 80 ka (Eruptive Epochs 4-5-6; Fig. 15d, e, f) through the emplacement of great volumes of (mostly) hydromagmatic pyroclastics and thick lava flows (*i.e.,* cordierite-bearing lavas), displaying a significant change of eruption types and progressive differentiation of involved magmas (see below in the text). During the latest phases of activity of M. S.Angelo, the M. Chirica stratocone was subordinately active with the effusion of thick lava flows from the W side of its summit crater rim (92-81 ka; Eruptive Epoch 6; Fig. 15f).

Renewal of volcanism on Lipari followed a prolonged period of dormancy and was characterized by the onset of rhyolite magmatism. The southern dome field of Lipari was constructed between ~42 and 22-21 ka through three successive Eruptions leading to the emplacement of endogenous lava domes and pumiceous pyroclastics (Eruptive Epochs 7-8; Fig. 15g, h). Volcanic activity under control of the main NNW-SSE tectonic trend followed a recurrent eruptive scenario characterized by strombolian to subplinian explosive phases of activity followed by dome effusion, with late explosive phases leading in places to partial

destruction of the dome surface. The M. Guardia pyroclastics, in particular, were emitted during a high-energy, subplinian eruption which is presently recorded on most of the Aeolian archipelago.

The activity of Lipari alternated with recurrent explosive activity from external source areas, which is recorded on Lipari during the past 70 ka by the emplacement in distinct stratigraphic positions of the Brown Tuff units (70-7 ka) from Vulcano Island, Grey Porri Tuffs (67-70 ka) and Lower Pollara Tuffs (~23 ka) from Salina Island and reknown Ischia Tephra (56 ka) from the Campanian Province (Fig. 14).

A series of N-S-aligned lava domes cropping out along the whole eastern side of Lipari Island (Fig. 15h) were emplaced during latest phases of Eruptive Epoch 8 (dated at between 16 and 8 ka), and signalled the progressive shifting to the north of active eruptive vents. The north-eastern sector of Lipari was in fact constructed between 11-8 ka and historical times through the emplacement of pumiceous pyroclastics and viscous lava coulees (Eruptive Epoch 9; Fig. 15i). Volcanic activity was controlled by the main NNW-SSE strike-slip system (and associated N-S to NE-SW extensional lineaments) and displayed three successive Eruptions characterized by the same eruptive pattern with initial strombolian (to sub-plinian)-type explosions followed by late coulee effusion. Based on historical reports, radiometric and archeomagnetic dating, the latest phases of activity on Lipari are those leading to the construction of M. Pilato pumice cone (*AD* 776) and effusion of the Rocche Rosse lava coulee (*AD* 1230).

Classification, petrography and mineral chemistry

Volcanic products of Lipari Island cover a wide compositional range from CA and high-K CA basaltic-andesite to rhyolite on the K_2O vs. SiO_2 classification diagram (Peccerillo and Taylor, 1976) (Fig. 16). The lowest exposed rocks with an age of 271 to 81 ka range from basaltic-andesites to andesites, showing a steep increase in K_2O from mafic to intermediate products. Starting from ~42 ka, after a 40 ka-long period of volcanic quiescence, rhyolitic lavas and pyroclastic products were erupted. There is a compositional gap at dacitic compositions, with the few samples plotting in the dacitic field showing petrographic evidences of magma mixing (i.e. banded pumices and magmatic enclaves) or containing considerable amounts of crustal xenoliths.

CA and high-K CA basaltic andesites dominate through the first four Eruptive Epochs (271-119 ka; Paleo-Lipari informal unit, Pianogrande and Scoglio Le Torricelle synthems). CA and high-K CA andesitic rocks are subordinate among the oldest rocks exposed on Lipari Island and are related to Eruptive Epochs 2 and 4 only, whereas they become predominant in Eruptive Epochs 5 and 6 (~105-81 ka; Bruca and Fontanelle synthems). High-K CA dacitic lavas (with less than 65% SiO_2) occur uniquely in Eruptive Epoch 4 (Timpone del Corvo

formation, M. S.Angelo lithosome) and 5 (Pulera formation, M. S.Angelo lithosome). Eruptive Epochs 7, 8 and 9 are almost entirely characterized by the emission of rhyolitic products (*i.e.,* Scogliera Sotto il Monte, Valle Muria and Vallone Fiume Bianco synthems). Among these Epochs, only two samples (*i.e.,* mafic enclaves-rich lavas of Falcone formation and banded pumices attributed to M. Guardia formation) plot in the dacitic field.

CA and high-K CA basaltic-andesitic lavas and scoriae are variably porphyritic (20-50%) with phenocrysts of dominant plagioclase and clinopyroxene, sometimes forming glomeroporphyric aggregates, and minor orthopyroxene and olivine.

Groundmass varies from hyalopilitic/pilotaxitic to micro- or cripto-crystalline and contains the same phases as the phenocrysts, plus Ti-magnetite. Plagioclase phenocrysts of both lava and scoriae (An_{91-63}) range from 1 to 5 mm in size, are euhedral and sometimes show sieved-textured zones. Clinopyroxene phenocrysts are generally euhedral and zoned, from diopsidic cores to augitic rims (Bargossi et al., 1989). Bronzitic to hypersthenic orthopyroxene is mostly overgrown by clinopyroxene reaction rims. Olivine (Fo_{91-64}) occurs as small euhedral to subeuhedral phenocrysts generally transformed to iddingsite. Groundmass plagioclase displays An_{68-48} composition, and clinopyroxene is pigeonitic. The glass is acidic in composition (SiO_2 = 71-72%; Bargossi et al., 1989).

CA and high-K CA andesitic lavas and juvenile pyroclasts show variably porphyritic to porphyritic seriate textures (PI ~ 35 to 60 in the lavas), with phenocrysts of plagioclase, clinopyroxene, orthopyroxene and Fe-Ti oxides, set in a hyalopilitic to pilotaxitic groundmass containing plagioclase needles, Fe-Ti oxides, and glass. Plagioclase (An_{76-56}) is the most abundant phase; clinopyroxene frequently occurs as subhedral and reversely zoned phenocrysts. Compositions are mostly augitic and more homogeneous than in basaltic-andesitic rocks. In andesitic products, orthopyroxene occurs in the same proportion as the clinopyroxene. Subhedral and partially reabsorbed, pale to dark green, Mg-hastingsitic amphibole phenocrysts only occur in high-K CA andesitic lavas and pyroclastic rocks of the Belvedere formation (Timpone Carrubbo lithosome, Eruptive Epoch 1). Ti-magnetite and apatite are the main accessory phases. Olivine is very rare. In the groundmass, plagioclase composition is An_{43} (Bargossi et al., 1989).

High-K CA dacitic lavas of Timpone del Corvo formation (Eruptive Epoch 4) have porphyritic texture, with prevalent plagioclase phenocrysts and subordinate clinopyroxene, orthopyroxene and ilmenite. Groundmass is hyalopilitic to pilotaxitic or micro- to cripto-crystalline with plagioclase and Fe-Ti oxides. The cordierite-bearing lavas of Pulera formation (Eruptive Epoch 5) have seriate to highly porphyritic texture (up to 50%) and contain subhedral to anhedral zoned plagioclase, skeletal and stumpy orthopyroxene, clinopyroxene, cordierite, garnet, K-feldspar and minor ilmenite, apatite, andalusite, spinel and sillimanite. They are also very rich in metapelitic, gneissic and gabbroic xenoliths (up to 20-30%).

Plagioclase phenocrysts have calcic nuclei (An_{77-70}) and show abrupt decrease of An towards the rims (An_{50-55}). Subhedral to anhedral diopsidic clinopyroxene is always overgrown by enstatitic orthopyroxene and glass rims. Cordierite occurs as euhedral to subhedral grains (generally < 4 mm, locally up to 10 mm or more) containing abundant silicate melt and mineral inclusions. Because of these features, cordierite grains have been interpreted as phenocrysts (Di Martino, 2010). Garnet occurs as variably resorbed grains, with variable size. Larger crystals are about 1 mm in diameter, are chemically zoned and contain melt and mineral inclusions. Smaller garnets are unzoned and do not contain melt inclusions, thus suggesting a xenocrystic origin (Di Martino, 2010). Sillimanite is anhedral and surrounded by coronitic association of spinel and cordierite. Andalusite forms large subhedral crystals (1-2 mm) with sieve-textured margin and plagioclase and spinel inclusions. The groundmass is hypocrystalline and contain plagioclase, cordierite, orthopyroxene, minor K-feldspar, biotite and rhyolitic glass.

Rhyolitic lavas and pyroclastic rocks show variable petrographic features. Most volcanic products of Eruptive Epochs 7 and 8 (P.ta del Perciato, Falcone and M. Giardina formations) are scarcely porphyritic with less than 5 vol% phenocrysts. Kfeldspar is the main phase, followed by plagioclase (An_{25-22}) and hornblende. Biotite, Ti-magnetite, zircon and apatite are the main accessories (Gioncada et al., 2005). Fa3 member of Falcone formation (Eruptive Epoch 7) is very rich in magmatic enclaves and xenocrysts of plagioclase and clinopyroxene. Pyroclastic rocks of M. Guardia formation (Eruptive Epoch 8) are characterized by white pumices showing the same paragenesis described above for the rhyolitic rocks, and grey pumices, latitic in composition, containing clinopyroxene, plagioclase (An_{76}), minor olivine, Ti-magnetite and apatite (De Rosa et al., 2003). White rhyolitic and dark latite pumices occur both as separated clasts and banded samples, indicating intermingling between felsic and intermediate magmas. Lava domes of P. S.Giuseppe formation (Eruptive Epoch 8) are aphyric, with some feldspar and Fe-Ti oxides microlites in the groundmass. Latitic enclaves are diffusely present. Pyroclastic rocks and lavas ranging in age between 16 and 8 ka (Colla, Castello and Capo Rosso formations; Eruptive Epoch 8) are aphyric to subaphyric, with eutaxitic texture. The same is reported for both lava coulees and pumiceous pyroclastic products of Eruptive Epoch 9 (V.ne del Gabellotto, Pomiciazzo, Pirrera, Serra dell'Arena and Fossa delle Rocche Rosse formations).

Petrography of xenoliths

Magmatic and metamorphic xenoliths are documented in volcanic rocks from Lipari. Metamorphic xenoliths (granulites, metapelites and quarzites) are dispersed in lavas and pyroclastic rocks from Lipari. Their abundance generally increases from basaltic andesites to andesites and dacites. Quartz-rich xenoliths are white-colored, angular shaped and

millimetric to centimetric in size, reaching maximum size of 20 cm in the basaltic-andesitic lavas of the Vallone Malopasso formation (Eruptive Epoch 2). They are almost completely made up of quartz grains (0.1-5 mm), rare feldspars and pyroxenes. Texture is mostly inequigranular with typical 120° triple junctions. No reaction rims at the boundary with host lava is reported (Di Martino, 2010). Metapelitic xenoliths containing cordierite, garnet, andalusite, sillimanite, biotite and oxides have been long observed in the renowned cordierite-bearing lavas (Bergeat, 1910; Pichler, 1980; Barker, 1987) of Pulera formation (Eruptive Epoch 5). The same xenoliths have been also recognized by Barker (1987) in the lavas of Le Puntazze formation (Eruptive Epoch 2). Metapelitic inclusions generally show zoning with garnet, andalusite and sillimanite grains forming in the internal part, surrounded by cordierite and hercynite.

Igneous xenoliths include both granular rocks and blobs of magmas intermingled with host lavas. Granular xenoliths consist of cumulus-textured assemblages of clinopyroxene, orthopyroxene, plagioclase and magnetite. Xenoliths entirely formed by plagioclase are rarely present.

Among rhyolitic products, a large quantity of magmatic enclaves and xenocrysts is documented for P. S.Giuseppe formation (Eruptive Epoch 8) and fa_3 member of Falcone formation (Eruptive Epoch 7). These enclaves have latitic composition and highly porphyritic texture (16-28 vol.%) with phenocrysts of plagioclase (An_{78-58}), augitic clinopyroxene and olivine (Fo_{63-68}; Gioncada et al., 2005). These phases sometimes exhibit disequilibrium texture with the groundmass. Magmatic enclaves have been also found by Davì et al. (2009) in the Rocche Rosse lava coulee (Fossa delle Rocche Rosse formation; Eruptive Epoch 9). These enclaves have latitic to trachytic composition and contain diopsidic to augitic clinopyroxene, plagioclase (An_{30-18}), sanidine, olivine (Fo_{70-90}), biotite and magnetite.

Petrology and geochemistry

This section reports on original major and trace element data, covering the whole stratigraphic succession reconstructed for Lipari. These data are combined with isotopic compositions of selected samples from the literature (Esperanca et al., 1992; Gioncada et al., 2003).

Major and trace elements

Selected major and trace element data representative of the Lipari's stratigraphic succession are reported in Table 4. A more complete set of analyses is given in the attached CD rom.

Variation diagrams of major and trace elements against SiO_2 are shown in Figs. 17 and 18. MgO, Fe_2O_3, CaO and TiO_2 decrease with increasing SiO_2, whereas K_2O increases. Na_2O, Al_2O_3 and P_2O_5 are almost constant in basaltic-andesitic to dacitic rocks, but change their behaviour increasing (Na_2O) or decreasing (Al_2O_3 and P_2O_5) in rhyolitic rocks (Fig. 17A-H).

Ferromagnesian trace elements (Cr, Ni, Co, Sc, V) generally decrease from basaltic andesites to rhyolites but show remarkable internal variations in each group of rocks. Some of them (e.g. Cr and Ni; Fig. 18A,B) define steep trends in basaltic andesitic rocks, which are typical of fractional crystallization processes involving fractionation of olivine, clinopyroxene and Fe-Ti oxide. Cr defines a nearly curvilinear trend from basaltic andesites to rhyolites (Fig. 18A), whereas Ni is much more scattered (Fig. 18B). Large Ion Lithophyle Elements (LILE: Rb, Ba, Th, U, LREE, etc.) and High Field Strength Elements (HFSE: Ta, Nb, Zr, Hf) generally define linear positive trends from basaltic andesitic to rhyolitic rocks on variation diagrams (Fig. 18E). Ba and Sr increase rapidly from basaltic andesites to dacites, then decrease towards the rhyolitic field (Fig. 18C,D). Among HFSE, Zr initially increases with silica, and remains almost constant through the dacitic and rhyolitic fields (Fig. 18F). LREE (e.g. La and Ce) show significant scattering, especially in the rhyolitic compositions. Notably, rhyolitic rocks, which have very similar major elements compositions, differ in some key trace element abundances (such as La and Th). In particular, La (Fig. 18G) and Th (Fig. 18H) content show a tendency to increase with time from Valle Muria and Scogliera Sotto il Monte synthems (Eruptive Epoch 7 and 8) to Vallone Fiume Bianco Synthem (Eruptive Epoch 9).

Inter-elements plots of incompatible trace elements with different degrees of incompatibility (e.g. Zr vs. Rb; Fig. 19A) show distinct linear positive trends for i) basaltic-andesitic to dacitic and for ii) rhyolitic products. These two groups of rocks are also characterized by different ratios of incompatible elements such as Zr/Nb (Fig. 19B), Zr/Hf, Th/Zr, U/La etc. REE fractionation is moderate but increases from basaltic andesites to dacites. Rhyolitic rocks define U-shaped patterns, with Eu negative anomaly. REE abundances generally increase from basaltic andesites to rhyolites (Fig. 20A,B). Incompatible elements normalized to primordial mantle for basaltic andesitic rocks show troughs at Nb and Ti, which are typical of volcanic arc-related magmas (Fig. 21).

Sr-Nd-Pb isotopes

Sr, Nd and Pb isotopic data from Esperanca et al. (1992) and Gioncada et al. (2003) are listed in Table 5, by conforming to the subdivision in different Eruptive Epochs proposed in our stratigraphic reconstruction. Whole rock $^{87}Sr/^{86}Sr$ (= 0.704275 to 0.706710) and $^{143}Nd/^{144}Nd$ (= 0.512418 to 0.512809) cover almost the whole range of isotopic compositions obtained for the other islands in the arc, except for Stromboli and Alicudi (Fig. 22A).

Basaltic-andesitic to dacitic rocks of Eruptive Epochs 1 to 6, display the larger isotopic range (Fig. 22B), in accordance with the extreme variability observed in the trace element variation diagrams. The cordierite-bearing lavas of Pulera formation (Bruca Synthem; Eruptive Epoch 5) and the andesitic lavas of Le Puntazze formation (Piano Grande Synthem; Eruptive Epoch 2), display the highest $^{87}Sr/^{86}Sr$ ratios and the lowest $^{143}Nd/^{144}Nd$ ratios (Fig. 22B). Sr and Nd isotopic compositions of these rocks are respectively lower and higher than the metapelitic rocks of the Serre Calabrian basement, but notably overlap the field of mafic basement lithologies (metagabbroic rocks) (Fig. 22A). Among rhyolitic rocks (Eruptive Epochs 7-9) two groups can be easily distinguished by their distinct $^{87}Sr/^{86}Sr$ values. In contrast, the two groups show very similar $^{143}Nd/^{144}Nd$ ratios (Fig. 22B).

Except for one sample, referred to the first activity of Mt. S. Angelo (Eruptive Epoch 4), and a couple of samples of cordierite-bearing lavas (Eruptive Epoch 5), Lipari rocks show small variations in $^{206}Pb/^{204}Pb$, $^{207}Pb/^{204}Pb$ and $^{208}Pb/^{204}Pb$ ratios, and fall within the fields defined by the other islands (Fig. 23A, B).

Sr, Nd and Pb isotope data, recently obtained by Forni F. (unpublished data), indicate a wider compositional range for Lipari volcanics. According to these preliminary results, Sr and Nd isotope ratios partially overlap the composition of the Calabrian Basement rocks.

Petrogenesis

Volcanic products from Lipari Island show a bimodal distribution with CA and high-K CA basaltic-andesites to high-K CA andesites, dominating from less than 271 to 81 ka, and the late appearance of rhyolitic rocks, occurring between ~42 ka and historical times (*AD* 1230). Rhyolitic magmatism took place at ~42 ka after a 40 ka-long period of quiescence from eruptive vents located in the southern sector of the island (*i.e.,* closer to Vulcano where also volcanism became dominantly rhyolitic), and successively migrated toward the north-eastern sector of Lipari.

There are several topics related to the magma genesis and evolution at Lipari, which have been amply discussed but are still poorly understood. They are the following: i) the reasons of the steep increase in K_2O contents from the early mafic CA products to younger intermediate and felsic rocks; ii) the role of continental crust in the magma evolution and, in particular, if magma contamination may have played a role in the steep increase in potassium observed at Lipari; iii) the origin of sialic rocks and the reason of their eruption during the latest stages of construction of Lipari Island; iv) the genetic relationships between Lipari volcanism and the analogous activity taking place at Vulcano, especially during the last 40 ka.

The steep increase in K_2O with time and the transition from mafic to intermediate products might indicate either the occurrence of complex and combined evolution processes (*i.e.,*

fractional crystallization, magma mixing and crustal assimilation) or the arrival of new magmas from a heterogeneous mantle source. The variation of potassium and enrichments in incompatible elements are common in the Aeolian archipelago and are generally attributed to the generation of distinct types of primary melts in a heterogeneous mantle (De Astis et al., 2000; Ellam et al., 1988; Francalanci et al. 1993). However, the same effects can be obtained by combined processes of fractional crystallisation, mixing and eruptions, starting from a single type of magmas, a process successfully modelled for Stromboli by Francalanci et al. (1989). Crisci et al. (1991) suggested that the high gradient of K_2O enrichment through time at Lipari reflects the occurrence of two mantle components with distinct enrichments in potassium inside the volcano plumbing system. One has a broadly tholeiitic composition, whereas the other has a potassic alkaline affinity akin to magma compositions encountered in central Italy. In addition to these mantle components, crustal components are also suggested to an important role essentially during the intermediate to late stages of activity of the Lipari volcanic system (Crisci et al., 1991). In accordance with Crisci et al. (1991), Esperanca et al. (1992) have proposed that the wide range of Sr, Nd and Pb isotopic compositions of Lipari volcanic rocks is the result of a complex interaction between magmas deriving from multiple sources. They also interpreted the rapid evolution of Lipari isotopic compositions towards crustal values and the increase of K_2O over Na_2O as the combined effect of crustal contamination and mixing between mantle-derived magmas and anatectic melts.

The interaction of mafic magmas with the continental crust represents a basic process in the magmatic evolution of most islands in the Aeolian archipelago, and it is particularly outlined at Lipari by the eruption of cordierite-bearing lavas (Eruptive Epoch 5, ~105 ka). These high-K CA dacitic lavas are characterized by the coexistence of typical igneous minerals (plagioclase, clinopyroxene and ortopyroxene) along with cordierite and garnet phenocrysts and a large amount of metapelitic, gneissic and gabbroic xenoliths (Barker, 1987). Esperanca et al. (1992) noticed that the contribution of the crust in the formation of cordierite-bearing lavas, which is evident from petrography, is also marked by the highest $^{86}Sr/^{87}Sr$ (= 0.706710) and lowest $^{143}Nd/^{144}Nd$ (= 0.512809) isotopic ratios measured for Lipari rocks. However, a significant contribution of the crust is not signaled by the Pb isotope ratios that plot very far from the field described by typical crustal values. The Authors suggested that isotopic compositions of the crust underneath the Aeolian Islands might have suffered significant changes (*i.e.,* volcanism preceding the formation of the arc) not experienced by the crustal section cropping out in southern Calabria. Based on detailed mineral chemistry, volcanological data and fluid inclusions investigation, Di Martino (2010) has recently interpreted the cordierite-bearing lavas as a product of mixing between a crustal anatectic

melt and mantle-derived CA magmas with the same compositional features of volcanic products characterizing the older magmatism of Lipari.

Rhyolitic rocks are abundant at Lipari and on the nearby island of Vulcano, and show a clear tendency to decrease away from the central sector of the archipelago. The origin of these magmas has been attributed by Crisci et al. (1991) to the increasing addition of the crustal component into the magmatic system. On the contrary, Esperanca et al. (1992) noticed that the geochemical and isotopic compositions of rhyolitic rocks are different from those of the Calabrian crust, arguing in favour of a mantle input in the petrogenesis of sialic melts. Detailed isotopic studies carried out by Gioncada et al. (2003) allow distinction between two different groups of rhyolitic rocks, one with high $^{86}Sr/^{87}Sr$ isotopic ratio and the other with low $^{86}Sr/^{87}Sr$ isotopic ratio. The Authors indicate assimilation and fractional crystallization (AFC; DePaolo, 1981) as the main genetic process for the high $^{86}Sr/^{87}Sr$ rhyolitic rocks. Instead, magma mixing between a Sr radiogenic rhyolitic end-member and a new fresh latitic magma is suggested to be responsible for the low $^{86}Sr/^{87}Sr$ rhyolites, as outlined by the presence of latitic enclaves and mingling textures in these rocks. The differentiation of rhyolitic melts starts from andesitic to latitic compositions (similar to those of enclaves) and involves fractionation of clinopyroxene, olivine, Fe-Ti oxides, plagioclase and K-feldspar. Based on petrography and microanalysis of the mafic enclaves, Gioncada et al. (2005) found that the latitic magmas are themselves the product of mixing events, which occurred shortly before the mixing with the rhyolitic end-members.

As for the relationships with the nearby volcanoes, it is noteworthy that the islands of Lipari, Vulcano and Salina are the subaerial portions of a wide volcanic structure aligned along the NNW-SEE Tindari Letojanni fault. Based on petrological and geochemical evidence, Gioncada et al. (2005) have suggested that Lipari and Vulcano are characterized by common plumbing system and magmatic evolution at least for the recent activity starting from 42 ka BP, which led to the emplacement of large volumes of rhyolitic rocks with similar geochemical characteristics on both islands. Ventura et al. (1999) and Gioncada et al. (2003) argued that the rhyolitic volcanic activity is linked to the activation of the Tindari-Letojanni strike-slip fault system and correlated N-S extensional faults, as indicated by the alignment of active vents on the two islands. This particular tectonic regime could have favoured the setting up of magmatic reservoirs in the continental crust, wherein mafic magmas could have evolved through AFC processes, thus generating different kinds of rhyolitic melts through time.

Overall, the petrographic and geochemical data presented by different authors indicate that the magmatic evolution of Lipari derives from a complex interplay between mantle-derived magmas and crustally-derived melts. The mantle-derived magmas mainly evolve through AFC and mixing processes, with the contribution of these differentiation processes

varying through time. However, there is still uncertainty on the roles of different crustal and mantle end-members and on the very nature of evolution processes, even in the light of the polybaric structure of the plumping system (see below in the text). As such, the complex magmatic evolution of Lipari, and the genetic relationships with the nearby Vulcano and Salina islands, hint at further investigations.

Origin of primary melts and composition of mantle sources

The complete absence of primitive rocks in the Lipari suite prevents from getting direct information about the nature of parental magmas and their mantle sources. The CA basaltic-andesitic rocks of Eruptive Epochs 1 and 2 represent in fact the most mafic products cropping out on the island. Both petrography and geochemistry of these rocks (*i.e.,* presence of metamorphic xenoliths, low Ni and Cr content) suggest that they might have suffered a pre-emplacement evolution, probably crystallization of mafic phases at depth and some kind of interaction with the crust. Moreover, these older rocks show wide variations in trace element (in particular HFSE) and isotopic ratios, also in the frame of single eruptions. This might be connected to the presence of distinct magma batches undergoing different evolution paths during their ascent to the surface. Differentiation processes at shallow depths, in fact, mainly affect HFSE and have little influence on LILE content (i.e. Ellam et al., 1988), whereas variable amount of crustal assimilation might be responsible for isotopic variations. The hypothesis of distinct magma batches would be also consistent with the field observations that clearly indicate the provenance of these products from different monogenic and polygenic scattered volcanic centres during the early stages of activity of Lipari.

Furtherly, the basaltic-andesitic rocks also show enrichment in LILE over HFSE, which is typical of subduction-related magmatism (Fig. 21). Fluids coming from the slab are able to carry considerable amounts of large ion lithophile elements and transfer them to the mantle wedge. Following Francalanci et al. (1993, 2007), fluids and silicate melts coming from the slab variously interact with the mantle wedge in the different sectors of the archipelago. In the central Aeolian sector, in particular, the mantle wedge is metasomatized mostly by aqueous fluids coming from the slab rather than by sediment melts. The nature of the pre-metasomatism mantle is supposed to be a MORB-like source, which has been subsequently metasomatized by LILE and LREE-rich aqueous fluids. This scenario is consistent with the relative low HFSE and HREE and the high LILE and LREE contents outlined for the Lipari basaltic andesites (Figs. 20, 21). The Pb isotopic compositions of Lipari rocks are shifted towards more radiogenic compositions with respect to those the Calabrian Basement field (Fig. 23A, B), which indicates the occurrence at Lipari of a high $^{206}Pb/^{204}Pb$ source. This high $^{206}Pb/^{204}Pb$ component (HIMU-like) has been suggested to derive from dehydration of the ancient subducting oceanic crust, which is characterized by high U/Pb and produced during

hydrothermal and subduction-related processes (Francalanci et al., 2007). However, an OIB-type mantle component similar to that of Mt. Etna (*i.e.,* FOZO) is another plausible explanation for the more radiogenic isotopic compositions of Lipari (Ellam et al., 1989).

Magmatic feeding system

Combined melt and fluid inclusions and petrochemical studies on Lipari rocks have provided information on the evolution of the plumbing system of Lipari volcano through time.

The early studies (De Rosa et al., 2003a; Gioncada et al., 2005) concentrated on the younger rhyolitic (and latitic) magmas of Eruptive Epochs 7-9 (<42 ka). Gioncada et al. (2005) have hypothesized the presence of a composite, vertically-distributed plumbing system with small-volume reservoirs of silicic (and mafic) magmas in the crust below southern Lipari, interacting (and mixing) during the eruptions. This is similar to what observed at Vulcano by Frezzotti et al. (2004). For the M. Guardia rhyolitic pyroclastic products (Eruptive Epoch 8, Eruption 8.1, 22-21 ka), in particular, De Rosa et al., (2003a) have proposed the occurrence of a mid-crustal reservoir of rhyolitic magmas located at depths generically greater than 6 km, on the basis of volatile contents (*i.e.,* H_2O and Cl) dissolved in rhyolitic melt inclusions.

A model for the plumbing system of mafic to intermediate magmas erupted during Eruptive Epochs 1-6 (from 270 to 81 ka) has been recently proposed by Di Martino et al. (2010) through the systematic studies of fluid inclusions (Fig. 24). This model is based on the methodological approach of Frezzotti et al. (2003) and Frezzotti and Peccerillo (2004), according to which the density of CO_2 fluid inclusions found in quartz-xenoliths within Lipari lavas provides an estimation of the geo-barometric conditions of fluid entrapment, as a consequence of magma rest in the crust.

Fluid inclusion density data for CA basaltic-andesite to andesite magmas erupted from the central-type volcano of Monte Mazzacaruso (Eruptive Epoch 2, ~270 ka) indicate the occurrence of a deep magma storage level located in the lower crust close to the Moho, at depths of 18-22 km (Fig. 24). A second shallower magma ponding level is identified at depths of 5-3 km, which correspond to the geophysical boundary between the intrusive complex and the underlying metamorphic basement (Ventura et al., 1999). An important change of the plumbing system during Eruptive Epochs 5-6 (between 105 and 81 ka) is given by the migration of the deep accumulation level toward shallower mid-crustal depths of 12-17 km (Fig. 24), whereas the depths of the shallower magma reservoirs did not vary (steady state behaviour at shallow depths). This is outlined by fluid inclusion data for the cordierite-bearing lavas of M. S. Angelo central-type volcano (Eruptive Epoch 5, Eruption 5.2) and the lava flows of M. Chirica-Costa D'agosto (Eruptive Epoch 6).

1471 This model for the magma plumbing system of central-type volcanoes at Lipari proposed
1472 by Di Martino et al. (2010) is in agreement with those obtained with the same methodology
1473 for other Aeolian volcanoes, *e.g.* Vulcano (Zanon et al., 2003; Peccerillo et al., 2006) and
1474 Alicudi (Frezzotti et al., 2003). Overall, models give description of a polybaric plumbing
1475 system with mafic magma ascent and ponding at lower and upper crustal levels, which
1476 seems to represent a long-term trait of regional significance in the whole Aeolian
1477 archipelago. Mafic magmas are suggested to have accumulated in lower-crust deep magma
1478 reservoirs located at minimum depths of 18 km, which possibly migrate towards the middle-
1479 crust in the course of time. These deep lower-mid crustal magma reservoirs were
1480 continuously supplied by mantle-derived mafic melts, and played a primary role in feeding
1481 magmas and triggering eruptions. During magma ascent, short (*i.e.,* day-to-week time)
1482 magma rests occurred at 3-5 km depth in shallow magma reservoirs.
1483 A different magma ascent path at Lipari has been reconstructed for the CA basaltic-
1484 andesite to andesite lavas erupted from fissural-type volcanoes during Eruptive Epochs 2
1485 and 4 (Di Martino et al., 2010). These are the N-S aligned Timpone Ospedale spatter cones
1486 and the Monte Chirica older products (Eruptive Epoch 2, 270-250 ka), and the E-W aligned
1487 Monterosa twin scoria cones (Eruptive Epoch 4, 116 ka). These volcanoes noteworthy reflect
1488 the activity of eruptive fissures located along N-S and E-W extensional structures, with the
1489 former being the expression of the Tindari-Letojanni NNW-SSE fault system, which is
1490 supposed to have influenced the magmatic and eruptive history of Lipari and the whole
1491 central sector of the Aeolian archipelago (De Astis et al., 2003; Ventura, 2011). Fluid
1492 inclusion data for these fissural volcanoes apparently indicate the occurrence of a single
1493 accumulation zone located in the middle crust at depths of ~14 km, with no evidence of a
1494 shallow magma reservoir (at depths of 3-5 km). This is explained by assuming that the
1495 regional tectonics has possibly favoured dyke propagation from lower-crustal accumulation
1496 zones, allowing “rapid” magma ascent along preferred structural pathways and resulting in
1497 intense strombolian-hawaiian explosive phases of activity.
1498 It is noteworthy that partial melting processes of the lower crust of Lipari have been
1499 invoked by Di Martino et al. (2010) to explain the origin of the cordierite-bearing lavas during
1500 Eruptive Epoch 5 (Eruption 5.2, 105 ka). These are in fact interpreted to be hybrid lavas
1501 containing restitic cordierite and garnet crystals, resulting from the mixing of mafic magmas
1502 and felsic (anatectic) melts. The occurrence of crustal anatexis processes bears a substantial
1503 influence on the rheology of the crust, with the presence of felsic (anatectic) melts at mid-
1504 crustal levels possibly acting as a density barrier for the ascent of mafic magmas from the
1505 deep reservoirs. This may have been the cause of the prolonged quiescence period occurred
1506 on Lipari between the eruption of cordierite-bearing lavas and latest phases of activity of the
1507 M. S.Angelo (at 105-81 ka) and the renewal of volcanism in the southern Lipari characterized

by the appearance of rhyolitic products (at ~42 ka). In fact, in the scenario proposed by Di Martino et al. (2010), it is likely that crustal anatexis processes at mid-crustal levels have determined the progressive ponding and cooling of (denser) mafic (and intermediate) magmas, which initiated magma differentiation processes leading to the development of latest rhyolitic melts.

Conclusions

Lipari is the subaerial summit of an articulated volcanic apparatus constructed by a large variety of lava flows, scoriaceous deposits, lava domes (coulees) and pyroclastics, originated from several eruptive vents partly overlapping in space (and time) and characterized by hydromagmatic to strombolian eruption types.

Stratigraphic analysis, combined with available radiometric ages and relative age constraints derived from the correlation of tephra layers and terraced marine deposits attributed to the last interglacial (MIS 5, 124-81 ka), allow reconstruction of the eruptive history of Lipari as the result of nine successive Eruptive Epochs (and related Eruptions). These develop between more than 271 ka and historical times (*AD* 776-1230) under control of major regional tectonic trends (N-S, NNW-SSE and minor E-W trend), and are interrupted by recurrent quiescence periods and volcano-tectonic collapse events.

Lipari rocks display a wide spectrum of magma compositions, varying through time from CA and high-K CA basaltic andesites to high-K rhyolites (with a notable gap in the dacites field), and showing a steep increase of K_2O content. The mafic and intermediate volcanics are erupted during Eruptive Epochs 1 to 6 (from 271 to 81 ka), whereas the sialic products are emplaced from ~42 ka to historical times (Eruptive Epochs 7 to 9).

The magmatic evolution of Lipari is characterized by the occurrence of different mantle-derived magmas mostly differentiating through AFC processes and magma mixing, in the frame of a polybaric plumbing system. The contribution of the crust is variable through time and reaches a maximum influence in the genesis of cordierite-bearing lavas (Eruptive Epoch 5, 105 ka), which are suggested to derive from the mixing between mafic magmas and crustal anatectic melts. These anatectic processes have influenced the magmatic (and eruptive) history of Lipari by possibly explaining the stratigraphic gap occurred before the late rhyolitic activity.

References

BARBERI, F., INNOCENTI, F., FERRARA, G., KELLER, J. & VILLARI, L. 1974. Evolution of Eolian arc volcanism (southern Tyrrhenian Sea). *Earth and Planetary Science Letters*, **21**, 269-276.

BARKER, D.S. 1987. Rhyolites contamined with metapelite and gabbro, Lipari, Aeolian Islands, Italy: products of lower crustal fusion or of assimilation plus fractional crystallization?. *Contributions of Mineralogy and Petrology*, **97**, 460-472.

BARGOSSI G.M., CAMPOS VENUTI M., GASPAROTTO G. & ROSSI P.L. 1989. Petrologia e stratigrafia delle successioni andesitiche l.s. di Lipari, Isole Eolie, Italia. *Mineralogica et Petrographica Acta*, **22**, 295-326.

BECCALUVA, L., GABBIANELLI, G., LUCCHINI, F., ROSSI, P.L. & SAVELLI, C. 1985. Petrology and K/Ar ages of volcanics dredged from the Aeolian seamounts: implications for geodynamic evolution of the Southern Tyrrhenian basin. *Earth and Planetary Science Letters*, **74**, 187-208.

BERGEAT, A. 1899. Die Äolischen Inseln (Stromboli, Panarea, Salina, Lipari, Vulcano, Filicudi, Alicudi). *Abhandlung math. Phys. Kl. Klg. Bayr. Akad. D. Wiss.* München, **20**, I. Abt., 274 p.

BERGEAT, A. 1910. Der Cordieritandesit von Lipari, seine andalusitführenden Einschlüsse und die genetischen Beziehungen zwischen dem Andalusit, Sillimanit, Biotit, Cordierit, Orthoklas und Spinell in den letzteren. *Neues Jahrb Mineral*, **30**, 575-627.

BERNABÒ-BREA, L. & KRONIG, W. 1978. Le Isole Eolie dal tardo antico ai Normanni. *Archivio Storico Siracusano, Nuova Serie*, **5**, 1-99.

BIGAZZI, G. & BONADONNA, F.P. 1973. Fission track dating of the obsidian of Lipari Island (Italy). *Nature*, **242**, 322-323.

BORGIA, A., LINNEMAN, S., SPENCER, D., MORALES, L.D. & BRENES ANDRE, J. 1983. Dynamics of lava flow fronts, Arenal Volcano, Costa Rica. *Journal of Volcanology and Geothermal Research*, **19**, 303-329.

CAGGIANELLI A., DEL MORO A., PAGLIONICO A., PICCARRETA G., PINARELLI L. & ROTTURA A. 1991. Lower crustal granite genesis connected with chemical fractionation in the continental crust of Calabria (Southern Italy). *European Journal of Mineralogy*, **3**, 159-180.

CALANCHI, N., LUCCHI, F., PIRAZZOLI, P., ROMAGNOLI, C., TRANNE, C.A., RADTKE, U., REYSS, J.L. & ROSSI, P.L. 2002. Late-Quaternary and recent relative sea-level changes and vertical displacements at Lipari (Aeolian Islands). *Journal of Quaternary Science*, **17** (5-6), 459-467.

CAS, R.A.F. & WRIGHT, J.V. 1987. Volcanic successions. Unwin Hyman, London, 528 p.

CHAPPELL, J. & SHACKLETON, N.J. 1986. Oxygen isotopes and sea level. *Nature*, **324**, 137-140.

COLELLA, A. & HISCOTT, R.N. 1997. Pyroclastic surges of the Pleistocene Monte Guardia sequence (Lipari Island, Italy): depositional processes. *Sedimentology*, **44**, 47-66.

CONTINISO, R., FERRUCCI, F., GAUDIOSI, G., LO BASCIO, D. & VENTURA, G. 1997. Malta escarpment and Mt.Etna: early stages of an asymmetric rifting process? Evidence from geophysical and geological data. *Acta Vulcanologica*, **9**, 39-47.

CORTESE, M., FRAZZETTA, G. & LA VOLPE, L. 1986. Volcanic history of Lipari (Aeolian islands, Italy) during the last 10 000 years. *Journal of Volcanology and Geothermal Research*, **27**, 117-133.

CORTESE, M. & SABATINI, V. 1892. Descrizione geologico-petrografica delle Isole Eolie. *Memorie Descrittive della Carta Geologica d'Italia*, **7**, 131 p.

CRISCI, G.M., DE ROSA, R., LANZAFAME, G., MAZZUOLI, R., SHERIDAN, M.F. & ZUFFA, G.G. 1981. Monte Guardia Sequence: a Late-Pleistocene Eruptive Cycle on Lipari (Italy). *Bulletin of Volcanology*, **44**(3), 241-255.

CRISCI, G.M., DELIBRIAS, G., DE ROSA, R., MAZZUOLI, R. & SHERIDAN, M.F. 1983. Age and petrology of the Late-Pleistocene Brown Tuffs on Lipari, Italy. *Bulletin of Volcanology*, **46**(4), 381-391.

CRISCI, G.M., DE ROSA, R., ESPERANCA, S., MAZZUOLI, R. & SONNINO, M. 1991. Temporal evolution of a three component system: the island of Lipari (Aeolian Arc, southern Italy). *Bulletin of Volcanology*, **53**, 207-221.

DAVÌ, M., BEHRENS, H. VETERE, F. & DE ROSA, R. 2008. The viscosity of latitic melts from Lipari (Aeolian Islands, Italy): Inference on mixing–mingling processes in magmas. *Chemical Geology*, **259**, 89–97.

DAVÌ, M., DE ROSA, R. & BARCA, D. 2009. A LA-ICP-MS study of minerals in the Rocche Rosse magmatic enclaves: Evidence of a ma!c input triggering the latest silicic eruption of Lipari Island (Aeolian Arc, Italy). *Journal of Volcanology and Geothermal Research*, **182**, 45–56

DE ASTIS, G., DELLINO, P., LA VOLPE, L., LUCCHI, F. & TRANNE, C.A. 2006. Geological map of the island of Vulcano (Aeolian Islands). University of Bari, University of Bologna, and INGV; printed by L.A.C., Firenze.

DE ASTIS, G., LUCCHI, F., DELLINO, P., LA VOLPE, L., TRANNE, C.A., FREZZOTTI, M.L. & PECCERILLO, A. 2011. Vulcano Island, in: LUCCHI, F., PECCERILLO, A., KELLER, J., TRANNE, C.A. & ROSSI, P.L. (Eds.), Geology of the Aeolian Islands (Italy). *Geological Society of London, Memoirs*, this volume.

DE ASTIS, G., PECCERILLO, A., KEMPTON, P.D., LA VOLPE, L. & WU, T.W. 2000. Transition from calcalkaline to potassium-rich magmatism in subduction environments: geochemical and Sr, Nd, Pb isotopic constraints from the Island of Vulcano (Aeolian arc). *Contributions of Mineralogy and Petrology*, **139**, 684-703.

DE ASTIS, G., VENTURA, G. & VILARDO, G. 2003. Geodynamic significance of the Aeolian volcanism (Southern Tyrrhenian Sea, Italy) in light of structural, seismological and geochemical data. *Tectonics*, **22** (4), 1040-1057.

DECRÉE, S., BERNARD, A., YANS, J. & DE PUTTER, TH. 2005. Poly-phase alteration history of the kaolonitized 'Cava di Caolino' volcanics (Lipari Island, southern Italy). *Clay Minerals*, **40**, 2, 153-165.

DELLINO, P. 1991. Metodi quantitativi applicati allo studio dei depositi piroclastici. Il caso di M. Pilato – Rocche Rosse. *Unpublished PhD Thesis, University of Bari, Italy*, 78 p.

DELLINO, P. & LA VOLPE, L. 1995. Fragmentation versus transportation mechanisms in the pyroclastic sequence of Monte Pilato – Rocche Rosse (Lipari, Italy). *Journal of Volcanology and Geothermal Research*, **64**, 211–232.

DELLINO, P., ISAIA, R., LA VOLPE, L. & ORSI, G. 2001. Statistical analysis of textural data from complex pyroclastic sequences: implications for fragmentation processes of the Agnano-Monte Spina Tephra (4.1 ka), Phlegrean Fields, southern Italy. *Bulletin of Volcanology*, **63**, 443-461.

DE PAOLO D.J. 1981. Trace elements and isotopic effects of combined wallrock assimilation and fractional crystallisation. *Earth and Planetary Science Letters*, **53**, 189-202.

DE ROSA, R. & SHERIDAN, M.F. 1983. Evidence for magma mixing in the surge deposits of the Monte Guardia sequence, Lipari. *Journal of Volcanology and Geothermal Research*, **17**, 313-328.

DE ROSA, R., DONATO, P., GIONCADA, A., MASETTI, M. & SANTACROCE, R. 2003a. The Monte Guardia eruption (Lipari, Aeolian Islands): an example of a reversely zoned magma mixing sequence. *Bulletin of Volcanology*, **65**, 530-543.

DE ROSA, R., GUILLOU, H., MAZZUOLI, R. & VENTURA, G. 2003b. New unspiked K-Ar ages of volcanic rocks of the central and western sector of the Aeolian Islands: reconstruction of the volcanic stages. *Journal of Volcanology and Geothermal Research*, **120**, 161-178.

DE VIVO, B., ROLANDI, G., GANS, P.B., CALVERT, A., BOHRSON, W.A. SPERA, F.J. & BELKIN, H.E. 2001. New constraints on the pyroclastic eruptive history of the Campanian Volcanic Plain (Italy). Mineralogy and Petrology, **73**, 47-65.

DI MARTINO, C., FREZZOTTI, M.L., LUCCHI, F., PECCERILLO, A., TRANNE, C.A. & DIAMOND, L.W. 2010. Magma storage and ascent at Lipari Island (Aeolian archipelago, southern Italy) during the old stages (223-81 ka): role of crustal processes and tectonic influence. *Bulletin of Volcanology*, DOI 10.1007/s00445-010-0383-6.

DI MARTINO, C., 2010. Evoluzione del sistema di alimentazione magmatica dell'Isola di Lipari (Isole Eolie, Italia). *Unpublished PhD Thesis, University of Bologna, Italy, 155 pp.*

1686 DOLOMIEU, U. (DE) 1783. Voyage aux Iles de Lipari, fait en 1781. *Paris, Acad. Roy. Sci.*, 208
1687 p.
1688
1689 ELLAM R.M., HAWKESWORTH C.J., MENZIES M.A & ROGERS N.W.1989. The volcanism of
1690 Southern Italy: role of subducion and the relationships between potassic and sodic alkaline
1691 amgmatism. *Journal of Geophysical Research*, **94**, 4589-4601.
1692
1693 ELLAM R.M., MENZIES M.A., HAWKESWORTH C.J., LEEMAN W.P., ROSI M. & SERRI G. 1988. The
1694 transition from calc-alkaline to potassic orogenic magmatism in the Aeolian Islands, Southern
1695 Italy. *Bulletin of Volcanology*, **50**, 386-398.
1696
1697 ESPERANCA, S., CRISCI, G.M., DE ROSA, R. & MAZZUOLI, R. 1992. The role of the crust in the
1698 magmatic evolution of the Island of Lipari (Aeolian Islands, Italy). *Contributions of Mineralogy*
1699 *and Petrology*, **112**, 450-462.
1700
1701 FINK, J.H. & ANDERSON, S.W. 2000. Lava domes and coulees, in: SIGURDSSON, H. (Ed.),
1702 Encyclopedia of volcanoes. *Academic Press,* 307-319.
1703
1704 FISHER, R.V. & SCHMINCKE, H.-U. 1984. Pyroclastic rocks. *Springer Verlag*, 472 p.
1705
1706 FRANCALANCI L., TAYLOR S.R., MCCULLOCH M.T. & WOOLHEAD J.D. 1993. Geochemical and
1707 isotopic variations in the calc-alkaline rocks of Aeolian arc, southern Tyrrhenian Sea, Italy:
1708 constraints on magma genesis. *Contributions of Mineralogy and Petrology*, **113**, 300-313.
1709
1710 FRANCALANCI L., AVANZINELLI R., TOMMASINI S. & HEUMAN A. 2007. A west-east geochemical
1711 and isotopic traverse along the volcanism of the Aeolian Island arc, southern Tyrrhenian Sea,
1712 Italy: Interferences on mantle source processes*. Geological Society of America Special*
1713 *Papers*, **418**, 235-263.
1714
1715 FREZZOTTI M.L. & PECCERILLO A. 2004. Fluid inclusion and petrological studies elucidate
1716 reconstruction of magma conduits. *Transactions of the American Geophysical Union*, **85**
1717 (16), 157.
1718
1719 FREZZOTTI M.L., PECCERILLO A. & BONELLI R. 2003. Magma ascent rates and depths of
1720 magma reservoirs beneath the Aeolian volcanic arc (Italy): inferences from fluid and melt
1721 inclusions in crustal xenoliths, in: BODNAR B., DE VIVO B. (Eds.) *Melt inclusions in volcanic*
1722 *systems*. Elsevier, Amsterdam, 185–206.

FREZZOTTI M.L., PECCERILLO A., ZANON V. & NIKOGOSIAN I. 2004. Silica-rich melts in quartz xenoliths from Vulcano island and their bearing on process of crustal anatexis and crust-magma interaction beneath the aeolian arc, southern Italy. *Journal of Petrology*, **45**, 3–26.

GAMBERI, F. & MARANI, M.P. 1997. Detailed bathymetric mapping of the eastern offshore slope of Lipari island (Tyrrhenian Sea): insight into the dark side of an arc volcano. *Marine Geophysical Researches*, **19**, 363-377.

GILLOT, P.Y. 1987. Histoire volcanique des Iles Eoliennes: arc insulaire ou complexe orogénique anulaire? *Doc. et Trav., Institut Géologique Albert-de-Lapparent*, **11**, 35-42.

GIONCADA, A., MAZZUOLI, R., BISSON, M. & PARESCHI, M.T. 2003. Petrology of volcanic products younger than 42 ka on the Lipari-Vulcano complex (Aeolian Islands, Italy): an example of volcanism controlled by tectonics. *Journal of Volcanology and Geothermal Research*, **122**, 191-220.

GIONCADA, A., MAZZUOLI, R. & MILTON, A.J. 2005. Magma mixing at Lipari (Aeolian Islands, Italy): insights from textural and compositional features of phenocrysts. *Journal of Volcanology and Geothermal Research*, **145**, 97-118.

HART S.R. 1984. A large-scale isotope anomaly in the southern hemisphere mantle. *Nature*, **309**, 753-757.

HONNOREZ, J. & KELLER, J. 1968. Xenolithe in vulkanischen Gesteinen der Aolischen Inseln (Sizilien). *Geologische Rundschau*, **57**, 719-736.

KELLER, J. 1967. Alter und Abfolge der vulkanischen Ereignisse auf den Äolischen Inseln. *Ber. Naturf. Ges.* Freiburg, **57**, 33-67.

KELLER, J. 1970. Detierung der obsidiane und bimstuffe von Lipari. *N. Jb. Geol. Mh.,* 90-101.

KELLER, J. 1980. The island of Salina. *Rendiconti della Società Italiana di Mineralogia e Petrologia*, **36**, 489-524.

KELLER, J. 2002. Lipari's fiery past: dating the medieval pumice eruption of Monte Pelato: International Conference „The fire between air and water", UNESCO-Regione Siciliana, Lipari, September 29th-October 2nd, oral presentation.

KELLER, J., LUCCHI, F., TRANNE, C.A. & GERTISSER, R. 2011. Salina Island, in: LUCCHI, F., PECCERILLO, A., KELLER, J., TRANNE, C.A. & ROSSI, P.L. (Eds.), Geology of the Aeolian Islands (Italy). *Geological Society of London, Memoirs*, this volume.

KLERX, J., DEUTSCH, S., HERTOGEN, J., DE WINTER, J., GIJBELS, R. & PICHLER, H. 1974. Comments on „Evolution of Eolian arc volcanism (southern Tyrrhenian Sea)" by BARBERI, F., INNOCENTI, F., FERRARA, G., KELLER, J. & VILLARI, L. *Earth and Planetary Science Letters*, **23**, 297-303.

KRAML, M., KELLER, J. & HENJES-KUNST, F. 1997. Dating of Upper Quaternary deep-sea sediments from the Ionian Sea (Eastern Mediterranean) with laser $^{40}Ar/^{39}Ar$ analyses on prominent tephra layers. EUG 97, *Terra Nova*, **9**, Abstract Supplement 1, 406.

LANZAFAME, G. & BOUSQUET, J.C. 1997. The Maltese escarpment and ist extension from Mt. Etna to Aeolian Islands (Sicily): importance and evolution of a lithospheric discontinuity. *Acta Vulcanologica*, **9**, 121-135.

LEOCAT, E., GILLOT, P.-Y. & PECCERILLO, A. 2010. Eruptive history of western and central Aeolian volcanoes (South Tyrrhenian Sea): insights from K/Ar dating. 44th Annual conference of the Volcanic and Magmatic Studies Group (VMSG), Geological Society of London and Mineralogical Society, 4th-6th January 2010, Abstract Volume.

LEOCAT, E., GILLOT, P.-Y. & PECCERILLO, A. 2009. Temporal evolution of the Western and Central volcanism of the Aeolian Island Arc (Italy, southern Tyrhhenian Sea). *EGU General Assembly, Geophysical Research Abstracts, **11**, EGU2009-13106.*

LOSITO, R. 1989. Stratigrafia, caratteri deposizionali e aree sorgente dei tufi bruni delle Isole Eolie. *Unpublished PhD Thesis, University of Bari, Italy.*

LUCCHI, F. 2000. Evoluzione dell'attività vulcanica e mobilità verticale delle Isole Eolie nel tardo Quaternario. *Unpublished PhD Thesis, University of Bologna, Italy*, 186 p.

LUCCHI, F. 2009. Late-Quaternary terraced marine deposits as tools for wide-scale correlation of unconformity-bounded units in the volcanic Aeolian archipelago (southern Italy). *Sedimentary Geology*, **216**, 158-178.

LUCCHI, F. & TRANNE, C.A. 2011. Stratigraphic methodology for the geological mapping of volcanic areas: insights from the Aeolian archipelago (Southern Italy), in: LUCCHI, F., PECCERILLO, A., KELLER, J., TRANNE, C.A. & ROSSI, P.L. (Eds.), Geology of the Aeolian Islands (Italy). *Geological Society of London, Memoirs*, this volume.

LUCCHI, F., TRANNE, C.A., CALANCHI, N., PIRAZZOLI, P., ROMAGNOLI, C., RADTKE, U., REYSS, J.L. & ROSSI, P.L. 2004a. Stratigraphic constraints to date late-Quaternary ancient shorelines and to evaluate vertical movements at Lipari (Aeolian Islands). *Quaternary international*, 115/116, 105-115.

LUCCHI, F., TRANNE, C.A., CALANCHI, N. & ROSSI, P.L. 2004b. Geological cartography in volcanic areas: the case of Lipari (Aeolian Islands), in: PASQUARÉ, G. & VENTURINI, C. (Eds.), Mapping Geology in Italy. *A.P.A.T. (Agenzia per la Protezione dell'Ambiente e per i servizi Tecnici), Dipartimento difesa del suolo, Geological Survey of Italy, printed by S.E.L.C.A.,* Firenze, 138-146.

LUCCHI, F., TRANNE, C.A., DE ASTIS G., KELLER, J., LOSITO, R. & MORCHE, W. 2008. Stratigraphy and significance of Brown Tuffs on the Aeolian Islands (southern Italy). *Journal of Volcanology and Geothermal Research*, **177**(1), 49-70.

LUCCHI, F., TRANNE, C.A. & KELLER, J. 2011. Regional stratigraphic correlations across the Aeolian archipelago (southern Italy), in: LUCCHI, F., PECCERILLO, A., KELLER, J., TRANNE, C.A. & ROSSI, P.L. (Eds.), Geology of the Aeolian Islands (Italy). *Geological Society of London, Memoirs*, this volume.

LUCCHI, F., TRANNE, C.A. & ROSSI, P.L. 2010. Stratigraphic approach to geological mapping of the late-Quaternary volcanic island of Lipari (Aeolian archipelago, Southern Italy), in: GROPPELLI, G. & VIERECK-GOETTE, L. (Eds.), Stratigraphy and Geology of Volcanic Areas. *Geological Society of America Special Papers*, **464**, 1–32, doi: 10.1130/2010.2464(01).

MACCARONE, E. 1963. Aspetti geochimico-petrografici di alcuni esemplari di andesite granato-cordieritifero dell'Isola di Lipari. *Periodico di Mineralogia*, **32**, 277-302.

MAZZUOLI, R., TORTORICI, L. & VENTURA, G. 1995. Oblique rifting in Salina, Lipari and Vulcano Islands (Aeolian Islands, Southern Tyrrhenian Sea, Italy). *Terra Nova*, **7**, 444-452.

PECCERILLO A. & TAYLOR S.R. 1976. Geochemistry of the Eocene calc-alkaline volcanic rocks from the Kastamonu area, northern Turkey. *Contribution of Mineralogy and Petrology*, **58**, 63-81.

PECCERILLO, A., FREZZOTTI, M.L., DE ASTIS, G. & VENTURA, G. 2006. Modeling the magma plumbing system of Vulcano (Aeolian Islands, Italy) by integrated fluid-inclusion geobarometry, petrology and geophysics. *Geology*, **34**, 17–20.

PICHLER, H. 1968. Zur Altersfrage des vulkanismus des Aeolischen Archipels und der Insel Ustica (Sizilien). *Geologische Mitteilungen*, **7**, 299-332.

PICHLER, H. 1976. Carta geologica dell'isola di Lipari. *Istituto di Vulcanologia, CNR, printed by L.A.C.,* Firenze.

PICHLER, H. 1980. The island of Lipari*. Rendiconti della Società Italiana di Mineralogia e Petrologia*, **36**, 415-440.

RICCI LUCCHI, F., CALANCHI, N., LANZAFAME, G. & ROSSI, P.L. 1988. Plant-rich pyroclastic deposits of Monte S.Angelo, Lipari (Aeolian Island*). Rendiconti della Società Italiana di Mineralogia e Petrologia*, **43**, 1227-1251.

ROMAGNOLI, C., CALANCHI, C., GABBIANELLI, G., LANZAFAME, G. & ROSSI, P.L. 1989. Contributi delle ricerche di geologia marina alla caratterizzazione morfostrutturale ed evolutiva dei complessi vulcanici di Salina, Lipari e Vulcano (Isole Eolie). *Bollettino GNV* (Gruppo Nazionale di Vulcanologia), **2**, 971-978.

SCHMIDT, R. & SCHMINCKE, H.-U. 2000. Seamounts and island building, in: SIGURDSSON, H., HOUGHTON, B.F., MCNUTT, S.R., RYMER, H. & STIX, J. (Eds.), Encyclopedia of Volcanoes. Academic Press, 683-694.

SHERIDAN, M.F., FRAZZETTA, G. & LA VOLPE, L. 1987. Eruptive histories of Lipari and Vulcano, Italy, during the past 22,000 years. *Geological Society of America Bulletin*, **212**, 29-34.

STACEY J.S. & KRAMERS J.D. 1975. Approximation of terrestial lead isotope evolution by a two-stage model. *Earth and Planetary Science Letters*, **26**, 207-221.

SUN S.S. & MC DONOUGH W.F. 1989. Chemical and isotopic systematics of oceanic basalts: implications fort he mantle composition and processes. In: Saunders A.D. and Norry M.J. (eds.), Magmatism in ocean basins. *Geol. Soc. London. Spec. Pub.*, **42**, 313-345.

TANGUY, J.C., LE GOFF, M., PRINCIPE, C., ARRIGHI, S., CHILLEMI, V., PAIOTTI, A., LA DELFA, S. & PATANÈ, G. 2003. Archeomagnetic dating of Mediterranean volcanics of the last 2100 years: validity and limits. *Earth and Planetary Science Letters*, **211**, 111-124.

TRANNE, C.A., LUCCHI, F., CALANCHI, N., LANZAFAME & G., ROSSI, P.L. 2002. Geological map of the island of Lipari (Aeolian Islands)(scale 1:12.500). *University of Bologna and INGV, printed by L.A.C.,* Firenze.

VENTURA, G. 2011. Geodynamic setting of the Aeolian volcanism (Italy) from geophysical data, in: LUCCHI, F., PECCERILLO, A., KELLER, J., TRANNE, C.A. & ROSSI, P.L. (Eds.), Geology of the Aeolian Islands (Italy). *Geological Society of London, Memoirs*, this volume.

VENTURA, G., VILARDO, G., MILANO, G. & PINO, N.A. 1999. Relationships among crustal structure, volcanism and strike-slip tectonics in the Lipari-Vulcano Volcanic Complex (Aeolian Islands, Southern Tyrrhenian Sea, Italy). *Physics of the Earth and Planetary Interiors*, **116**, 31-52.

VESPERMANN, D. & SCHMINCKE, H.-U. 2000. Scoria cones and tuff rings, in: SIGURDSSON, H., HOUGHTON, B.F., MCNUTT, S.R., RYMER, H. & STIX, J. (Eds.), Encyclopedia of Volcanoes. Academic Press, 683-694.

WAELBROECK, C., LABEYRIE, L., MICHEL, E., DUPLESSY, J.C., MCMANUS, J.F., LAMBECK, K., BALBON, E. & LABRACHERIE, M. 2002. Sea-level and deep water temperature changes derived from foraminifera isotopic records. *Quaternary Science Reviews,* **21**, 295-305.

WOLFF, J.A. & SUMNER, J.M. 2000. Lava fountains and their products, in: SIGURDSSON, H., HOUGHTON, B.F., MCNUTT, S.R., RYMER, H. & STIX, J. (Eds.), Encyclopedia of Volcanoes. Academic Press, 321-329.

ZANCHETTA, G., SULPIZIO, R., ROBERTS, N., CIONI, R., EASTWOOD, W.J., SIANI, G., PATERNE, M. & SANTACROCE, R. 2010. Tephrostratigraphy and climatic events of the Mediterranean: an overview. *The Holocene*, in press.

ZANON V., FREZZOTTI M.L., PECCERILLO A. 2003. Magmatic feeding system and crustal magma accumulation beneath Vulcano Island (Italy): evidence from CO_2 fluid inclusions in quartz xenoliths. *Journal of Geophysical Research*, **108**, 2298–2301. doi:10.1029/2002JB002140

ZARTMAN R.E. & HAINES S.M. 1988. The plumbotectonic model fro Pb isotopic systematics among major terrestrial reservoirs – a case for bidirectional transport. *Geochimica et Cosmochimica Acta*, 52, 1327-1339.

Figure captions

Fig. 1. A - Localization of Lipari Island in the Aeolian archipelago, southern Tyrrhenian Sea (bathymetry from Beccaluva et al., 1985, modified). B - Morphostructural sketch map of the Vulcano, Lipari and Salina volcanoes, which form a NNW-SSE-oriented volcanic belt aligned along the Tindari-Letojanni structural system (simplified from Romagnoli et al., 1989). Coordinates conform to the Gauss-Boaga System (IGM). Depth contour lines in metres below sea level.

Fig. 2. Morphostructural sketch map of the island of Lipari based on a DEM shaded relief image processed by L.A.C. (Firenze). Coordinates conform to the Gauss-Boaga System (IGM). Numbered points in the figures indicate metres above sea level.

Fig. 3. Outcrop exposure of marine terraces related to paleoshorelines I (43-45 m *asl*) and II (23-27 m *asl*) along the western coastal cliffs of Lipari near Cala Fico (A) and P. del Cugno Lungo (B). Paleoshorelines I, II, III are attributed to the main high sea-level peaks during MIS 5 on the basis of stratigraphic relations with dated volcanic products and age of fossils (C). See below in the text for age references. Note that the successive paleoshorelines are arranged in a downstepping stacking pattern with older terraces (paleoshoreline I) located at higher elevations (B).

Fig. 4. Stratigraphic framework of unconformity-bounded units recognized at Lipari. Grey areas indicate the time-intervals of formation of allogenic unconformities (U_I, U_{II}, L_3, I_c, I_d) by linking with specific segments of the sea-level curves (a=Chappell and Shackleton, 1986; b=Waelbroeck et al., 2002).

Fig. 5. Sketch geological map of Lipari Island according to the designated unconformity-bounded units and corresponding Eruptive Epochs (from a simplified reduction of the 1:10,000 geological map in the attached CD). Symbols conform to Fig. 2. Coordinates conform to the Gauss-Boaga System (IGM).

Fig. 6. Schematic stratigraphic succession of Lipari described by 21 UBUs and the informal Paleo-Panarea unit, 26 lithosomes and several lithostratigraphic units (simplified from the legend of the 1:10,000 geological map in the attached CD). Successive Eruptive Epochs (and eruptions) and main inter-eruption periods are defined according to the corresponding UBUs and unconformities. References cited for the correlation of stratigraphic units: * De Astis et al., 2011; ** Keller et al., 2011. References cited: ([1]) Barker, 1987; ([2]) Bigazzi and

Bonadonna, 1973; ([3]) Colella and Hiscott, 1997; ([4]) Cortese et al. (1986); ([5]) Crisci et al., 1981; ([6]) Crisci et al., 1983; ([7]) Crisci et al., 1991; ([8]) De Astis et al., 2006; ([9]) Dellino and La Volpe, 1995; ([10]) De Rosa et al., 2003b; ([11]) De Vivo et al., 2001; ([12]) Gillot, 1987; ([13]) Keller, 1970; ([14]) Keller, 1980; ([15]) Keller, 2002, pers. comm.; ([16]) Kraml et al., 1997; ([17]) Leocat et al., 2010; ([18]) Leocat et al., 2009; ([19]) Lucchi et al., 2004a; ([20]) Lucchi et al., 2008; ([21]) Pichler, 1980; ([22]) Ricci Lucchi et al., 1988; ([23]) Tanguy et al., 2003; ([24]) Tranne et al., 2002; ([25]) Zanchetta et al., 2010.

Fig. 7. Outcrop photographs of the older volcanic products of Lipari cropping out along its western coasts (from south to north). A) The Timpone Carrubbo volcano is representative of Eruptive Epoch 1 (Paleo-Lipari) and is mostly composed of lava flows and scoriaceous products with diffuse hydrotermalization (sb=S. Bianco formation). Near P. le Grotticelle, the inner portion of the volcano with its vertical feeding dykes is exposed. B) Pyroclastic-breccias and lava flows building up the N-S-aligned spatter cones of Timpone Pataso, Timpone Ospedale and Valle di Pero (Eruptive Epoch 2). C) The Chiesa Vecchia volcano (Eruptive Epoch 2) is mostly made up of massive and blocky lava flows exposed in the NW sector of Lipari (pu=Puddino formation). In all photographs, the older volcanic products of Lipari are cut by marine terraces related to paleoshorelines I and III, which are covered by more recent detrital deposits and pyroclastics (bt=Brown Tuffs). This stratigraphic motif is particularly exposed on the sides of the NW-SE-oriented conjugate normal faults (F1 and F2) affecting the NW coast of Lipari (C). Numbered points in the figures indicate metres above sea level.

Fig. 8. Eruptive Epoch 4 volcanic products (119-116 ka). Numbered points in the figures indicate metres above sea level. A) Outcrop photograph (and interpretative scheme) of the easternmost side of the Monterosa scoria cones constructed by scoriaceous products and lavas of the Sciarra di Monterosa (sci_1, sci_2), Pignataro di Fuori (pf) and U Mazzuni formations (ma_1). The Sciarra di Monterosa pyroclastics (sci_1), in particular, consists of hydromagmatic lapilli-tuffs (a) gradually upward passing to strombolian scoriae (b) which build up the flank of a basal scoria cone, successively filled by massive lava flows (sci_2). B) In the central-western sector of Lipari, the Timpone Ricotta pyroclastic products (tr) originated from the M. S.Angelo stratocone unconformably overlie the volcanic products of M. Mazzacaruso volcano, represented by scoriaceous products and lava flows of the Bagni termali di S. Calogero formation (bt_1, bt_2), emplaced during Eruptive Epoch 2, and the older hydrotermalized lavas of Vallone dei Lacci formation (vla_2) related to Eruptive Epoch 1. This erosional unconformity is the field evidence in this area of the major unconformity U_I. C) In the area of Porto Pignataro, eastern Lipari, the Timpone Ricotta pyroclastic products coming

from the M. S.Angelo volcano notably contain several bomb-sags originated from the opposite direction, which corresponds to the location of Monterosa scoria cones.

Fig. 9. Leaf-bearing pyroclastics originated from the M. S.Angelo volcano (Eruptive Epoch 5). A) In the area of Timpone Carrubbo, the two distinct sheet-like horizons of leaf-bearing pyroclastics (tp=Timpone Pataso formation; sp=Serra Pirrera formation) are separated by a widespread red paleosol. Note the passage from the well-stratified appearance of primary pyroclastics (a) to the massive or poorly bedded lahar-type lithofacies (b) (see the text for further explanation). The two horizons are representative of successive eruptions during Eruptive Epoch 5 (namely 5.1 and 5.2). This stratigraphic motif is diffused throughout Lipari Island. B) Near Timpone Pataso, the Timpone Pataso leaf-bearing pyroclastics constitute a lentiform body representing the regularly-stratified filling of a small tectonic lake (tp_a) formed as a consequence of tectonic activity along N-S structures (F). See the text for further explanation. Numbered points in the figures indicate metres above sea level.

Fig. 10. Correlative framework of composite, synthetic stratigraphic sections across the island of Lipari, showing the correlation of key stratigraphic units, *e.g.* leaf-bearing pyroclastics (tp=Timpone Pataso formation; sp=Serra Pirrera formation), Brown Tuff pyroclastics from Vulcano (pi=Pianoconte formation; gr=Piano Grotte dei Rossi formation), Grey Porri Tuffs from Salina (rb=Rocce di Barcone formation), M.Guardia (gu) and Vallone del Gabellotto formations (vg). The correlation of the various unconformities and most of lithostratigraphic units is also outlined (labels conform to Fig. 6 and Tab. 3). Vertical scale is in metres above sea level.

Fig. 11. Volcanic products of Eruptive Epochs 5-6 and their stratigraphic relationships with the paleoshoreline II marine deposits (MIS 5c-100 ka). Near to Bruca (A-B), the paleoshoreline II conglomerates are located above the leaf-bearing pyroclastics (sp=Serra Pirrera formation) and 105ka old cordierite-bearing lavas (pu=Pulera formation), related to Eruptive Epoch 5. In B, the stratigraphic relationship with the cordierite-bearing lavas is reconstructed on the basis of the abundance of this lithotype in the boulders of paleoshoreline II (cordierite-bearing boulders are notably absent in the paleoshoreline I deposits), cutting at the front these lava flows originated from the M. S.Angelo volcano. The older paleoshoreline I deposits are located at lower elevations as a consequence of localized displacement along a series of normal faults (f)(see Lucchi, 2009, for a wider explanation). At Cala Sciabeca (C), the paleoshoreline II is represented by beach sands and gravels (cl_a member) showing cross-stratification (*) upward passing to low-angle plane parallel-stratification (**). These deposits are covered by the thick massive lava flows originated from

2030 the M. Chirica volcano during Eruptive Epoch 6 (cc=Monte Chirica-Costa d'Agosto
2031 formation). All these stratigraphic successions are capped by pyroclastics deposited during
2032 the inter-eruption period younger than MIS 5 (*e.g.,* Brown Tuffs, Grey Porri Tuffs and M.
2033 Guardia pyroclastics). Field evidence of unconformities U_I, U_{II} and L_3 is shown.
2034
2035 Fig. 12. Rhyolite volcanic products in the southern sector of Lipari (Eruptive Epochs 7-8). A)
2036 At V. Muria, the M. Guardia pyroclastics (gu), related to Eruptive Epoch 8, climb over
2037 scoriaceous products related to the Timpone Carrubbo stratocone (bel_1 member), which are
2038 affected by vc3 collapse. This is the field evidence of U_{II} unconformity. The M. Guardia
2039 pyroclastics are capped by M. Giardina domes (gi). B) Along the coastal cliff of P. del
2040 Perciato it is exposed a natural stratigraphic section showing the superposition of pumiceous
2041 pyroclastics (pe_2, fa_1 members and gu) and domes (pe_1 member and gi) building up the
2042 southern dome field of Lipari. The Intermediate Brown Tuffs (pi), including the tephra layer
2043 more likely correlated with Y5/Campanian Ignimbrite, are interbedded, separating volcanics
2044 of Eruptive Epoch 7 from those related to Eruptive Epoch 8. C) At Punta della Crapazza, the
2045 fa_3 black dacite lava dome cuts the Falcone domes (fa_2 member), representing the unique
2046 field evidence of more mafic magmas in the southern sector of Lipari. The domes are capped
2047 by Intermediate Brown Tuffs (pi=Pianoconte formations) and M.Guardia pyroclastics (gu).
2048 Labels conform to Fig. 6.
2049
2050 Fig. 13. Volcanic products of the north-eastern dome field of Lipari (Eruptive Epoch 9). A) at
2051 Spiaggia della Papesca, the M. Pilato (Sciarra dell'Arena formation, sa_1) and Vallone del
2052 Gabellotto pumiceous pyroclastics (vg) are separated by a reddish paleosol. These deposits
2053 unconformably cover the highly altered endogenous domes of Capo Rosso (cr), related to
2054 Eruption 8.2, outlining the field evidence of unconformity L_5. B) The Rocche Rosse coulee
2055 (Fossa di Rocche Rosse formation, frr_2) is outpoured from the crater area of M. Pilato cone,
2056 which is constructed by sa_1 pumiceous pyroclastics. Note that both flanks of M. Pilato cone
2057 (at the sides of Rocche Rosse coulee) are deeply cut by pumice quarries. Labels conform to
2058 Fig. 6.
2059
2060 Fig. 14. Correspondence between the unconformity-bounded stratigraphy of Lipari and
2061 reconstructed Eruptive Epochs (and Eruptions) and inter-eruption periods, the chronology of
2062 which is shown by linking with specific segments of the sea-level curves (a=Chappell and
2063 Shackleton, 1986; b=Waelbroeck et al., 2002). Distinctive eruptive vents, eruption types and
2064 composition of erupted products for each Eruptive Epoch are synthetically described.
2065

Fig. 15. Sketch maps showing the distribution of active eruptive vents during the Eruptive Epochs defined for Lipari volcano. Symbols: 1=crater rim; 2=spatter cones; 3=lava dome foliation; 4=presumed transport direction of pyroclastic products; 5=main lava flow; 6=caldera-type collapse rim.

Fig. 16. K_2O *vs.* SiO_2 classification diagram (Peccerillo and Taylor, 1976) for Lipari rocks.

Fig. 17. Major element *vs.* SiO_2 variation diagrams for Lipari rocks. Symbols as in Fig. 16.

Fig. 18. Trace element *vs.* SiO_2 variation diagrams for Lipari rocks. Symbols as in Fig. 16.

Fig. 19. Zr *vs*. Rb (A) and Nb/Zr *vs*. Zr (B). Symbols as in Fig. 16.

Fig. 20. REE patterns normalized to chondrite values (Sun and Mc Donough, 1989) for Lipari basaltic andesite to dacite rocks (A) and rhyolite rocks (B). Symbols as in Fig. 16.

Fig. 21. Incompatible trace element pattern normalized to primordial mantle (Sun and Mc Donough, 1898) for Lipari basaltic andesite rocks. Symbols as in Fig. 16.

Fig. 22. Nd *vs.* Sr isotope variation of Lipari volcanics (data from Esperanca *et al*., 1992 and Gioncada *et al*., 2003) and Calabrian Basement rocks (data from Caggianelli *et al*., 1991). Compositional fields of Aeolian Islands for comparison (data from Peccerillo *et al*., 2004).

Fig. 23. Pb isotope variation of Lipari volcanics (data from Esperanca *et al*., 1992 and Gioncada *et al*., 2003) and Calabrian Basement rocks (data from Caggianelli *et al.*, 1991). Symbols as in Fig. 23. Compositional field of Aeolian Islands for comparison (data from Peccerillo *et al.*, 2004). Northern Hemispher Reference Line (NHRL) from Hart (1984). Pb isotope evolution curve for the upper crust from Zartman and Haines, 1988. Model growth for the average crust from Stacey and Kramers, 1975 (S&K).

Fig. 24. Sketch diagram showing the pressures (P) and corresponding depths of fluid trapping and reequilibration of fluid inclusions at Lipari. Data related to both Type I and Type II fluid inclusions are shown: according to Zanon et al. (2003), the early Type I inclusions are assumed to have been trapped before the ascent of the host xenoliths, whereas the Type II inclusions are trapped during the magma ascent.

These are assumed to display the magma accumulation levels below the studied volcanic edifices and the evolution through time of the magma feeding system of Lipari. Main crustal lithological boundaries conform to Peccerillo et al. (2006).

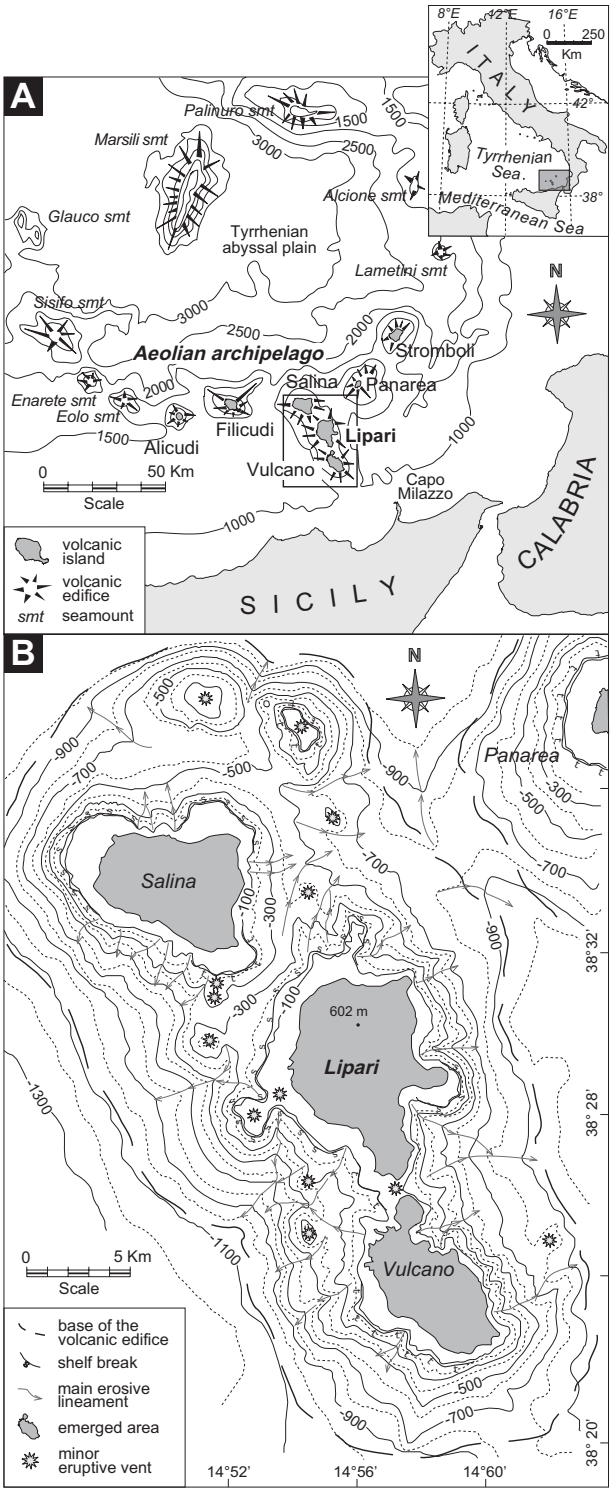

Fig. 1 - Forni et al.

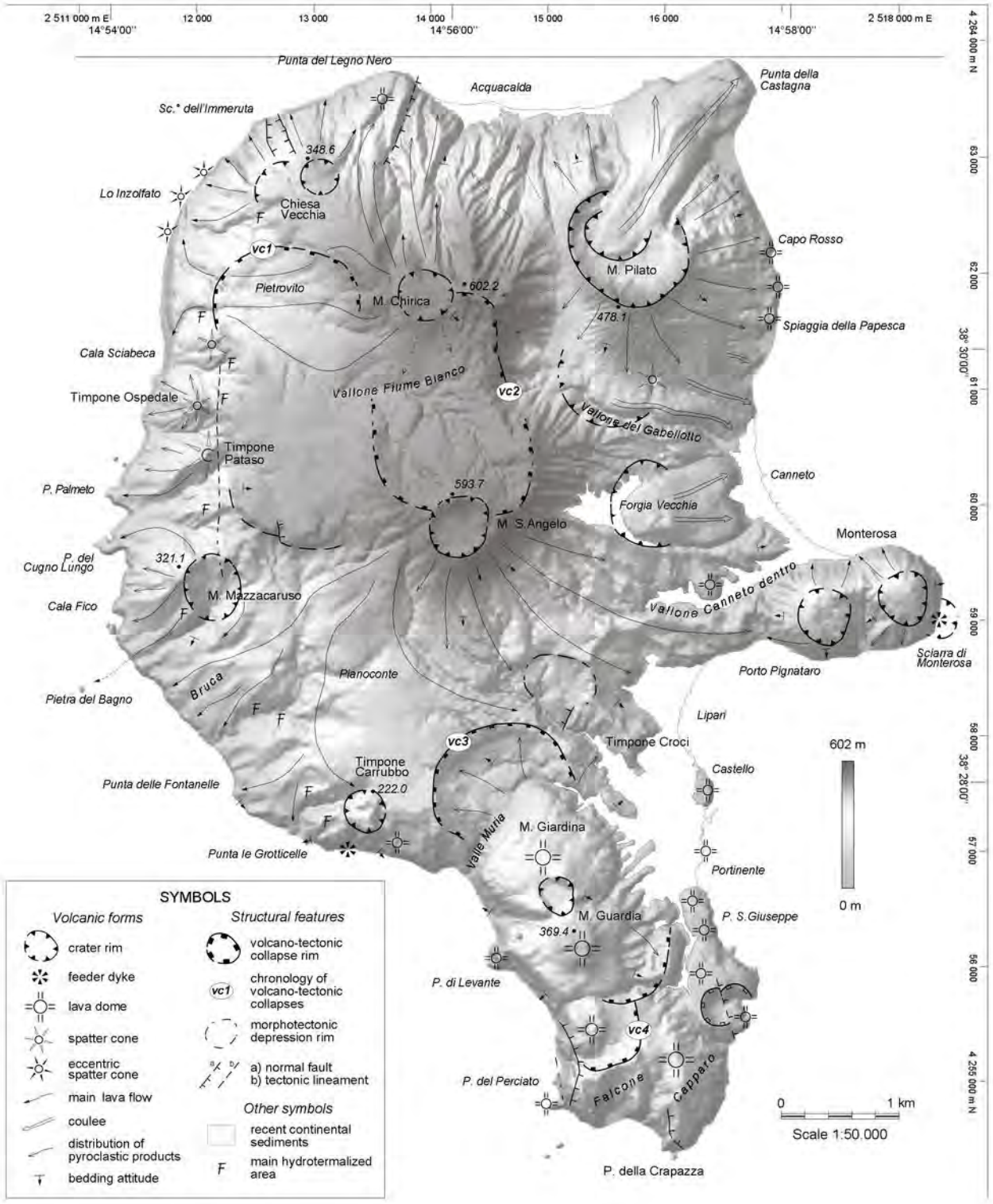

Fig. 2 - Forni et al.

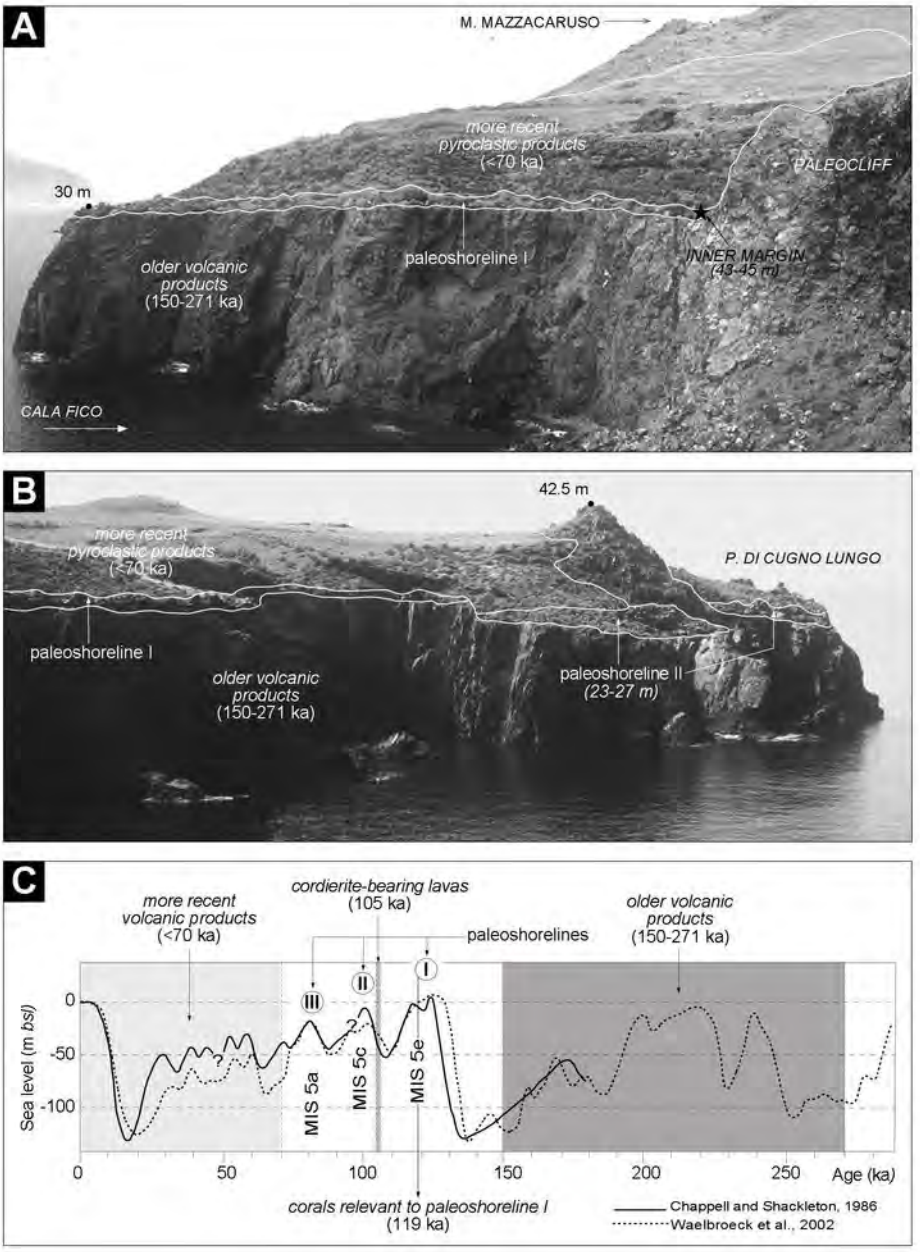

Fig. 3 - Forni et al.

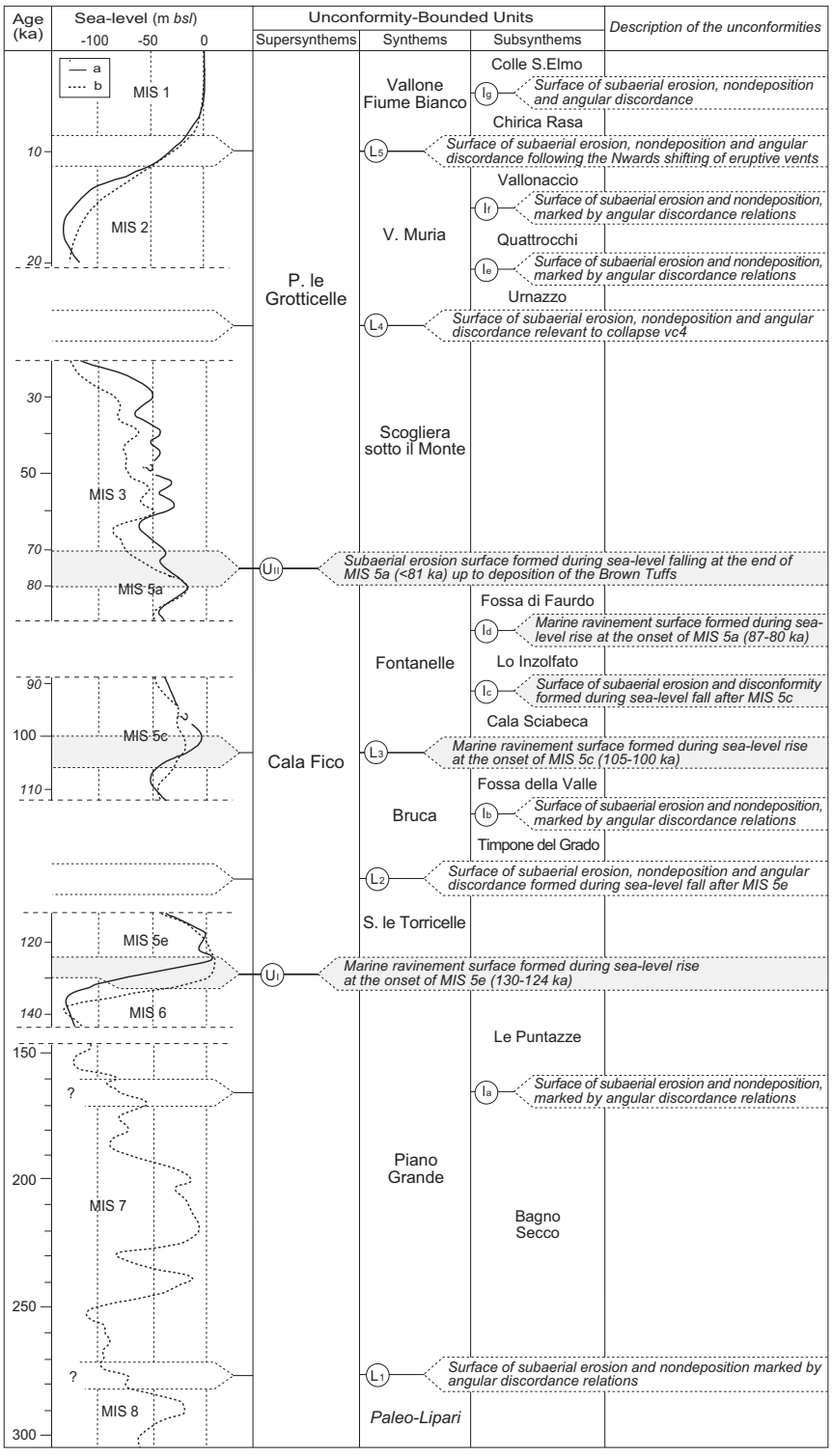

Fig. 4 - Forni et al.

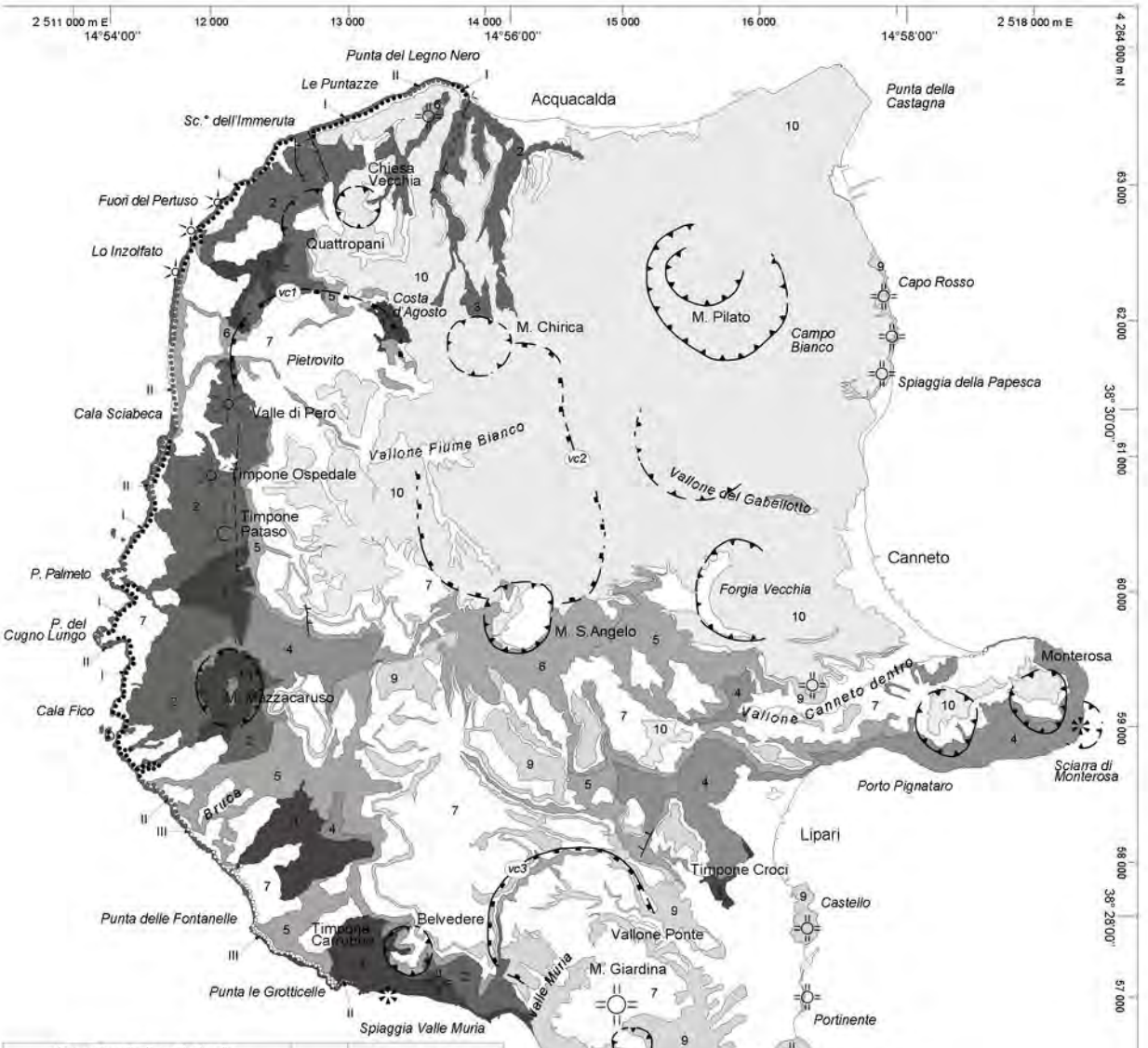

Unconformity-bounded units				Eruptive history
Supersynth.	Synthems	Subsynthems		
P. le Grotticelle	Vallone Fiume Bianco (L4)		10	eruptive epoch 9
	V. Muria (L4)		9	eruptive epoch 8
	Scogliera sotto il Monte		8	eruptive epoch 7
			7	*external pyroclastites (Brown Tuffs)*
(U II)				
Cala Fico	Fontanelle (L3)	Fossa di Faurdo (Id)	III	*paleoshoreline III*
		Lo Inzolfato (Ic)	6	eruptive epoch 6
		Cala Sciabeca	II	*paleoshoreline II*
	Bruca (L2)		5	eruptive epoch 5
	Sc. le Torricelle		4	eruptive epoch 4
			I	*paleoshoreline I*
(U I)				
	Piano Grande (L1)	Le Puntazze (Ia)	3	eruptive epoch 3
		Bagno Secco	2	eruptive epoch 2
	Paleo-Lipari		1	eruptive epoch 1

Fig. 5 - Forni et al.

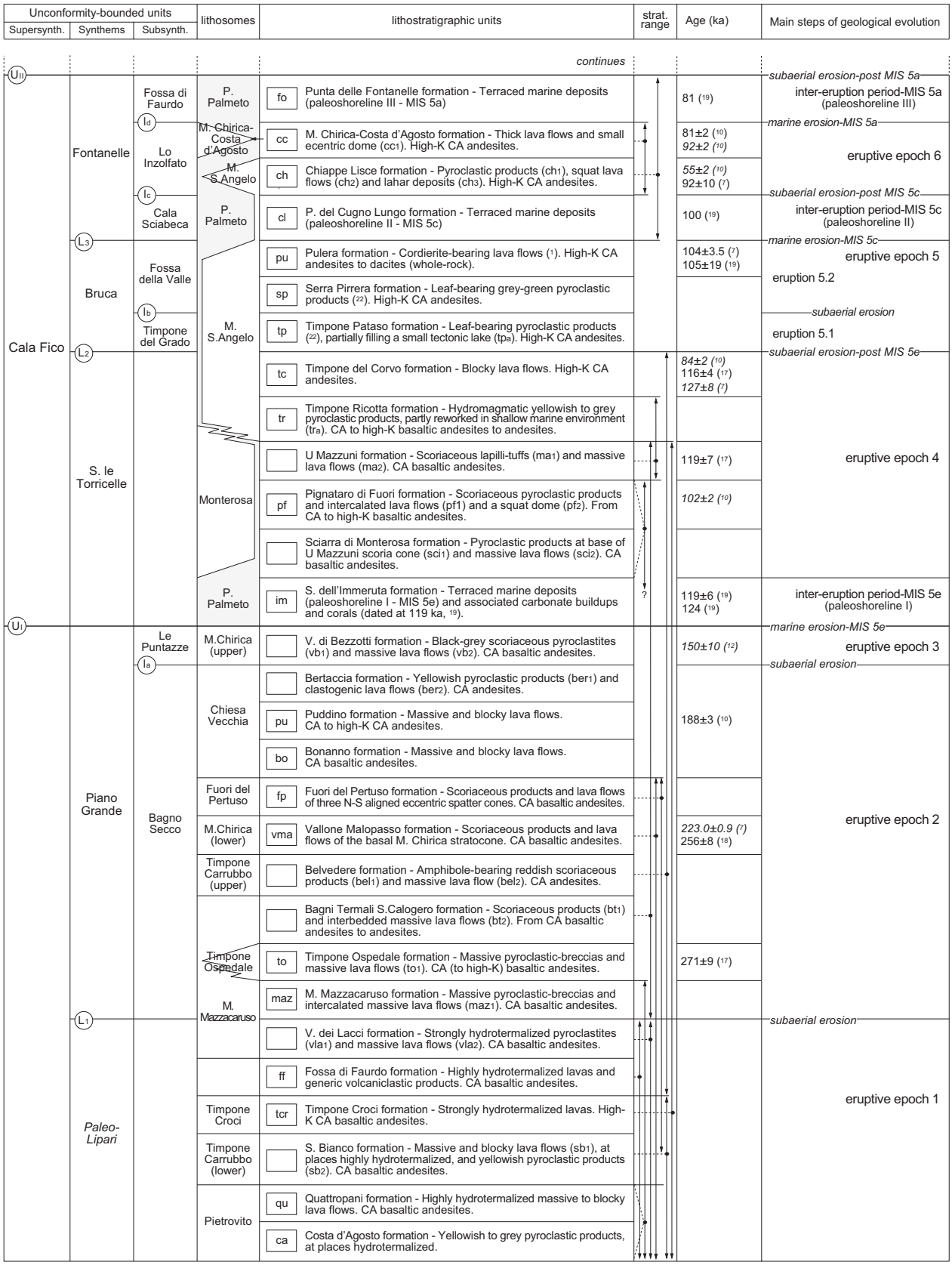

Fig. 6A - Forni et al.

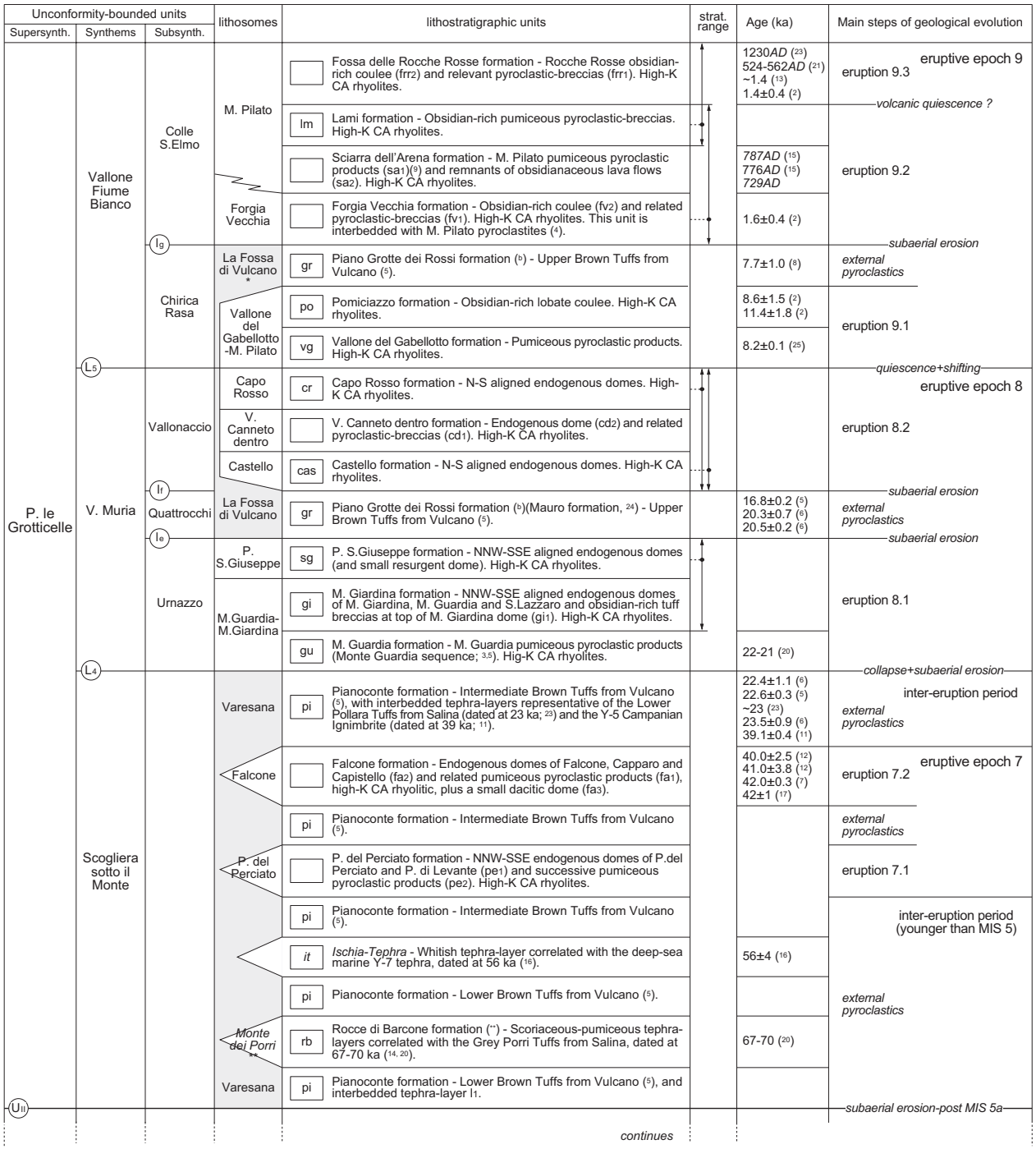

Fig 6B - Forni et al.

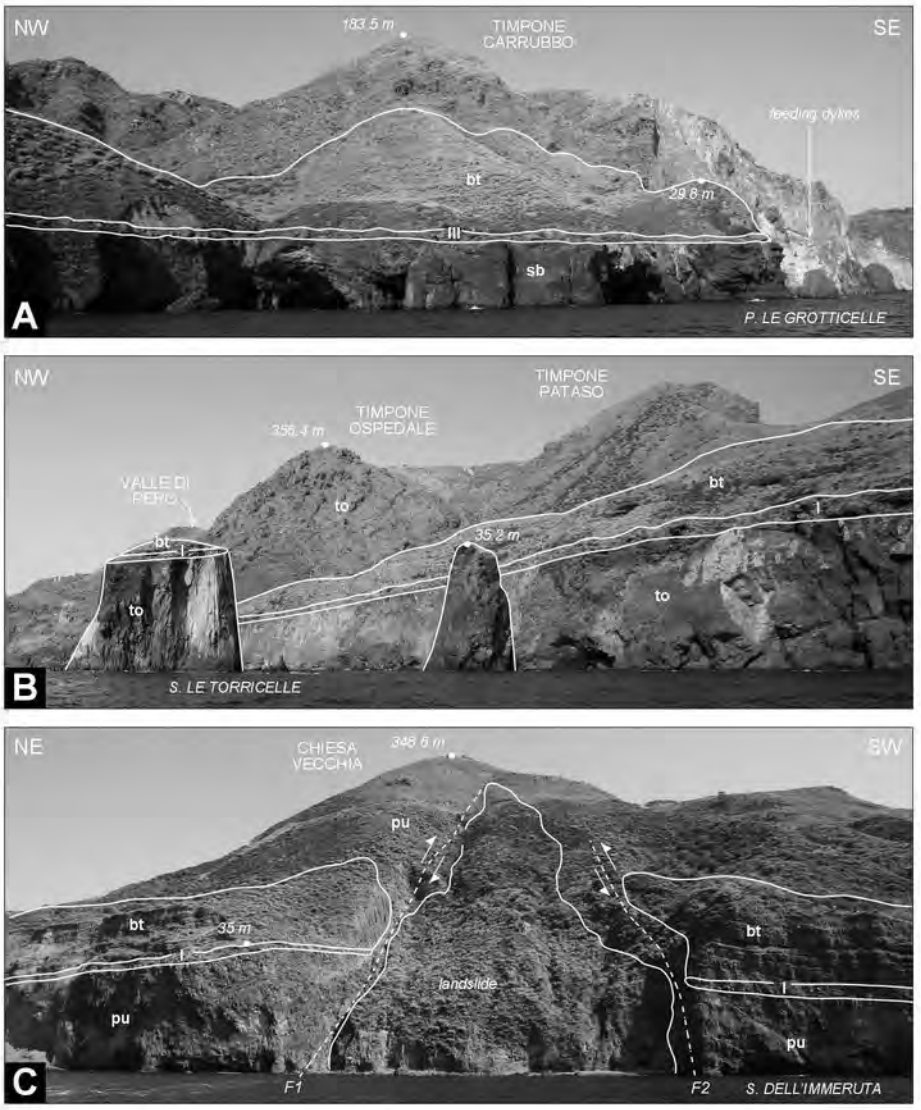

Fig. 7 - Forni et al.

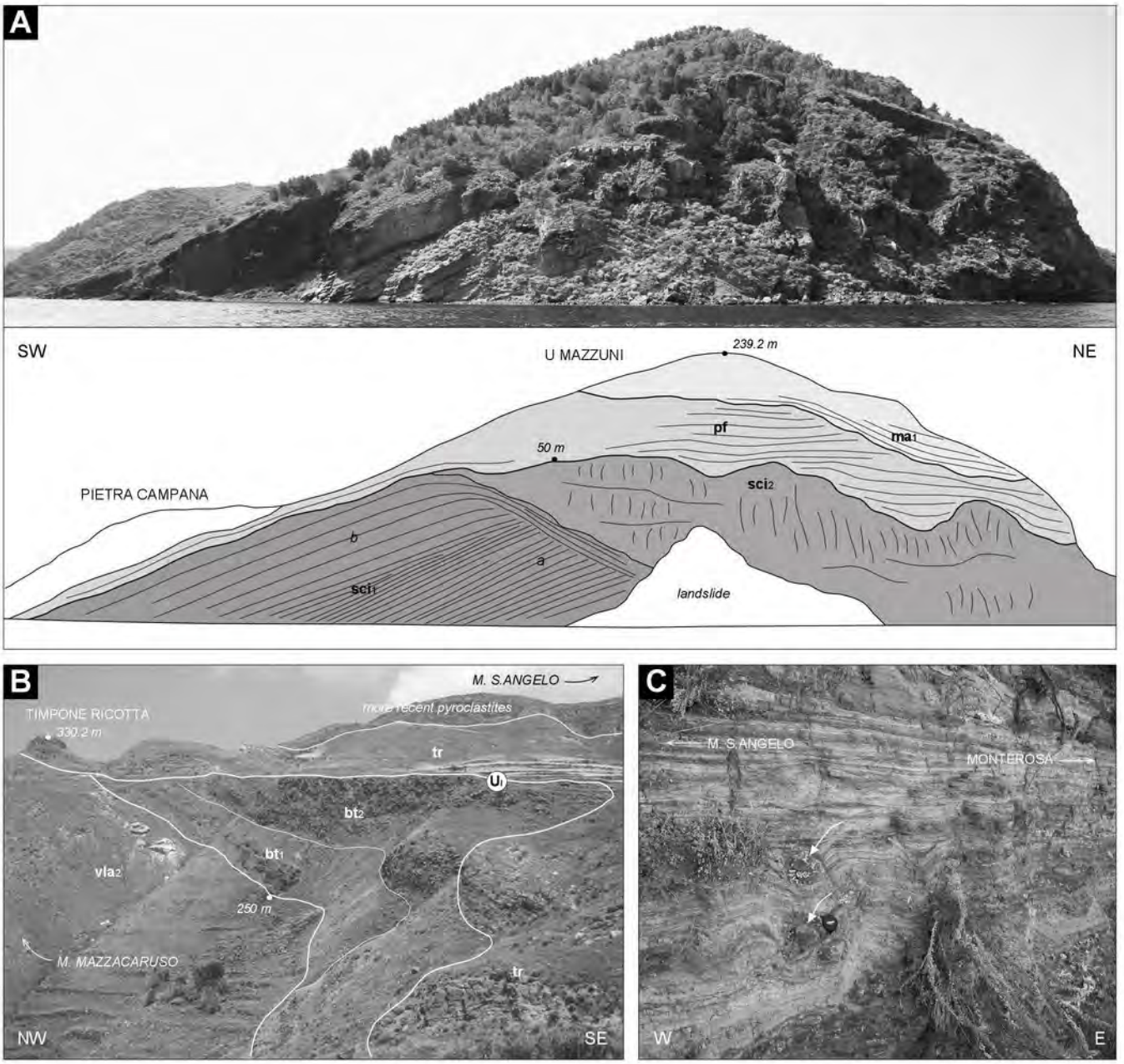

Fig. 8 - Forni et al.

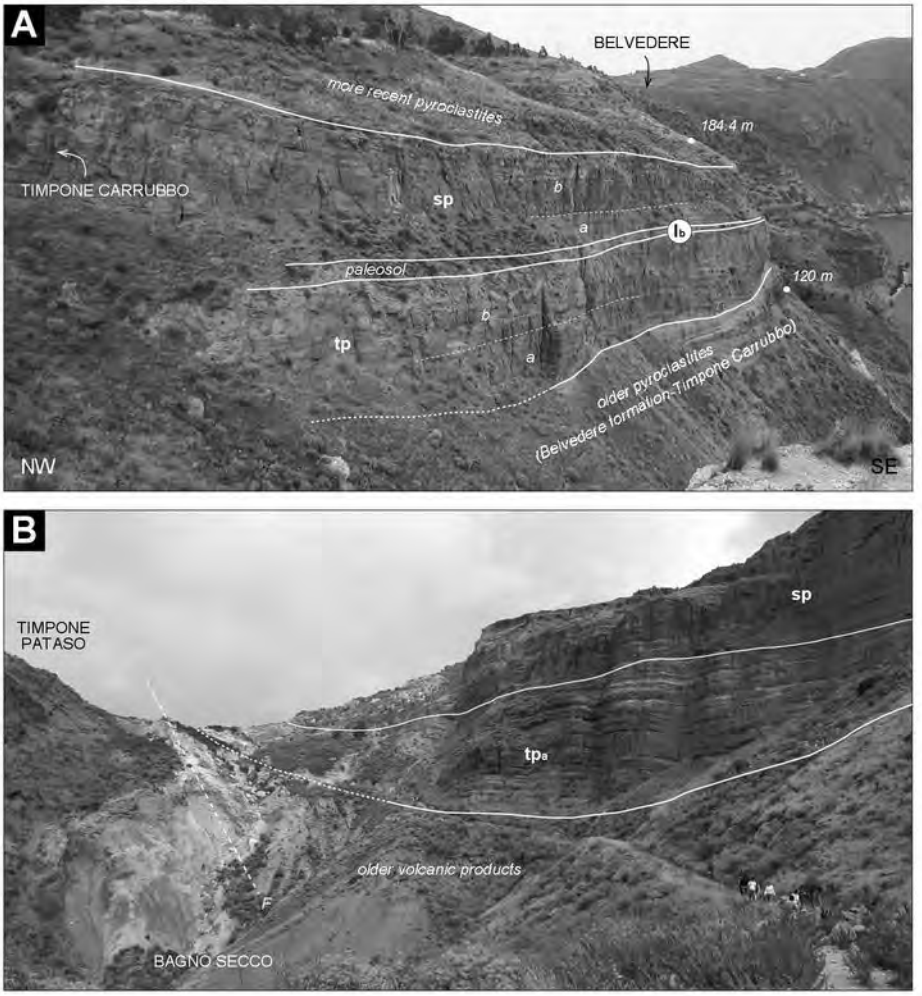

Fig. 9 - Forni et al.

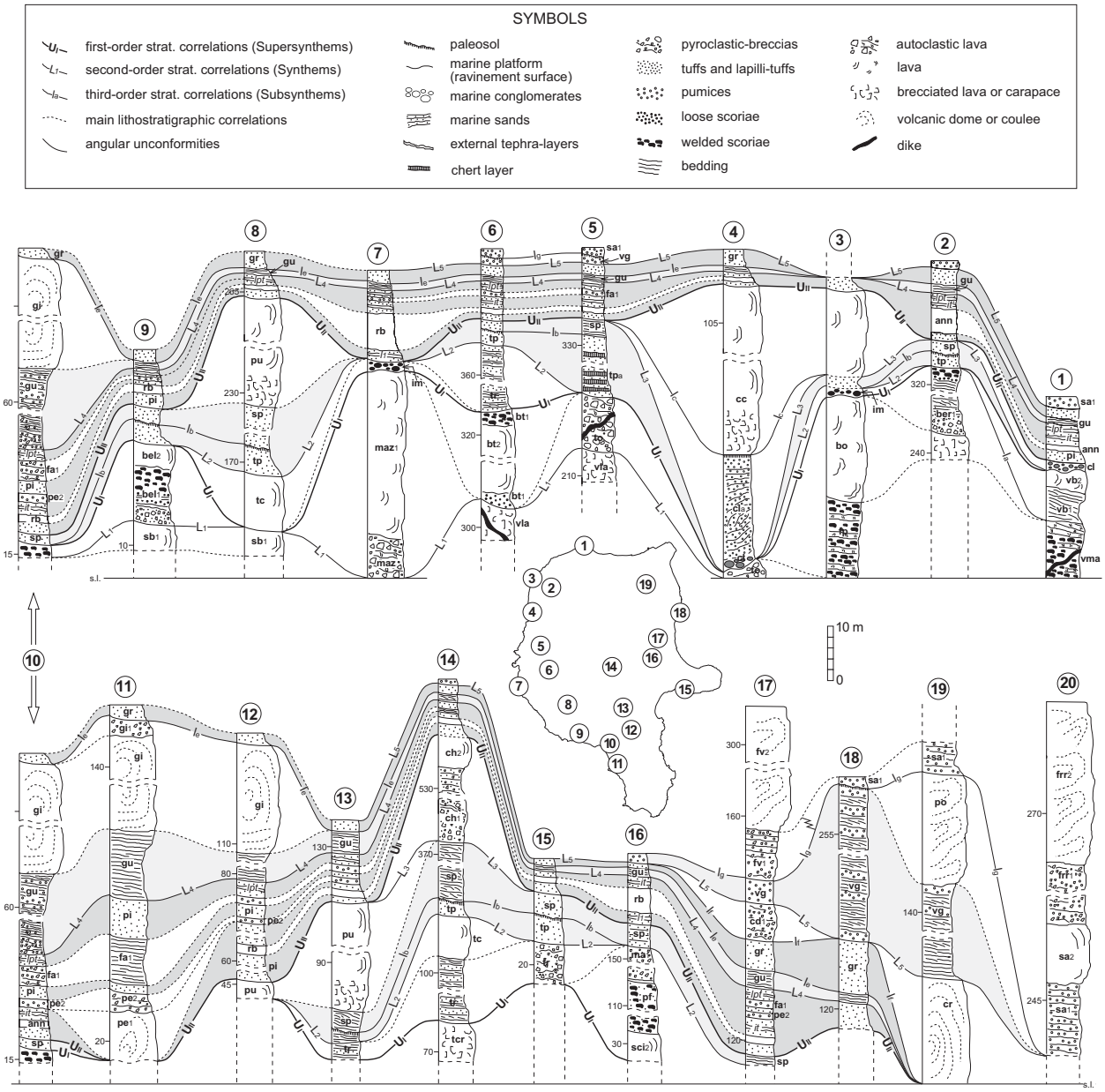

Fig. 10 - Forni et al.

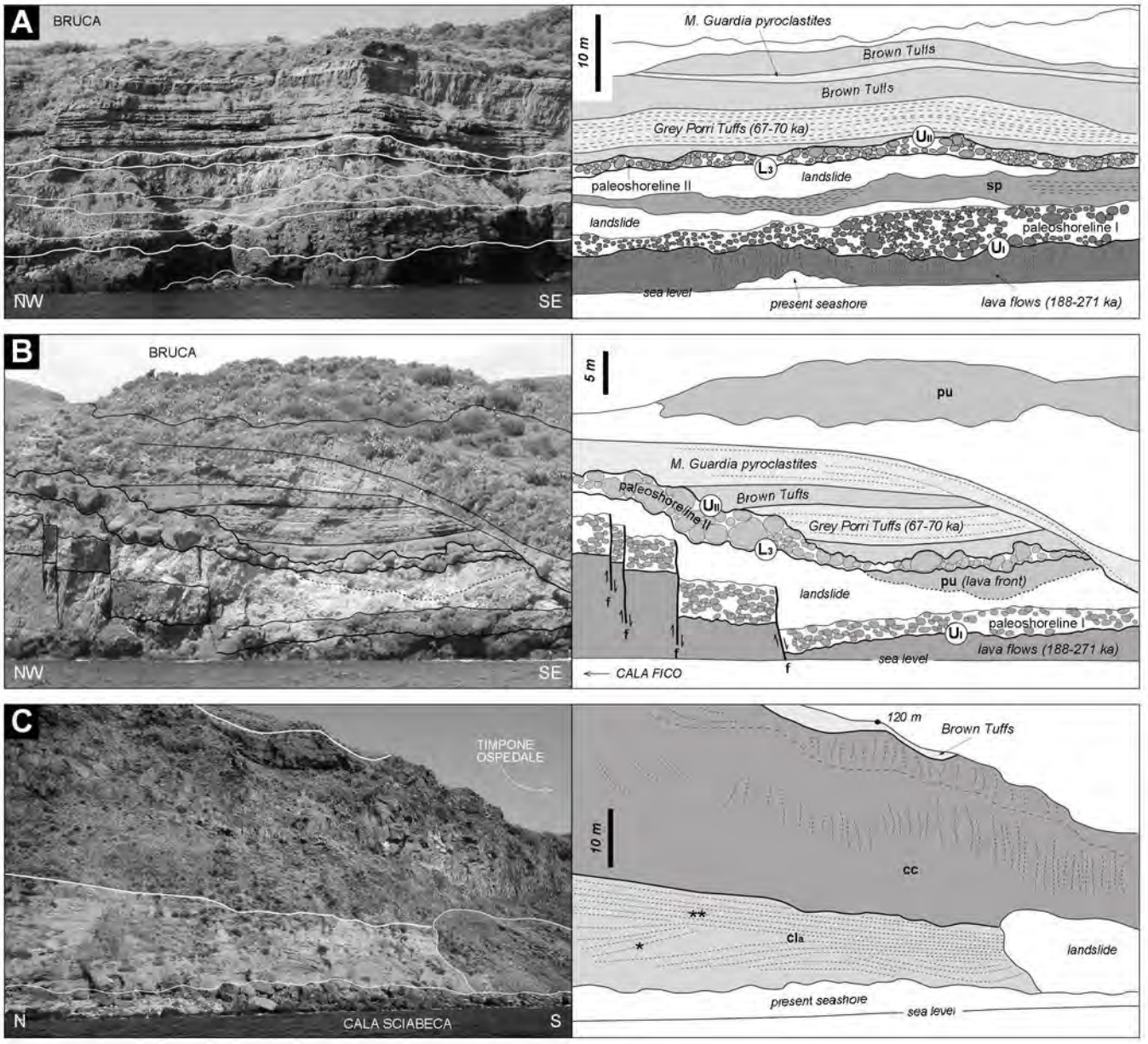

Fig. 11 - Forni et al.

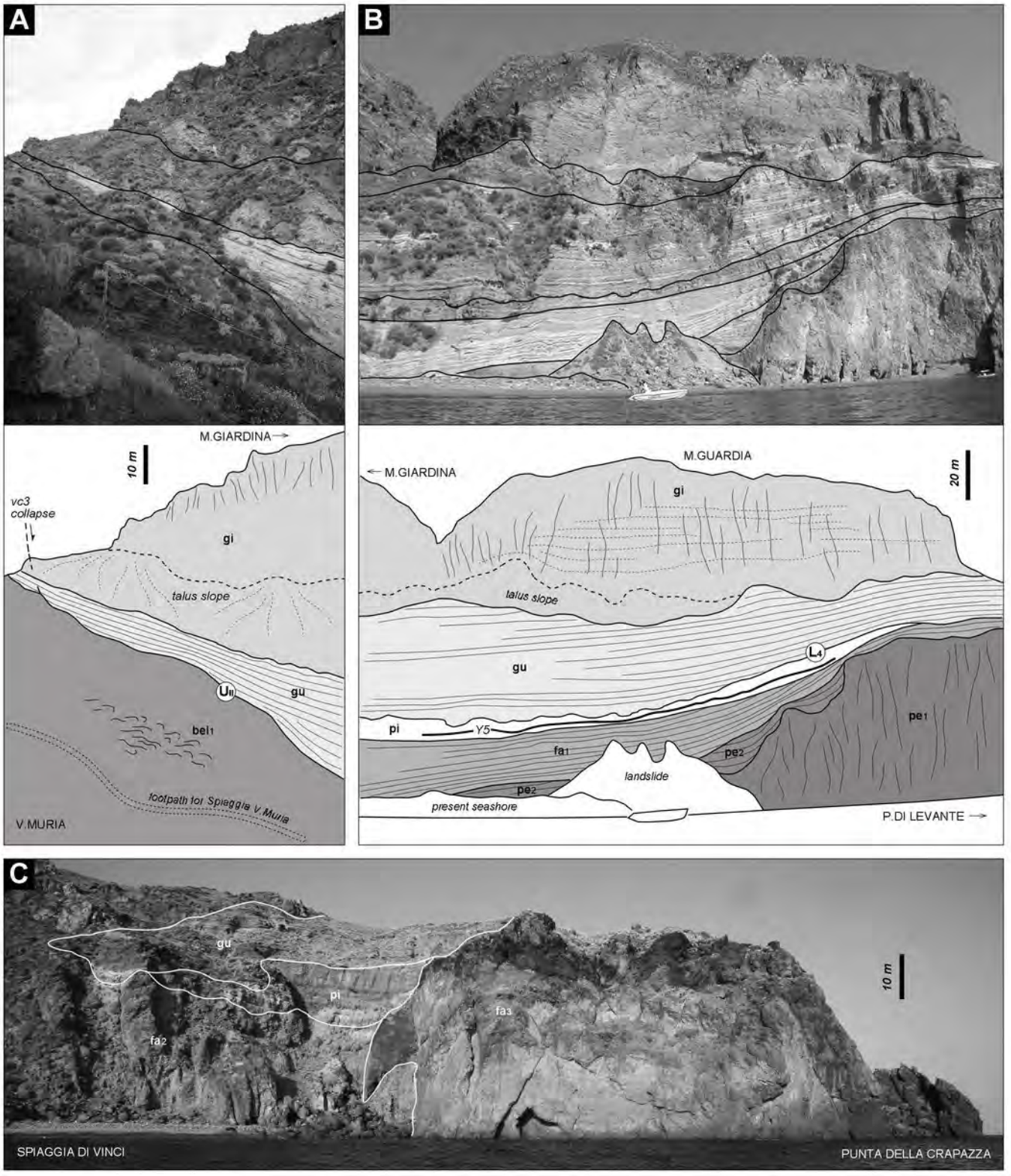

Fig. 12 - Forni et al.

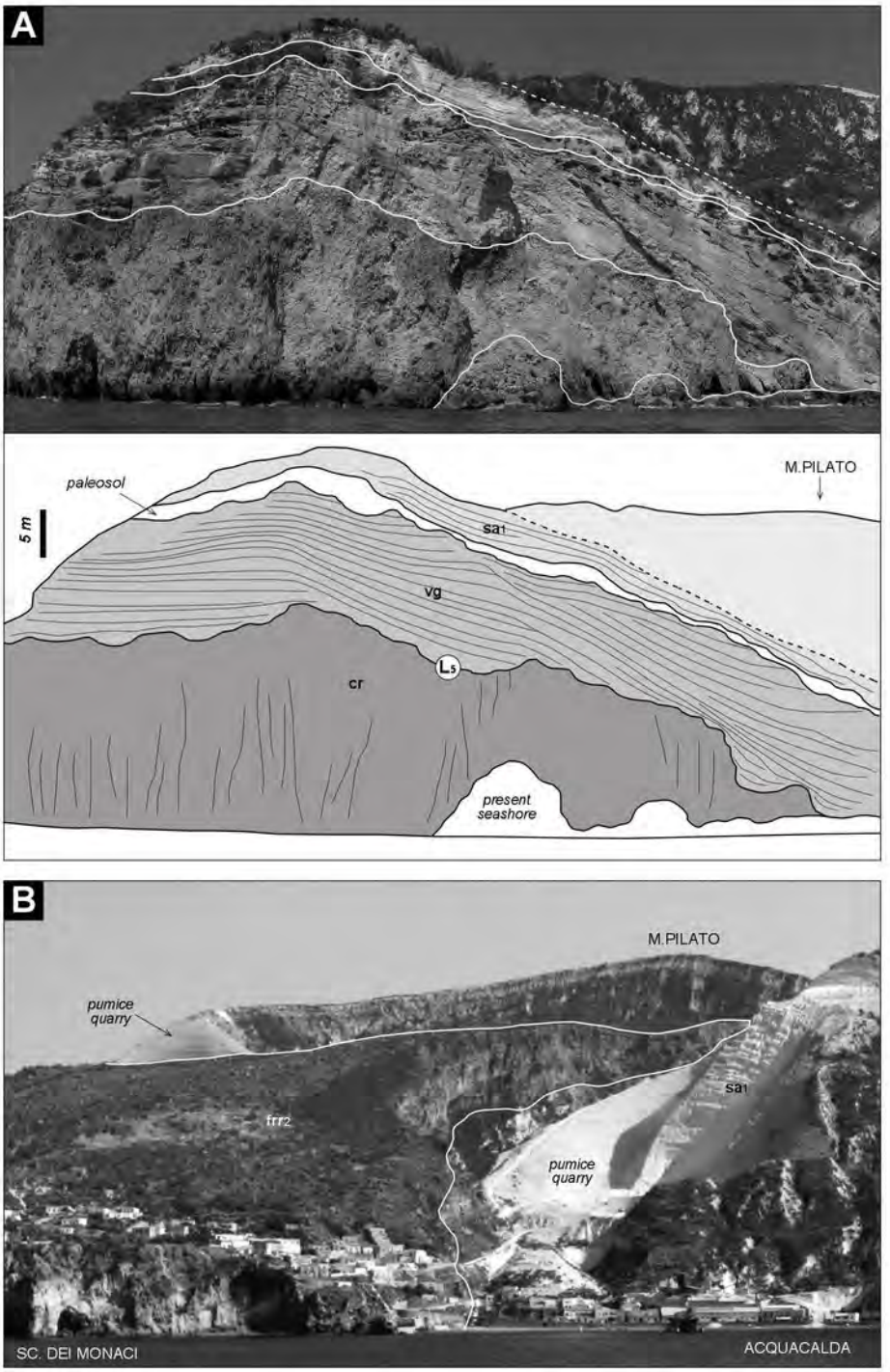

Fig. 13 - Forni et al.

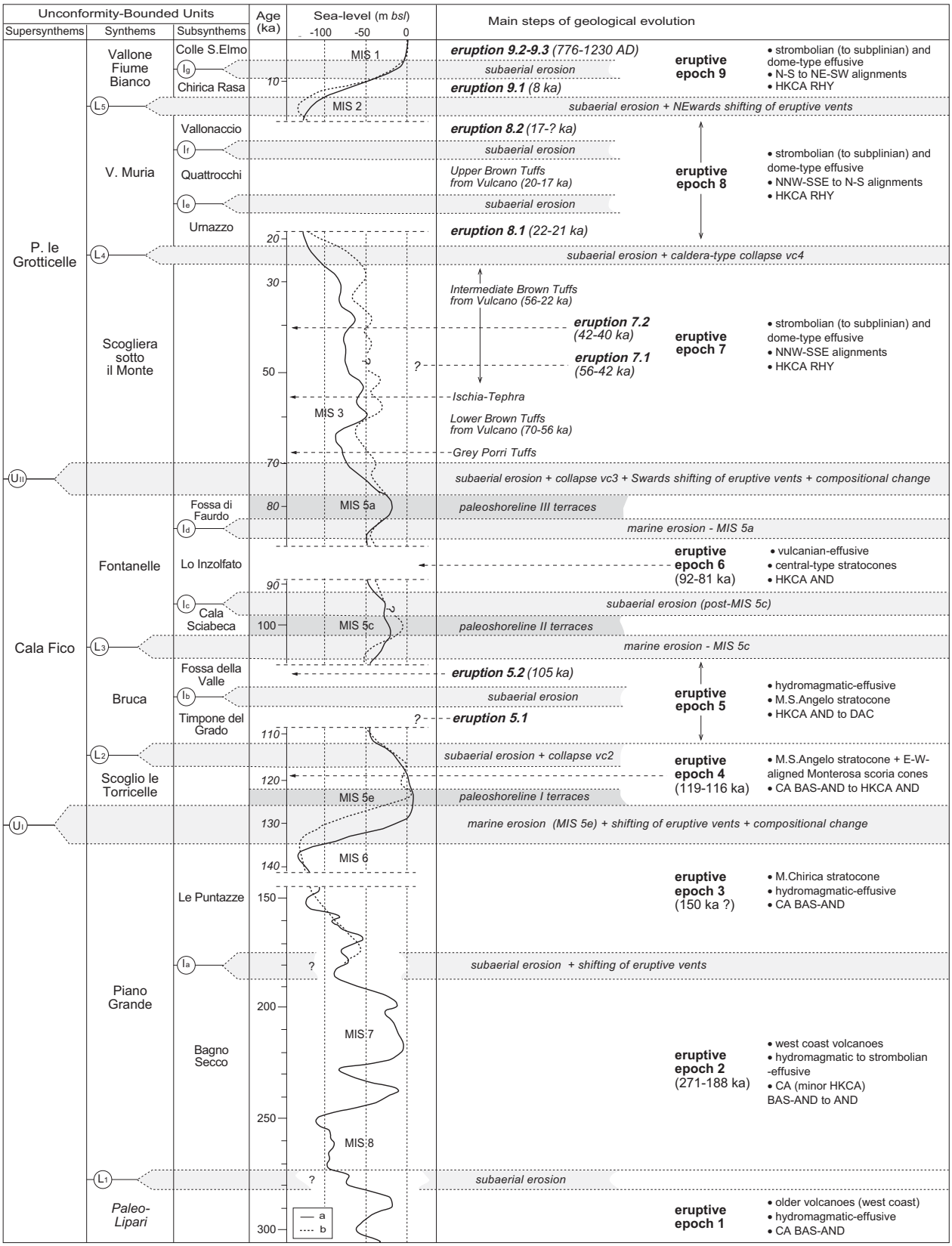

Fig. 14 - Forni et al.

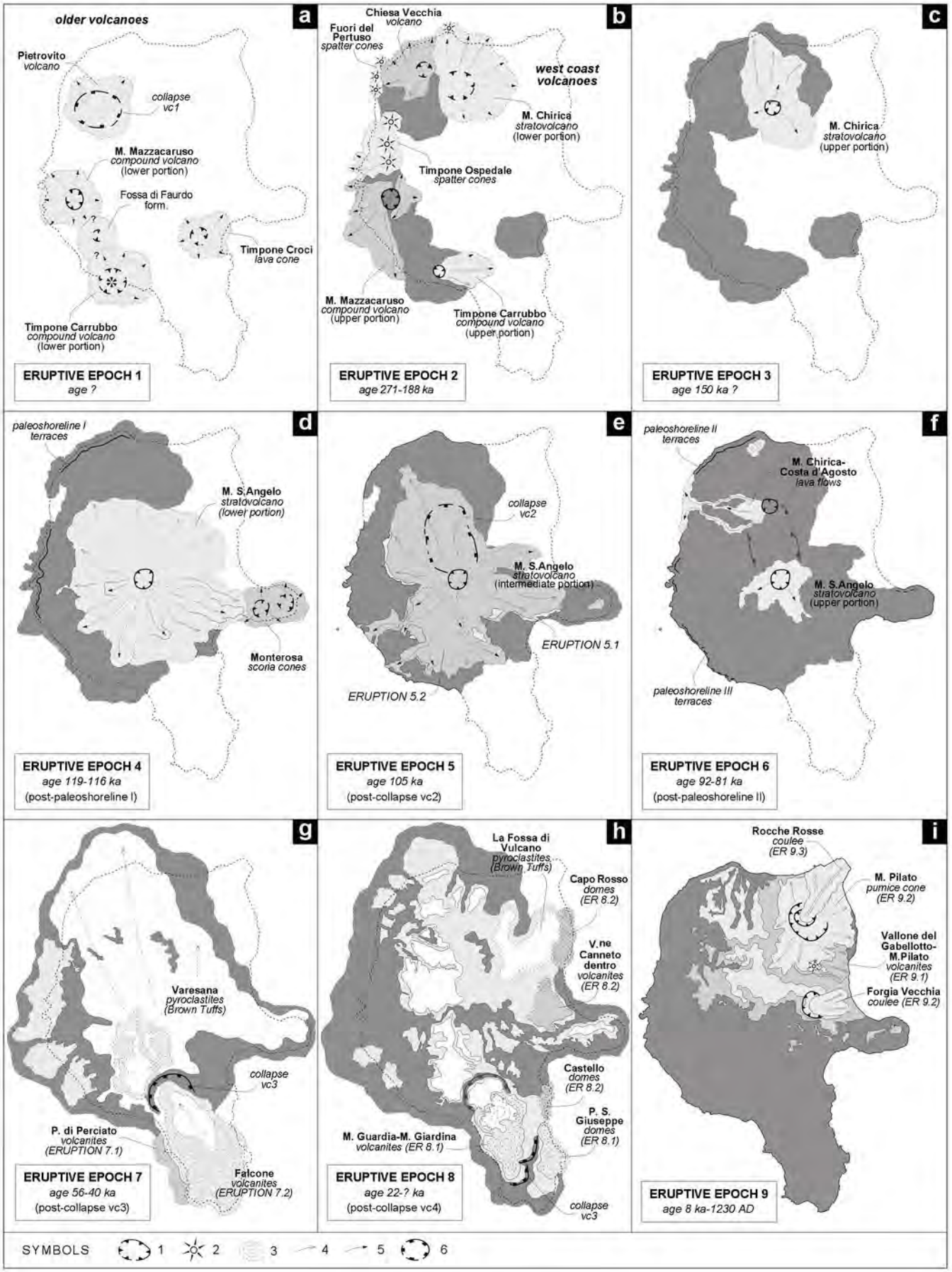

Fig. 15 - Forni et al.

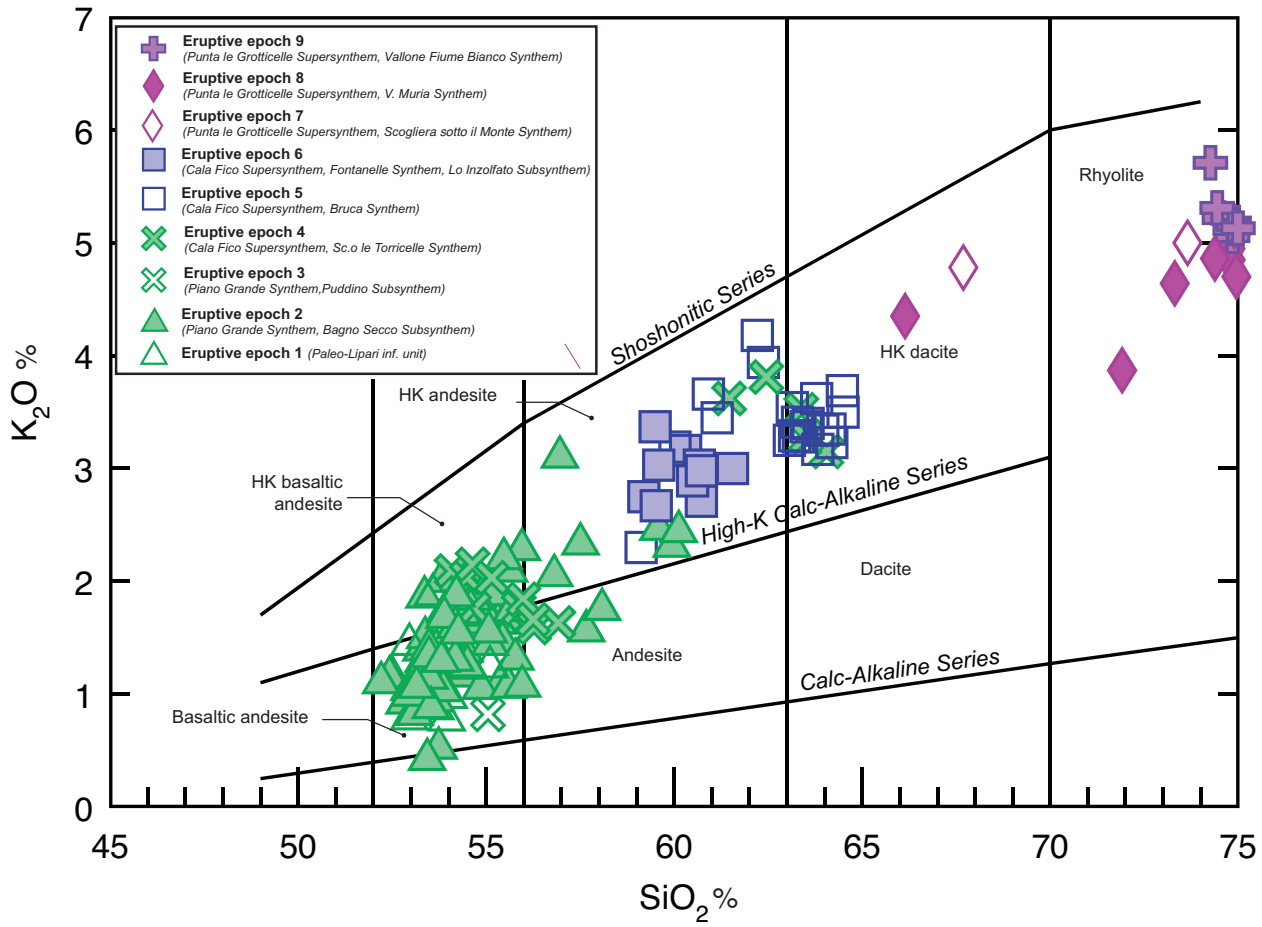

Fig. 16 - Forni et al.

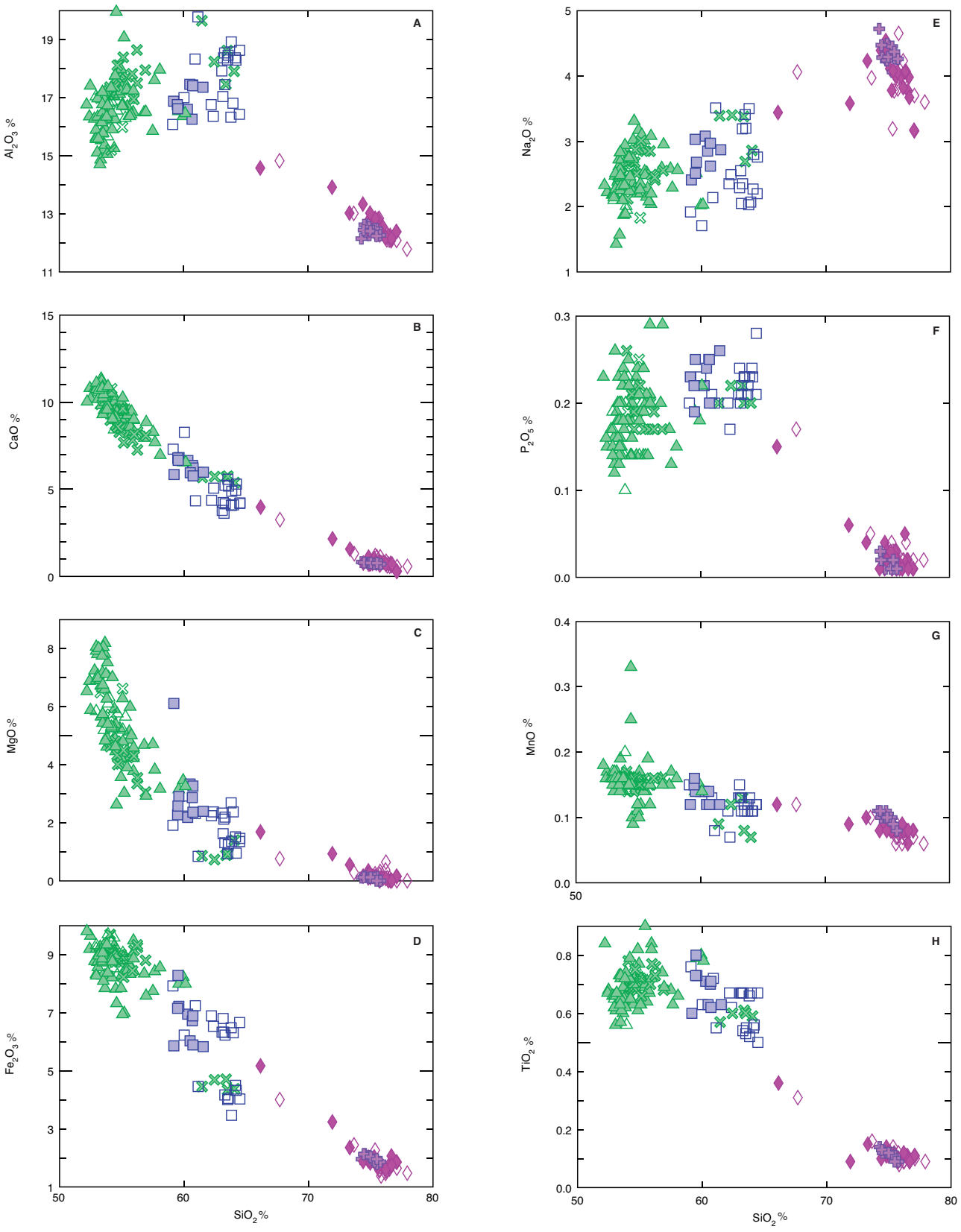

Fig. 17 - Forni et al.

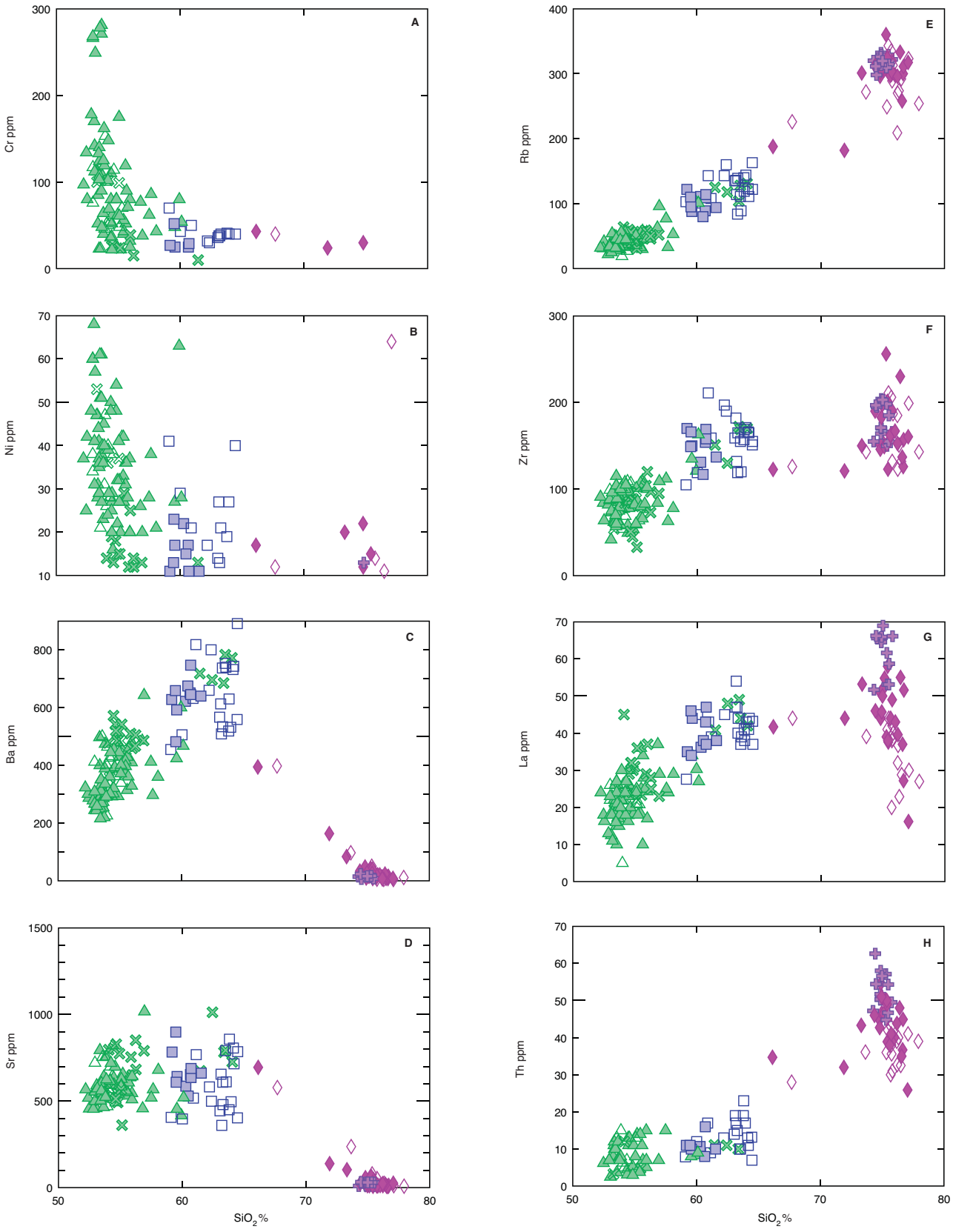

Fig. 18 - Forni et al.

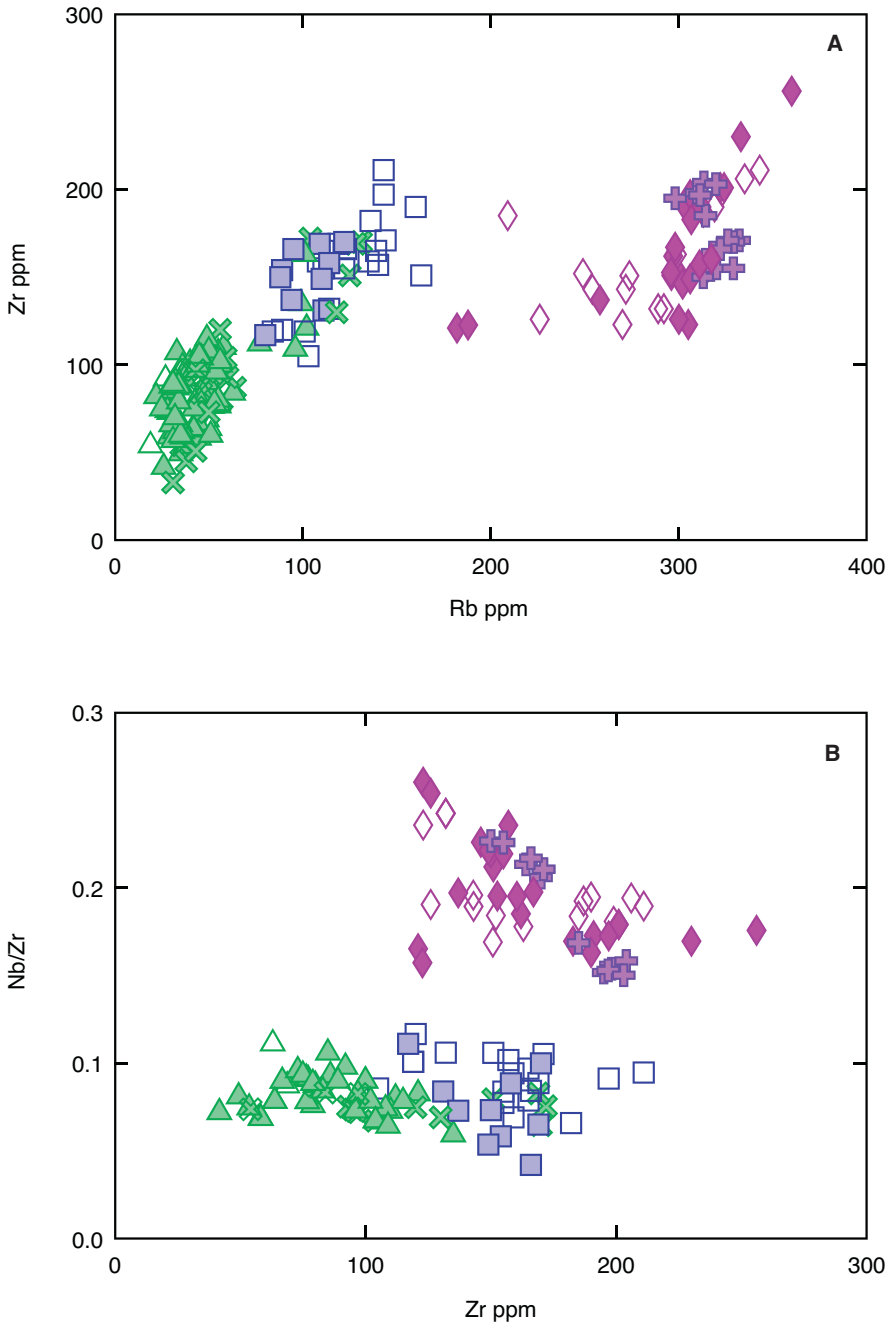

Fig. 19 - Forni et al.

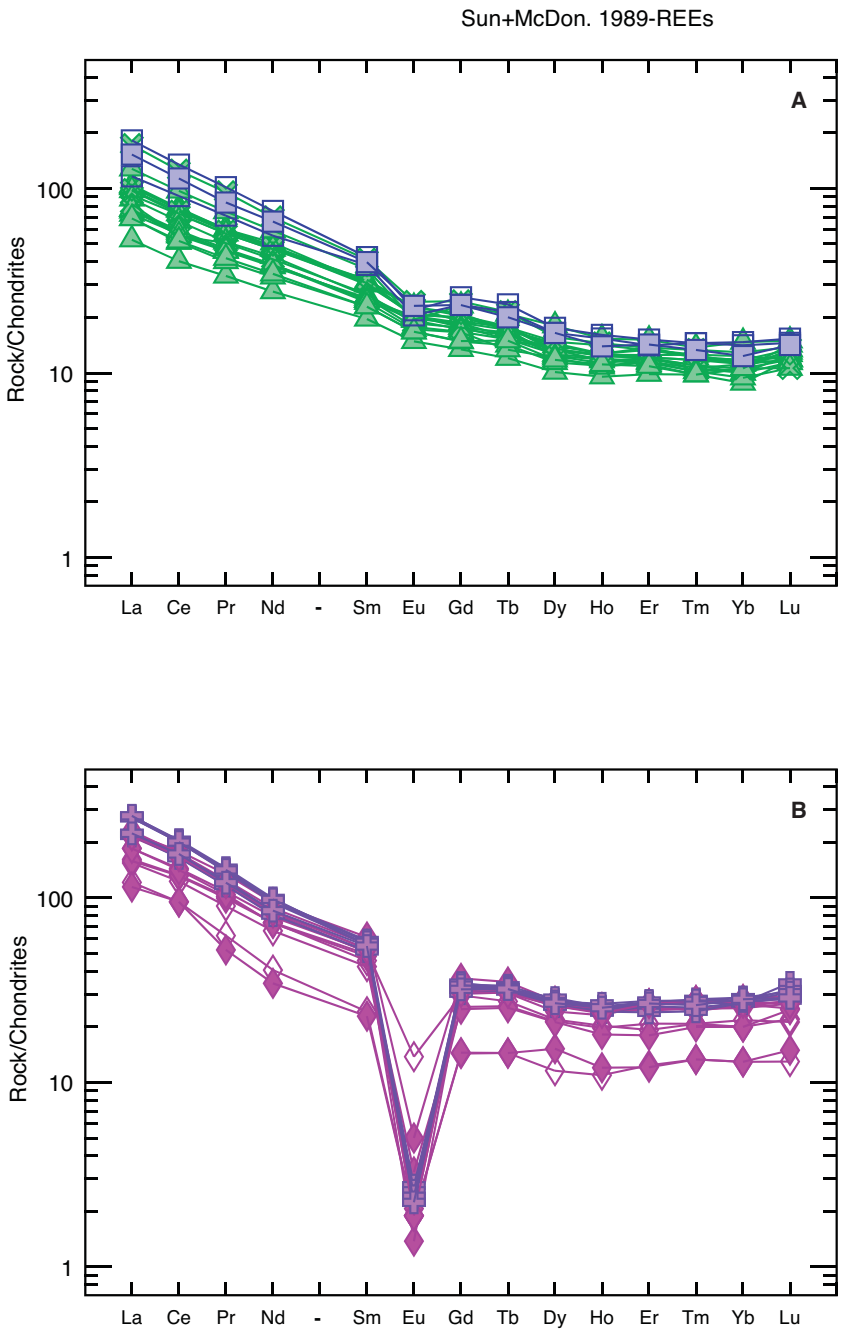

Fig. 20 - Forni et al.

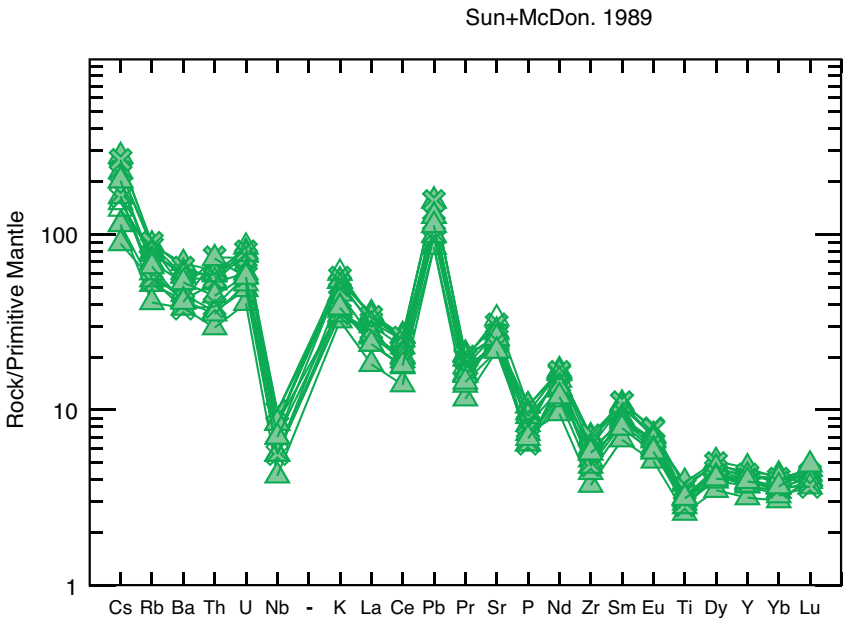

Fig. 21 - Forni et al.

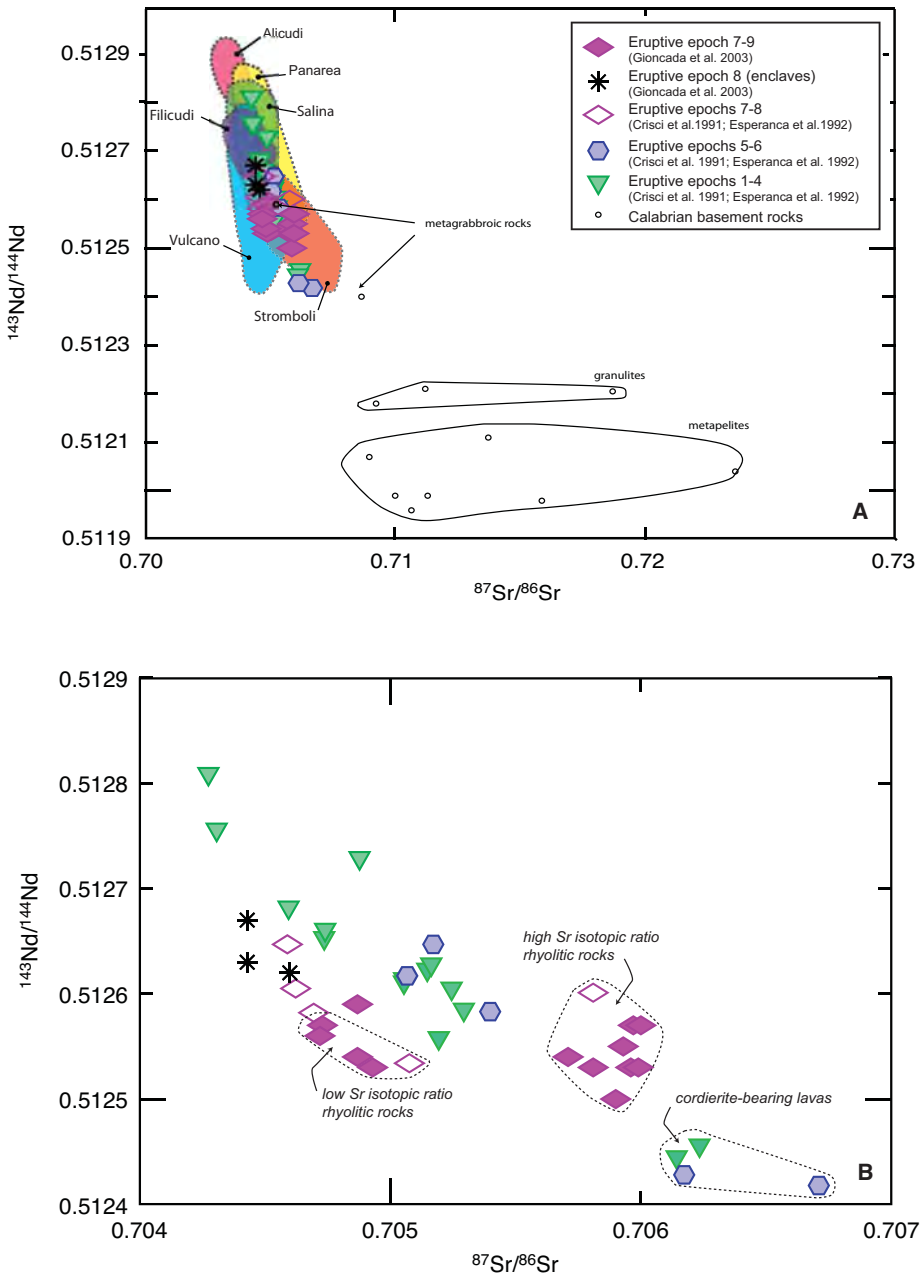

Fig. 22 - Forni et al.

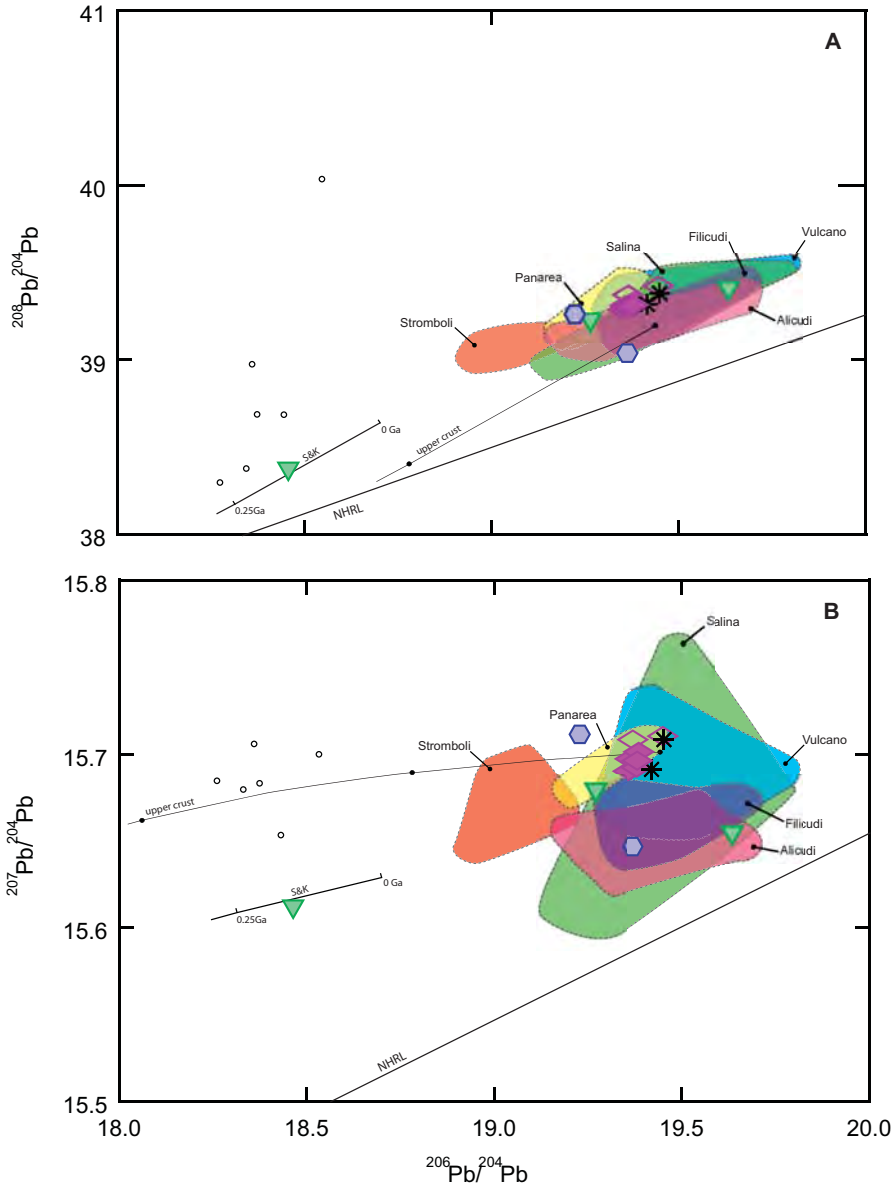

Fig. 23 - Forni et al.

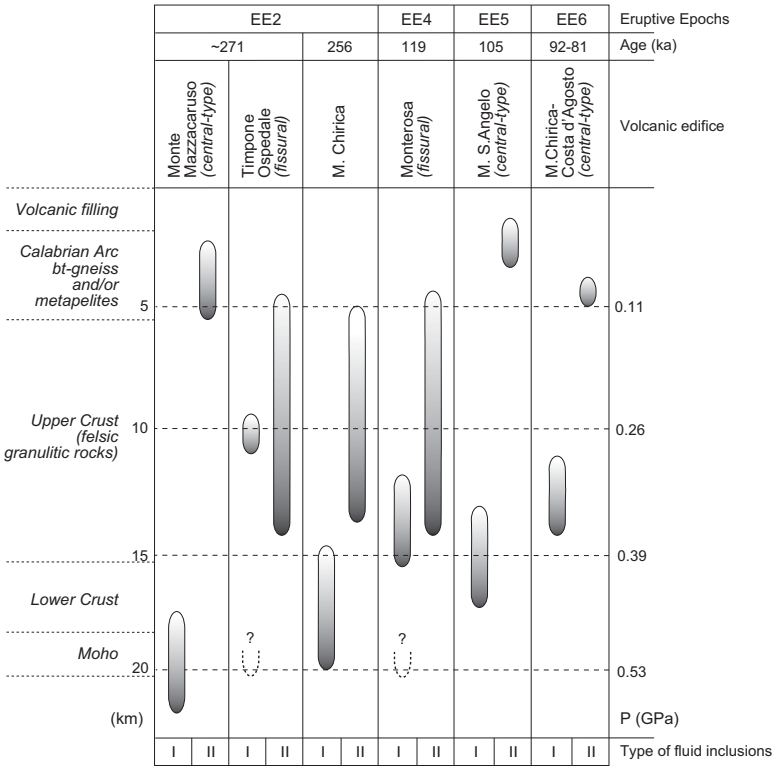

Fig. 24 - Forni et al.

Table 1 - Summary table of tephra-layers reported on Lipari Island (in stratigraphic order)

tephra	*field locality*	*description*	*thickness*	*chemistry*	*mineralogy*	*provenance*	*stratigraphic unit*	*age*
Lower Pollara Tuffs	widespread	poorly coherent, normal graded lapilli tuffs made up of black scoriae and yellowish pumices	30-45 cm	CA to high-K CA andesitic	cpx, amp, ol, opx	Pollara eruptive vent, Salina Island (Aeolian archipelago)	Punta Fontanelle formation	23 ka ([b])
Y-5	Capparo, P. di Levante (S Lipari)	whitish tuffs	few cms	trachy-phonolitic		Phlegrean Fields	"Campanian Ignimbrite"	39.1±0.4 ([c])
Y-7 Ischia-Tephra	western coast	whitish tuffs	up to 30 cm	trachytic	kf, bt, plg, cpx, ac, ti, zr	Ischia Island (Campanian area)	"Tufo Verde Epomeo"	56 ka ± 4 ([a])
Grey Porri Tuffs	widespread (central-western Lipari)	cf. Monte dei Porri, Rocce di Barcone formation	up to 6 m	CA basaltic andesitic to dacitic	opx, cpx, ol, amp	Monte dei Porri, Salina Island (Aeolian archipelago)	Rocce di Barcone formation	67-70 ka ([b])
I_1	V.ne dei Lacci (W Lipari)	medium bedded, normal graded, pumiceous lapilli tuffs	20 cm	CA andesitic	plg, cpx, bt, kf, lc	Monte dei Porri ?, Salina Island (Aeolian archipelago)	?	? (between 67-70 and 81 ka)

Age references: ([a]) Kraml et al., 1997; ([b]) Lucchi et al., 2008, and references therein; ([c]) De Vivo et al., 2001
Symbols - Mineralogy: kf=sanidine; plg=plagioclase; cpx=clinopyroxene; opx=orthopyroxene; bt=biotite; ol=olivine; amp=amphibole; ti=titanite; ac=acmite; zr=zircon.

Table 2 - Summary of unconformities on Lipari Island (in stratigraphic order)

	Rank	Areal extent	Descriptive features	Genetic processes	Time duration
I_g	3	NE sector of Lipari	Surface of subaerial erosion and angular discordance marked by a widespread red paleosol separating the Vallone del Gabellotto (age of 8 ka) and M. Pilato rhyolitic pyroclastites (776 *AD*), the latter included in the Sciarra dell'Arena formation	Volcanic quiescence	~7 ka (from 8 ka BP to 776 *AD*)
L_5	2	Lipari Island	Surface of subaerial erosion marked by the angular discordance between the Vallone del Gabellotto pyroclastites (age of 8 ka) and underlying products represented by rhyolitic domes and pyroclastites of the southern (and subordinately central) sector of Lipari and most of the Brown Tuffs.	Volcanic quiescence and Nwards shifting of eruptive vents (from the southern and central sectors to the NE area of Lipari)	? (>8 ka BP)
I_f	3	eastern strip of Lipari Island	Surface of subaerial erosion and angular discordance between N-S-aligned domes of V.ne Canneto dentro, Castello and Capo Rosso and underlying Upper Brown Tuffs (17-20 ka)	Volcanic quiescence and shifting of eruptive vents (towards N-S fractures along the eastern strip of Lipari Island)	? (<17 ka BP)
I_e	3	S sector of Lipari Island	Surface of subaerial erosion and angular discordance between the Upper Brown Tuffs (17-20 ka) and underlying domes and pyroclastites of M.Guardia and P. S.Giuseppe (dated at between 22-21 ka)	Volcanic quiescence	~1 ka (from 22-21 to 20 ka BP)
L_4	2	S sector of Lipari Island	Surface of subaerial erosion associated to volcano-tectonic collapse vc4, exposed in the S sector of Lipari. The unconformity is marked by the high-angle angular discordance between domes and pyroclastites of M.Guardia and P. S.Giuseppe (dated at between 22-21 ka) and underlying products represented by the older Falcone and P. di Perciato volcanites (42-40 ka) and Lower-Intermediate Brown Tuffs (22-70 ka)	Volcanic quiescence	<1 ka (from 22 to 22-21 ka BP)
U_{II}	1	Aeolian archipelago	Surface of subaerial erosion demonstrated by lithological change and angular discordance between MIS 5 terraced marine deposits and overlying products represented by 70-ka-old Brown Tuffs and rhyolitic domes-pyroclastites in the southern sector of Lipari	Subaerial erosion during sea-level fall at the end of MIS 5a (<81 ka) up to renewal of rhyolitic volcanism in the southern (and northern) sector of Lipari	~10 ka (from 81 to 70 ka BP)
I_d	3	limited sectors of Lipari	Ravinement surface at base of MIS 5a terraced marine deposits (paleoshoreline III) demonstrated by the cross-cutting relations between marine terraces attributed to MIS 5a (paleoshoreline III) and MIS 5c (paleoshoreline II)	Marine erosion during MIS 5a transgression (from 87 to 81 ka BP)	~6 ka
I_c	3	W coastal sector of Lipari	Surface of subaerial erosion marked by the sharp lithological change between MIS 5 terraced marine deposits (paleoshoreline II) and overlying lavas of M.Chirica-Costa d'Agosto (92-81 ka)	Subaerial erosion during sea-level falling at the end of MIS 5c (<100 ka) up to renewal of volcanic activity	~8 ka (from 100 to 92 ka BP)
L_3	2	most of the Aeolian archipelago	Ravinement surface at base of MIS 5c terraced marine deposits (paleoshoreline II), overcutting leaf-bearing pyroclastites (*i.e.,* Serra Pirrera formation) and 104-105 ka-old cordierite-bearing lavas (*i.e.,* Pulera formation) from the M. S.Angelo volcano	Marine erosion during MIS 5c transgression (from 105 to 100 ka BP)	~5 ka (from 105 to 100 ka BP)
I_b	3	wide sectors of Lipari	Surface of subaerial erosion and angular discordance marked by a widespread red paleosol separating the older (*i.e.,* Timpone Pataso formation) and younger (*i.e.,* Serra Pirrera formation) horizons of leaf-bearing pyroclastites from the M. S.Angelo volcano	Volcanic quiescence	?
L_2	2	Lipari Island	Surface of subaerial erosion at top of MIS 5e terraced marine deposits (paleoshoreline I) and volcanites of the M. S.Angelo volcano-lower portion and Monterosa scoria cones. The unconformity is sealed by the widespread leaf-bearing pyroclastites and cordierite-bearing lavas relevant to the M. S.Angelo volcano-intermediate portion	Volcanic quiescence developed mostly during sea-level falling at the end of MIS 5e (<118 ka)	~13 ka (from 118 to 105 ka BP)
U_I	1	Aeolian archipelago	Ravinement surface at base of MIS 5e terraced marine deposits (paleoshoreline I) sitting on volcanites dated at 127-256 ka. Away from coastal areas, the unconformity is represented by the surface of subaerial erosion formed during contemporaneous volcanic quiescence	Marine erosion during the 130 m sea-level rise at the onset of MIS 5e (from 130 to 124 ka BP) *plus* volcanic quiescence	
I_a	3	northern Lipari Island	Surface of subaerial erosion and angular discordance between volcanites relevant to the upper portion of M. Chirica volcano (~150 ka) and underlying volcanic products related to the western volcanoes (dated at between 271 and 188 ka)	Volcanic quiescence and Nwards shifting of eruptive vents from the western coast to the northern sector of Lipari	~30 ka (from 188 to 150 ka BP)
L_1	2	western Lipari Island	Surface of subaerial erosion and angular discordance developed between Paleo-Lipari volcanoes and overlying products related to more recent volcanoes along the western coast of Lipari (dated at 271-188 ka)	Volcanic quiescence	? (>271 ka BP)

Notes - Unconformities U_I, L_3, and U_{II} are widely correlated to most of the Aeolian archipelago (cfr. Lucchi et al., 2011).

Table 3 - List of lithostratigraphic units introduced at Lipari (cf. stratigraphy of Fig. 6). Map labels are in bold letters

UNIT	*LITHOLOGIC PROPERTIES*	*INTERPRETATION*	*PETROCHEM.*	*AGE (ka)*
PALEO-LIPARI INFORMAL UNIT				
Pietrovito lithosome				
Costa d'Agosto formation (ca)	Thinly bedded, planar stratified yellow lapilli-tuffs alternating with massive grey tuffs (with lithic-rich pyroclastic breccias at the base), in places highly hydrotermalized (60 m thick). They crop out at an oblique angle to the slope of Quattropani-Costa d'Agosto (N Lipari).	Hydromagmatic dilute PDC eruption units of the Pietrovito tuff cone.	CA AND	
Quattropani formation (qu)	Massive and brecciated lava flows cropping out in the sector of Bonanno. They are intensely hydrotermalized with only few remnants of the original lava products.	Effusive activity of the Pietrovito volcano.	CA BAS-AND	
Timpone Carrubbo lithosome (lower portion)				
Sc.° Bianco formation				
sb_1 member	M-thick, massive to blocky lava flows interbedded with thickly bedded, normal graded scoriaceous tuff-breccias. A 15 m-thick succession of thin lava flows is reported near Sc.° Bianco. A squat lava dome (15 m large) with onion-type foliation crops out near Timpone Carrubbo. These products are frequently hydrotermalized to kaolin-rich varicoloured deposits (*e.g.* at Timpone Carrubbo). Near P. le Grotticelle, the unit is cut by several subvertical feeding dykes (*i.e.,* crater area).	Effusive activity and strombolian fallout eruption units.	CA BAS-AND	
sb_2 member	Yellowish pyroclastics (45 m thick) exposed along the SW coastal cliff of Sc.° Bianco, interbedded with the sb_1 member. They consist of thickly and planar bedded tuff-breccias, upwards passing to thinly bedded, planar and cross-stratified lapilli-tuffs. Highly hydrotermalized near Sp. Valle Muria.	Hydromagmatic dilute PDC eruption units.		
Timpone Croci formation (tcr) (=lithosome)	Massive and brecciated lavas exposed in correspondence of the Timpone Croci relief, central Lipari. They are pervasively hydrotermalized and eroded (with only rare traces of the original lava lithotypes).	Effusive activity.	High-K CA BAS-AND	
Fossa di Faurdo formation (ff)	Massive and brecciated lavas, with minor generic volcaniclastic products, exposed in the area of Fossa di Faurdo, central-western Lipari. They are characterized by intense hydrotermalization with only few remnants of the original lithotypes.	Generic effusive activity (minor explosive) of an undefined vent	CA BAS-AND	
M. Mazzacaruso lithosome				
Vallone dei Lacci formation				
vla_1 member	Intensely hydrotermalized, medium bedded, planar stratified lapilli-tuffs (20 m thick), with interbedded layers of loose, poorly sorted scoriaceus lapillit-tuffs (i), exposed along the V. dei Lacci gorge, W Lipari.	Dilute PDC (i=strombolian fallout) eruption units		
vla_2 member	Massive and blocky lava flows cropping out between V. dei Lacci and Bagno Secco. Hydrotermalization is very intense, frequently giving rise to kaolin-rich brecciated rocks.	Effusive activity	CA BAS-AND	
PIANO GRANDE SYNTHEM - BAGNO SECCO SUBSYNTHEM				
M. Mazzacaruso lithosome				
M.Mazzacaruso formation (maz)	Thickly bedded, massive pyroclastic-breccias composed of matrix-supported, subrounded to angular, poorly vesiculated lava clasts and less scoriae. Thin lava flows (<1 m thick) are discontinuously interbedded, together with layers of loose scoriaceous lapilli-tuffs or thinly bedded, planar- to cross-laminated lapilli-tuffs (i). These products are found along the W flanks of M.Mazzacaruso volcano and in the coastal sector between Punta delle Fontanelle and Punta Palmeto, cropping out also in corrispondence of the Pietra del Bagno isolated rock. Thick (35 m) massive lava flows with foliation and jointing crop out along the coastal cliff at P. del Cugno Lungo and Cala Fico (**maz_1 member**).	Hawaiian-strombolian fallout and effusive activity (see the text), (i=hydromagmatic dilute PDC eruption units)	CA BAS-AND, very porphyritic (mm-sized plg and cpx)	
Bagni Termali S.Calogero formation	Two thick (25 m) massive lava flows with discontinuous basal carapace and well developed columnar joints (**bt_2 member**) exposed near Timpone Ricotta. These lavas are interbedded with thickly bedded, well sorted, loose scoriaceous tuff-breccias and lapilli-tuffs passing upwards to very thickly bedded, poorly sorted, welded scoriaceous pyroclastic-breccias (**bt_1 member**). Dm- to m-thick layers of thinly bedded lapilli-tuffs with bomb sags are visible in places (i).	Effusive activity and strombolian-hawaiian fallout eruption units (i=hydromagmatic dilute PDC eruption units).	CA BAS-AND to AND	
Timpone Ospedale formation (to) (=lithosome)	Volcanics comparable to the M. Mazzacaruso formation building up the N-S aligned cones of Timpone Pataso, Timpone Ospedale and Valle di Pero. Thick (30 m), massive and columnar jointed lava flows crop out along the coastal cliffs at Sc.° le Torricelle and P. Palmeto (**to_1 member**). The unit is cut by several dykes between Timpone Pataso and Timpone Ospedale.	Fissural-type hawaiian-strombolian and effusive activity (i=minor dilute PDC eruption units).	CA (minor high-K) BAS-AND, poorly porphyritic	271±9 [18]
Timpone Carrubbo lithosome				
Belvedere formation				
bel_1 member	Poorly sorted, lithic-rich (with few rounded boulders) massive, welded scoriaceous pyroclastic-breccias gradually upward passing to widely distributed, poorly sorted, non-coherent, thickly bedded scoriaceous tuff-breccias. A bed of thinly bedded lapilli-tuffs with bomb-sags is present at the base, in near-vent areas.	Strombolian fallout deposits (hydromagmatic PDC eruption units at the base).	CA AND, highly porphyritic (mm-size amp)	
bel_2 member	Massive, 10 m-thick lava flow with evident blocky carapaces and diffused jointing	Effusive activity		
M. Chirica lithosome (lower portion)				
Vallone Malopasso formation (vma)	Massive lava flows (2.5 m) alternating with thick layers of well sorted, welded to loose scoriaceous lapilli-tuffs exposed along the deep valleys on the N flanks of M. Chirica (70-80 m thick). Thicker massive lava flows (10 m thick) are present in places (at the outlet of Vallone Malopasso). Near P. del Legno Nero, welded scoriaceous pyroclastic-breccias and a succession of dm-thick massive lava flows are visible.	Alternating effusive activity and strombolian-hawaiian fallout eruption units.	CA BAS-AND	256±8 [19] *223.0±0.9* [7]
Fuori del Pertuso formation (fp) (=lithosome)	Massive lava flows (2 m) alternating with thick layers of well-sorted scoriaceous lapilli and blocks building up three N-S aligned spatter cones exposed on the lowermost portion of the NW coastal cliff. Scoriaceous products are characterized by decreasing degree of welding from near-vent areas (poorly stratified spatter agglomerates) to distal areas (loose scoriaceous lapilli-tuffs).	Alternating lava flow and strombolian-hawaiian fallout eruption units	CA BAS-AND	
Chiesa Vecchia lithosome				

Bonanno formation (pt)	Massive and blocky lava flows (up to 25 m thick along the coastl cliff) cropping out in the sector of Bonanno-Bertaccia.	Generic effusive activity.	CA BAS-AND	
Puddino formation (pu)	Massive to blocky lava flows, frequently strongly brecciated, cropping out in the coastal sector between Le Puntazze and Sc. dell'Immeruta. Their best exposure is along the road Quattropani-Acquacalda, where two massive lava flows (10 and 15 m thick) with well developed flow foliation and columnar jointing are visible. Thinly bedded lapilli-tuff layers (i) are interbedded in places.	Effusive activity (i= minor PDC eruption units) from the Chiesa Vecchia volcano.	CA AND to high-K CA AND	188±3 [11]
Bertaccia formation				
ber$_1$ member	Planar, medium-bedded lapilli-tuffs (65 m thick) with intraformational channels, in places strongly hydrotermalized. Massive lithic-rich pyroclastic-breccias are visible at the base. A m-thick layer of loose scoriaceous lapilli-tuffs, in places passing to a welded scoriaceous agglomerate, is present at the top.	Hydromagmatic dilute PDC eruption units passing to late strombolian activity.		
ber$_2$ member	M-thick lava flows (average=4 metres) tipically consisting of flattened spatter clasts.	Clastogenic lava flows.	CA AND	
PIANO GRANDE SYNTHEM - LE PUNTAZZE SUBSYNTHEM				
M. Chirica lithosome (upper portion)				
Vallone di Bezzotti formation				
vb$_1$ member	Pyroclastics (up to 60 m thick) exposed along the cliffs of the deep valleys on the N flank of M. Chirica relief. They consist of alternating thin to medium beds (thickening upwards) of i) well sorted, normal graded grey tuffs and ii) cross-stratified or normal graded, loose, subangular black scoriaceous lapilli-tuffs. Lithic-rich deposits (with bomb sags) are exposed in the lower portion and in near-vent areas (strongly hydrotermalized). Beds of inverse-graded lapilli-tuffs are reported (iii).	Alternating fallout (i) and dilute PDC eruption units (ii) of M.Chirica volcano (iii=grain flow processes).	CA BAS-AND	150±10 [13]
vb$_2$ member	Massive lavas, in places strongly hydrotermalized, exposed on the N flank of M. Chirica.	Late effusive activity.	CA BAS-AND	
CALA FICO SUPERSYNTHEM - SCOGLIO LE TORRICELLE SYNTHEM				
P. Palmeto lithosome (lower portion)				
Scoglio dell'Immeruta formation (im)	Thick (up to 2 m), coarse (dmax=2 m), poorly sorted rounded pebbles to boulders lying on sharp erosional surfaces (*i.e.,* ravinement). They mostly crop out on the coastal cliffs as sub-horizontal to gently dipping horizons representing the sections of marine terraces with inner margins at 43-45 m *asl* ([20]). Very poorly sorted, crudely bedded coarse conglomerates locally form lentiform bodies (up to 15 m thick and few tens of m large) lying on irregular erosional surfaces. Isolated subspherical carbonate buildups are visible at 40-45 m *asl*. They consist of a vermetid-rich framework of calcareous algae and serpulids englobing mollusc shells and fragments of *Cladocora caespitosa* corals (the latter dated at 119 ka ± 6)([20]).	Paleoshoreline I marine terraces (MIS 5e, 124 ka). The lentiform bodies derive from submarine slumping processes. Carbonate buildups indicate maximum flooding dep. conditions ([20]).	Clast composition reflects that of adjacent volcanic lithotypes	124 [20] 119±6 [20]
Monterosa lithosome				
Sciarra di Monterosa formation				
sci$_1$ member	Pyroclastics (up to 30 m thick) exposed on the eastern side of the Monterosa cape and consisting of i) thinly bedded lapilli-tuffs with bomb sags that gradually and alternately pass upwards to ii) thickly bedded, welded (in near-vent areas) to loose (towards distal areas), scoriaceous lapilli-tuffs and tuff-breccias	Hydromagmatic dilute PDC eruption units (i) passing to strombolian deposits (ii).	CA BAS-AND	
sci$_2$ member	Thick (up to 15 metres) massive lava flows.	Effusive activity.	CA BAS-AND	
Pignataro di fuori formation (pf)	Well sorted, thickly bedded, normal graded, welded scoriaceous pyroclastic-breccias (up to 80 m thick), with intercalated discontinuous thin lava flows and thinly bedded lapilli-tuff layers (i). At base, a succession of alternating thin lava flows and welded scoriaceous layers crops out along the valley between the reliefs of Pietra Campana and U Mazzuni. Few m-thick massive lava flows (3 m) with well defined carapaces are exposed along the S side of the Pietra Campana cone (**pf$_1$ member**), together with a squat lava dome (diameter of 30 m) with well evident onion-skin type foliation (**pf$_2$ member**).	Strombolian fallout eruption units and lava flows (i=hydromagmatic dilute PDC eruption units) building the main portion of Monterosa scoria cones.	Scoriae are high-K CA BAS-AND, whereas both pf$_1$ and pf$_2$ are CA BAS-AND to AND	*102±2* [11]
U Mazzuni formation				
ma$_1$ member	Well-sorted, normal to reverse graded, black/yellow scoriaceous lapilli-tuffs (2 m thick). A thinly bedded, varicoloured tuff layer (2 m thick) with bomb sags and rip-up structures is visible at base (i). Massive, lithic-rich tuff-breccias (up to 20 m thick) are exposed between the reliefs of Pietra Campana and U Mazzuni	Strombolian fallout eruption units (i=dilute, wet-type PDC eruption units).	CA BAS-AND	
ma$_2$ member	Succession of massive lava flows (average thickness=5 m) with well developed carapaces and jointing.	Latest effusive activity.	CA BAS-AND	119±7 [19]
M. S.Angelo lithosome (lower portion)				
Timpone Ricotta formation (tr)	Thin to medium (thicknening upwards) planar beds of yellowish to grey, massive to cross-stratified tuffs and lapilli-tuffs (up to 40 m thick) exposed along the flanks of M. S.Angelo relief with best exposure in the area of Timpone Ricotta. The lower portion is lithic-rich. Along the coast-road Lipari-Canneto, near Marina di Porto Salvo (E Lipari), the unit is represented by lentiform, medium bedded tuffaceous breccias containing numerous lava and scoriaceous lithics and revealing diffuse rip-up structures and plastic deformation of strata (i). Discontinuous scoriaceous tuff-breccia layers and numerous lava lithic blocks are interbedded in the site of Timpone Croci (central-E Lipari). Both these outcrop sites reveal the occurrence of impact sags (up to 40 cm large) originated from the eastern quadrangles (N120°E to N90°E). Near Marina di Porto Salvo (E Lipari), clastogenic lavas are discontinuously visible (**tr$_a$ member**).	Hydromagmatic dilute, (dry-type) PDC eruption units (i=syn-depositional marine reworking; see the text). Strombolian and/or ballistic fallout from eccentric eruptive vents is revealed in E Lipari.	CA BAS-AND to AND (juvenile clasts)	
Timpone del Corvo (tc)	Thick (up to 15-20 m), lobate, massive and blocky lava flows cropping out along the southern flanks of M. S.Angelo volcano. Their best exposure is at Marina di Porto Salvo (E Lipari), along the coast-road Lipari-Canneto, where the lava front with sub-spherical flow foliation is visible.	Effusive activity	high-K CA AND	116±4 [18] *127±8* [7] *84±2* [11]
CALA FICO SUPERSYNTHEM - BRUCA SYNTHEM - TIMPONE DEL GRADO SUBSYNTHEM				
M. S.Angelo lithosome (intermediate portion)				

Timpone Pataso formation (tp)	Widespread, massive, sheet-like horizons of grey-green lapilli-tuffs (up to 15 m thick), showing various grading patterns (normal, reverse or both) and numerous unburnt fossil plant relicts („leaf-bearing horizons"; [23]). In places, an higher content of lithic blocks is reported at the base (*i.e.,* substrate erosion). These leaf-bearing deposits reveal topographically-controlled thickness variations (valley ponding), and are diffusely hydrotermalized in the area of kaolin quarry. Thinly to medium bedded, grey to pink lapilli-tuffs with low-angle cross-stratification, ephemeral channels, scour structures and rare accretionary lapilli (primary pyroclastics) are visible in places, particularly along the flanks of the M. S.Angelo cone. Minor poorly stratified, well sorted (fines-depleted) scoriaceous lapilli-tuffs are interbedded. In the area of Marina di Porto Salvo (E Lipari), symmetrical ripples are reported. South of Timpone Pataso, this unit forms a lentiform body (**tp_a member** - up to 100 m thick, 400 m large) exposed on a subvertical cliff and composed of alternating thin to medium, planar beds of primary pyroclastics and varicoloured aphanitic chert deposits (up to 85% SiO_2 content, fossils absent) with faint varve-like lamination.	Lahar deposits (see the text). Primary pyroclastics are hydromagmatic dilute (dry-type) PDC eruption units and strombolian fallout deposits from the M. S.Angelo cone. Symmetrical ripples reveal marine reworking. The tp_a member reflects the progressive filling of a small lacustrine basin (see text).	Whole-rock composition is high-K CA AND	

CALA FICO SUPERSYNTHEM - BRUCA SYNTHEM - FOSSA DELLA VALLE SUBSYNTHEM

M. S.Angelo lithosome (intermediate portion)

Serra Pirrera formation (sp)	Leaf-bearing pyroclastics fully comparable with the Timpone Pataso formation. They are widely dispersed on Lipari directly overlying a lateral persistent red paleosol developing on Timpone Pataso pyroclastic products. Primary pyroclastics (up to 60 m thick) diffusely outcrop on the S flank of the M. S.Angelo cone, and are also reported in distinct sectors of the W coast of Lipari, e.g. at Bruca and Cala Sciabeca. At Cala Sciabeca, they are exposed in the basal portion of the coastal cliff and form a lenticular body composed of subangular to subrounded, cross-stratified, granules to sands (P. del Cugno Lungo form.-cl_a member).	Lahar deposits and PDC eruption units of M.S.Angelo stratocone (cf. Timpone Pataso form.). cl_a member reflects marine reworking processes (see below).	Whole-rock composition is high-K CA AND	
Pulera formation (pu)	Widespread, thick (up to 20 m), blocky lava flows with well developed carapaces and flow foliation, known as "cordierite-bearing lavas" for their high content of megacrysts of cordierite and garnet ([1]). They are exposed along the S flanks of the M. S.Angelo volcano, branching out in different lobes mostly along the coastal sector between Bruca and Punta delle Fontanelle (for a total length of up to 3 km).	Effusive activity of the M. S.Angelo stratocone.	Whole-rock is high-K CA AND, with DAC-RHY glass	104.0±3.5 [7] 105±19 [20]

CALA FICO SUPERSYNTHEM - FONTANELLE SYNTHEM - CALA SCIABECA SUBSYNTHEM

P. Palmeto lithosome (intermediate portion)

Punta del Cugno Lungo formation (cl)	Very coarse (dmax=3 m), poorly sorted, clast-supported conglomerates (up to 2 m thick) with rounded pebbles to boulders lying on sharp ravinement surfaces ([20]). They are related to terraces exposed along the entire W coast of Lipari from P. del Legno Nero (to the N) to P. le Grotticelle (to the S), with inner margins at elevations of 23-27 m *asl*. Isolated carbonate buildups (cfr. Sc. dell'Immeruta formation) are documented at 20-30 m *asl*, directly overlying the conglomerates. Finer-grained deposits made up of well sorted, cross-stratified rounded granules to sands are reported in places, particularly on the basal portion of the coastal cliff near Cala Sciabeca, where they form a lentiform body (**cl_a member** - up to 20 m thick, 600 m large) with large-scale cross-stratification (foreset inclination of 20-30° and orientation normal to parallel to present shoreline) upward passing to plane parallel and low-angle cross stratification. Clast composition reflects that of leaf-bearing pyroclastics (cf. Serra Pirrera formation).	Paleoshoreline II marine terraces (MIS 5c, 100 ka). The cl_a member reflects progradation of a submerged beach deposit in shallow marine environments, under sediment supply of leaf-bearing pyroclastics.	Clast composition = adjacent volcanic lithotypes	100 [20]

CALA FICO SUPERSYNTHEM - FONTANELLE SYNTHEM - LO INZOLFATO SUBSYNTHEM

M. S.Angelo lithosome (upper portion)

Chiappe Lisce formation

ch_1 member	Non-coherent, poorly bedded, massive (locally stratified or normal graded) pyroclastic-breccias (up to 20 m thick) with numerous bread-crust bombs mostly exposed along the flanks of the M. S.Angelo cone (30-35° slope angles). Towards distal areas, they laterally (and gradually) pass to thinly bedded tuff-breccias and lapilli-tuffs with plane parallel- and cross-stratification.	Vulcanian-type dilute PDC eruption units (*plus* ballistic fallout) of M. S.Angelo stratocone.	High-K CA AND	
ch_2 member	Two squat, m-thick blocky lava flows with poorly developed basal carapace, exposed on the S and W crater rims of the M. S.Angelo cone (for a total length of only 250 m).	Latest effusive activity of M. S.Angelo cone.	High-K CA AND	92±10 [13] *55±2* [11]
ch_3 member	Poorly bedded tuffaceous-breccias with substantial valley-ponding effect (up to 20 m thick), exposed at the foot of the SW flanks of M. S.Angelo cone, gradually lying on ch_1 member.	Lahar depositional units.		
M. Chirica-Costa d'Agosto formation (cc) (=lithosome)	Succession of three thick (up to 50 m) massive lava flows with well developed carapaces, onion-skin foliation structures and columnar joints. They discontinuously crop out along the W side of the M. Chirica volcano and are particularly exposed along the steep coastal cliff between Lo Inzolfato and Cala Sciabeca, displaying a 1.5 km-large and 120 m thick lava front. These lava flows are dated at 81 ka. A squat (up to 15 m thick), massive lava dome with similar stratigraphy and composition crops out near P. del Legno Nero (**cc_1 member**), N Lipari.	Latest effusive activity of M. Chirica. The cc_1 member reflects effusion from an eccentric dyke.	high-K CA AND	*92±2* [11] 81±2 [11]

CALA FICO SUPERSYNTHEM - FONTANELLE SYNTHEM - FOSSA DI FAURDO SUBSYNTHEM

P. Palmeto lithosome (upper portion)

Punta delle Fontanelle formation (pf)	Thick (up to 1.5 metres), coarse (dmax=2 m), poorly sorted, clast-supported conglomerates with rounded pebbles to boulders lying on sharp ravinement surfaces representing the cover of narrow marine terraces (inner margins at ~12 m *asl*), which sections are exposed along the southern part of W Lipari ([20]). Poorly sorted conglomerates with rounded pebbles to boulders occur at 2-3 m *asl* in two small outcrops on the N side of the Monterosa cape (**fo_a member**).	Terraced marine deposits corresponding to paleoshoreline III (MIS 5a, 81 ka).	Clast comp.= adjacent volcanic lithotypes	100 [20]

P. LE GROTTICELLE SUPERSYNTHEM - SCOGLIERA SOTTO IL MONTE SYNTHEM

Varesana lithosome

Pianoconte formation (pi)	Massive, poorly coherent to coherent, brown-reddish ash-rich pyroclastic deposits dominantly formed by millimetric glass fragments (and subordinate cpx crystals, in places abundant), exposed on most of Lipari ([21]). Carbonized wood fragments are diffused. These pyroclastics are organized in thick to very thick beds frequently amalgamated in lithologically homogeneous successions, the thickness of which is characterized by strong valley ponding effect ranging from a maximum of 15 m to few dms. Lithic blocks embedded from the volcanic substrate are reported in S Lipari. In places, they are enriched in lava lithics, particularly along the W stratigraphic profiles at the foot of Paleo-Lipari volcanic reliefs. This unit lies below the M. Guardia pyroclastics (22-20 ka) and includes the l1 tephra layer (cf. Tab. 2), and tephra layers correlated with GPT (cf. Rocce di Barcone formation; 67-70 ka, [21]), IT (56 ka; [17]) and LPT (~23 ka; [21]), together with interbedded local volcanics (cf. Punta del Perciato and Falcone formations). Distinct layers have been dated through ^{14}C methodology on embedded charcoal fragments ([5, 6]).	Fallout eruption units and subordinate dilute and turbulent PDC eruption units (in S Lipari) originated from Vulcano Island ([21]). They are representative of the Lower (70-56 ka) and Intermediate Brown Tuffs (56-22 ka), based on the interbedding of *IT.*	Glass composition is TRA-AND to RHY with phenocrysts of cpx, plg, kf, ol, amp	67-70 [21] 70-56 [21] 56 [17] 56-22 [21] 22.6±0.3 [5] 23.5±0.9 [6] ~23 ka [21] 22.4±1.1 [6]
Monte dei Porri lithosome *(from Salina)*				
Rocce di Barcone formation (rb) *(from Salina)*	Pyroclastic products widely cropping out in the N and central-W Lipari, interbedded within the Pianoconte formation. Irregularly mantling the pre-depositional topography with a general W-to-E thickness decrease (up to 15 m along the W coast), they consist of two layers separated by a thin Brown Tuff unit. The lower layer consists of thickly to thinly bedded, normal (to reverse) graded, massive or plane parallel laminated, poorly sorted lapilli-tuffs made up of dark grey scoriae (up to 60-80%) and grey pumices. Thickness (and grain-size) notably decrease from W to E. The upper layer (almost constantly 1 m thick) consists of medium bedded, poorly coherent, normal-graded lapili-tuffs made up of light grey scoriae (40%), yellowish pumices (40%) and lithics (20%).	Fallout eruption units (and few distal PDC eruption units within the lower layer) correlated with the *GPT* from the M. dei Porri at Salina (67-70 ka)([21]).	Scoriae are CA BAS-AND, whereas pumices are AND (typical of *GPT,* [15])	67-70 [21]
Punta del Perciato formation (=lithosome)				
pe_1 member	NNW-SSE aligned, endoenous lava domes with thick blockier pumiceous upper carapace and poorly developed columnar joints, which remnants are exposed along the SWmost coastal sector of Lipari (including the isolated rocks of le Formiche, Pietralunga and Pietra Menalda). The onion-skin foliated inner structure of one of these domes is visible along the coastal cliff to the N of P. del Perciato.	Oldermost dome-type effusive activity in the S sector of Lipari.	High-K CA RHY, few phenocrysts, no enclaves	
pe_2 member	Pumiceous pyroclastics characterized by thickness decrease from S (up to 2 m at V. Muria) to N with substantial valley ponding and parallel lateral facies variations. Poorly sorted, massive and coherent, lithic-rich (dome-type), white (to reddish) pumiceous pyroclastic-breccias occur in near-vent areas (*e.g.*, P. di Iacopo). Normal-graded tuff beds with cross-lamination, bomb sags and accretionary lapilli are intercalated in places. Towards distal areas, thickly to thinly bedded, planar- to cross-stratified lapilli-tuffs (60% ash) and massive tuffs (80% ash) become prevalent, *e.g.* near V. Muria (where isolated bomb sags are visible). In distal outcrops, a white pumiceous tuff layer is discontinuously reported, interbedded within the Pianoconte formation. Similar (fining-upward) vertical facies variations are documented.	Dilute and turbulent PDC eruption units (moving from S to N Lipari) related to late explosive activity in the area of P. del Perciato, likely destructing the summit of pe_1 domes.	Pumices are high-K CA RHY	
Falcone formation (=lithosome)				
fa_1 member	Pumiceous pyroclastics cropping out in most of Lipari, interbedded within the Pianoconte formation. They are characterized by peculiar lateral (and vertical) facies variations and rapid S-to-N thickness decrease (up to 15 m along the SW coasts), with slight valley-ponding effect. Massive to normal graded (minor inverse graded), lithic-rich (more than 30%), pumiceous tuff-breccias and lapilli-tuffs with bomb sags crop out at the base of the succession in near-vent areas. Medium to thinly bedded, cross-laminated pumiceous lapilli-tuffs and tuffs become gradually prevalent towards distal areas, where metric sandwave structures (wavelength up to 2 m) are reported.	Nwards spreading, dilute and turbulent PDC eruption units generated from explosive activity in the area of Falcone, giving rise to a large tuff ring (presently covered).	Pumices are high-K CA RHY	
fa_2 member	Endogeneous lava domes with blocky carapaces and well developed flow foliation exposed at Capparo (where xenoliths are diffused), Falcone and Capistello, S Lipari. The Falcone dome is best preserved and shows elliptical shape with average diameter of 800 metres. These domes are deeply eroded and weathered, (particularly in correspondence of the wide morphologic depression behind Spiaggia di Vinci) and are displaced by intense tectonic and volcano-tectonic activity (collapse vc4).	Second stage of dome-type effusive activity in the S sector of Lipari.	High-K CA RHY, few phenocrysts, LAT enclaves (plg, px)	42.0±0.3 [7] 41.0±3.8 [13] 40.0±2.5 [13]
fa_3 member	Small black lava dome cropping out near Punta della Crapazza, cutting the fa_1 domes.	Dome-type effusion along an eccentric dyke.	High-K DAC (porphyritic)	
P. LE GROTTICELLE SUPERSYNTHEM - V. MURIA SYNTHEM - URNAZZO SUBSYNTHEM				
M. Guardia-M.Giardina lithosome				
M. Guardia formation (gu)	Widespread pumiceous pyroclastics („Monte Guardia sequence"; [3, 5, 10]) with substantial valley ponding effect and thickness ranging from 50-60 m in S Lipari to few dms. Juvenile fragments are white, highly vesiculated pumices and minor grey, mildly vesicular pumices and banded pumices ([10]).Fine-grained salmon-coloured ash-rich key-beds with accretionary lapilli allow subdivision into several depositional units with rapid S-to-N thickness decrease and parallel lateral (and vertical) facies variations ([3]). Very thick, lithic-rich massive lapilli-tuffs and tuff-breccias of lapilli and angular blocks (50% pumice content) occur in near-vent areas. They rapidly laterally pass to thickly bedded, massive lapilli-tuffs with inverse-grading (and rounding of clasts), diffuse bomb sags and well-developed clast embedding at the base of each bed. Subordinate coarse-grained, fines-depleted well-sorted pumiceous lapilli layers are reported (i). Thinly to medium bedded lapilli-tuffs and tuffs become prevalent towards distal areas. They display planar crude stratification laterally passing to cross-stratification with bedform wavelength varying from metres to tens of cms (at 1-2 km N of the vent), and planar to low-angle oblique lamination (at 4-6 km N of the vent). In areas distant from the vent, massive tuff layers display accretionary lapilli in places. Distal tephras are documented at Vulcano ([8]), Panarea, Basiluzzo and Salina ([21]).	Dilute and turbulent, dry-type (subordinately wet-type) PDC eruption units originated from the M. Guardia eruptive vent (i=minor fallout deposits from an associated eruption plume). M. Guardia explosive activity was mostly driven by magmatic volatile fragmentation mechanisms, with subordinate impulsive magma-water interaction.	White pumices are RHY ([10]), with low crystal content (kf, cpx, amp, zr). Grey pumices are LAT to high-K DAC ([10]), with high crystal content (cpx, plg, ol, ti, ap). Porphyritic (cpx, plg) LAT enclaves.	22-21 [21]
gu_1 member	Lentiform (up to 10 m thick and 200 m large), medium-bedded volcaniclastics cropping out at Vallone Ponte (near to Lipari village), at top of M. Guardia formation. It consists of alternating primary pyroclastics (cf. M. Guardia formation) and minor clay and limonite-rich layers (*i.e.,* secondary deposits).	Volcaniclastic filling of a small lacustrine basin.		
M. Giardina formation (gi)	NNW-SSE-aligned endogenous lava domes of S.Lazzaro, M. Guardia, and M. Giardina. They have subcircular shape, diameter up to 850 m (the S.Lazzaro dome is 450 m large) and thickness more than 100 m, and consist of a sub-vertical lava front encircled by a thick collar of unstable steep talus slope deposits. Well developed flow foliation, consisting of interbanded obsidian and lithic rhyolite layers, and rampart structures are reported. Lava is glassy and highly vesicular.	Third stage of dome-type effusive activity in S Lipari.	High-K CA RHY, low porphyritic (kf, plg, amp) LAT enclaves	

gi_1 member	Poorly sorted, thickly bedded (thickening upward), massive and coherent tuff-breccias and lapilli-tuffs building up a crater structure (15-20 m high and 300 m large) at top of M. Giardina lava dome and rapidly thinning along the slopes of M. Giardina and M. Guardia domes (thicknening between the two reliefs). They mostly consist of reddish (oxidized) obsidian and rhyolite angular clasts (dome-type), with minor vesiculated clasts. Finer-grained lapilli-tuff layers with planar- to cross-lamination are intercalated (i).	Fallout eruption units (i=subordinate dilute PDC eruption units) disrupting the summit of M. Giardina dome.		
P. S.Giuseppe formation (sg) (=lithosome)	Three NNW-SSE-aligned, endogenous lava domes exposed in the sector of P. S.Giuseppe, S Lipari. The southernmost and bigger dome is elliptical in plan with maximum elongation of 800 m and up to 40-50 m thick, whereas the other domes are squat, sub-circular, and 200 m large. Flow foliation and rampart structures are visible along the coastal profiles. A small subcircular dome is visible near P. di Costa, located in the middle of an elliptical, ~300 m large morphologic depression at top of the southermost dome (furtherly displaced by a NNW-SSE fault).	Effusive activity coeval with M.Giardina domes. The resurgent small dome near P. di Costa is assumed to fill a steep-walled collapse structure.	High-K CA RHY, aphyric, with cpx-rich magmatic enclaves and xenocrysts	
P. LE GROTTICELLE SUPERSYNTHEM - V. MURIA SYNTHEM - QUATTROCCHI SUBSYNTHEM				
La Fossa di Vulcano lithosome *(from Vulcano)*				
Piano Grotte dei Rossi formation (gr) *(from Vulcano)* - (ex Mauro formation, [25])	Massive ash-rich deposits mantling most of Lipari Island with substantial thickening in paleo-valleys (up to 10 m), decreasing from S to N (together with grain size). Their field attitude strictly conforms to the Pianoconte formation, although lighter in colour (light brown to grey), less coherent and with frequent internal bands of different colour or grain-size (coarse *vs* fine ashes). Discontinuous cross-lamination is reported in some outcrops of S and central Lipari. This unit overlies the M. Guardia pyroclastics (22-21 ka) and includes the l_2 tephra layer (see below). Distinct layers are dated by means of 14C methods on embedded charcoal fragments ([5, 6]).	Dilute PDC eruption units (in S Lipari) and fallout deposits originated from Vulcano Island ([21]), representing the Upper Brown Tuffs (21-7 ka).	Glass clasts are TRA-AND to RHY with phenocrysts of cpx, plg, kf, ol	21-7 [21] 16.8±0.2 [5] 20.5±0.2 [6] 20.3±0.7 [6]
l_2 tephra layer	Medium bedded, lithic-rich, pumiceous lapilli-tuff layer (1-2 m thick) with massive, plane-parallel and cross-stratified beds intercalated within the Piano Grotte dei Rossi formation between V.ne Canneto Dentro and Vallonaccio (E Lipari).	Near-vent dilute PDC eruption units (undefined local source).	Pumices are high-K CA RHY, aphyric	
P. LE GROTTICELLE SUPERSYNTHEM - V. MURIA SYNTHEM - VALLONACCIO SUBSYNTHEM				
Castello formation (cas) (=lithosome)	N-S-aligned, small endogenous lava domes discontinuously cropping out in the intensely urbanized area of Lipari village, between Castello and Portinente. They show well developed flow foliation along the coastal cliff of Castello relief.	Dome-type effusive activity along N-S tectonic lineaments.	High-K CA RHY, aphyric (LAT encl.)	
V.ne Canneto dentro formation (=lithosome)				
cd_1 member *(Canneto Dentro tephra, [4])*	Thickly bedded, normal graded, obsidian-rich, pumiceous pyroclastic-breccias (up to 4 m thick) with intercalated thinly bedded tuff beds and bomb sags. They are exposed in the area between V.ne Canneto dentro and the Vallonaccio valley, E Lipari.	PDC eruption units from the V.ne Canneto dentro eruptive vent.	High-K CA RHY, aphyric	
cd_2 member	Squat endogenous lava dome (50 m-thick and 300 m-large) with well developed flow foliation exposed at V.ne Canneto dentro. This is correlated with a small lava dome localized S of Vallone del Gabellotto due to comparable stratigraphic position and composition.	Dome-type effusive activity along N-S tectonic lineaments.	High-K CA RHY, aphyric (LAT encl.)	
Capo Rosso (cr) (=lithosome)	Three N-S-aligned endogenous lava domes well developed flow foliation cropping out along the coastal cliff of the NE sector of Lipari Island. They are strongly hydrotermalized.	Dome-type effusive activity along N-S lineaments.	High-K CA RHY, aphyric	
P. LE GROTTICELLE SUPERSYNTHEM - VALLONE FIUM BIANCO SYNTHEM - CHIRICA RASA SUBSYNTHEM				
Vallone del Gabelloto-M. Pilato lithosome *("Gabellotto-Fiume Bianco volcano-stratigraphic unit", [4])*				
Vallone del Gabellotto formation (vg) *(„Lower Pumice Series, PIV-1"; [22])*	Widespread, thick (up to 130 m), whitish pumiceous pyroclastics, best exposed on the S steep wall of the Vallone del Gabellotto gorge. They mostly consist of medium to thick beds of massive and planar- to cross-stratified (with large-scale bedforms), pumiceous lapilli-tuffs and tuff-breccias with rhyolitic and obsidian lithic clasts. These deposits are characterized by lateral, proximal-to-distal decrease of grain-size and thickness (down to few dms on Monterosa), and wavelength (from tens of m to tens of cm). Pumices are poorly vesicular, angular to subrounded, blocky and equant ([4]). Crude-layered, normal graded, well sorted, pumiceous lapilli-tuff and tuff beds are interlayered (i). Tuff layers with accretionary lapilli are reported in N Lipari. Distal tephra layers are found on Panarea and Vulcano ([20]), and even in Adriatic and Tyrrhenian deep-sea cores (E-1 tephra layer, 8.2 ka ±0.1; [26]).	Hydromagmatic dilute, dry-type PDC eruption units (i= subordinate fallout deposits) related to the Vallone del Gabellotto eruptive vent.	High-K CA RHY, aphyric	8.2±0.1 [26]
Pomiciazzo formation (po)	Large obsidian-rich coulee (up to 30 m thick) with well developed flow foliation, forming three ~450 m-large lava lobes along the E coastal sector of Lipari nearby Pomiciazzo.	Vallone del Gabellotto effusive activity.	High-K CA RHY, aphyric	11.4±1.8 [2] 8.6±1.5 [2]
La Fossa di Vulcano lithosome *(from Vulcano)*				
Piano Grotte dei Rossi formation (gr) *(from Vulcano)*	This is the most recent Upper Brown Tuff unit on Lipari, which is exposed between the Vallone del Gabellotto (8 ka) and M. Pilato pyroclastics in the stratigraphic profiles of the Vallone Fiume Bianco pumice quarry and along the coastal cliff of the NE sector of Lipari, nearby Capo Rosso. By correlation with Vulcano, this unit is dated at 7.7 ± 1.0 ([8])	Upper Brown Tuffs - Fallout eruption units originated from Vulcano Island ([21]),	Glass compositions are TRA-AND to RHY	7.7±1.0 [8]
P. LE GROTTICELLE SUPERSYNTHEM - VALLONE FIUM BIANCO SYNTHEM - COLLE S.ELMO SUBSYNTHEM				
Forgia Vecchia formation (=lithosome)				
fv_1 member	Massive pumiceous lapilli-tuffs and tuff-breccias (up to 7 m thick) with minor lava and obsidian clasts (up to 40 cm in diameter), crude layering and poorly developed normal grading. Plane parallel- to cross-stratified lapilli-tuff beds are reported. A few massive tuff layers are interbedded (see the text). This unit is limitedly exposed nearby the Pirrera village (best exposure along the steep sides of Vallonaccio gorge) with rapid proximal-to-distal thickness and grain-size decrease.	Near-vent dilute PDC eruption units in the area of Forgia Vecchia-Serra Pirrera.	High-K CA RHY, aphyric	
fv_2 member	Tongue-like (30 m thick) obsidian-rich lava coulee with basal carapace, foliation structures, blocky and rough surface with curved cracks. This coulee is generated in the area of Pirrera-Forgia Vecchia and flows down towards the coast forming two lava lobes standing at the back of the Canneto village.	Coulee-type effusive activity.	High-K CA RHY, aphyric	1.6±0.4 [2]
M. Pilato lithosome *("Monte Pilato-Rocche Rosse volcano-stratigraphic unit", [4])*				
Sciarra dell'Arena formation				

sa_1 member *(„Upper Pumice Series, PIV-2", [22]; „Monte Pilato sequence", [9])*	Widespread pumiceous pyroclastics (up to 150 m thick) building up the M. Pilato cone (350m high, 1km large crater rim open to the NE, average slope angles of 25°), best exposed on the walls of the pumice quarries in NE Lipari. They mantle the topography overlying the red paleosol developing on Vallone del Gabellotto pyroclastics, and are mostly subdivided into four lithofacies ([9]). Litofacies 1 (dominant) consists of well sorted, normal graded, medium to thick beds of highly vesiculated pumiceous lapilli-tuffs with minor obsidian and lava clasts. Litofacies 2 is represented by poorly sorted, medium beds of matrix-supported pumiceous lapilli-tuffs and tuffs with scattered lithics, inverse and normal grading and substantial valley fill effect, whereas litofacies 3 is demonstrated by thin beds of plane parallel-laminated tuffs with bomb sags. These three lithofacies are interbedded mostly in near-vent areas. Litofacies 4 becomes gradually prevalent in the upper part of the unit and with distance from the vent, being represented by dm- to m-thick layers of medium-bedded, plane parallel-laminated tuffs with accretionary lapilli (30% in vol). Distal tephra layers are reported on Vulcano, Stromboli and Panarea ([21]). Carbonized plant fragments contained within the basal portion of M. Pilato pyroclastics gave age of 1241 years ± 31 (^{14}C; Keller, 2002), which corresponds to a calibrated calendar age of 776 AD (+110/-90). This is approximately consistent with the age constraints provided by the historical reports (729 and 787 *AD*).	M. Pilato strombolian to subplinian explosive activity ([9]): lithofacies 1=fallout eruption units from a sustained eruption column; lithofacies 2 and 3=high-concentration or dilute PDC eruption units, respectively; lithofacies 4=wet-type dilute PDC eruption units.	Pumices are high-K CA RHY and aphyric	*787 AD* [16] 776 *AD* [16] (+100/-90) *729 AD*
sa_2 member	Obsidian-rich coulees very limitedly exposed on the N side of M. Pilato cone.	M. Pilato effusive activity.		
Lami formation (lm) *("pipernoid pumice cone", [22])*	Medium to thickly bedded pyroclastic succession (10 m thick) cropping out (and morphologically independent) at the foot of the southern flank of M. Pilato, near Lami. It mostly consists of variably sorted tuff-breccias composed of pumices, lithic clasts, diffused obsidian clasts (from glassy to spherulitic) and bread-crust bombs. Transitional pumice-obsidian clasts are peculiar. Variably stratified, medium sorted layers and massive tuff layers (the latter correlated to the sa_1 member by [4]) are interbedded. A m-thick layer of highly vesicular, welded and flattened pumiceous lapillli and blocks is present at the top ("pipernoid pumice deposits", [22]).	Fallout deposits (and mionor PDC eruption units) related to an eccentric eruptive vent on the flank of the M. Pilato cone.	Pumices are high-K CA RHY	
Fossa delle Rocche Rosse formation				
frr_1 member *(„Upper Pumice Series, PIV-3",[22]; „Rocche Rosse sequence", [9])*	Crudely normal graded, medium to thickly bedded pumiceous (vesiculated) lapilli-tuffs (up to 15-20 m thick) with diffused obsidian and (minor) lava lithics building up a 30-m-high and 400-m-large crater inside the M.Pilato crater area. Hydrotermalized dense lava lithics are abundant in the basal portion of the succession. Minor thin to medium beds of pumiceous lapilli-tuffs with accretionary lapilli are reported ([9]).	Small-scale fallout (and minor dilute PDC) eruption units of the Fossa delle Rocche Rosse vent	Pumices are high-K CA RHY and aphyric	
frr_2 member *(„Rocche Rosse coulee")*	Tongue-like (up to 60 m thick and 2 km long) obsidian-rich lava coulee with thick basal carapace outpoured from the NE side of M. Pilato crater area. Its surface, best exposed along the coast road, is tipically blocky and rough with concentric curved cracks. The internal structure is characterized by steep, sub-vertical, sheet-like flow ramp structures curving down to sub-horizontal flow foliation. Flow foliation consists of dense interbanding of obsidian (in places spherulitic or perlitized) and lithic rhyolite layers and is frequently folded.	Latest coulee-type effusive activity of M. Pilato-Fossa delle Rocche Rosse cone.	High-K CA RHY, aphyric to subaphyric, with few LAT to TRA enclaves	524-562 *AD* [22] 1.4±0.4 [2] ~1.4 [14] 1230 *AD* (± 0.4) [24]

Symbols - Tephra layers: GPT=Grey Porri Tuffs; IT=Ischia-Tephra; LPT=Lower Pollara Tuffs. Eruption types: PDC=pyroclastic density current. Composition: CA=calcalkaline; TRA=trachyte; LAT=latite; BAS=basalte; AND=andesite; DAC=dacite; RHY=rhyolite. Mineralogy: plg=plagioclase; cpx=clinopyroxene; opx=orthopyroxene; bt=biotite; ol=olivine; amp=amphibole (hornblende); ti=titanite; ap=apatite; zr=zircon. Composition and mineralogy mostly conform to the present work, Crisci et al., 1991 (general framework), Gioncada et al., 2033, 2005 (rhyolites), Davi et al., 2008, 2009 (more recent Rocche Rosse rhyolites). References (in italic, age measurements not fully consistent with the general stratigraphic framework or not attributable with certainty to any introduced lithostratigraphic unit due to imprecise location of samples in the original papers): ([1]) Barker, 1987; ([2]) Bigazzi and Bonadonna, 1973; ([3]) Colella and Hiscott, 1997; ([4]) Cortese et al., 1986; ([5]) Crisci et al., 1981; ([6]) Crisci et al., 1983; ([7]) Crisci et al., 1991; ([8]) De Astis et al., 2006; ([9]) Dellino and La Volpe, 1995; ([10]) De Rosa et al., 2003a; ([11]) De Rosa et al., 2003b; ([12]) De Vivo et al., 2001; ([13]) Gillot, 1987; ([14]) Keller, 1970; ([15]) Keller, 1980; ([16]) Keller, 2002 - personal communication; ([17]) Kraml et al., 1997; ([18]) Leocat et al., 2010; ([19]) Leocat et al., 2009; ([20]) Lucchi, 2009; ([21]) Lucchi et al., 2008; ([22]) Pichler, 1980; ([23]) Ricci Lucchi et al., 1988; ([24]) Tanguy et al., 2003; ([25]) Tranne et al., 2002; ([26]) Zanchetta et al., 2010.

Table 4 - Major (wt%) and trace (ppm) elements composition of Lipari volcanics.

Eruptive Epoch	**1**			**2**					**3**	**4**		**5**
Synthem	PALEO-LIPARI			PIANO GRANDE						SC.° LE TORRICELLE		BRUCA
Lithosome	Timp. Carrubbo (lower portion)	Timpone Croci	M. Mazza-caruso	M. Mazza-caruso	Timpone Ospedale	M.Chirica (lower portion)	Fuori del Pertuso	Chiesa Vecchia	M.Chirica (upper portion)	Monterosa	M. S.Angelo (lower portion)	M. S.Angelo (interm. portion)
Formation	Scoglio Bianco	Timpone Croci	Vallone dei Lacci	M. Mazza-caruso	Timpone Ospedale	Vallone Malopasso	Fuori del Pertuso	Le Puntazze	Vallone di Bezzotti	U'Mazzuni	Timpone del Corvo	Pulera
	sb1	tcr	vla	maz	to	vma	fp	pt	vb2	ma2	tc	pu
Sample	A3	T17	A26	A16	Lip134	B3	Lip114	T9	Lip211	Lip139	Lip157	LS90013
SiO_2	53.84	53.59	54.94	54.10	54.06	54.83	53.96	59.26	52.35	55.31	60.53	64.47
TiO_2	0.68	0.77	0.67	0.81	0.64	0.68	0.69	0.79	0.61	0.70	0.56	0.67
Al_2O_3	16.75	16.99	16.19	17.26	16.93	17.21	15.13	16.17	16.69	17.66	19.36	16.43
Fe_2O_3	9.36	9.60	8.84	8.67	9.06	8.50	9.23	8.14	8.82	8.69	4.39	6.66
MnO	0.16	0.16	0.16	0.14	0.25	0.14	0.32	0.15	0.16	0.16	0.09	0.12
MgO	5.25	4.74	5.61	4.42	4.91	4.43	5.86	3.42	6.38	4.24	0.86	1.36
CaO	8.89	9.42	8.88	8.89	9.96	8.93	10.14	6.47	9.71	8.20	5.59	4.19
Na_2O	2.36	2.10	2.22	2.49	2.23	2.98	2.28	2.00	2.32	2.84	3.34	2.20
K_2O	1.65	1.54	1.62	1.56	1.15	1.10	1.37	2.28	1.05	1.70	3.56	3.69
P_2O_5	0.23	0.18	0.20	0.23	0.14	0.14	0.18	0.18	0.14	0.17	0.20	0.21
LOI	0.83	0.91	0.67	1.43	0.67	1.06	0.84	1.14	1.76	0.33	1.52	0.00
Sc	30	31	32	27	38	30	34	23	35	27	-	15
V	305	264	259	250	269	305	278	217	251	275	56	136
Cr	40	52	70	80	80	40	110	80	100	-	10	40
Co	27.8	32	28.6	31.3	30.3	27.8	39	23.9	33.2	27.8	7.5	15.3
Ni	33	26	42	48	48	33	50	63	53	29	13	40
Rb	44	53.9	50.4	55.2	35.1	44	33	102	35.4	56.9	125	163
Sr	531	567	580	531	595	531	512	417	501	649	674	403
Y	19.1	19.3	17.9	20.1	16.8	19.1	17.4	23.9	18.3	19.5	22.3	25.4
Zr	66.8	77.1	63.8	79	49.4	66.8	58.1	121	54.2	80.3	151	151
Nb	6	7	5	6	4	6	4	10	4	7	12	16
Cs	1.6	1.8	1.1	2.2	0.7	1.6	0.9	4.4	1.3	2.1	4.7	6.1
Ba	372	342	403	478	318	372	296	600	264	452	718	559
La	18.3	21.8	20.8	24	16.3	18.3	17.9	30.3	19.5	23.3	40.8	43.2
Ce	36.2	44.3	40.7	47.2	31.3	36.2	35.5	59.4	33.8	45.9	76.6	82.5
Pr	4.47	5.42	4.88	5.75	3.82	4.47	4.35	7.13	4.81	5.56	9.07	9.66
Nd	18.1	21.8	20	22.7	15.5	18.1	17.6	27.6	19.3	22.3	32.6	35.3
Sm	3.8	4.9	4	4.8	3.5	3.8	3.9	5.6	4.1	4.9	6.3	6.5
Eu	1.12	1.32	1.14	1.2	0.97	1.12	1.03	1.13	1.08	1.3	1.41	1.27
Gd	3.54	4.31	3.81	4.12	3.04	3.54	3.43	4.75	3.62	3.92	5.03	5.29
Tb	0.6	0.64	0.59	0.64	0.53	0.6	0.57	0.78	0.62	0.66	0.8	0.88
Dy	3.44	3.67	3.4	3.57	2.9	3.44	3.21	4.58	3.14	3.34	3.98	4.46
Ho	0.7	0.72	0.66	0.72	0.62	0.7	0.68	0.87	0.64	0.72	0.82	0.91
Er	2.01	2.27	1.99	2.21	1.91	2.01	1.88	2.5	1.98	2.01	2.27	2.51
Tm	0.3	0.31	0.28	0.32	0.27	0.3	0.26	0.35	0.28	0.3	0.34	0.37
Yb	2	2	1.7	2.1	1.7	2	1.8	2.5	1.8	1.9	2.2	2.5
Lu	0.29	0.31	0.29	0.3	0.32	0.29	0.34	0.38	0.27	0.32	0.35	0.39
Ta	-	-	-	-	-	-	-	-	-	-	-	-
Hf	-	3	-	3	-	-	-	4	-	3	5	5
Pb	-	-	-	11	-	-	-	19	-	11	18	21
Th	3.8	6.3	4.6	5.3	3.1	3.8	4.5	8.3	3.3	4.8	11.1	13.2
U	1.22	1.54	1.62	1.67	1.02	1.22	1.27	2.66	1.22	1.68	3.68	3.77

Major and trace elements were determined by XRF. Cs, Ta, Hf, U and REE were determined by ICP-AES and ICP-MS.
Reported trace element data are higher than the double of the detection limit.
n.d.= not determined

Table 4 - Major (wt%) and trace (ppm) elements composition of Lipari volcanics.

Eruptive Epoch	**6**		**7**			8				9		
Synthem	FONTANELLE		SCOGLIERA SOTTO IL MONTE			V. MURIA				VALLONE FIUME BIANCO		
Lithosome	M. S.Angelo (upper portion)	M.Chirica-Costa d'Agosto	Punta del Perciato	Falcone		M.Guardia-M.Giardina		Castello	Capo Rosso	V. Gabellotto-M.Pilato	Forgia Vecchia	M.Pilato
Formation	Chiappe Lisce	M.Chirica- C. d'Agosto	Punta del Perciato	Falcone		M.Guardia	M. Giardina	Castello	Capo Rosso	Pomiciazzo	Forgia Vecchia	F. Rocche Rosse
	ch2	cc	pe1	fa2	fa3	gu	gi	cas	cr	po	fv2	ffr2
Sample	Lip283	Lip281	Lip97	Lip287	Lip288A	Lip277	Lip294	Lip285	Lip297	Lip265	Lip272	Lip273A
SiO_2	59.12	60.31	75.12	73.34	66.92	72.77	73.56	74.34	74.77	74.93	74.20	74.50
TiO_2	0.73	0.71	0.09	0.12	0.31	0.11	0.12	0.12	0.12	0.09	0.12	0.12
Al_2O_3	16.66	16.60	11.99	12.25	14.66	12.40	12.01	12.41	12.61	12.15	12.48	12.21
Fe_2O_3	7.11	6.95	1.53	1.74	3.96	1.86	1.81	1.92	1.92	1.95	2.01	2.02
MnO	0.15	0.14	0.07	0.09	0.12	0.10	0.09	0.11	0.10	0.09	0.10	0.11
MgO	2.27	2.19	0.64	0.10	0.76	0.11	0.12	0.12	0.16	0.01	0.11	0.13
CaO	6.76	6.65	0.86	0.69	3.22	0.70	0.74	0.73	0.75	0.76	0.75	0.77
Na_2O	3.01	3.08	3.89	3.68	4.01	4.42	3.95	4.33	4.09	4.34	4.26	4.47
K_2O	3.35	3.16	4.37	4.79	4.73	4.82	5.12	5.07	5.02	4.94	5.07	5.15
P_2O_5	0.22	0.22	0.01	0.01	0.17	0.01	0.02	0.03	0.01	0.02	0.02	0.00
LOI	0.63	0.00	1.43	3.20	1.14	2.70	2.47	0.82	0.45	0.72	0.88	0.52
Sc	23	17	-	-	-	-	-	-	-	-	-	-
V	158	152	-	-		53	-	-	-	-	-	-
Cr	-	-	-	-		40	30	-	-	-	-	-
Co	20	16.9	-	-		8.4	1.2	-	-	-	-	-
Ni	13	22	-		14	12	22	15	-	-	-	-
Rb	110	111	270	289	226	296	305	315	306	329	332	329
Sr	898	586	12.2	10.9	578	18	8.8	12.5	12.3	10.1	12.8	13.1
Y	25	22	32.8	39.9	33.3	40.6	41.3	41	42.5	42.6	43.2	43.9
Zr	149	131	123	132	126	151	123	155	149	155	171	170
Nb	8	11	29	32	24	32	32	34	33	35	36	35
Cs	n.d.	2.4	9.5	14.9	10.8	15.8	16	16.5	14.9	17	17.9	17.5
Ba	659	622	8	6.2	398	21.3	8.5	14.6	16.2	14.8	16.7	16.3
La	46	36.2	36.7	38.4	44	50.9	37.6	51.7	54.8	53.1	65.7	65.7
Ce	82	69.4	75.4	81.4	88.5	102	80.7	103	107	106	125	126
Pr	n.d.	7.98	8.59	9.68	10.3	11.1	9.48	11.4	11.9	11.5	13.6	13.8
Nd	n.d.	30.9	31	34.4	36.9	38.1	34.4	38.7	41.2	39.9	45.4	46.5
Sm	n.d.	6.1	6.5	7	7.9	7.8	7.6	7.8	8.6	8.4	9	8.5
Eu	n.d.	1.34	0.14	0.13	0.8	-	0.12	0.11	0.14	0.13	0.15	0.14
Gd	n.d.	4.8	5.28	6.21	6.09	6.51	6.34	6.39	6.59	6.57	6.97	7.11
Tb	n.d.	0.75	0.97	1.15	1.03	1.14	1.16	1.17	1.18	1.2	1.25	1.22
Dy	n.d.	4.19	5.45	6.61	5.57	6.16	6.73	6.78	6.9	6.83	7.14	6.93
Ho	n.d.	0.79	1.12	1.37	1.15	1.31	1.39	1.41	1.44	1.44	1.43	1.45
Er	n.d.	2.36	3.45	4.19	3.19	4.37	4.07	4.41	4.39	4.44	4.47	4.49
Tm	n.d.	0.34	0.53	0.64	0.53	0.62	0.64	0.71	0.68	0.67	0.7	0.72
Yb	n.d.	2.1	3.7	4.3	3.4	4.5	4.5	4.6	4.8	4.8	4.9	4.9
Lu	n.d.	0.36	0.54	0.68	0.56	0.64	0.7	0.73	0.75	0.73	0.79	0.71
Ta	n.d.	-	2	2.2	1.5	2.2	2.2	2.3	2.2	2.3	2.5	2.5
Hf	n.d.	4	6	6	5	6	5	6	6	6	7	7
Pb	17	13	26	29	26	30	31	30	34	30	33	32
Th	11	10.7	32.7	35.6	28	44.8	38.9	46.6	46.5	46.7	50.2	51.3
U	n.d.	3.19	11.8	11.9	9.3	14.3	13	14.8	14.8	15.1	16	16

Major and trace elements were determined by XRF. Cs, Ta, Hf, U and REE were determined by ICP-AES and ICP-MS.
Reported trace element data are higher than the double of the detection limit.
n.d.= not determined

Table 5 - Isotopic composition of Lipari volcanics from Esperanca et al. (1992) and Gioncada et al. (2003). Major (%) and trace (ppm) element data from the same authors are also reported.

Data Source	*Esperanca et al., 1992*																			
Eruptive Epoch	**1 - 2 - 3 - 4**															**5 - 6** cordierite-bearing lavas				
Sample	LIP 69	LIP 130	LIP 187	LIP 177	LIP 182	LIP 183	LIP 11	LIP 49	LIP 56	LIP 60	LIP 71	LIP 101	LIP 113	LIP 193	LIP 195	LIP 16	LIP 99	LIP 54	LIP 76	LIP 110
SiO_2	53.6	56.0	54.7	59.3	53.3	54.3	59.1	62.7	56.3	57.6	54.2	55.3	62.2	59.3	54.7	61.4	63.0	61.9	60.5	58.4
TiO_2	0.66	0.87	0.61	0.81	0.64	0.65	0.79	0.60	0.89	0.78	0.67	0.82	0.65	0.69	0.77	0.68	0.65	0.7	0.72	0.69
Al_2O_3	16.6	18.2	18.3	17.1	16.5	16.0	17.3	18.6	12.5	18.4	16.7	17.9	18.1	16.7	18.0	16.3	17.3	20.5	17.3	17.1
FeOtot	8.17	7.62	7.95	7.35	8.72	7.71	7.22	3.99	8.45	7.08	8.24	7.85	5.39	6.11	8.27	5.49	5.69	4.95	5.94	6.14
MnO	0.30	0.11	0.14	0.13	0.16	0.15	0.13	0.09	0.16	0.14	0.17	0.14	0.1	0.1	0.14	0.11	0.14	0.08	0.12	0.33
MgO	5.91	3.06	3.69	2.94	5.96	6.55	2.98	1.01	7.86	2.21	6.01	4.21	1.69	2.55	3.07	2.36	2.32	1.91	2.09	2.21
CaO	10.90	9.05	9.33	6.76	10.90	10.50	6.64	5.48	9.66	7.63	10.30	9.08	5.74	6.37	8.37	3.9	4.36	4.31	6.29	6.6
Na_2O	1.86	2.19	2.33	2.07	1.78	1.88	2.32	3.28	1.94	2.66	1.78	2.11	2.41	3.95	3.27	2.03	1.77	1.99	2.73	2.68
K_2O	0.96	1.84	1.81	2.58	1.01	1.22	2.55	3.66	1.19	2.57	0.92	1.52	2.92	3.28	2.22	3.85	3.89	2.87	3.38	3.06
P_2O_5	0.14	0.22	0.2	0.17	0.10	0.12	0.18	0.20	0.11	0.19	0.13	0.20	0.22	0.23	0.2	0.19	0.2	0.27	0.23	0.23
LOI	0.55	0.28	0.36	0.58	0.58	0.46	0.59		0.51	0.54	0.54	0.34	0.45	0.28	0.59	2.37	0.33	0.17	0.42	0.37
Sc																				
V	299	293	258	214	272	243	212			211	314	289	157	175	286	145	103	74	156	163
Cr	122	57	20	60	160	93	59	4		19	118	94	19	21	17	64	37	5	20	23
Co																				
Ni	38	22	15	36	47	67	27	6		12	43	29	10	14	16	28	23	4	12	14
Rb	27	54	46	98	24	39	98	120	53	84	25	73	93	103	64	157	145	103	109	106
Sr	553	669	828	476	484	487	485	801	723	788	567	611	562	662	809	402	487	912	643	651
Y	14	24	18	33	15	13	26	28	21	23	20	23	22	28	19	33	34	22	26	27
Zr	50	93	75	134	57	68	133	174	90	122	53	88	145	153	98	196	184	162	160	151
Nb	3	5	7	10	4	6	9	12	8	9	5	7	10	10	4	15	16	12	12	10
Cs																				
Ba	378	448	494	491	255	297	467			560	410	468	608	626	499	483	597	646	634	602
La	14	24	19	34	14	16	35			34	15	30	38	35	25	45	47	71	38	38
Ce	28	47	40	64	23	31	70			67	31	57	74	72	49	94	96	141	82	77
Pr																				
Nd	13.6	21.8	19.7	28.5	12.5	15.1	27.8	33.3	22	27.2	14.3	25.4	32.1	30.9	24.4	38.1	36.7	42.1	31.6	30.7
Sm	3.03	4.47	4.09	5.63	2.85	3.29	5.52	6.2	4.56	5.34	3.21	5.23	6.14	5.98	5.01	7.13	6.85	6.39	6.08	5.96
Eu																				
Gd																				
Tb																				
Dy																				
Ho																				
Er																				
Tm																				
Yb																				
Lu																				
Ta																				
Hf																				
Sb																				
Th																				
U																				
$^{87}Sr/^{86}Sr$	0.70431	0.70488	0.70474	0.70623	0.70460	0.70529	0.70614	0.70525	0.70519	0.70515	0.70428	0.70474	0.70506	0.70506	0.70516	0.70671	0.70617	0.70540	0.70517	0.70507
$^{143}Nd/^{144}Nd$	0.51276	0.51273	0.51265	0.51246	0.51268	0.51259	0.51245	0.51261	0.51256	0.51262	0.51281	0.51266	0.51261	0.51261	0.51263	0.51242	0.51243	0.51258	0.51265	0.51262
$^{206}Pb/^{204}Pb$						19.264					19.629				18.461	19.363	19.223			
$^{207}Pb/^{204}Pb$						15.679					15.655				15.613	15.647	15.711			
$^{208}Pb/^{204}Pb$						39.24					39.42				38.39	39.05	39.27			

Table 5 - Isotopic composition of Lipari volcanics from Esperanca et al. (1992) and Gioncada et al. (2003). Major (%) and trace (ppm) element data from the same authors are also reported.

Data Source	Esperanca et al., 1992					*Gioncada et al., 2003*															
Eruptive	**7 - 8**					**7 - 8 - 9**															
Epoch											enclave					enclave			enclave		
Sample	LIP 18	LIP 29	LIP 32	LIP 44	LIP 46	LIP 1	LIP 3	LIP-9	LIP-6	LIP-16	LIP-13	LIP-59s	LIP 59c	LIP-2	LIP-8	LIP-66A	LIP-66B	LIP-20	LIP-19	LIP-21	LIP-22
SiO_2	64.7	75.9	67.2	76.1	60.3	73.7	72.8	74.81	74.36	71.2	58.49	62.47	71.4	74.68	74	58.86	72.45	73.35	59.76	74.5	74.32
TiO_2	0.39	0.09	0.29	0.08	0.47	0.08	0.16	0.08	0.08	0.11	0.59	0.45	0.12	0.09	0.08	0.54	0.11	0.1	0.48	0.09	0.09
Al_2O_3	14.1	13.2	15.5	12.7	17.5	12.1	12.2	12.61	12.44	12.3	15.19	14.01	12.39	12.4	12.46	15.08	12.86	12.7	14.27	12.56	12.75
FeOtot	4.86	1.65	3.55	1.44	5.19	1.74	1.82	1.79	1.84	2.11	6.85	5.56	2.2	1.9	1.84	6.27	2.29	2.17	6.04	1.96	2.07
MnO	0.11	0.05	0.09	0.06	0.12	0.1	0.1	0.1	0.1	0.1	0.14	0.13	0.11	0.1	0.1	0.13	0.11	0.11	0.13	0.11	0.11
MgO	2.97	0.06	0.86	0.12	2	0.15	0.17	0.19	0.16	0.58	3.29	2.48	0.37	0.15	0.15	5.26	0.4	0.34	4.78	0.27	0.16
CaO	4.56	0.65	3.26	0.62	5.46	0.63	0.66	0.61	0.64	1.01	6.7	4.43	1.04	0.67	0.64	5.27	1.01	0.92	5.63	0.68	0.67
Na_2O	3.59	3.4	4.04	3.95	3.73	3.67	3.76	4.34	3.81	3.85	3.13	2.87	3.12	3.94	3.66	3.14	3.88	4.02	3.37	4.4	4.14
K_2O	4.08	4.77	4.63	4.79	4.4	4.53	4.58	4.6	4.6	4.63	3.44	3.61	4.89	4.55	4.72	4.37	4.69	4.6	4.03	4.59	4.69
P_2O_5	0.14		0.18	0.01	0.31		0.01	0.01		0.01	0.23	0.19	0.03	0.01		0.32	0.03	0.02	0.26	0.01	0.01
LOI	0.35	0.08	0.29	0.02	0.14	3.29	3.8	0.87	1.96	4.09	1.95	3.81	4.35	1.5	2.34	0.76	2.17	1.67	1.23	0.84	0.99
Sc						3	3		2	4	19	17			2			3	21	2	3
V	100		54		106	1			1	15	194	146						10	155	1	1
Cr	69	3	16	2	23					9	59	42						10	170	1	
Co										2	22	16						2	23		
Ni	18	2	7	2	8	1	1		1	3	18	14			1			3	33	1	1
Rb	193	280	211	284	131	271	271		264	269	134	174			269			267	170	273	284
Sr	541	12	692	25	1231	13	13		11	72	850	657			11			52	706	16	16
Y	40	59	46	50	30	42	42.4		42.8	41	27.4	33.2			42.9			44.1	32.3	44.5	45.1
Zr	127	153	138	147	131	180	181	182	176	162	70	92	175	184	177	93	203	202	105	224	239
Nb	21	31	24	32	18	30.5	30.5		30.9	30	14.9	19			30.7			32	19.6	33.4	34.6
Cs						16.3	16.3		16.1	15.2	6.5	8.6			16.2			17	9.3	17.3	18.1
Ba	356	15	405	24	721	7.9	6.2		6.8	48	540	428			8.2			42	523	16	18
La	39	39	44	35	48	38	40		39	38	37	37			38			50	53	56	68
Ce	90	86	90	75	98	77	82		79	77	72	73			78			97	102	105	123
Pr						9.1	9.5		9.3	9.1	8.6	8.7			9.3			11	11.9	12	13.4
Nd	34.4	34.3	36.8	32	38	33	34		35	32	33	32			34			39	43	41	46
Sm	7.18	7.42	7.51	7.06	7.3	7.7	8.1		7.5	7.4	6.9	7.1			7.6			8.1	8.7	8.5	8.8
Eu						0.11	0.12		0.11	0.18	1.22	0.92			0.12			0.17	1.08	0.13	0.13
Gd						6.3	6.1		6.5	6.1	5.6	5.7			6.3			6.7	6.9	7.2	7
Tb						1.1	1.11		1.12	1	0.81	0.86			1.09			1.12	0.98	1.13	1.17
Dy						6.6	6.6		6.9	6.1	4.7	5.3			6.8			6.9	5.4	7.1	7.2
Ho						1.41	1.41		1.42	1.35	0.93	1.08			1.4			1.48	1.06	1.52	1.54
Er						4.1	4.2		4.2	3.7	2.6	3			4.1			4.2	2.9	4.4	4.5
Tm						0.63	0.64		0.7	0.62	0.41	0.48			0.69			0.72	0.46	0.75	0.76
Yb						4.2	4.22		4.17	3.58	2.46	2.77			4.02			4.46	2.73	4.36	4.62
Lu						0.6	0.61		0.63	0.63	0.35	0.46			0.6			0.63	0.4	0.65	0.66
Ta						2.32	2.4		2.34	2.12	0.99	1.23			2.35			2.4	1.34	2.57	2.64
Hf						5.4	5.4		5.4	4.8	3.3	3.7			5.2			6.2	4.2	6.7	7.2
Sb						25.1	24.4		25.5	19.7	14.2	13.6			26.9			26.6	27.6	27	28.5
Th						39.1	38.9		40.6	36.4	17.9	21.2			39.8			46.7	26.8	50.1	54.4
U						11.9	11.8		12	10.9	5.3	6.4			11.9			13.5	7.9	14.5	15.8
$^{87}Sr/^{86}Sr$	0.70470	0.70581	0.70462	0.70508	0.70459	0.70581	0.70571	0.70593	0.70596	0.70493	0.70460	0.70487	0.70487	0.70597	0.70600	0.70443	0.70473	0.70472	0.70443	0.70590	0.70599
$^{143}Nd/^{144}Nd$	0.51258	0.51260	0.51261	0.51253	0.51265	0.51253	0.51254	0.51255	0.51253	0.51253	0.51262	0.51259	0.51254	0.51257	0.51257	0.51267	0.51257	0.51256	0.51263	0.51250	0.51253
$^{206}Pb/^{204}Pb$				19.364	19.444	19.352	19.357									19.447	19.374	19.38	19.414		19.376
$^{207}Pb/^{204}Pb$				15.708	15.71	15.69	15.697									15.708	15.692	15.701	15.691		15.696
$^{208}Pb/^{204}Pb$				39.38	39.43	39.30	39.32									39.39	39.31	39.34	39.33		39.32

CHAPTER 2

Petrogenesis of the mafic to intermediate rocks referred to the Eruptive Epochs 1-6 (270-80 ka)

2.1 - Introduction

The magmatic evolution of Lipari from 270 to 80 ka is characterized by a wide compositional range of the volcanic products (from CA and HKCA basaltic andesites to HKCA dacites) with a steep increase in K_2O from the early mafic to intermediate rocks (Fig.1). The volcanic history (270-80 ka) is described by six successive Eruptive Epochs, which are fully detailed in Chapter 1 (Forni et al., accepted for publication). During Eruptive Epochs 1, 2, 3 and 4 (271-116 ka) the volcanic activity concentrates on a series of scattered monogenic and polygenic volcanic centres both of central-type (M. Chirica, Chiesa Vecchia, Pietrovito, M. Mazzacaruso, Timpone Carrubbo and M. S.Angelo volcanoes) and fissural-type (Fuori del Pertuso, Timpone Ospedale spatter cones and Monterosa scoria cones), mostly distributed along the main tectonic trends (NNW-SSE, N-S and minor E-W). The associated products range in composition from CA and HKCA basaltic andesites to andesites. Eruptive Epoch 5 is dominated by the activity of M. S.Angelo stratocone and is characterized by the emplacement of HKCA andesitic to dacitic products, including the cordierite-bearing lavas (CBL; 105 ka). During Eruptive Epoch 6 (92-81 ka), with the effusion of a series of andesitic lava flows related to the activity of M. S.Angelo and M. Chirica stratocones, the mafic to intermediate volcanism at Lipari comes to an end and is followed by a 40 ka-long of quiescence interrupted by the emission of the rhyolitic products of Eruptive Epochs 7-9.

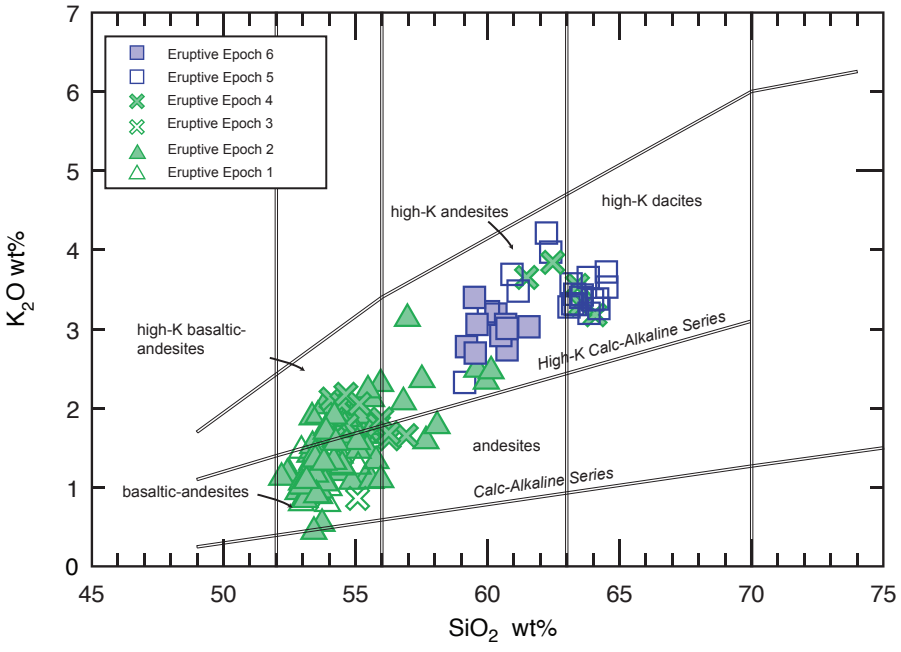

Fig.1 - K_2O vs. SiO_2 classification diagram (Peccerillo & Taylor, 1976) for the mafic to intermediate rocks of Eruptive Epochs 1-6 (270-80 ka).

Previous studies (Crisci et al., 1991; Esperanca et al., 1992 do not give a complete outline of the magmatic evolution of Lipari from 270 to 80 ka (cf. Chapter 1). Indeed, several petrogenetic problems, such as the role of the continental crust and its interaction with the mantle-derived melts, the nature and relative roles of magma evolution processes through time and the genetic relationships with the nearby island of Vulcano, still represent a matter of debates. In this Chapter these problems are discussed on the basis of new geochemical, mineral chemistry and Sr-Nd-Pb isotope data and in the light of the structure of Lipari pluming system, recently reconstructed by Di Martino et al. (2010).

2.2 - Petrographic features

A detailed petrographic description of the magmatic products referred to Eruptive Epochs 1 to 6 is reported in Chapter 1 (Forni et al., accepted for publication). Petrography and mineral chemistry data for the CBL (Eruptive Epoch 5) are reported in Chapter 3 (Di Martino et al., accepted for publication). In this section a brief summary of the petrographic features with new mineral chemistry data for representative rocks from Lipari (Tables 2, 3, 4, and 5; cf. Appendix) is presented.

CA and HKCA basaltic-andesitic and andesitic rocks (Eruptive Epochs 1-4) are

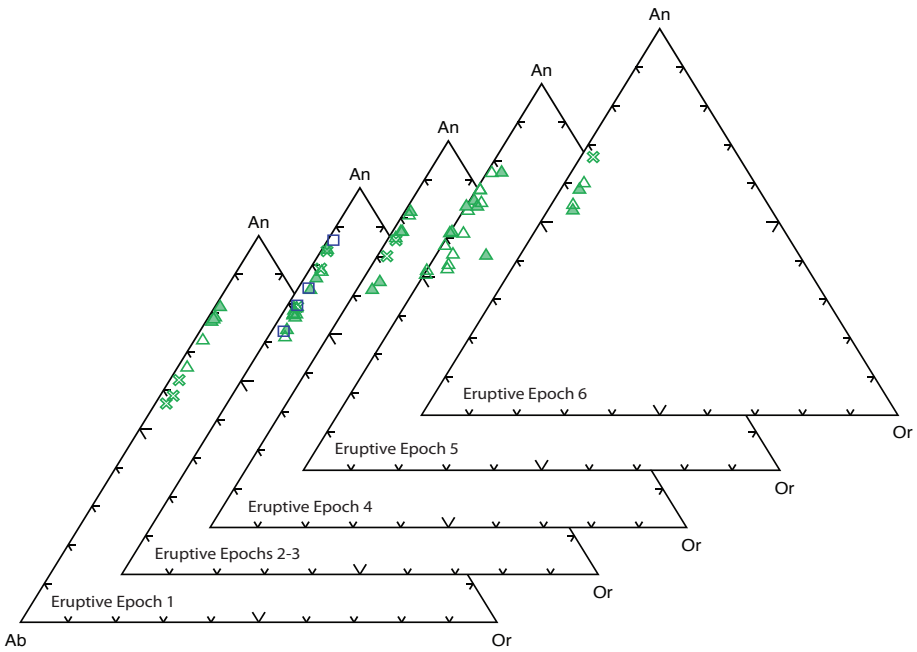

Fig.2 - Classification of plagioclases in the rocks of Eruptive Epochs 1-6 (additional data from Di Martino et al., accepted for publication; cf. Chapter 3). Full triangles: cores; empty triangles: rims; Crosses: microfenocrysts; Squares: plagioclase xenocrysts or plagioclases within the metamorphic xenoliths.

variably porphyritic (20-60%) with phenocrysts of plagioclase, clinopyroxene and orthopyroxene. Plagioclase phenocrysts are directly or inversely zoned and range in composition from An_{84} to An_{61}, whereas microcrysts in the groundmass vary from An_{74} to An_{57} (Fig.2). Clinopyroxene is zoned and changes in composition from diopside to augite (Fig.3). Orthopyroxene is from pigeonitic to enstatitic (Fig.3) and is frequently overgrown by clinopyroxene (augite) reaction rims. Ti-magnetite occurs as microcrysts in basaltic andesites and as phenocrysts in andesites (Fig.4). The andesitic rocks of Puddino formation (Eruptive Epoch 2) also contain ilmenite (Fig.4). Olivine (Fo_{78}), always altered to iddingsite, is scarcely present in basaltic andesitic and andesitic rocks. Apatite is an accessory phase in andesitic rocks. Mg-hastingitic amphibole (Bargossi et al., 1989) only occurs in pyroclastic rocks and lavas of Bervedere formation (Eruptive Epoch 1). Among the CA and HCKA basaltic-andesitic to andesitic rocks mixing textures (i.e. patches of magma with different compositions) and cognate xenocrysts (mostly clinopyroxene) have been frequently recognized.

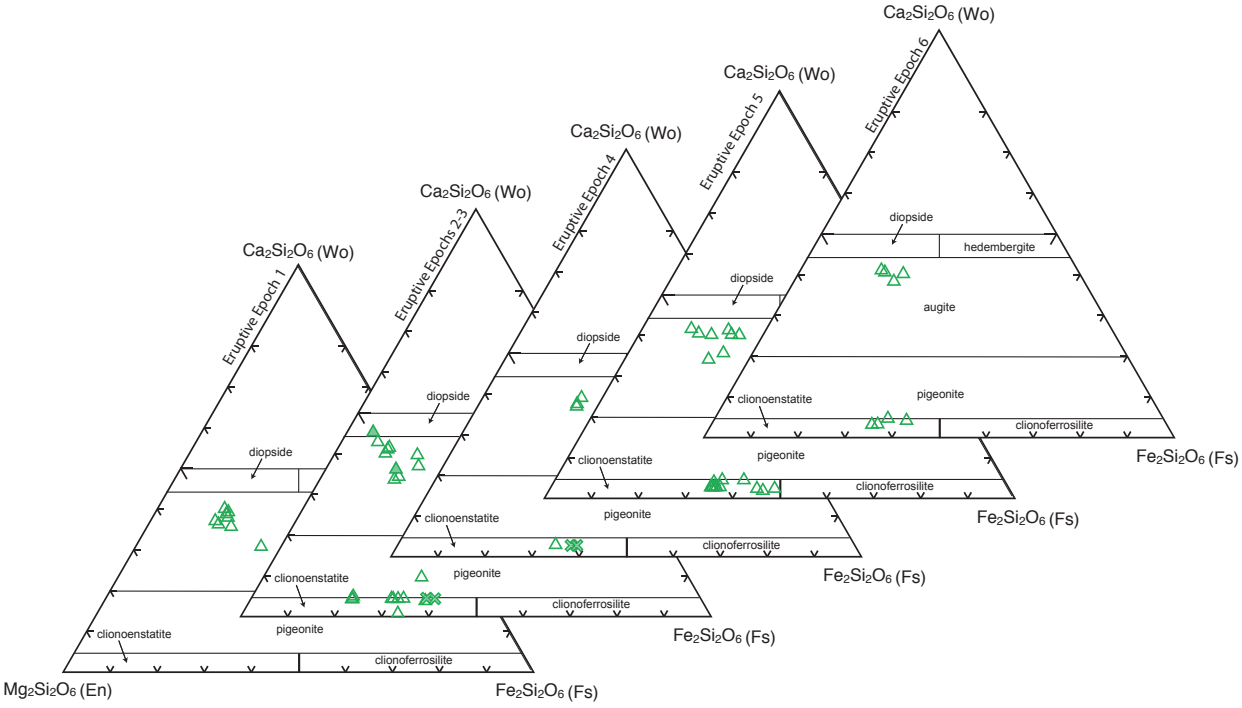

Fig.3 - Composition of pyroxenes in the rocks of Eruptive Epochs 1-6 (additional data from Di Martino et al., accepted for publication; cf. Chapter 3). Empty triangles: pyroxene from basaltic-andesites and andesites of Eruptive Epochs 1, 2, 3, 4 and 6; full triangles: pyroxenes within the gabbroic xenoliths; crosses= pyroxenes within the metamorphic xenoliths.

The HKCA dacitic lavas of Timpone del Corvo formation (Eruptive Epoch 4) contain mostly plagioclase, subordinate clinopyroxene, orthopyroxene and Ti-magnetite phenocrysts.

The HKCA andesitic to dacitic lavas of Pulera formation (CBL; Eruptive Epoch 5) have highly porphyritic texture (up to 50%) and contain plagioclase, orthopyroxene, clinopyroxene, cordierite, garnet (Fig.5 e-f), K-feldspar and minor ilmenite, apatite, andalusite (Fig.5 g-h), spinel and sillimanite. They are also very rich in metapelitic (Fig.5 c-d) and gabbroic xenoliths (up to 20-30%). The groundmass is hypocrystalline and contains plagioclase, cordierite, orthopyroxene, K-feldspar, biotite and glass. Plagioclase phenocrysts have calcic cores (An_{77-70}) and become abruptly more albitic towards the rims (An_{50-55}) (Fig.2). Clinopyroxene, diopsidic to augitic in composition (Fig.3), is always surrounded by fine-grained orthopyroxene. Cordierite occurs in coarse euhedral to subhedral phenocrysts (generally < 4 mm, locally up to 10 mm, or more), very rich in silicate melt and mineral inclusions. Garnet grains have different morphologies: subhedral/euhedral grains with resorbed margins always associated with cordierite and anhedral and resorbed grains with embayed outlines (Fig.5 e-f). Compositionally different orthopyroxene has been recognized: stumpy microphenocrysts and crystal aggregates rimming clinopyroxene are enstatic in composition (Mg# =0.68-0.65; low Al_2O_3 and CaO), whereas orthopyroxene associated with cordierite and garnet has lower Mg# (=0.55) and higher Al_2O_3 and CaO (Di Martino et al., accepted for publication; cf. Chapter 3).

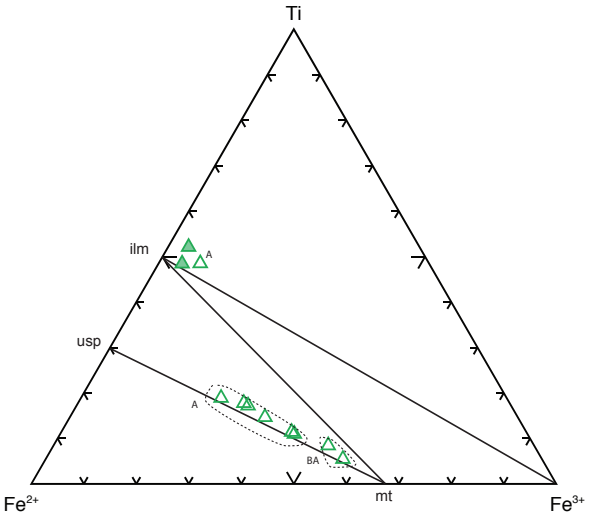

Fig.4 - Classification of Fe-Ti oxides in the rocks of Eruptive Epochs 1-6. Full triangles: Fe-Ti oxides in CBL (Eruptive Epoch 5); empty triangles: Fe-Ti oxides in basaltic-andesitic (BA) to andesitic (A) rocks of Eruptive Epochs 1, 2, 3, 4 and 6.

The HKCA andesitic rocks of Eruptive Epoch 6 show highly porphiritic (35-60%) to porphiritic seriate texture and contain phenocrysts of plagioclase (An_{67-53}) (Fig.2), orthopyroxene, clinopyroxene and Ti-magnetite within a hyalopilitic groundmass.

Magmatic gabbroic xenoliths consisting in cumulus-textured assemblages, made up of clinopyroxene, orthopyroxenes, plagioclase (An_{67}) (Fig.2), olivine (Fo_{77}) and Ti-Fe oxides, are documented in the basaltic-andesitic to dacitic rocks (Eruptive Epochs 1-6). Metamorphic xenoliths (granulites, metapelites and quarzites) are extensively diffuse in lavas and pyroclastic rocks from Lipari. Their abundance generally increases from basaltic andesites to andesites and dacites.

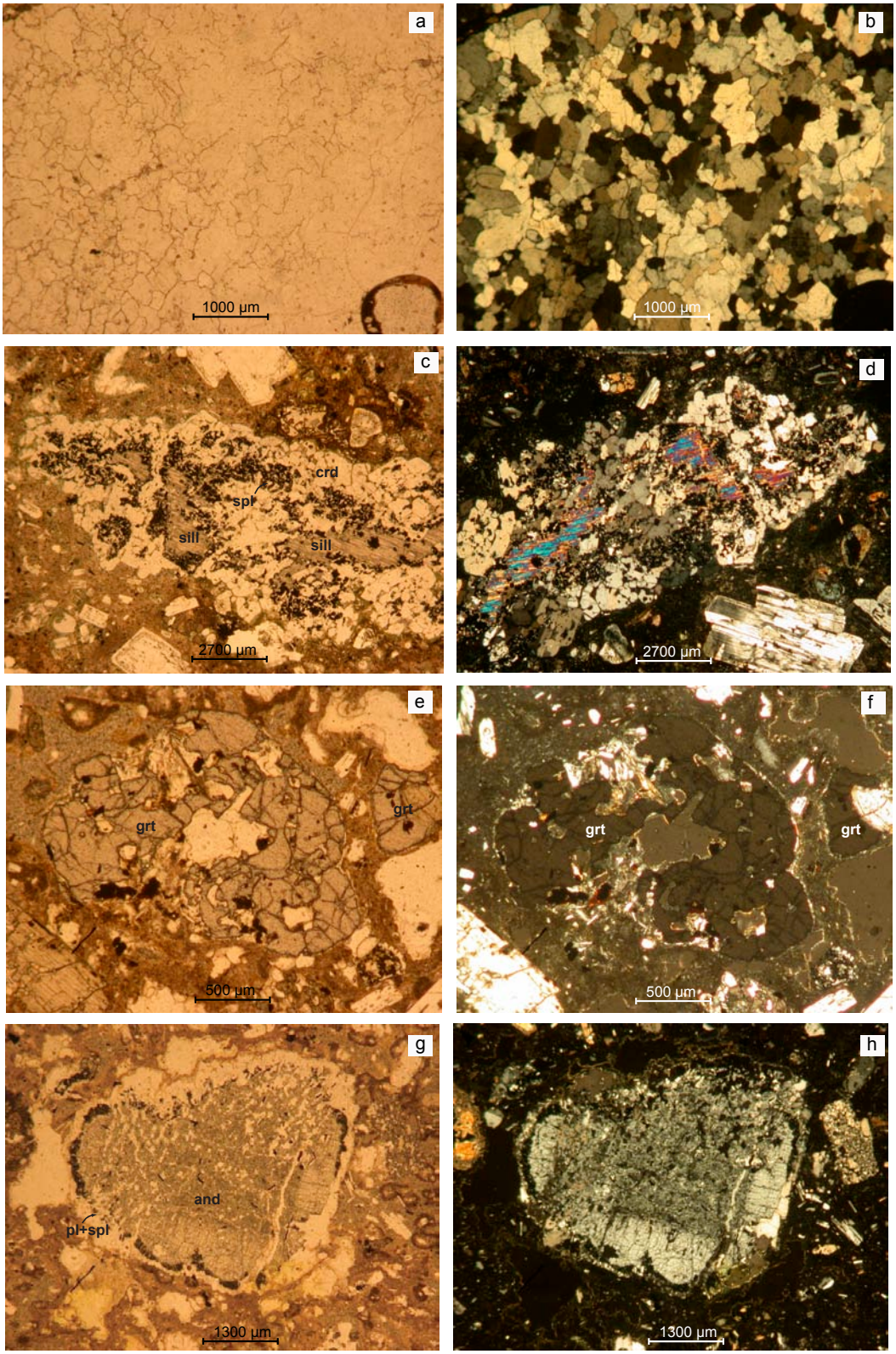

Fig.5 - Quartz-rich xenolith within the HKCA andesitic rocks of Epuptive Epoch 2 (V.ne Malopasso fm.) (a-b); metamorphic xenolith containing relict of sillimanite (=sill) surrounded by cordierite (=crd) and spinel (=spl) coronas (c-d), scheletric garnet (=grt) grains (e-f) and andalusite with plagioclase (=pl) and spinel coronas (g-h) in the CBL of Eruptive Epoch 5 (Pulera fm.).

Quartz-rich xenoliths are white-colored, angular shaped and millimetric to centimetric in size (Fig.5 a-b). Exceptionally they reach the maximum size of 20 cm. They are almost completely made up of quartz grains (0.1-5 mm), rare feldspars and pyroxenes. The texture is mostly inequigranular with typical 120° triple junction (Fig.5). No reaction rims at the boundary with host lava is reported. Mesoscopic metapelitic xenoliths containing cordierite, garnet, andalusite, sillimanite, biotite and oxides have been long observed in the renowned cordierite-bearing lavas (Bergeat, 1910; Pichler, 1980; Barker, 1987) of Eruptive Epoch 5 (Fig.5 c-d). Barker (1987) recognized xenoliths with similar characteristics within the lavas of Eruptive Epoch 2 (Puddino formation). These HKCA andesitic lavas also include a considerable amount of metamorphic xenoliths made up of plagioclase (An_{86-61}; Fig.2) and patches of orthopyroxene (enstatite; Fig.3) and spinel (hercynite) with no mineral preferred orientations and appear highly resorbed and transformed.

2.3 - Analytical methods

A number of 132 whole-rock samples, representative of Eruptive Epochs 1-6 (270-80 ka), were analyzed for major and trace elements by X-ray fluorescence at Dipartimento di Scienze della Terra (University of Bologna). Data were corrected for matrix effect using the method described by Franzini et al. (1975) and Leoni & Saitta (1976). Loss of ignition (LOI) was determined by heating at 950°C.

A subset of these samples (n=20) was analyzed for trace and rare earth elements (REE), by ICP-AES and ICP-MS at SGS Laboratory (Toronto, Canada). Precision is better than 10% for Cr, 5% for Sc, 1% for V, Co, Ni, Rb, Sr, Zr, Nb, Cs, Ba, La, Ce, Nd, Ta, Hf and Pb and 0.1% for the other trace elements.

Mineral chemistry analyses were performed using a Philips 515b scanning electron microscope (SEM), equipped with Edax dx4 microprobe (EDS) at University of Bologna. Operating conditions were: acceleration voltage 15 kv and beam current 2 nA.

Basing on major and trace elements variations, 23 representative whole-rock samples were selected and prepared for radiogenic isotope analysis. Sr, Nd and Pb isotopic ratios were determined using a multicollector automated Finnigan-MAT 262 mass spectrometer at the U.S. Geological Survey, Reston, VA. Detailed analytical technique for Pb, Nd and Sr are given in Ayuso & Schulz (2003) and Ayuso et al. (2009). Sr and Nd isotope data were reported relative to international standards: La Jolla standard ($^{143}Nd/^{144}Nd$ average value =0.511850±5) and NIST-SRM 987 standard ($^{87}Sr/^{86}Sr$ average value =0.710250±6). Pb isotopic ratios were corrected for mass

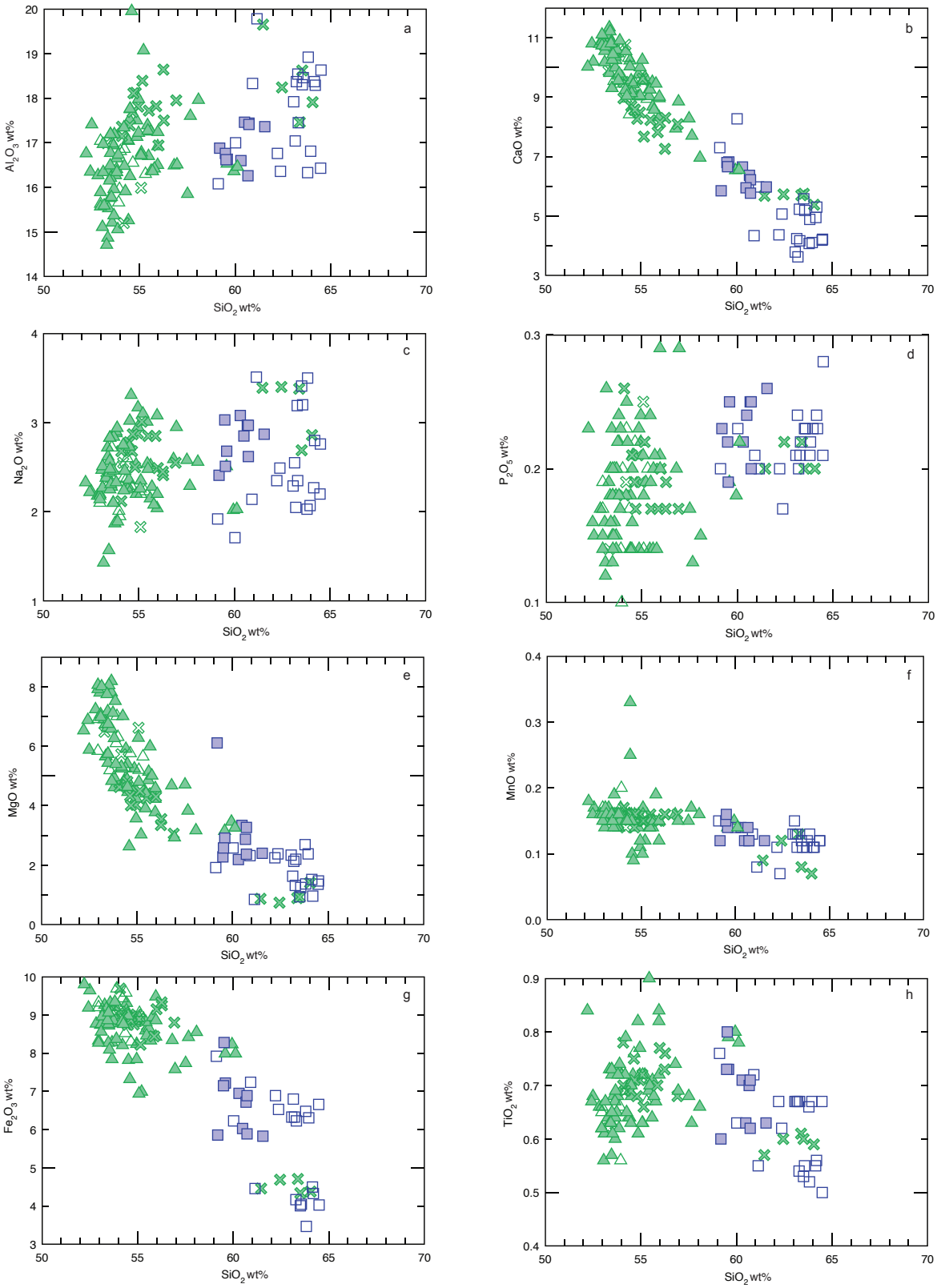

Fig.6 - Variation diagrams of major elements vs. SiO_2 for Lipari mafic to intermediate rocks (270-80 ka). Symbols as in Fig.1.

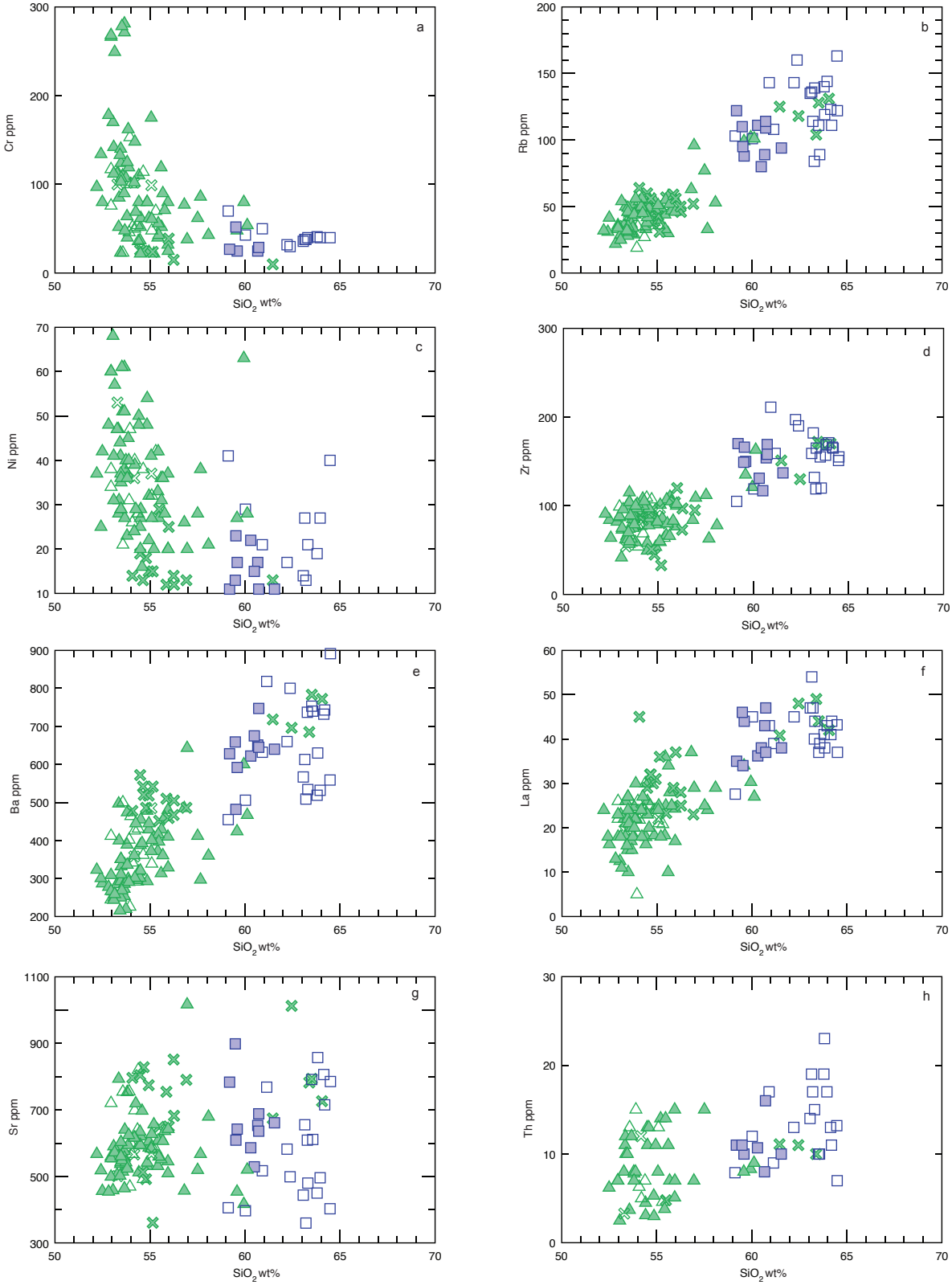

Fig.7 - Variation diagrams of trace elements vs. SiO_2 for Lipari mafic to intermediate rocks (270-81 ka). Symbols as in Fig.1.

fractionation by 0.08%, 0.12% and 0.16% amu-1 at 2sigma for $^{206}Pb/^{204}Pb$, $^{207}Pb/^{204}Pb$ and $^{208}Pb/^{204}Pb$ respectively, according to replicate measurement of NBS 981.

2.4 - Major and trace elements

Major and trace element data for representative samples from Lipari are reported in Table 1 (cf. Appendix). Variation diagrams of major and trace elements against SiO_2 are shown in Figs.6 and 7.

MgO, Fe_2O_3 and CaO linearly decrease with SiO_2, whereas K_2O increases. Al_2O_3 and P_2O_5 roughly increase with SiO_2, showing wide variations in basaltic andesites. Na_2O is almost constant, while TiO_2 increases in basaltic andesites, than decreases from andesites to dacites (Fig.6).

Ferromagnesian trace elements (e.g. Cr and Ni; Fig.7 a-c) generally decrease with SiO_2 defining in basaltic andesitic rocks steep trends, which are typical of fractional crystallization processes involving early fractionating phases such as olivine, clinopyroxene and Fe-Ti oxide. In particular, Cr describes nearly curvilinear trends, whereas Ni is much more scattered. Large Ion Lithophyle Elements (LILE: Rb, Ba, Th, U, LREE, etc.) and High Field Strength Elements (HFSE: Ta, Nb, Zr, Hf) generally define linear positive trends from basaltic andesites to dacites (e.g. Rb, Zr, La and Th; Fig.7 b-d-f-h). Sr appears widely scattered (Fig.7 g), indicating that plagioclase plays a secondary role as a fractionating phase. Ba increases from basaltic andesites to andesite than steeply descrese in dacitic rocks (Fig.7 e).

Fractionation between LREE and HREE is moderate but increases from basaltic andesites to dacites. No significant Eu negative anomaly has been observed. (Fig.8).

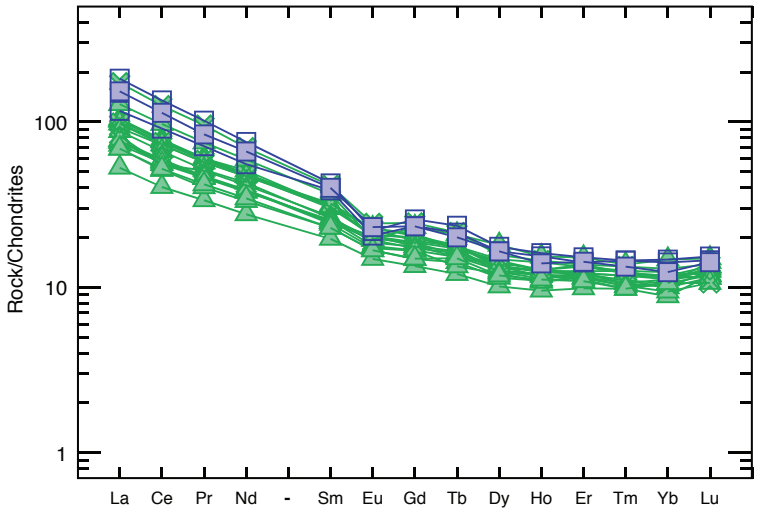

Fig.8 - REE patterns normalized to chondrite values (Sun & Mc Donough, 1989) for Lipari mafic to intermediate rocks (270-81 ka). Symbols as in Fig.1.

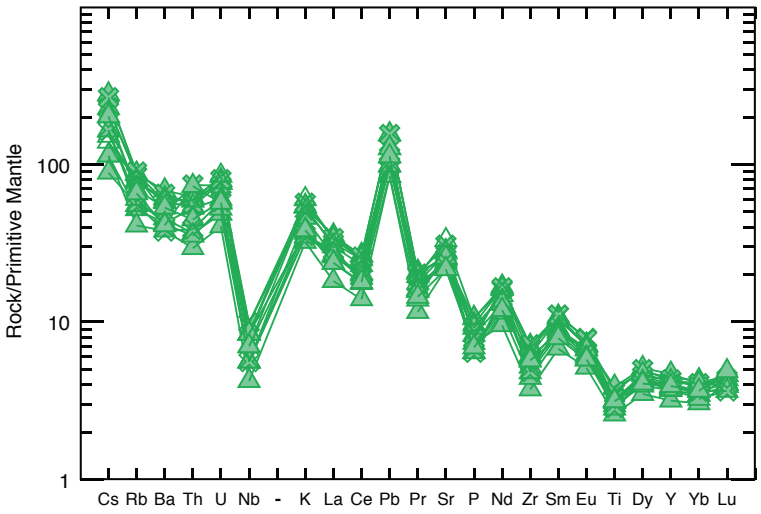

Fig.9 - Incompatible trace element patterns normalized to primordial mantle (Sun & Mc Donough, 1989) for Lipari mafic to intermediate rocks (270-81 ka). Symbols as in Fig.1.

Incompatible elements normalized to primordial mantle for basaltic andesitic terms show toughs at Nb and Ti, which are typical of volcanic arc-related magmas and a positive spike at Pb (Fig.9).

2.5 - Sr, Nd and Pb isotopes

Sr, Nd and Pb isotope data for Lipari samples are reported in Table 1 (cf. Appendix).

Samples referred to Eruptive Epochs 1 to 4 display the widest range of Sr and Nd isotope compositions ($^{87}Sr/^{86}Sr$ =0.705115-0.706752; $^{144}Nd/^{143}Nd$ =0.512311-0.512714) (Fig.10). Overall, the analyzed samples from Lipari partially overlap the fields of Panarea, Vulcano and Stromboli. Just few samples referred to Eruptive Epoch 2 bear similarities with Salina and Filicudi isotopic compositions. Exceptionally sample T9 (Puddino Formation; Eruptive Epoch 2) show the highest values of Sr and the lowest values of Nd isotope ratios ($^{87}Sr/^{86}Sr$ =0.706991; $^{144}Nd/^{143}Nd$ =0.511937) measured for Lipari rocks, whereas cordierite-bearing lavas of Eruptive Epoch 5 range in $^{87}Sr/^{86}Sr$ from 0.706133 to 0.706685 and in $^{144}Nd/^{143}Nd$ from 0.512176 to 0.512431, approaching the isotopic compositions of the Calabrian Basement metapelitic rocks. Sr and Nd isotope ratios correlate respectively positively and negatively with SiO_2 (Fig.11) and incompatible trace elements (not shown).

Except for sample T9 (Puddino Formation; Eruptive Epoch 2) Lipari rocks show small variations in Pb isotope ratios and fall within the fields described by the other islands, save Stromboli (Fig.12). Samples referred to Eruptive Epoch 2 display the most scattered values, especially for $^{207}Pb/^{206}Pb$ ratios, whereas cordierite-bearing lavas (Eruptive Epoch 5) form weak trends towards the crustal compositions (Fig.12).

Notably, Sr, Nd and Pb isotopic compositions of sample T9 (Puddino Formation; Eruptive Epoch 2) indicate that a relatively low $^{87}Sr/^{86}Sr$, low $^{144}Nd/^{143}Nd$ and Th-U-depleted component probably contributed to the genesis of these lavas. Coherently with petrographic observations, this component might be identified with the mafic granulites of the lower crust, but it requires more investigations.

Compared with data from Esperanca et al. (1992) and Gioncada et al. (2003), Sr, Nd and Pb isotope data presented in this study indicate a wider range of isotopic compositions for Lipari rocks.

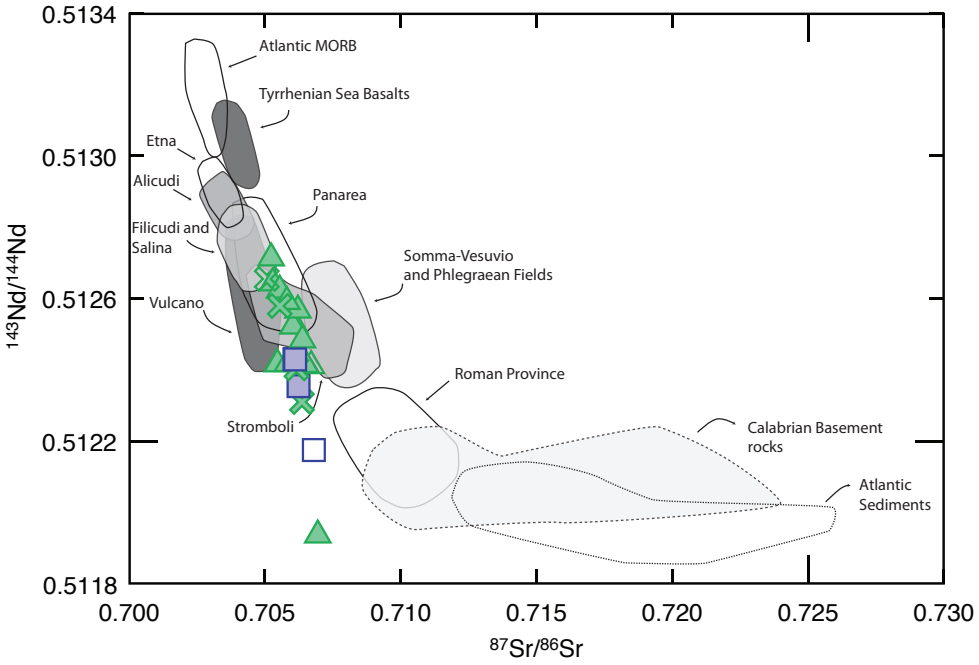

Fig.10 - Nd vs. Sr isotope variations for Lipari mafic to intermediate rocks (270-81 ka). Symbols as in Fig.1. Compositional fields of Calabrian basement rocks (Caggianelli et al., 1991), Alicudi (Peccerillo & Wu, 1992; Peccerillo et al., 1993; Peccerillo et al. 2004), Filicudi (Santo et al., 2004), Salina (Ellam et al., 1989; Francalanci et al., 1993;Gertisser & Keller, 2000), Panarea (Calanchi et al., 2002), Vulcano (De Astis et al., 1997, 2000; Gioncada et al., 2003), Stromboli (Ellam et al., 1989; Francalanci et al., 1993), Atlantic Sediments (Plank & Langmuir,1998), Roman Province (Hawkesworth & Vollmer, 1979; Rogers et al., 1985; D'Antonio et al., 1996; Conticelli et al., 1997; Di Battistini et al., 2001; Gasperini et al., 2002; Perini et al., 2004), Mt. Somma-Vesuvius and Phlegraean Fields (Hawkesworth & Vollmer, 1979; Civetta et al., 1991; Ayuso et al., 1998; D'Antonio et al., 1999; Pappalardo et al., 2002) , Tyrrhenian Sea Basalts ODP site (Beccaluva et al., 1990), Atlantic MORB (Cohen et al., 1980; Ito et al., 1987) and Etna (Tonarini et al., 1995; D'Orazio, 1997; Armienti et al., 2004) are reported for comparison.

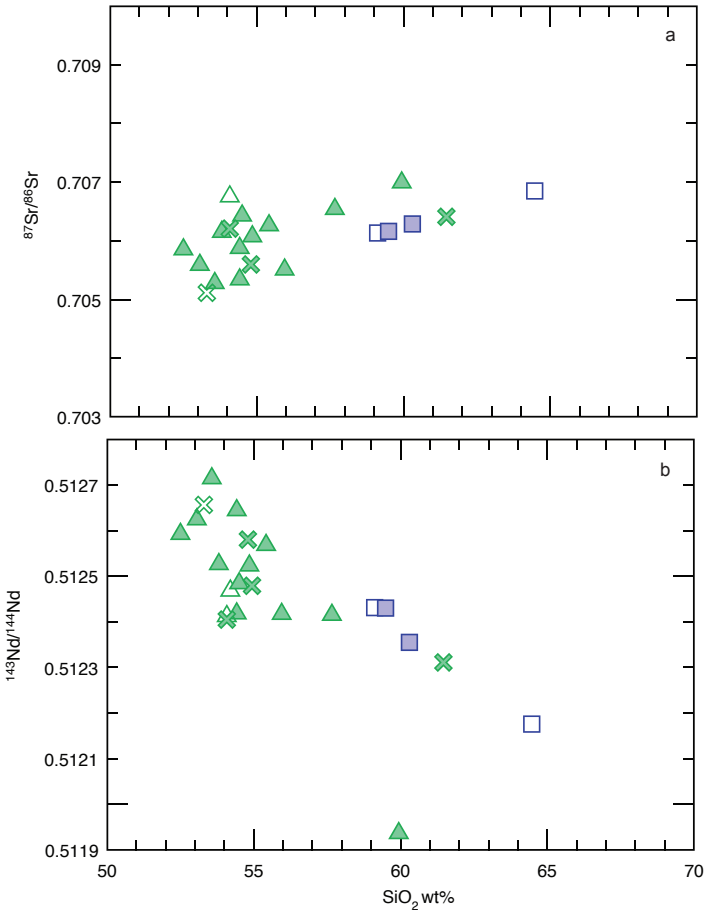

Fig.11 - Variation diagrams of Sr and Nd isotope ratios vs. SiO_2 for Lipari mafic to intermediate rocks (270-81 ka). Symbols as in Fig.1.

2.6 - Magma evolutionary processes

2.6.1 - Eruptive Epochs 1, 2, 3 and 4 (270-116 ka)

The CA and HKCA basaltic-andesitic to andesitic pyroclastics and lavas of Eruptive Epochs 1, 2, 3 and 4 (270-116 ka) are related to the activity of different monogenic and polygenic volcanic centers and are characterized by wide variations in trace element ratios (in particular LILE/HFSE and HFSE/HFSE; Figs.14, 16) and isotopic compositions (Fig.10, 12).

CA basaltic andesites represent the oldest and most primitive rocks on the island. Compared to the Tyrrhenian Sea basalts and the mafic rocks from Alicudi island, which represent the most primitive rocks of the entire Aeolian archipelago, they display lower Ni and Cr concentrations (Fig.13), suggesting some pre-emplacement evolution involving crystallization of mafic phases at depth. Furthermore, the relatively low Nd and high Sr isotopic ratios (Fig.10) suggest that interaction of mafic magma with the continental crust might have been effective during fractional crystallization processes.

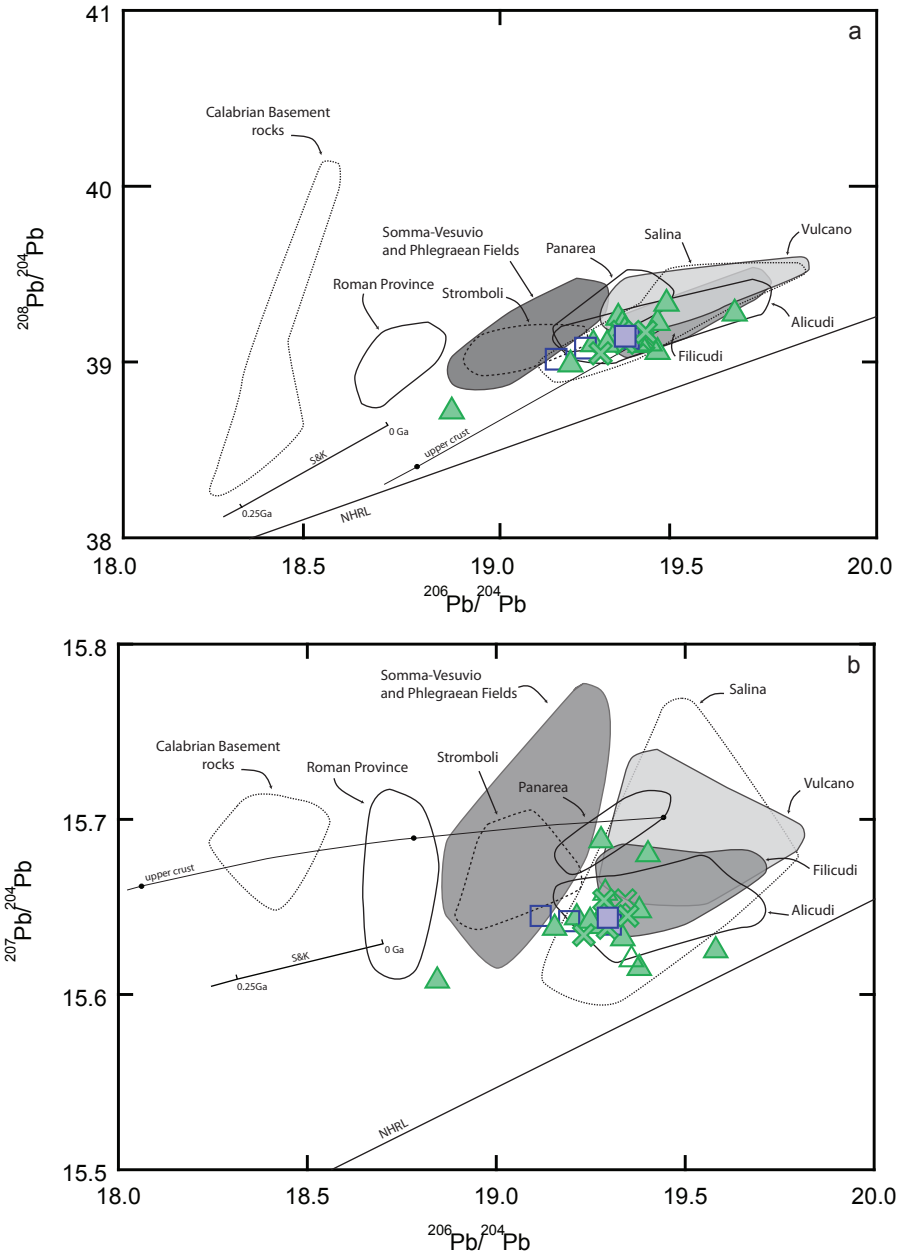

Fig.12 - Pb isotope variations for Lipari mafic to intermediate rocks (270-81 ka). Symbols as in Fig.1. Compositional fields of Calabrian Basement rocks (Caggianelli et al., 1991), Alicudi (Peccerillo & Wu, 1992; Peccerillo et al., 1993; Peccerillo et al. 2004), Filicudi (Santo et al., 2004), Salina (Ellam et al., 1989; Francalanci et al., 1993;Gertisser & Keller, 2000), Panarea (Calanchi et al., 2002), Vulcano (De Astis et al., 1997, 2000; Gioncada et al., 2003), Stromboli (Ellam et al., 1989; Francalanci et al., 1993), Roman Province (Hawkesworth & Vollmer, 1979; D'Antonio et al., 1996; Conticelli et al., 1997; Di Battistini et al., 2001; Gasperini et al., 2002; Perini et al., 2004), Somma-Vesuvius and Phlegraean Fields (Civetta et al., 1991; Ayuso et al., 1998; D'Antonio et al., 1999; Pappalardo et al., 2002) are reported for comparison. Northern Hemispher Reference Line (NHRL) from Hart (1984). Pb isotope evolution curve for the upper crust from Zartman & Haines (1988). Model growth for the average crust from Stacey & Kramers (1975; S&K).

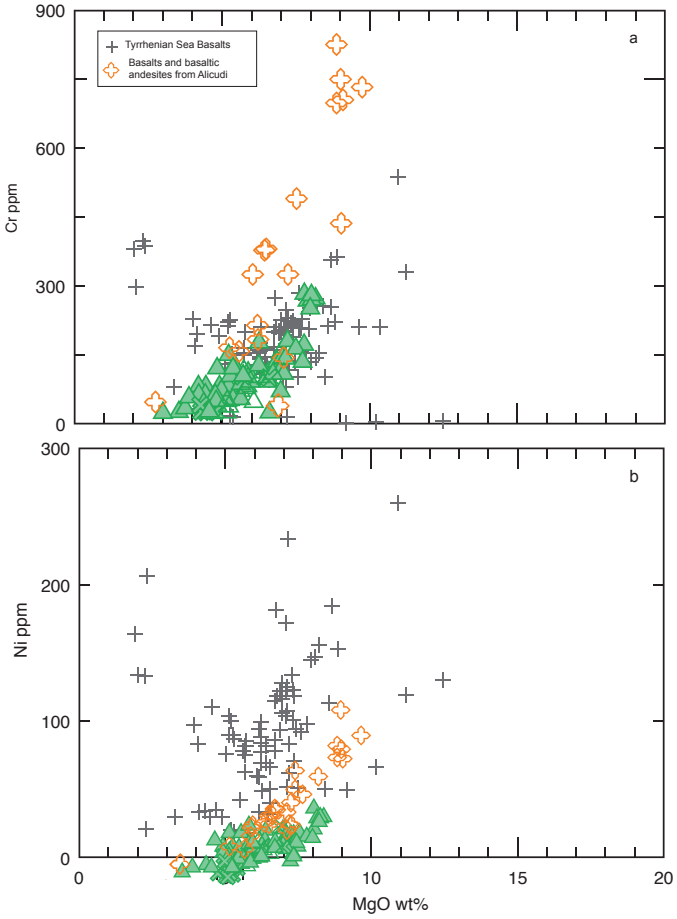

Fig.13 - Plots of ferromagnesian trace elements vs. MgO for the CA basaltic-andesitic rocks of Lipari (Symbols as in Fig.1). Tyrrhenian Sea Basalts ODP site (Beccaluva et al., 1990) and mafic rocks from Alicudi (Peccerillo & Wu, 1992; Peccerillo et al., 1993; Peccerillo et al. 2004) for comparison.

The magmatic evolution in time from CA basaltic andesites to HKCA andesites might have been hence ruled by similar processes, as indicated by the positive correlations of $^{87}Sr/^{86}Sr$ with SiO_2 (Fig.11 a) and some key incompatible trace elements and ratios, in concert with petrographic observations indicating the increasing abundance of metamorphic xenoliths from basaltic andesites to andesites. These features are not compatible with simple fractional crystallization processes (FC) therefore assimilation and fractional crystallization (AFC; De Paolo, 1981) modelling have been tested.

AFC models carried out using incompatible trace element ratios (LILE/HFSE and HFSE/HFSE) and Cr vs. $^{87}Sr/^{86}Sr$ are reported in Fig.14. Sample Lip113 (Eruptive Epoch 2) has been used as parent (Co) in these models on the basis of its relatively high content in ferromagnesian trace elements and primitive isotopic compositions (Lip105 cannot be used as parent because of its high porphyritic index). Trace elements and isotopic compositions of the Calabrian Basement rocks from Caggianelli et al. (1991) have been also reported in the plots. Extreme compositions have been used as assimilants (Ca) in each model. Partition coefficients have been estimated from trace elements variation diagrams (Figs.7 and 14) and according to the least-squares mass balance calculations based on major element data (Table 6, cf. Appendix).

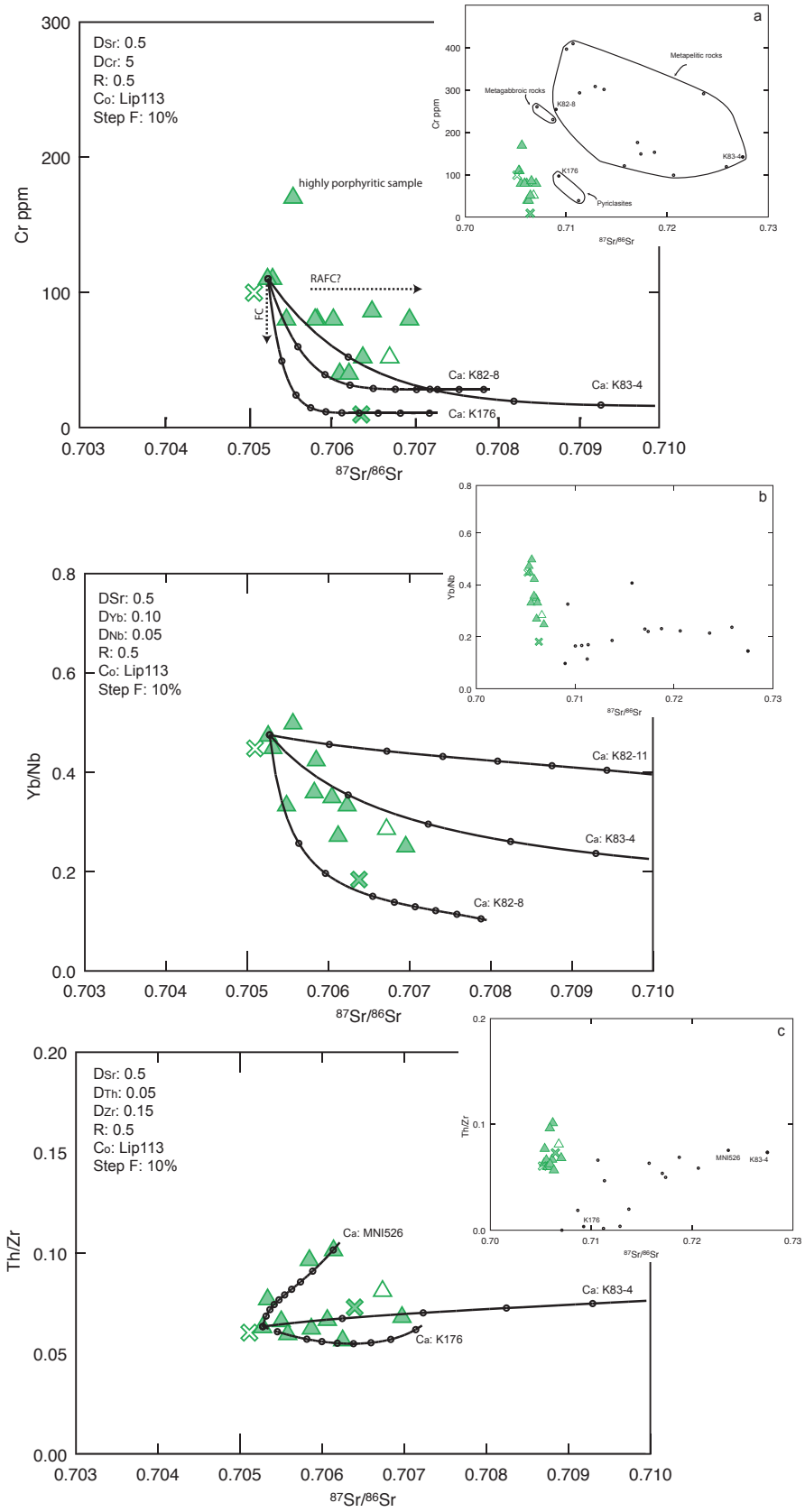

Fig.14- AFC models for Lipari rocks (Eruptive Epochs 1-4; 270-116 ka). Symbols as in Fig.1. Trace elements and isotopic compositions of the Calabrian Basement rocks (Caggianelli et al., 1991) are reported in the insets.

For example, the values of 0.5 and 5 have been attributed to Sr (D_{Sr}) and Cr (D_{Cr}) respectively, because clinopyroxene is supposed to play a more important role as fractionating phase with respect to plagioclase. Estimated partition coefficients fall within the ranges reported in literature (Rollinson, 1993). The wide range of $^{87}Sr/^{86}Sr$ isotopic compositions and the small geochemical variations hint at high rates of assimilation vs. fractional crystallization (r=0.5).

Incompatible trace element ratios vs. $^{87}Sr/^{86}Sr$ models give positive results, considering that most geochemical and isotopic variations described by Lipari samples are included within the different AFC paths (Fig.14 b-c). In contrast, the $^{87}Sr/^{86}Sr$ vs. Cr AFC model (Fig.14 a) does not fit the horizontal trends delineated by some samples with similar Cr contents that progressively tend towards higher $^{87}Sr/^{86}Sr$ isotope ratios. These variations may be theoretically obtained by increasing the rate of assimilation vs. fractional crystallization until r=1, which is very unlikely. A more realistic possibility is represented by the occurrence of replenishment, assimilation and fractional crystallization processes (RAFC; O'Hara, 1977) that imply the continuous mixing between the resident magma and fresh mafic magmas coming from the source. These processes have been successfully related to the magmatic evolution of the oldest rocks of Vulcano Island by De Astis et al. (1997) and give good explanation for the small depletions in compatible elements during fractionation of mafic phases (Fig.14 a). Moreover, these observations are in accordance with the fluid inclusion density data for the rocks of Eruptive Epoch 2 (Di Martino et al., 2010), which indicate the presence of a main zone of magma accumulation, located at the lower crust-mantle boundary (18-22 km). High-pressure conditions, in fact, typically prevent the plagioclase of being a fractionating phase during fractional crystallization processes and relatively high depths of magma accumulation favour injections of mafic magmas from the mantle source (De Astis et al., 1997; Peccerillo et al., 2006). Besides, the presence of mixing textures and xenocrysts of clinopyroxene within the basaltic-andesitic and andesitic rocks from Lipari confirms that fresh mafic magmas might have interacted with the resident fractionating magmas.

2.6.2 - Cordierite-bearing lavas (CBL), Eruptive Epoch 5 (105 ka)

The CBL, dated at ~105 ka and related to the activity of M. S.Angelo stratocone (Eruptive Epoch 5), represent the clearest evidence of the fundamental role played by the interaction between mantle-derived magma and the continental crust in the magmatic evolution of Lipari. In fact, these rocks, ranging in bulk-composition from HKCA andesites to dacites, are characterized by the coexistence of typical igneous minerals (plagioclase and pyroxenes) along with phenocrysts of cordierite and garnet

and a large amount of gabbroic and metamorphic xenoliths.

Because of their peculiar characteristics the CBL have been subjected to numerous studies (Bergeat, 1910; Barker, 1987; De Vivo et al., 1987; Crisci et al., 1991; Esperanca et al., 1992). Most of them attribute to the CBL a genesis by assimilation and fractional crystallization, but do not exclude the possible occurrence of crustal melting processes.

A detailed study focused on the petrogenesis of the CBL is reported in Chapter 3 (Di Martino et al., accepted for publication). In this study, based on mineral chemistry, melt inclusions and Sr-Nd whole rock and mineral isotope data, the cordierite-bearing lavas are interpreted as the product of mixing and consequent hybridization of mantle-derived magmas (akin to Lipari rocks of Eruptive Epochs 1-2) and crustal anatectic melts.

2.6.3 - Eruptive Epoch 6 (92-81 ka)

The volcanic activity, which follows the eruption of the CBL, is characterized by the emission of HKCA andesitic lavas constructing the upper portions of the M. S.Angelo stratocone and M. Chirica volcano (Eruptive Epoch 6). These rocks do not exhibit petrographic evidences of interaction with the crust; moreover, with respect to the CBL, they display lower Sr and higher Nd isotope ratios and show lower contents in incompatible trace elements. On the contrary, they bear remarkable similarities with the most evolved terms of the AFC suite (Eruptive Epochs 1-4), in particular with the high $^{87}Sr/^{86}Sr$ and high Rb, HKCA andesite of Timpone del Corvo formation (Eruptive Epoch 4). This suggests a possible genetic link between these products and the volcanic activity preceding the eruption of the CBL, therefore new AFC models, carried out using trace elements and Sr isotope ratios, have been tested (Fig.15). In these models sample Lip113 (Eruptive Epoch 2) has been used as parent (Co) and extreme compositions of the Calabrian Basement rocks (Caggianelli et al., 1991) have been taken on as assimilants (Ca). Partition coefficients have been estimated on the basis of the geochemical behavior of trace elements in variation diagrams (Fig.7) and are consistent with the ranges reported in literature (Rollingson, 1993).

Least-square major elements mass balance calculations (Table 7, cf. Appendix) indicate that plagioclase and clinopyroxene are the most important fractionating phases in the differentiation from basaltic-andesitic to andesitic compositions, thus suggesting that the partition coefficients of Sr and Cr must be relatively high (D_{Sr}=1 and D_{Cr}=5). Crystallization of plagioclase is favoured by low pressures, therefore the fractionation of large amounts of this phases requires important changes of the geo-barometric conditions, which occur during fractional crystallization processes. This is corroborated by the fluid inclusion data that indicate an upward migration of the deep

level of magma accumulation to mid-crustal depths (12-17 km) during Eruptive Epochs 5 and 6 (Di Martino et al., 2010).

Different petrogenetic models obtained using these parameters confirm that andesitic rocks of Eruptive Epoch 6 may likely represent fractionated products of the AFC paths (Fig.15).

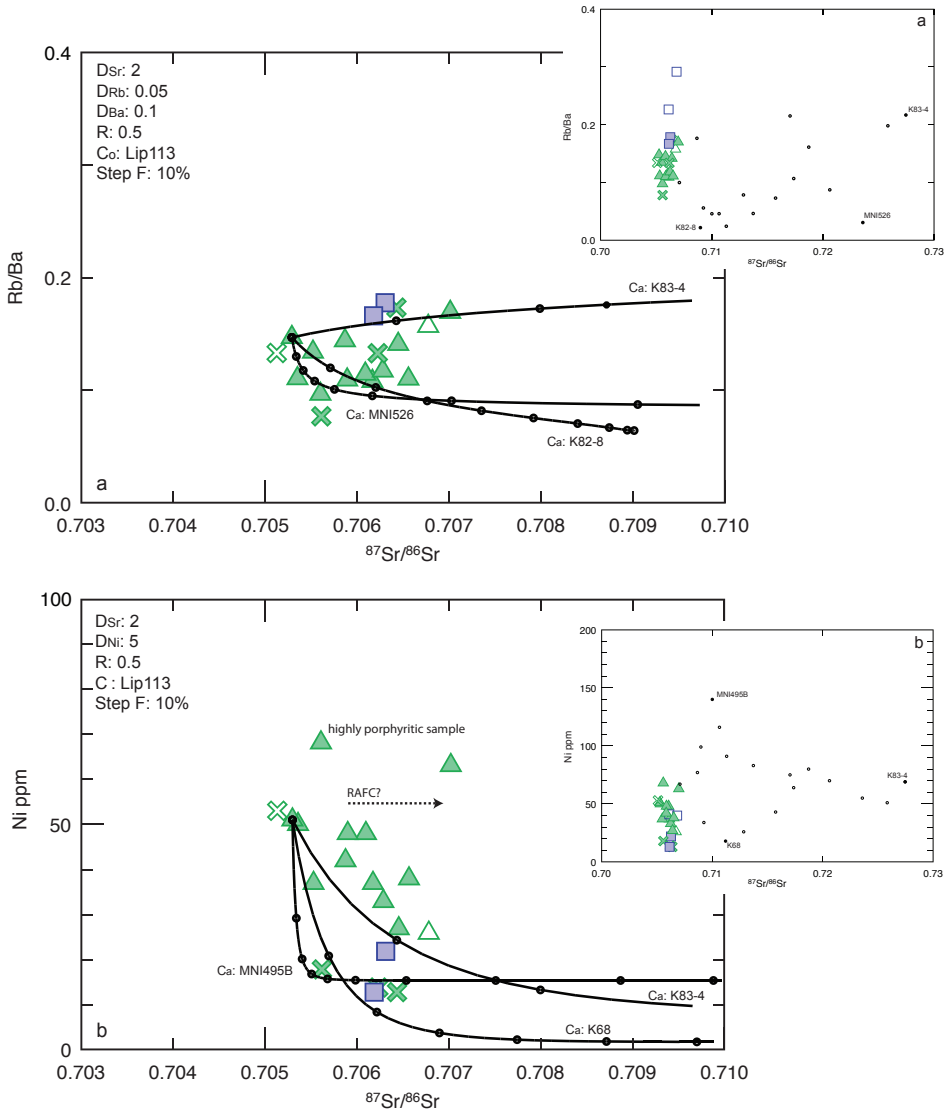

Fig.15 - Rb/Ba (a) and Ni (b) vs. $^{86}Sr/^{87}Sr$ AFC models for the andesitic rocks of Lipari (Eruptive Epoch 6; 92-81 ka). Symbols as in Fig.1. Trace element and isotopic composition of the Calabrian Basement rocks (Caggianelli et al., 1991) are reported in the insets.

2.7 - The Lipari-Vulcano system

The islands of Lipari and Vulcano, together with Salina, are part of the same volcanic structure developing along the NNW-SSE-oriented Tindari-Letojanni strike-slip fault (i.e. Mazzuoli et al., 1995; Ventura et al., 1999). The presence of this lithospheric discontinuity of regional importance and the associated N-S and minor E-W faults, are supposed to have influenced the magmatic history of the whole central sector of the Aeolian archipelago (De Astis et al., 2003). The influence of tectonics is particularly outlined at Lipari and Vulcano by the spatial distribution of the active vents, which develop along the main tectonic lineaments, and, at depth, by the structure of the plumbing system. Based on petrological and geochemical data, Gioncada et al. (2003) and recently Davì et al. (2010) have highlighted important similarities between the volcanic activity at Lipari and Vulcano in the last 40 ka. This activity, which is strongly connected to the activation of the regional fault systems, has been traced back to the presence of a similar magmatic system underneath the two islands.

Our data show possible connections between the volcanic activity at Lipari and Vulcano even prior to 40-50 ka. Investigating the occurrence of possible genetic links between the CA-HKCA rocks of Lipari (270-116 ka) and the HKCA-SHO rocks of Vulcano (120-30 ka) is strongly related to the still controversial debate on the genesis of mafic magmas with variable K_2O enrichment in volcanic arc settings (e.g. Ellam et al., 1989; Francalanci et al., 1989; Esperanca et al., 1992; Ellam & Harmon, 1990; De Astis et al., 2000). In order to get information on the mantle sources and early evolutionary processes, we compare the most primitive compositions (SiO_2 < 56 wt% and MgO > 3.5 wt%) erupted during the first stages of volcanic activity at Lipari and Vulcano (270-116 ka and 120-30 ka, respectively). From this comparison it emerges that the mafic rocks from Vulcano display higher contents of incompatible trace elements (especially LILE; Fig. 17 a), REE fractionation (Fig. 17 b) and K_2O (Fig.19 a) with respect to the mafic rocks from Lipari. The two groups of rocks however, display very similar variations in most major elements (not shown), compatible trace elements (Fig. 16 a) and incompatible trace element ratios (e.g. Zr/Nb; Fig.17, b-c). As for the isotopic signature, the rocks from Vulcano show smaller ranges of isotopic compositions and display higher Nd, lower Sr and higher Pb isotope ratios (Figs.10, 12). Geochemical features suggest that these magmas underwent similar evolutionary processes. In fact, both for Lipari (this study) and Vulcano (De Astis et al., 1997), AFC and RAFC petrogenetic models involving fractionation of mafic phases (mostly olivine and clinopyroxene, with a minor role of plagioclase), assimilation of wall rocks and mixing with newly injected mafic magmas, have been proposed to explain the

evolution of the mafic products. Moreover, these observations perfectly fit the modes of Vulcano and Lipari plumbing systems (Peccerillo et al., 2006; Di Martino et al., 2010) that indicate the presence of a main zone of magma accumulation, located at the lower crust-mantle boundary (17-21 km and 18-22 km, respectively). These conditions in fact prevent the crystallization of plagioclase and favour the injection of mafic magmas from the source.

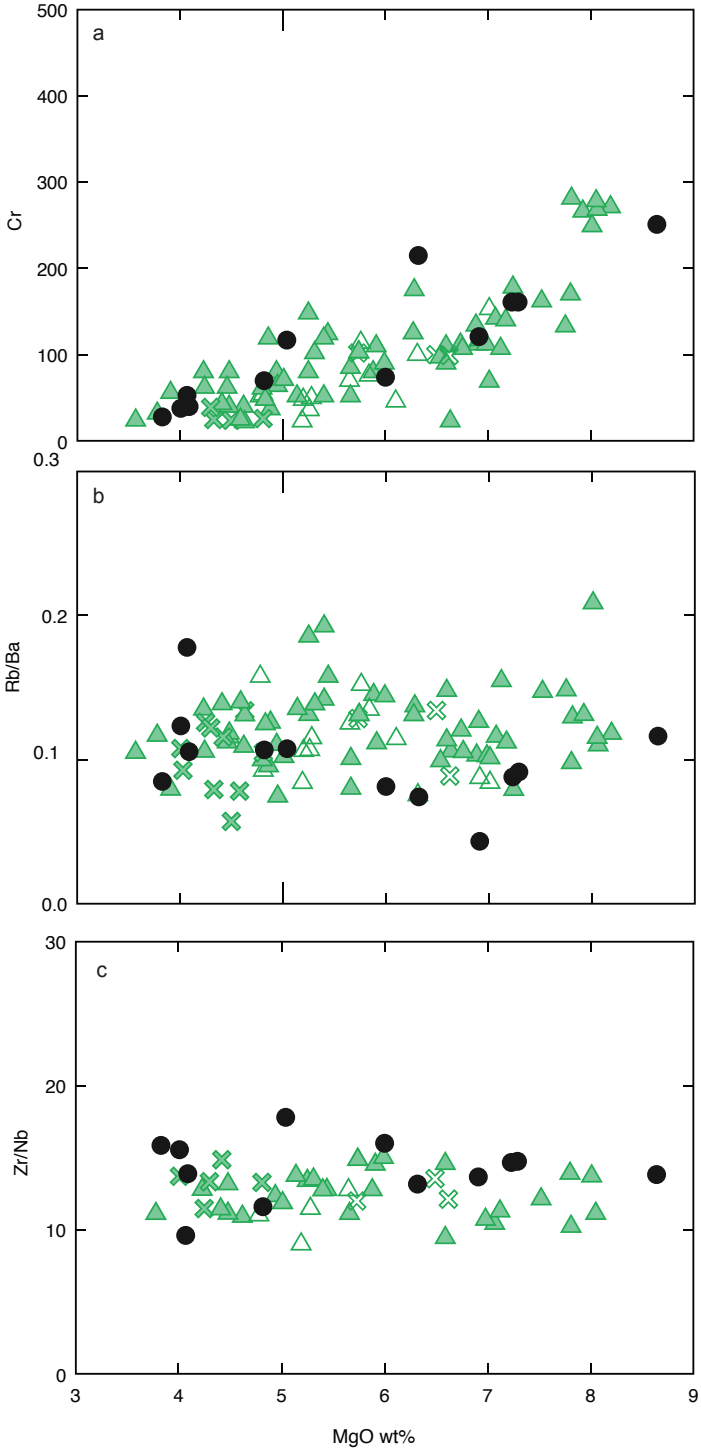

Fig.16 - Plot of compatible trace element (a) and incompatible trace element ratios (b, c) vs. MgO for the mafic rocks (SiO_2 < 56wt% and MgO > 3.5wt%) from Lipari (270-81 ka) and Vulcano (120-30 ka). Symbols as in Fig.1 for the samples from Lipari. Black dots indicate the samples from Vulcano (De Astis et al., 1997; 2000).

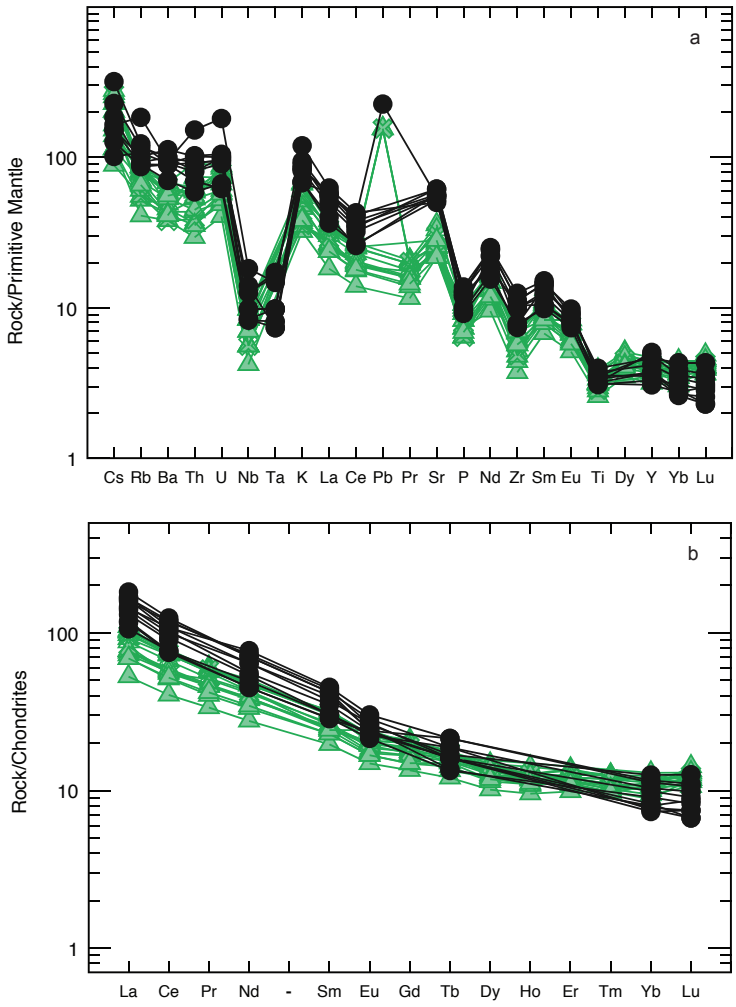

Fig.17 - Incompatible trace element pattern normalized to primordial mantle (Sun & Mc Donough, 1989) (a) and REE patterns normalized to chondrite values (Sun & Mc Donough, 1989) (b) for the mafic (SiO_2 <56 wt% and MgO >3.5 wt%) of Lipari (symbols as in Fig.1) and Vulcano (black dots; De Astis et al., 1997).

Isotopic data instead reveal that crustal assimilation processes were likely more effective at Lipari than at Vulcano, as suggested by the presence of lower crustal metamorphic xenoliths of some of Lipari lavas (Puddino formation, Eruptive Epoch 2) which indicate prolonged interactions of mantle-derived magmas with the mafic granulites of the lower crust.

At Lipari, the volcanic products of Eruptive Epochs 1-4 have been attributed to the activity of scattered monogenic and polygenic volcanic centers, variably controlled by the regional tectonics (cf. Chapter 1). Following Di Martino et al. (2010), the activation of the tectonic systems might have favoured a fast magma ascent with no ponding at shallow levels, beneath fissural type-volcanoes (e.g. Timpone Ospedale, Monterosa, M. Chirica). Differently, at central type-volcanoes (M. Mazzacaruso, M. S.Angelo, M. Chirica-Costa d'Agosto), which are not directly controlled by tectonics, a secondary shallow magma reservoir, located within the upper crust (5.5-3.5 km), has been detected. Therefore, the oldest volcanic activity at Lipari might be related to the presence of distinct magma batches subjected to different ascending pathways.

During their ascent to the surface these magmas variably interact with the basement rocks generating a large spectrum of isotopic compositions. On the contrary, at Vulcano, the oldest products (120-30 ka) are related to the activity of a single composite volcano (Primordial Vulcano) and to the post-collapse activity (Piano Caldera in-fill products) (De Astis et al., 1997). Magmas come directly for the deep reservoir and likely follow less branched ascending pathways, suggesting that crustal assimilation processes might have acted to a lesser extent, thus causing minor $^{87}Sr/^{86}Sr$, $^{206}Pb/^{204}Pb$, $^{207}Pb/^{204}Pb$ and $^{208}Pb/^{204}Pb$ enrichments, with respect to Lipari rocks. Moreover, because of the higher contents of Sr observed in the mafic rocks from Vulcano, Sr isotope ratios in these rocks are less sensitive to the adding of crustal material.

These observations indicate that crustal assimilation processes might have been responsible for the larger range of isotopic compositions observed in the mafic rocks from Lipari. Moreover, they exclude that the K_2O and trace element enrichment, displayed by the oldest series of Vulcano, might be related to crustal assimilation or other evolutionary processes. Compositional differences in the mantle source (e.g. different styles of metasomatism) would produce magmas with more variable incompatible trace element ratios. Therefore, different degrees of partial melting of the source (possibly in a stratified mantle; Crisci et al., 1991) might have been responsible for the geochemical features observed in the mafic rocks from Lipari and Vulcano. High degree of partial melting (20-30%) in fact, are deemed to generate CA magmas (i.e. Green, 1976; Ulmer, 2001) similar to the ones observed at Lipari, whereas, lower degree of partial melting, which favour the incorporation of incompatible elements in the magma and lead to higher REE fractionation, might be responsible for the formation of the HKCA to SHO magmas of Vulcano. Changes of the partial melting conditions in the mantle source would have occurred around 100-120 Ka. In this period at Vulcano the subaerial volcanic activity started and at Lipari, with the eruption of the cordierite-bearing lavas and the andesitic lavas of M. S.Angelo and M.Chirica volcanoes, the CA to HKCA volcanism came to an end and was followed by a 40 ka-long period of quiescence. Following Di Martino et al. (2010), crustal anatexis, responsible for the formation of the cordierite-bearing lavas, induced by prolonged ponding of the mafic magmas in the deep magma chamber, might have prevented the rising of new magmas during the 40 ka-long period of dormancy. During this period, the volcanic activity might have started at Vulcano with the emission of HKCA to SHO magmas. Variations of the degree of partial melting with time, might have been favoured by an isotherm upraise, leading to lower degrees of partial melting of a shallower mantle source (Crisci et al., 1991). Indeed seismological data indicate the presence of mantle upwelling below the Lipari-Vulcano complex (De Astis et al., 2003).

2.8 - The role of crustal assimilation and source heterogeneities in the magmatic evolution of the Aeolian Arc

The interaction of mantle-derived magmas with the crust is an essential process in the magmatic evolution of arc-related magmas, especially the ones located on continental crust. Previous studies, which have investigated the nature of evolutionary processes operating during the volcanic history of the Aeolian Island (e.g. Francalanci et al., 1989; Ellam et al., 1990; Esperanca et al., 1992; Peccerillo et al., 2004; De Astis et al., 1997; Gertisser & Keller, 2000; Calanchi et al., 2002; Santo et al., 2004), outlined that crustal assimilation, coupled with fractional or equilibrium crystallization, represents the most important process leading to magma differentiation in the frame of the magmatic evolution of every single island. At Lipari, in particular, interactions of mafic magmas with the crust are remarkably strong and culminate at 105 ka (Eruptive Epoch 5) with the generation of the cordierite-bearing lavas.

Although crustal assimilation has a relevant role in determining isotope and trace element variations, especially at local scale, it results quite unfit to explain the wide variations observed at regional scale. These variations have been mostly attributed to heterogeneities of the mantle sources due to the action of metasomatizing agents, such as aqueous fluids and sediments coming from the slab (e.g. Francalanci et al., 2007 and references therein). Metasomatizing fluids have little effect on isotope ratios but produce changes in trace element ratios, especially the ones involving mobile trace elements (Rb, Sr, K, Ba etc.) and immobile elements (Nb, Zr, Ce etc.) (e.g. Scambelluri et al., 2001). These fluids, in fact, are able to transport mobile elements, thus leading to an increase of the LILE/HFSE ratios in the mantle source. The addition of sediments to the mantle source instead generally causes the increase of $^{87}Sr/^{86}Sr$ and the decrease of Nd and Pb isotope ratios.

In Fig.19 the mafic rocks (SiO_2 < 56 wt% and MgO > 3.5 wt%) from Lipari and from the other islands in the Aeolian archipelago have been compared in order to evaluate the different roles of magma sources and evolutionary processes. In diagrams of $^{87}Sr/^{86}Sr$ vs. trace element ratios (Fig.19 b-c), the mafic rocks from Lipari and Stromboli display wider isotopic variations and minor variations in LILE/HFSE ratios, compared to the mafic rocks from Filicudi, Alicudi, Salina, which show steep trends, indicating large LILE/HFSE ratios variations and small ranges of $^{87}Sr/^{86}Sr$. Two distinct groups of mafic rocks characterized by different K_2O enrichment and $^{87}Sr/^{86}Sr$ ratios, are easily recognizable both at Stromboli (HKCA and SHO series) and Panarea (CA and HKCA-SHO series) (Fig.19 a). Similarly, at Vulcano two different groups of mafic rocks (HKCA-SHO and SHO) have been distinguished on the basis of different trace element

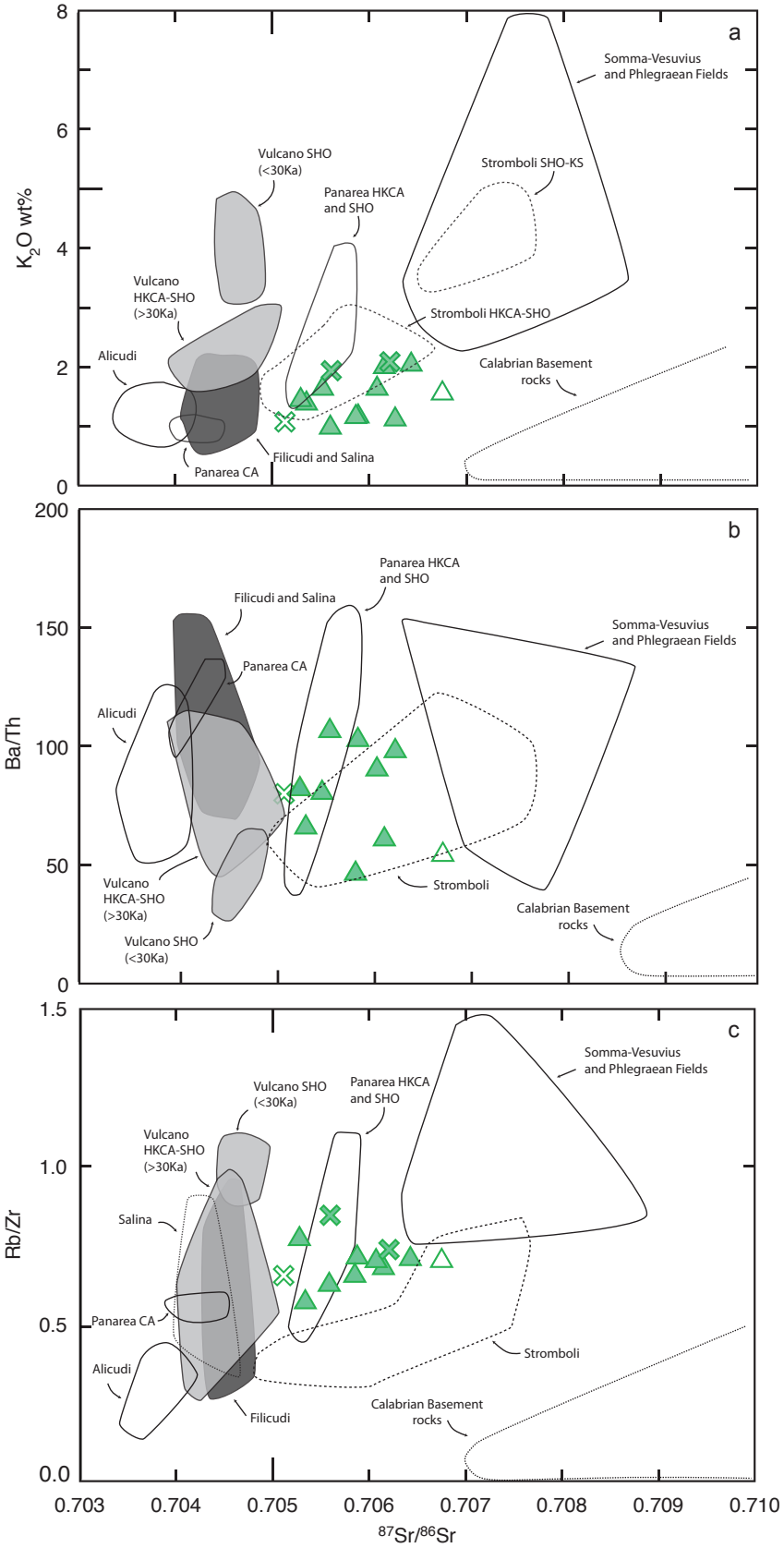

Fig.19 - Plots of K_2O and trace element ratios vs. Sr isotope ratio for the mafic rocks (SiO_2 < 56 wt% and MgO > 3.5 wt%) of Lipari (symbols as in Fig.1) and the other islands of the Aeolian archipelago (data source as in Fig.9). Fields of the Somma-Vesuvius, Phlegraean Field and Calabrian Basement rocks are reported for comparison (data source as in Fig.9).

ratios and K_2O content. The HKCA-SHO rocks referred to the old volcanic activity (>30 ka) display larger variations of $^{87}Sr/^{86}Sr$ ratios compared to the SHO rocks (>30 ka), while variations of trace element ratios are very similar to the ones observed in the mafic rocks from Lipari (Fig.19 a).

The local variations of isotope and trace element ratio suggest that:

1) AFC processes (with high rate of crustal assimilation) are responsible for the geochemical and isotopic variations observed in the mafic rocks of Lipari;

2) at Vulcano the same processes occurred to a lesser extent, thus causing a lower increase of Sr isotope ratios;

3) the wide variations of $^{87}Sr/^{86}Sr$ and $^{143}Nd/^{144}Nd$ ratios, displayed by the mafic rocks of Stromboli and Panarea, might theoretically derive from crustal assimilation, however similar variations in isotope ratios would require very high rates of crustal assimilation (r~1), which are very unlikely;

4) the steep patterns described by the mafic rocks of Filicudi, Salina and Alicudi indicate that magma differentiation has been ruled mostly by fractional crystallization processes, with a minor role of crustal assimilation.

Instead, the regional variations of isotope and trace element ratio suggest that:

1) the mafic rocks of Salina, Vulcano and Filicudi derive from mantle sources variably contaminated by aqueous fluids, with minor additions of sediments;

2) Lipari mafic rocks plots at higher Sr isotope ratios than the mafic rocks from Salina, Vulcano and Filicudi. This might theoretically derive from higher additions of sediments to the mantle source of Lipari, but geochemical data, together with structural and tectonic observations, speak in favour of a common source for Lipari and Vulcano (>30 ka) mafic magmas. At Vulcano lower degrees of partial melting of the mantle source caused a general enrichment of incompatible trace elements and K_2O in the old mafic melts, maintaining trace element ratios almost unaltered (Figs.16, 19). Crustal contamination, which is more evident at Lipari with respect to Vulcano, because of the abundance of metamorphic xenoliths in the old rocks, is responsible for the higher $^{87}Sr/^{86}Sr$ and lower $^{143}Nd/^{144}Nd$ ratios observed in Lipari mafic rocks;

3) the mafic rocks from Stromboli and Panarea derive from heterogeneous mantle sources (Francalanci et al., 1993; Calanchi et al., 2002). As outlined by Peccerillo (2001), at Stromboli the presence of a mantle source akin to the potassic rocks of Somma-Vesuvio and Phlegraean Fields is strongly highlighted by the similarities observed in diagrams of trace elements vs. isotope ratios and isotope ratios (Figs.10, 12, 19). At Panarea, the isotopic and geochemical compositions of the CA rocks overlap the fields of Filicudi and Salina, whereas the HKCA-SHO rocks are shifted towards the HKCA-SHO rocks of Stromboli (Fig.19). This suggests a derivation from two different

sources for the CA and the HKCA-SHO magmas. The first is similar to the source of Filicudi and Salina and the other is likely a mixture between the first and the source of Stromboli magmas (Calanchi et al., 2002). Moreover, the adding of sediments to the mantle sources might have also favoured the increase of $^{87}Sr/^{86}Sr$ ratios in the eastern sector of the archipelago;

4) the mafic rocks from Alicudi are the most primitive rocks of the whole archipelago. Their low Sr and high Nd isotope ratios suggest that the mantle source of these rocks underwent no or very little sediment additions. Relatively low LILE/HFSE ratios indicate bland fluid metasomatism.

References

Ayuso R.A., De Vivo B., Rolandi G., Seal II R.R. & Paone A. 1998. Geochemical and isotopic (Nd-Pb-Sr-O) variations bearing on the genesis of volcanic rocks from Vesuvius, Italy. J. Volcanol. Geotherm. Res., 82, 53-78.

Ayuso R.A. & Schulz K.J. 2003. Nd, Pb, Sr isotope geochemistry and origin of the Ordovician Bald Mountain and Mount Chase massive sulfide deposits, northern Maine. In: Goodfellow W.D., McCutcheon S.R., Peter J.M. (Eds.), Volcanogenic Massive Sulfide deposits of the Bathurst District and Northern Maine. Economic Geology Monograph, 11, 611-630.

Ayuso R.A., Haeussler P.J., Bradley D.C., Farris D.W., Foley N.K. & Wandless G.A. 2009. The role of the ridge subduction in determining the geochemistry and Nd, Sr, Pb isotopic evolution of the Kodiak batholith in Southern Alaska. Tectonophysics, 464, 137-163.

Armienti P., Tonarini S., D'Orazio M., Innocenti F. 2004. Genesis and evolution of Mt. Etna alkaline lavas: petrological and Sr-Nd-B isotope constraints. Per Mineral., 73, 29-52.

Bargossi G.M., Campos Venuti M., Gasparotto G. & Rossi P.L. 1989. Petrologia e stratigrafia delle successioni andesitiche l.s. di Lipari, Isole Eolie, Italia. Mineralogica et Petrographica Acta, 22, 295-326.

Beccaluva L., Bonatti E., Dupuy C., Ferrara G., Innocenti F., Lucchini F., Macera P., Petrini R., Rossi P.L., Serri G., Seyler M. & Siena F. 1990. Geochemistry and mineralogy of the volcanic rocks from ODP sites 650, 651, 655 and 654 in the Tyrrhenian Sea. In: Kastens K.A., Mascle J. et al. (Eds.). Proc. Ocean Drilling Program, Scientific Results, 107, 49-74.

Bergeat A. 1910. Der Cordieritandesit von Lipari, seine andalusitführenden Einschlüsse und die genetischen Beziehungen zwischen dem Andalusit, Sillimanit, Biotit, Cordierit, Orthoklas und Spinnel in den letzteren. N. Jb. Mineral., Beil., 30, 575-627.

Barker D.S. 1987. Rhyolites contaminated with metapelite and gabbro, Lipari, Aeolian Islands, Italy: products of lower crustal fusion or of assimilation plus fractional crystallization? Contrib. Mineral. Petrol., 97, 460-472.

Calanchi N., Peccerillo A., Tranne C.A., Lucchini F., Rossi P.M., Kempton P.D., Barbieri M. & Wu T.W. 2002. Petrology and geochemistry of the Island of Panarea: implications

for mantle evolution beneath the Aeolian island arc (Southern Tyrrhenian Sea, Italy). J. Volcanol. Geotherm. Res., 115, 367-395

Caggianelli A., Del Moro A., Paglionico A., Piccarreta G., Pinarelli L. & Rottura A. 1991. Lower crustal granite genesis connected with chemical fractionation in the continental

crust of Calabria (Southern Italy). European Journal of Mineralogy, 3, 159-180.

Cohen R.S., Evensen M.S., Hamilton P.J. & O'Nions R.K. 1980. U-Pb, Sm-Nd and Rb-Sr systematic sod mid-ocean ridge basalts glasses. Nature, 283, 149-153.

Civetta L., Carluccio E., Innocenti F., Sbrana A. & Taddeucci G. 1991. Magma chamber evolution under Phlegraean Field during the last 10 ka: trace element and isotope data. Eur. J. Mineral., 3 , 415-428.

Conticelli S., Francalanci L., Manetti P., Cioni R. & Sbrana A. 1997. Petrology and geochemistry of the ultrapotassic rocks from the Sabatini volcanic district, central Italy: the role of evolutionary processes in the genesis of variably enriched alkaline magmas. J. Volcanol. Geotherm. Res., 75, 107-136.

Crisci G.M., De Rosa R., Esperanca S., Mazzuoli R. & Sonnino M. 1991. Temporal

evolution of three component system: the island of Lipari (Aeolian Arc, southern Italy). Bull. Volcanol., 53, 207-221.

D'Antonio M., Civetta L. & Di Girolamo P. 1999. Mantle source heterogeneity in the Campanian Region (south Italy) as inferred from geochemical and isotopic features of mafic volcanic rocks with shoshonitic affinity. Mineral. Petrol., 67, 163-192.

D'Antonio M., Tilton G.R. & Civetta L. 1996. Petrogenesis of Italian alkaline lavas deduced from Pb-Sr-Nd isotope relationships. In: Basu A. & Hart S.R. (Eds.) Isotopic Studies of Crust-Mantle Evolution. Am. Geophys. Un. Mon., 95, 253-267.

Davì M., De Rosa R. & Holtz F. 2010. Mafic enclaves in the rhyolitic products of Lipari historical eruptions; relationships with the coeval Vulcano magmas (Aeolian Islands, Italy). Bull Volcanology, DOI 10.1007/s00445-010-0376-5.

De Astis G., La Volpe L., Peccerillo A. & Civetta L. 1997. Volcanologic and petrological evolution of Vulcano Island (Aeolian Arc, Southern Tyrrhenian Sea). J. Geophisical Res., 102, 8021-8050.

De Astis G., Peccerillo A., Kempton P.D., La Volpe L. & Wu T.W. 2000. Transition from calcalkaline to potassium-rich magmatism in subduction environments: geochemical

and Sr, Nd, Pb isotopic constraints from the Island of Vulcano (Aeolian arc). Contributions of Mineralogy and Petrology, 139, 684-703.

De Astis G., Ventura G. & Vilardo G. 2003. Geodynamic significance of the Aeolian volcanism (Southern Tyrrhenian Sea, Italy) in light of structural, seismological and geochemical data. Tectonics, 22 (4), 1040-1057.

D'Orazio M., Tonarini S., Innocenti F. & Pompilio M. 1997. Northern Valle del Bove volcanic succession (Mt. Etna, Siciliy): petrography, geochemistry and Sr-Nd isotope data. Acta Vulcanol., 9, 73-86.

De Vivo B., Maiorani A. & Trigilia R. 1987. On the origin of the cordierite bearing rhyolites from M. S.Angelo (Lipari, Italy): fluid inclusions and petrological studies. Periodico di Mineralogia 56, 71-84.

De Paolo D.J. 1981. Trace element and isotopic effects of combined wallrock assimilation and fractional crystallization. Earth Planet. Sci. Lett., 53, 189-202.

Di Battistini G., Montanini A., Vernia L., Venturelli G. & Tonarini S. 2001. Petrology of melilite-bearing rocks from the Montefiascone volcanic complex (Roman Magmatic Province): new insights into the ultrapotassic volcanism of Central Italy. Lithos, 59, 1-24.

Di Martino C. 2010. Evoluzione del sistema di alimentazione magmatica dell'Isola di Lipari (Isole Eolie, Italia). Unpublished PhD Thesis, University of Bologna, Italy, 155 pp.

Di Martino C., Forni F., Frezzotti M.L., Palmeri R., Webster J.D., Ayuso R.A., Lucchi F. & Tranne C.A. Anatexis and magma-hybridization in the lower-crust: petrogenesis of cordierite-bearing lavas from Lipari, Aeolian Arc, Italy. Contribution to Mineralogy and Petrology, accepted for publication.

Di Martino C., Frezzotti M.L., Palmeri R., Lucchi F., Peccerillo A., Tranne C.A. & Diamond L.W. 2010. Magma storage and ascent at Lipari Island (Aeolian archipelago, Southern Italy) at 223–81 ka: the role of crustal processes and tectonic influence. Bull. of Volcanology, DOI 10.1007/s00445-010-0383-6.

Ellam R.M. & Harmon R. S. 1990. Oxygen isotope constraints on the crustal contribution to the subduction-related magmatism of the Aeolian Islands, Southern Italy. Journal of Volcanology and Geothermal Research 44, 105–122.

Ellam R.M., Hawkeswort C.J., Menzies M.A & Rogers N.W.1989. The volcanism of Southern Italy: role of subducion and the relationships between potassic and sodic

alkaline magmatism. Journal of Geophysical Research, 94, 4589-4601.

Esperanca S., Crisci G.M:, De Rosa R. & Mazzuoli R. 1992. The role of the crust in the magmatic evolution of the island of Lipari (Aeolian Islands, Italy). Contr. Mineral. Petrol., 112, 450-462.

Forni F., Lucchi F., Peccerillo A., Tranne C.A., Rossi P.L., Di Martino C., Frezzotti M.L. & Ayuso R.A. Lipari. In: Lucchi, F., Peccerillo A., Keller J., Tranne C.A. & Rossi P.L. (Eds.), Geology of the Aeolian Islands (Italy). Geological Society of London, accepted for publication.

Francalanci L., Avanzinelli R., Tommasini S. & Heuman A. 2007. A west-east geochemical and isotopic traverse along the volcanism of the Aeolian Island arc, southern Tyrrhenian Sea, Italy: Interfereces on mantle source processes. In: Beccaluva L., Bianchini G. & Wilson M. (Eds.), Cenozoic Volcanism in the Mediterranea Area. Geological Society of America Special Paper 418, 235-263.

Francalanci L., Manetti P. & Peccerillo A. 1989. Volcanological and magmatological evolution of Stromboli volcano (Aeolian Island): the roles of fractional crystallisation, magma mixing, crustal contamination and source heterogeneity. Bull. Volcanology, 51, 355-378.

Francalanci L., Tayolor S.R., McCulloch M.T. & Woodhead J.D. 1993. Geochemical and isotopic variations in the calc-alkaline rocks of Aeolian arc, southern Tyrrhenian Sea, Italy: constraints on magma genesis. Contributions of Mineralogy and Petrology, 113, 300-313.

Franzini M., Leoni L. & Saitta M., 1975. Revisione di una metodologia analitica per la fluorescenza-X, basata sulla correzione completa degli effetti di matrice. Rend. Soc. Ital. Mineral. e Petrol. 31, 2, 36-378.

Gasperini D., Blichert-Toft J., Bosch D., Del Moro A., Macera P. & Albarede F. 2002 Upwelling of deep mantle material through a plate window: evidence from the geochemisty of Italian basaltic volcanics. J. Geophys. Res. 107(B12), 2367, doi:10.1029/2001JB000418.

Gertisser R. & Keller J. 2000. From basalt to dacite: origin and evolution of the calcalkaline series of Salina, Aeolain Arc, Itlay. Contrib. Mineral. Petrol., 139, 607-626.

Green D. H. 1976. Experimental testing of ‘equilibrium’ partial melting of peridotite under water-saturated, high pressure conditions, Can. Mineral., 14, 255-268.

Gioncada A., Mazzuoli R., Bisson M. & Pareschi M.T. 2003. Petrology of volcanic products younger than 42 ka on the Lipari-Vulcano complex (Aeolian Island, Italy): an example of volcanism controlled by tectonics. J. Volcanol. Geotherm. Res., 122, 191-220.

Hart S.R. 1984. A large-scale isotope anomaly in the southern hemisphere mantle. Nature, 309, 753-757.

Hawkesworth C.J. & Vollmer R. 1979. Crustal contamination vs. enriched mantle: 143Nd/144Nd and 87Sr/86Sr evidence from the Italian volcanics. Contrib. Mineral. Petrol., 69, 151-165.

Ito E., White W.M. & Gopel C. 1987. The O, Sr, Nd and Pb isotope geochemistry of MORB. Chem. Geol., 62, 157-176.

Leoni L. & Saitta M. 1976. X-ray fluorescence analysis of 29 trace elements in rock and mineral standard. Rend. Soc. Mineral. Petrol., 32, 479-510.

Lucchi F., Tranne C.A., Forni, F. & Rossi, P.L. Geological map of Lipari Island, scale 1:10,000 (Aeolian archipelago), in: Lucchi F., Peccerillo A., Keller J., Tranne C.A. & Rossi P.L. (Eds.), Geology of the Aeolian Islands (Italy), Geological Society of London, Memoirs, accepted for publication.

Mazzuoli R., Tortorici L. & Ventura G. 1995. Oblique rifting in Salina, Lipari and Vulcano islands (Aeolian islands, Southern Italy). Terra Nova, 7, 444–452.

O'Hara M.J. 1977. Geochemical evolution during fractional crystallization of a periodically refilled magma chamber. Nature, 266, 503-507.

Pappalardo L., Piochi M., D'Antonio M., Civetta L. & Petrini R. 2002. Evidence for multistage magmatic evolution during the past 60 kyr at Campi Flegrei (Italy) deduced from Sr, Nd and Pb isotope data. J. Petrol., 43, 1415-1434.

Peccerillo A. 2001. Geochemical similarities between the Vesuvius, Phlegraean Fields and Stromboli Volcanoes: petrogenetic, geodynamic and volcanological implications. Mineralogy and Petrology, 73, 93-105

Peccerillo A., Dallai L., Frezzotti M.L. & Kempton P.D. 2004. Sr-Nd-Pb-O isotopic evidence for decreasing crustal contamination with ongoing magma evolution at Alicudi volcano (Aeolian Arc, Italy): implication for style of magma-crust interaction and for mantle soure compositions. Lithos, 78, 217-233.

Peccerillo A., Frezzotti M.L., De Astis G. & Ventura G. 2006. Modeling the magma plumping system of Vulcano (Aeolian Island, Italy) by integrated fluid-inclusion geobarometry, petrology and geophysics. Geology, 34, 17-20.

Peccerillo A., Kempton P.D., Harmon R.S., Wu T.W., Santo A.P., Boyce A.J. & Tripodo A. 1993. Petrological and geochemical characteristics of the Alicudi Volcano, Aeolian Island, Italy: implications for magma genesis and evolution. Acta Vulcanol. 3, 235-249.

Peccerillo A. & Taylor S.R. 1976. Geochemistry of the Eocene calc-alkaline volcanic rocks from the Kastamonu area, northern Turkey. Contrib. Mineral.Petrol., 58: 63-81.

Peccerillo A. & Wu T.W. 1992. Evolution of calc-alkaline magmas in continental arc volcanoes: evidence from Alicudi, Aeolian Arc (Southern Tyrrhenian Sea, Italy). J. Petrol., 33, 1295-1315.

Perini G., Francalanci L., Davidson J.P. & Conticelli S. 2004. The petrogenesis of Vico Volcano, Central Italy: an example of low scale mantle heterogeneity. J. Petrol., 45, 139-182.

Plank T. & Langmuir C. H. 1998. The chemical composition of subducting sediment and its consequences for the crust and mantle. Chem. Geol. 145, 325–394.

Pichler H. 1980. The island of Lipari. Rendiconti della Società Italiana di Mineralogia e Petrologia, 36, 415-440.

Rogers N.W., Hawkesworth C.J, Parker R.J. & Marsh J.S. 1985. Geochemistry of potassic lavas from Vulsini, central Italy, and implications for the mantle enrichment processes beneath the Roman region. Contrib. Mineral. Petrol., 90, 244-257.

Rollinson H. 1993. Using geochemical data: evaluation, presentation, interpretation (Longman Geochemistry). Pearson, Edinburg Gate, 352 pp.

Santo A.P., Jacobsen S.B., Barker J. 2004. Evolution and genesis of calc-alkaline magmas at Filicudi volcano, Aeolian Arc (Southern Tyrrhenian Sea, Italy). Lithos, 72, 73-96.

Scambelluri M., Rampone E. & Piccardo G. 2001. Fluid and trace element cycling in subducted serpentinite: a trace element study of the Erro-Tobbio high-pressure ultramafics (Western Alps, NW Italy). J. Petrol., 42, 55-67.

Stacey J.S. & Kramers J.D. 1975. Approximation of terrestial lead isotope evolution by a two-stage model. Earth and Planetary Science Letters, 26, 207-221.

Sun S.S. & MC Donough W.F. 1989. Chemical and isotopic systematics of oceanic basalts: implications fort he mantle composition and processes. In: Saunders A.D. and Norry M.J. (eds.), Magmatism in ocean basins. Geol. Soc. London. Spec. Pub., 42, 313-345.

Tonarini S., Armienti P., D'Orazio M., Innocenti F., Pompilio M. & Petrini R. 1995. Geochemical and isotopic monitoring of Mt. Etna 1989-93 eruptive activity: bearing on the shallow feeding system. J. Volcanol. Geotherm. Res., 64, 95-155.

Ulmer P. 2001. Partial melting in the mantle wedge – the role of H2O in the genesis of mantle-derived "arc-related" magmas. Phys Earth Planet Intr., 127, 215-232.

Ventura G., Vilardo G., Milano G. & Pino N. 1999. Relationships among crustal structure, volcanism and strike-slip tectonics in the Lipari-Vulcano volcanic complex (Aeolian Islands, Southern Tyrrhenian Sea, Italy). Physic Earth Planetary Interior 116, 31-52.

Zartman R.E. & Haines S.M. 1988. The plumbotectonic model fro Pb isotopic systematics among major terrestrial reservoirs – a case for bidirectional transport. Geochimica et Cosmochimica Acta, 52, 1327-1339.

CHAPTER 3

Di Martino C., Forni F., Frezzotti M.L., Palmeri R., Webster J.D., Ayuso R.A., Lucchi F. & Tranne C.A. Anatexis and magma-hybridization in the lower-crust: petrogenesis of cordierite-bearing lavas from Lipari, Aeolian Arc, Italy. Contribution to Mineralogy and Petrology, accepted for publication

Editorial Manager(tm) for Contributions to Mineralogy and Petrology
Manuscript Draft

Manuscript Number:

Title: Anatexis and magma-hybridization in the lower-crust: petrogenesis of cordierite-bearing lavas from Lipari, Aeolian Arc, Italy
Article Type: Original Paper

Keywords: Lipari Island; cordierite-bearing lavas; crustal anatexis; biotite dehydration melting; peritectic phases; magma hybridization

Corresponding Author: Maria Luce Frezzotti, PhD

Corresponding Author's Institution:

First Author: Corrado Di Martino

Order of Authors: Corrado Di Martino;Francesca Forni;Maria Luce Frezzotti, PhD;Rosaria Palmeri;Jim Webster;Robert Ayuso;Federico Lucchi;Claudio Tranne

Abstract: Cordierite-bearing lavas (CBL; ~105 ka) erupted from the Monte S. Angelo volcano at Lipari (Aeolian Arc, Italy) are high-K andesites (whole-rock) resulting from the peculiar coexistence of megacrysts of Ca-plagioclase and clinopyroxene, euhedral crystals of cordierite and garnet, microphenocrysts of orthopyroxene (Opx I, II, and III) and plagioclase, and crustal xenoliths set in a heterogeneous groundmass of rhyodacitic-rhyolitic composition. Mineral phase compositions correlate well with textural characteristics of CBL between a mafic magma type akin to Lipari rocks of Eruptive Epochs 1 and 2 (223-127 ka) (e.g., high MgO/FeO in clinopyroxene and orthopyroxene (I), and high-CaO plagioclase cores) and a high-K peraluminous rhyolitic magma type of crustal origin (i.e., due to the presence of peritectic cordierite, garnet, and orthopyroxene (III), and the composition of melt inclusions in cordierite).
The crustal anatectic melts were generated through dehydration-melting reactions of metapelites in the lower crust of Lipari. Two main peritectic reactions have been reconstructed:
1)Biotite+Aluminosilicate+Quartz+Albite=Garnet+Cordierite +K-feldspar+Melt, and
2)Biotite+Garnet+Quartz=Orthopyroxene+Cordierite+K-feldspar+Melt,
and their position in a petrogenetic grid, suggests that melting of metapelitic rocks occurred at 725 < temperature < 900 Â°C and pressure = 0.4-0.45 GPa by extensive emplacement of basic magmas in the lower crust. Petrogenetic modeling based on Sr and Nd isotope data confirms mixing processes involving mantle-derived and crustally derived magmas; this magma mixing generated hybrid melts having the isotopic composition of CLB whole-rock samples. Magma hybridization and eruption are proposed to have occurred in response to the entrance of fresh mafic mantle-derived magmas into the deep crustal basic-magma accumulation zone.

Anatexis and magma-hybridization in the lower-crust: petrogenesis of cordierite-bearing lavas from Lipari, Aeolian Arc, Italy

Corrado Di Martino[1], Francesca Forni[1], Maria Luce Frezzotti[2]*, Rosaria Palmeri[3], James D. Webster[4], Robert A. Ayuso[5], Federico Lucchi[1], Claudio A. Tranne[1]

1-Dipartimento di Scienze della Terra e Geologico-Ambientali, Università di Bologna, Piazza di Porta San Donato 1, I-40126 Bologna

2-Dipartimento di Scienze della Terra, Università di Siena, Via Laterina 8, I-53100, Siena

3-Museo Nazionale Antartide-Sezione di Scienze della Terra, Via Laterina 8, I-53100, Siena

4-Department of Earth and Planetary Sciences, AMNH, Central Park West, 79th St., New York, NY 10024-5192, USA

5- U.S. Geological Survey, 954 National Center, Reston, VA 20192, USA

** Corresponding author*

E-Mail address: frezzottiml@unisi.it

Tel: ++39 0577233929

Fax: ++39 0577233938

Running Title: Anatexis and magma-hybridization in the lower-crust of Lipari

Key words: Lipari Island; cordierite-bearing lavas; crustal anatexis; biotite dehydration melting; peritectic phases; magma hybridization

Abstract

Cordierite-bearing lavas (CBL; ~105 ka) erupted from the Monte S. Angelo volcano at Lipari (Aeolian Arc, Italy) are high-K andesites (whole-rock) resulting from the peculiar coexistence of megacrysts of Ca-plagioclase and clinopyroxene, euhedral crystals of cordierite and garnet, microphenocrysts of orthopyroxene (Opx I, II, and III) and plagioclase, and crustal xenoliths set in a heterogeneous groundmass of rhyodacitic-rhyolitic composition. Mineral phase compositions correlate well with textural characteristics of CBL between a mafic magma type akin to Lipari rocks of Eruptive Epochs 1 and 2 (223-127 ka) (e.g., high MgO/FeO in clinopyroxene and orthopyroxene (I), and high-CaO plagioclase cores) and a high-K peraluminous rhyolitic magma type of crustal origin (i.e., due to the presence of peritectic cordierite, garnet, and orthopyroxene (III), and the composition of melt inclusions in cordierite).

The crustal anatectic melts were generated through dehydration-melting reactions of metapelites in the lower crust of Lipari. Two main peritectic reactions have been reconstructed:

1) Biotite+Aluminosilicate+Quartz+Albite=Garnet+Cordierite+K-feldspar+Melt, and

2) Biotite+Garnet+Quartz=Orthopyroxene+Cordierite+K-feldspar+Melt,

and their position in a petrogenetic grid, suggests that melting of metapelitic rocks occurred at 725 < temperature < 900 °C and pressure = 0.4-0.45 GPa by extensive emplacement of basic magmas in the lower crust. Petrogenetic modeling based on Sr and Nd isotope data confirms mixing processes involving mantle-derived and crustally derived magmas; this magma mixing generated hybrid melts having the isotopic composition of CLB whole-rock samples. Magma hybridization and eruption are proposed to have occurred in response to the entrance of fresh mafic mantle-derived magmas into the deep crustal basic-magma accumulation zone.

INTRODUCTION

The cordierite-bearing lavas (CBL) cropping out at Lipari in the Aeolian Arc represent one of the most exotic lithologies associated with orogenic volcanism in Italy and worldwide. Although classified as high-K andesites or dacites (Pichler 1980), these rocks show peculiar petrographic characteristics given by the coexistence of typical igneous minerals, such as zoned plagioclase, clinopyroxene, and orthopyroxene, along with less typical i) euhedral to subhedral phenocrysts of cordierite and garnet; ii) metapelitic, gneissic, and gabbroic xenoliths (up to 20-30 %); iii) a heterogeneous groundmass with variable composition; and iv) variable geochemical and isotopic composition for single lava bodies (Barker 1987; Crisci et al. 1991; Esperança et al. 1992; Maccarone 1963). The eruption of CBL at about 105 ka marks a turning point in the volcanological and magmatic evolution of Lipari Island, when mafic to intermediate magmatism (from basaltic andesites to andesites and minor dacites; 223-81 Ka) comes to an end, and an important migration of the lava emission points occurred from the western to the central sector of the island (Di Martino et al. 2010; Lucchi et al. 2010; Tranne et al. 2002).

Because of its textural, compositional, and stratigraphic significance, the CBL have been the subject of several studies. Barker (1987) and De Vivo et al. (1987) focused their attention on the chemical characters of metamorphic xenoliths and glasses, and proposed that the origin of the CBL could be related to the evolution of a mafic magma by crustal assimilation and fractional crystallization or, as an alternative, to crustal partial melting processes. Crisci et al. (1991) and Esperança et al. (1992) further showed that fractional crystallization plus crustal assimilation were responsible for the geochemical and isotopic variability of CBL. These authors also highlighted a possible role of partial melting of a heterogeneous lower crust to account for the whole evolution of Lipari's magmatism.

Extensive melting of the lower crust, however, implies a significant energy supply from the mantle. Although petrological and geochemical evidence is indicative of a hybrid nature of the CBL, in which both mantle and crustal end-members contribute, the processes behind this hybridism are still controversial.

Study of the textures and compositions of minerals has proven to be a simple and most effective means of interpreting processes of generating hybrid magmas, because minerals commonly preserve evidence of diverse and complex histories, even in magmas that are chemically homogeneous (Ginibre et al. 2002, 2007; Jerram and Kent 2006, and references therein). Therefore, we investigated the petrography and glass and mineral chemistry of the CBL to establish the relative roles of the various processes responsible for the particular composition of these lavas. To determine the source characteristics of the different components that contributed to the genesis of CBL, we interpret Sr and Nd radiogenic isotope ratios of mineral and whole-rock samples, which are diagnostic of magma sources and of evolutionary processes (i.e., crustal assimilation and magma mixing; Hawkesworth and van Calsteren 1984), but unaffected by fractional crystallization. These results provide an opportunity to reconstruct crustal processes and magma dynamics that occurred in the lower crust beneath Lipari at about 100 ka.

VOLCANOLOGICAL BACKGROUND AND PREVIOUS STUDIES

Lipari island is located in the central sector of the Aeolian archipelago (Fig. 1), a volcanic island arc built on a ~20-25 km thick continental crust in the Southern Tyrrhenian Sea (Piromallo and Morelli 2003). The eruptive history of Lipari is described by five main Eruptive Epochs, according to Lucchi et al. (2010) (Fig. 1). Eruptive Epochs 1 and 2 (223-127 ka) are characterized by the emplacement of predominant basaltic andesites and subordinate

andesites and dacites. However, andesitic to dacitic magmas become ubiquitous during Eruptive Epoch 3 that includes CBL (105-81 ka). After a 40-ka time gap in volcanic activity, the Eruptive Epochs 4 and 5 (42 ka-776 D.C.) led to younger rhyolitic magma emplacement. This geochemical variation is accompanied also by changing volcanological patterns from strombolian-effusive activity (Eruptive Epochs 1, 2 and 3) to more explosive phases (Eruptive Epochs 4 and 5), driving the deposition of pumiceous pyroclastic products and final effusion of superimposed viscous domes and coulées. These geochemical and volcanological variations have been also found in other islands of the central sector of the Aeolian arc, and may reflect a dramatic modification of the internal structure of volcanoes (e.g., Esperança et al. 1992; Peccerillo et al. 2006).

The cordierite-bearing lavas of Monte S. Angelo volcano (Fig. 1; Eruptive Epoch 3; 105 ka) are deemed to be clear evidence of the fundamental role played by interaction between mantle-derived magmas and the crust in the origin and differentiation of Lipari magmas (Barker 1987). In fact, one of the most remarkable characteristics of CBL, which are high-K andesites in composition, is the occurrence of phenocrysts and/or xenocrysts of plagioclase, clinopyroxene, orthopyroxene, cordierite, garnet, K-feldspar, andalusite, biotite, quartz, and sillimanite (in decreasing order of abundance) of extremely variable size, along with numerous and irregularly distributed gabbroic and metamorphic xenoliths (Bergeat 1910; Honnorez and Keller 1968).

Through a detailed study of xenoliths and megacrysts, Barker (1987) proposed that: i) metamorphic xenoliths consist of gneisses and granulites; ii) most garnet, cordierite, and andalusite are xenocrystic in origin; and iii) alkali-feldspar, plagioclase, Fe-rich orthopyroxene, and quartz represent microphenocrysts crystallized from a rhyodacitic/rhyolitic groundmass. The xenolithic fragments are interpreted as remnant, dispersed micro-enclaves of lower crustal origin, equilibrated at about 0.5±0.1 GPa and

800±100 °C (Barker 1987), whereas the rhyolitic glass of the groundmass represents the final product of fractional crystallization from a mafic magma, following important assimilation of lower-crustal rocks. According to Barker (1987), however, the participation of melts generated through partial melting processes of the lower crust cannot be excluded, since the calculated P-T equilibria in metamorphic xenoliths are well above the P-T conditions of water-present melting conditions for metapelites, at the considered pressures.

Crisci et al. (1991) and Esperança et al. (1992) tested this hypothesis by studying the geochemical and isotopic signature of the CBL. These authors interpreted the whole-rock isotopic signature ($^{87}Sr/^{86}Sr$= 0.7064; $^{143}Nd/^{144}Nd$ = 0.5120) as representative of contamination of mafic calc-alkaline magmas akin to Lipari's older volcanic stages (223-127 ka) by crustal materials and/or crustal melts. One proposed scenario involves an isotherm increase within the upper mantle as a consequence of doming beneath Lipari and, probably, the whole Aeolian arc, and consequent crustal melting. Although the whole-rock data of these studies turned out to be quite unfit to characterize the nature of the different components involved in the genesis of the CBL, no isotope study based on mineral separates is documented in the literature.

SAMPLING AND ANALYTICAL TECHNIQUES

The CBL mainly outcrop on the SW sector of Lipari, spreading from the summit of Monte S. Angelo stratocone (~600 m in altitude) toward the western coast, where they branch out in different lobes reaching the steep cliff near the *Punta delle Grotticelle* locality (Fig. 1). Lavas are 20-m thick, blocky, locally flow-foliated, and overlie the pyroclastic deposits emplaced by the earlier eruptions of Monte S. Angelo. The lava flows fill the fluvial incisions

affecting the southwestern flank of the edifice and appear more viscous than the older basaltic-andesites (>127 ka), since these show a lower aspect ratio.

Petrographic investigations were conducted on 5 CBL samples collected from lava outcropping in the *Terme di S. Calogero* locality (Fig. 1). The lava is massive, porphyritic, and contains abundant metamorphic xenoliths (up to 30% vol.) having different sizes (generally less than 2 cm). Meter-scale variation in xenolith amounts are observed. Studied samples were selected in the field based on the absence of macroscopic crustal and accidental material, in order to collect lava samples with limited xenolithic contribution (e.g., rock fragments and single xenocrysts). Bulk chemical analyses were not performed on the lavas, because of the extreme heterogeneity of the samples.

In-situ chemical compositions (major, minor, and trace elements) of mineral phases and glasses were determined with EPMA using the Cameca SX/100 electron microprobe at the American Museum of Natural History, USA, and the CAMECA SX/50 electron microprobe at the IGAG, CNR in Roma. Operating conditions were: acceleration voltage of 15kV, probe current of 10 nA, with a beam diameter that varied from 30 to 10 μm. In particular, to minimize Na and K migration, the glass inclusions were moved constantly under the defocused beam. The concentrations of these elements in the internal standard glasses and minerals were also determined to monitor analytical accuracy and instrumental drift.

Isotopic analyses were performed on whole-rock samples and mineral separates. Representative samples of CBL (n=3) were collected at *Terme di S. Calogero*. A subset (n=2) was used for bulk-rock analyses and another one (n=1) for mineral separation. Pure separates of cordierite, plagioclase, clinopyroxene ,and orthopyroxene were obtained using combined mechanical and gravity methods and by hand-picking. A calc–alkaline basaltic-andesitic lava of Eruptive Epoch 2 was also analyzed as bulk rock. Sr and Nd isotope ratios were determined using a multicollector, automated Finnigan-MAT 262 mass spectrometer at the U.S.

Geological Survey, Reston, VA. Detailed analytical techniques for Nd and Sr are given in Ayuso and Schulz (2003) and Ayuso et al. (2009). Nd and Sr isotope data are reported relative to international standards: La Jolla standard ($^{143}Nd/^{144}Nd$ average value= 0.511850±5) and NIST-SRM 987 standard ($^{87}Sr/^{86}Sr$ average value =0.710250±6).

PETROGRAPHY

The high-K andesitic chemical composition of CBL is the result of a multiplicity of textural features. The lava samples vary from seriate to highly porphyritic (porphyritic index up to 50%) and contain plagioclase, orthopyroxene, clinopyroxene, cordierite, garnet, and minor ilmenite, apatite, andalusite, spinel, biotite, and sillimanite. Plagioclase and pyroxene phenocrysts represent ~20 % and ~7% by volume, respectively, whereas cordierite and garnet are relatively less abundant (7% by volume). The remaining mineral phases and groundmass represent 10% and more than 50% by volume, respectively. It is noteworthy that cordierite and garnet appear evenly distributed through the lava flows.

Plagioclase

Plagioclase is the most abundant phenocryst (20 % by mode) present with two distinct morphologies. Large subhedral phenocrysts (1-5 mm) are typically zoned (Fig. 2a), and often contain dusty sieve-textured nuclei marked by abundant large (≤ 100 μm) unconnected melt inclusions. They often occur associated with clinopyroxene. Prismatic microphenocrysts showing albitetwinning (< 300 μm) are commonly distributed through the rock.

Pyroxene

Clinopyroxene generally occurs as large, subhedral grains from 1 to 4 mm in length, often forming glomerocrystic aggregates in association with plagioclase. Clinopyroxene is generally unzoned, and always surrounded by a corona of variable thickness (10 to 200 μm) consisting of fine-grained orthopyroxene (Opx II) and glass (Fig. 2b and c). Orthopyroxene is present as: I) unzoned, skeletal (Fig. 2d) and stumpy euhedral phenocrysts (100-500 μm in size) evenly distributed through the lava, II) as tiny crystals forming coronas surrounding clinopyroxene (Fig. 2b and c), or III) as rare euhedral phenocrysts (100-500 μm in size) associated with biotite, cordierite, and garnet (Fig. 3e and h). Orthopyroxene I contains silicate melt, apatite, and plagioclase inclusions (Table 1), while orthopyroxene III contains inclusions of cordierite, garnet, and plagioclase (Table 1 and Fig. 2e).

Cordierite

Cordierite, with a typical lavender color, occurs mainly as euhedral (Fig. 2a and f) and subhedral phenocrysts generally <4 mm in size, but locally attaining 10 mm or larger, and as microphenocrysts or glomerocrysts in the groundmass. Cordierite phenocrysts show embayed boundaries and fractures, while no alteration (i.e., pinite) is detected. The embayed margins likely formed while the crystals were partly resorbed, and the glomerocrysts are the late aggregation of small resorbed grains as described by Hogan (1993). Phenocrysts contain abundant silicate melt and mineral inclusions, the latter including apatite, sillimanite needles, chloritized biotite, quartz, orthopyroxene, and minor ilmenite and Fe-oxides (Table 1; Fig. 2f and g). Because of its abundance, large dimensions, and the presence of melt inclusions, phenocrysts of cordierite do not appear as xenocrystic material; moreover, the sillimanite needles and the rare biotite mineral inclusions suggest an early formation. On the contrary,

small cordierite crystals and glomerocrysts, as described in Hogan (1993), likely formed at a later stage.

Garnet

Pale-pink garnet is present with two distinct morphologies. The first type consists of abundant subhedral/euhedral grains ≤ 1 mm in size and showing resorbed margins. These grains are always found in association with cordierite (Fig. 2f) and commonly contain inclusions of apatite, biotite, sillimanite needles, quartz, ilmenite, feldspar, Fe-oxides, and glass (Table 1; Fig. 2f). The second type of garnet consists of anhedral grains with embayed outlines and of variable size (< 600 μm; Fig. 2h). The anhedral garnet is more-strongly resorbed, suggesting two possibilities for its formation: i) a xenocrystic origin, or ii) a late involvement as a reactant in dehydration-melting reactions.

Accessory phases

Sillimanite is present as rare needles within cordierite and garnet, and as anhedral crystals in the groundmass, where it is surrounded by a coronitic association consisting of spinel and cordierite (Fig. 3a). Andalusite occurs as large subhedral crystals (1 to 2 mm in diameter) showing sieve-textured margins including small resorbed crystals of cordierite, plagioclase, and Fe-oxides (Table 1 and Fig. 3b). A symplectitic texture consisting of a fine intergrowth (<20 μm) of plagioclase and spinel surrounding phenocrysts of andalusite (Fig. 3b). These textural features allow us to consider sillimanite as a relic of metamorphic origin, whereas andalusite, because of its size and shape, likely formed in the presence of a silicate melt. As a consequence, these two aluminosilicates represent two different stages of evolution of the CBL.

Euhedral apatite microphenocrysts occur associated with orthopyroxene I. Occasional resorbed biotite, that is variably altered, occurs in association with garnet, cordierite, and orthopyroxene III. Spinel is present only in the polycrystalline associations around sillimanite and/or andalusite (Fig. 3 a and b).

MINERAL CHEMISTRY

Plagioclase

The plagioclase composition, including phenocrysts and microphenocrysts, is reported in Table 2. Phenocrysts are characterized by calcic nuclei (An_{77-70}) which are succeeded towards the rim of the grains by an abrupt decrease of An (An_{50-55}). At the rims, the An content rises again to An_{60-64}. The most calcic compositions of the phenocryst nuclei overlap with the compositions of plagioclase in mafic lavas from Lipari (Bargossi et al. 1989). Microphenocrysts show inverse zoning with An_{50} cores and An_{60} rims.

Pyroxene

The clinopyroxene is diopside (Table 3) with Mg# (Mg# = Mg/Mg+Fe^{2+}) usually equal to 0.72-0.73. Rare zoning preserved in a few crystals indicates a rim with slightly lower Mg# (i.e., 0.67-0.68). We note that Barker (1987) reported clinopyroxene with similar Mg# of 0.75. Orthopyroxene, occurringboth in stumpy microphenocrysts and in crystal aggregates rimming diopside (Opx I and II; Table 3), is an enstatite showing similar and restricted ranges of Mg# (0.68-0.65; Table 3), low Al_2O_3, and CaO. Conversely, a lower Mg# of 0.55 and lower CaO, and higher Al_2O_3 have been measured in orthopyroxene III associated with cordierite and garnet (cf., Table 3).

Cordierite

On the basis of MnO content and Mg# values (Table 4), we distinguish two main chemical groups which correspond to the two textural types of cordierite (phenocrysts and microcrysts). Figure 4 illustrates the relationships between textural and chemical features of cordierite crystals. Both types show variable MnO (0.18-0.73 wt%) and Mg# (0.47-0.66) with an overlapping of their compositional fields. However, phenocrysts have lower MnO (0.18-0.35 wt%) and higher Mg# values (0.57-0.66) with respect to microphenocrysts (MnO 0.24-0.73 wt%; Mg# 0.49-0.64) (Fig. 4; Table 3).

Cordierite is generally zoned: phenocrysts are characterized by a decrease of Mg# coupled by an increase of MnO towards the rim (normal zoning; Erdmann et al. 2004); the opposite trend (i.e., reverse zoning) is observed in microphenocrysts. According to Erdmann et al. (2004), normal zoning in cordierite can be indicative of a peritectic crystallization; conversely reverse zoning can result from several processes including magma recharge and increasing T, increasing fO_2, metasomatic reactions, and pressure quenching.

Garnet

Table 5 reports the compositions of the two texturally different garnet crystals. The triangular plots (Fig. 5) suggest two different chemical trends. In the Ca-Fe+Mg-Mn and Mg-Fe-Ca+Mn diagrams (Fig. 5a and b), garnet forms two distinct chemical groups. Euhedral/subhedral garnet crystals display a narrow distribution of values; they are unzoned and richer in Fe+Mg (Fig. 5). In Fig. 5b, the euhedral garnet field shows a very slight increase in Mg and a subsequent decrease in Fe toward the rim of crystals (Table 5 and Fig. 5b); the Ca+Mn content does not have any significant variation. Resorbed (anhedral) crystals display a more scattered and heterogeneous distribution; they are characterized by the highest Mn content and show a chemical zoning with increasing Fe+Mg and decreasing Mn toward the

rim (Fig. 5a). Both the general higher Mn content of anhedral crystals and the nearly homogeneous composition - with a slight increase of the Mg content at the rim - for the euhedral crystals suggest that the latter mainly formed under a steady state for temperature, even if their rims indicate an increase of temperature during their late crystallization. On the other hand, the higher Mn content and marked zoning for anhedral crystals can be interpreted as garnet consumption (Alvarez-Valero et al. 2007) due to its involvement as reactant in a melting reaction.

SILICATE MELT INCLUSIONS AND GROUNDMASS GLASS

Cordierite and orthopyroxene I contain abundant silicate melt inclusions (10 and 80 μm in size) homogeneously distributed through single crystals. Rare, tiny, inclusions (≤ 10 μm in size) are also observed in large zoned garnet crystals. In cordierite and garnet, melt inclusions occur in syngenetic association with the mineral inclusions (e.g., quartz, biotite, sillimanite) in the same growth zones.

Silicate melt inclusions are homogenous, generally have negative crystal shapes, and their distribution is indicative of a primary origin (Fig. 2g; c.f., Frezzotti 2001). They consist of clear glass ± a small shrinkage bubble (less than 10 % in volume), but no daughter mineral phases. Within the bubble, gas phases (e.g, CO_2) are absent or below the detection limit of Raman spectrometry.

The composition of the glass within the melt inclusions hosted in cordierite is rhyolitic, peraluminous (aluminum saturation index; ASI of about 1.13-1.16) andcorundum normative (1.7-2.8 %), and has high K_2O (> 5 wt%; Na_2O/K_2O = 0.32-0.39) (Table 6; Fig. 6). A common characteristic to all analyzed melt inclusions, is that they have very high EPMA totals,

indirectly suggesting low abundances of water, from less than 0.5 to about 2 wt%. Low and variable amounts of F, Cl, and P_2O_5 have been measured (Table 6).

In orthopyroxene I, silicate melt inclusions also have rhyolitic composition but are distinctly less peraluminous with ASI of 1.05-1.12, have significantly higher Na_2O/K_2O ratios (0.58-0.65), and lower K_2O and FeO contents (Table 6; Fig. 6). These differences suggest that orthopyroxene I could not have grown in the melt preserved by inclusions in cordierite. Evolved chemical compositions probably reflect crystallization of pyroxene on the cavity walls.

The groundmass glass is strongly heterogeneous (gray area in Fig. 6a), with a composition varying from rhyodacitic to rhyolitic, and shows an extremely variable K_2O content (3.5-7.4 wt%) and ASI (1.05-1.25) (Table 6).

Sr AND Nd ISOTOPE DATA

Isotope data of whole-rock samples and mineral separates are reported in Table 6. Because of the extreme heterogeneity of the CBL, whole-rock samples display slightly different isotopic compositions, ranging in $^{87}Sr/^{86}Sr$ from 0.706133 to 0.706850 and $^{143}Nd/^{144}Nd$ from 0.512176 to 0.512431 (Fig. 7a). The isotopic composition of the mafic lava referred to Eruptive Epoch 2, plots within the field defined by Esperança et al. (1992) and Gioncada et al. (2003) for Lipari rocks (Fig. 7a). Among mineral separates, cordierite shows the highest $^{87}Sr/^{86}Sr$ (=0.710228) and lowest $^{143}Nd/^{144}Nd$ (=0.511999) isotope ratios and plots within the field of the Calabrian Basement metapelitic rocks (Fig. 7a). Plagioclase with $^{87}Sr/^{86}Sr$ =0.707650 and $^{143}Nd/^{144}Nd$ =0.512064, plots close to the field of the crustal metamorphic rocks (Fig. 7a). On the contrary, isotopic compositions of pyroxenes appear more similar to the compositions of Lipari magmatic rocks (Fig. 7a). In detail, clinopyroxene

shows lower $^{87}Sr/^{86}Sr$ (=0.705848) and lower $^{143}Nd/^{144}Nd$ (=0.512320) isotope ratios than orthopyroxene ($^{87}Sr/^{86}Sr$ =0.706562 and $^{143}Nd/^{144}Nd$ =0.512458).

DISCUSSION

Significance of mineral textures and compositions

The variability of the isotopic compositions and the distinct textures occurring at the mm scale within the CBL indicate different environments and processes of formation for the mineral phases (Fig. 7a). Large clinopyroxene phenocrysts most likely crystallized from a mafic magma similar to the old Lipari rocks, because of their high CaO and Mg #. However, the higher $^{87}Sr/^{86}Sr$ (=0.705848) and lower $^{143}Nd/^{144}Nd$ (=0.512320) values reflect hybridization processes with a new component of crustal origin (Fig. 7a), petrographically demonstrated by growth of orthopyroxene II coronae around clinopyroxene phenocrysts (Fig. Fig. 2b and c). The chemical and isotopic composition of orthopyroxene I also supports a crystallization from a mafic magma, and skeletal growth may reflect rapid crystallization.

Large plagioclase phenocrysts record a distinct crystallization history. In particular, the highly anorthitic cores suggest the onset of crystallization from a mafic parent magma, while the abrupt normal zoning indicates a variation in the magma crystallization conditions. Results from isotope studies indicate that most of the plagioclase crystallization occurred as a result of magma hybridization with a crustal component, i.e., $^{87}Sr/^{86}Sr$ =0.707650 and $^{143}Nd/^{144}Nd$ =0.512064. Abrupt growth of more sodic plagioclase suggests also a rapid temperature drop or a reduced water fugacity in melt. The formation of reverse zoning continuous as the system re-approaches equilibrium. The similar An content in the rims of large plagioclase phenocrysts and the composition of microphenocrysts indicates that only the final stages of plagioclase growth occurred during crystallization of the groundmass.

Rare orthopyroxene III, coexisting with cordierite and garnet, has a different composition as compared to the other types of orthopyroxene (e.g., higher alumina content, lower Mg#), and contains cordierite inclusions (Fig. 2e). Various metamorphic mineral inclusions are also observed in cordierite and garnet, i.e., biotite, quartz, and sillimanite needles (Table 1). Radiogenic isotopes indicate a metamorphic origin for cordierite, from rocks similar to the metapelites of the Calabrian basement (Fig. 7a; Caggianelli et al. 1991) However, the shape and compositional zoning of cordierite phenocrysts and of euhedral garnets suggest that these are not xenocrysts left after digestion of metasedimentary xenoliths by magma.

The association of biotite, quartz, sillimanite, and glass (melt) as inclusions in cordierite and garnet - and of cordierite in orthopyroxene III - is important evidence for crystallization from a silicate melt in the presence of minerals of metamorphic origin (now preserved mainly as inclusions). Based on the these observations, we interpret cordierite, garnet, and orthopyroxene III as peritectic phases formed as results of incongruent melting reactions of metamorphic rocks to produce anatectic melts.

The composition of the anatectic melts is preserved in melt inclusions hosted in peritectic cordierite. The melts are equivalent to high-K peraluminous rhyolites, containing very low volatile contents. A major characteristic of anatectic melts is that, although classified as leucogranites, they do not have minimum eutectic compositions in the haplogranite system (Fig. 6a and b). The measured glass compositions are similar to melts experimentally produced from partial-melting processes induced by fluid-absent biotite break-down at high temperatures and variable pressures (e.g., 0.5 GPa – 900°C; Fig. 6a and b; Droops et al. 2003; Stevens et al. 1995), and are within the compositional ranges measured in melt inclusions hosted in restitic phases of partially melted volcanic xenoliths and of migmatites from many localities (cf., Acosta-Vigil et al 2010, Cesare et al. 2009, and Frezzotti et al. 2004).

Sequence of petrogenetic events

Texture features and mineral chemistry allow us to identify two consequent processes leading to the petrogenesis of the CBL: 1) partial crustal melting with generation of anatectic melts of rhyolitic composition, and 2) hybridization of mafic magmas with anatectic felsic melts and restitic phases. The principal lines of evidence are the: i) presence of peritectic cordierite, garnet, and orthopyroxene III assemblages; ii) distinct Sr and Nd radiogenic isotope compositions in mineral phases; iii) chemical disequilibrium between clinopyroxene, and orthopyroxene II; and iv) the increase of MgO/MnO ratio at and near the rims of garnet and cordierite.

Stage 1: Crustal partial-melting processes:

Biotite-dehydration melting has been considerably studied through experimental petrology (e.g., Le Breton and Thompson 1988; Stevens et al. 1997; Vielzeuf and Holloway 1988; Vielzeuf and Clemens 1992) and through theoretical petrogenetic treatments (e.g. Grant, 1985; Spear et al. 1999; White et al. 2001). The univariant (for KFMASH and NaKFMASH systems) fluid-absent peritectic reaction (Spear et al. 1999; Vielzeuf and Schmidt 2001):

Biotite+Aluminosilicate+Quartz+Albite=Garnet+Cordierite+K-feldspar+Melt (R1)

is compatible with the microtextural and chemical observations reported above for Monte S. Angelo CBL rocks. The above reaction is constrained in the range of ≈ 680 to 850 °C under pressures between 0.25-0.85 GPa (Fig. 8).

The presence in the rocks of euhedral crystals of orthopyroxene III including cordierite (Fig. 3e; Mg# 0.54-0.55) suggests that a likely further increase of temperature induced another melt-producing reaction (Fig. 8):

Biotite+Garnet+Quartz+Albite= Orthopyroxene+Cordierite+K-feldspar+Melt (R2)

which also justifies a number of textural and chemical features of some minerals, such as resorption in anhedral garnet, and inverse zoning in microphenocrysts of cordierite. This reaction in the P-T grid of Fig. 8 develops at a minimum temperature of 800 °C at nearly 0.5 GPa.

The lack of peritectic crystals of K-feldspar in the assemblage of anatectic lavas, as expected by the development of reactions R1 and R2, opens the controversy about the presence or not of K-feldspar as a product in the above reactions (e.g., Carrington and Watt 1995). However, experimental work on reaction R1 by Stevens et al. (1997), shows that, in Ti-bearing magma compositions (indicated in our case by the presence of ilmenite), K-feldspar begins to appear only between 875 and 900 °C as melting progresses, and it definitively disappears at 950 °C from 0.5 to 1 GPa.

From the P-T grid of Figure 8, the formation of anatectic melt together with peritectic garnet and cordierite for CBL is constrained to temperatures between 725-800 °C: the lower temperature limit (725 °C) is inferred from the intersection between reaction R1 with the cordierite isopleth Mg_{60} which represents the composition of cordierite phenocrysts. The higher temperature limit (800 °C) is derived from the intersection between the same cordierite isopleth with the reaction (R2) involving orthopyroxene among the products (Fig. 8). The lack of K-feldspar as peritectic phase, however, indicates 900°C as the highest possible temperature attained by the CBL (Stevens et al. 1997).

In the P-T grid (Fig. 8) the reaction:

Garnet+Sillimanite+Quartz=Cordierite (R3)

represents a good geobarometer. The coexistence of garnet and cordierite (Mg_{60}) along the representative curve for the above reaction, indicates that the anatexis process developed between 0.4-0.5 GPa. Such a pressure range is in keeping with independent pressure estimates by fluid inclusion studies in metamorphic xenoliths, which indicate values around 0.4 – 0.45 GPa at 800 - 850°C (cf., Fig. 8; Di Martino et al. 2010).

The present interpretation for the origin of the different textural and chemical types of cordierite and garnet, and also for orthopyroxene (III) and the estimated temperatures under which the two main anatexis reactions developed suggest that the temperatures of 800±100°C of Barker (1987) based on metamorphic equilibria in crustal xenoliths from CBL correspond, indeed, to crustal anatexis processes at Lipari.

Stage 2: Magma mixing

There is overwhelming evidence to indicate that CBL records hybridization of melts with distinct compositions. Clinopyroxene, orthopyroxene I, and the core of plagioclase phenocryst compositions resemble calcalkaline basaltic rocks from Lipari, suggesting a composition for the mafic magma end-member akin to the primitive mantle-derived mafic magmas characterizing the older activity (223 – 90 ka) at Lipari. Conversely, peritectic assemblages testify for the participation of a rhyolitic anatectic melt, coexisting with abundant restitic phases and refractory rocks retained from zones of crustal melting.

The identification of peritectic assemblages (e.g., cordierite and garnet) does not preclude assimilation processes *per se*. Formation of peritectic phase assemblages prior to

digestion by assimilation processes and following melting of wall rocks is known to occur in magma chambers. Such processes, however, generate dm- to m-thick zones with high-cordierite and -garnet concentrations in hybrid rocks, representing post-assimilation accumulations rather than *in-situ* melt products (Erdmann et al. 2007). Local cordierite and/or garnet concentrations are not observed in the CBL, where peritectic phases are evenly distributed in the lava at the thin-section scale. In addition, if peritectic phases were derived from melting and assimilation processes of metapelites, the presence of 5 vol. % of cordierite would imply about 25 vol. % of assimilated country rock material in basaltic rocks (Erdmann et al. 2007). Such a value, although not impossible, appears exceedingly energetically high for a mafic magma, which in addition is at sub-liquidus conditions.

A mixing model, based on Sr and Nd isotopic compositions of bulk-rock samples and mineral separates of cordierite, plagioclase, clinopyroxene, and orthopyroxene is presented in Fig. 7b. The isotopic composition of the crustal end-member in the mixing model is represented by the composition of a Calabrian basement metapelitic rock (Caggianelli et al. 1991), which plots very close to the cordierite in the $^{87}Sr/^{86}Sr$ vs. $^{143}Nd/^{144}Nd$ diagram (Fig.7b). Cordierite, in fact, is supposed to form during dehydration melting processes of metapelites in the lower crust, therefore, its isotopic composition likely represents the composition of the anatectic melt. As for the mafic end-member, the isotopic composition of clinopyroxene cannot be used although phenocrysts did grow in the mafic melt. Clinopyroxene phenocrysts, in fact, are always surrounded by orthopyroxene II coronas, developing in the hybrid melt, which contribute to a shift in the isotopic composition of the mineral toward crustal values (Fig. 7b). Therefore, a calcalkaline basaltic-andesitic lava erupted during Eruptive Epoch 2 has been used as a representative mafic end-member.

A mixing hyperbola fits the compositions of both minerals and whole-rock samples (Fig. 7b), thus bolstering the observations based on petrographic, and glass and mineral

chemistry investigations. Mixing calculations indicate that the isotopic composition of clinopyroxene results from crystallization of a magma involving 70-80% of the mafic end-member and 20-30% of the crustal end-member. Coherently with mineral chemistry data, the isotopic composition of plagioclase derives from 10-20% of the mafic end-member, in which plagioclase phenocrysts start to crystallize, with a substantial contribution of the crustal end-member (80-90%). The abrupt compositional change from cores to rims registered in plagioclase phenocrysts, in fact, testifies to drastic modifications of the liquid composition. Separated phenocrysts of orthopyroxene include both the magmatic (Opx I) and the peritectic phase (Opx III), because they are not optically distinguishable.

Whole-rock samples, which plot on the curve at 10% and 50-60% of crustal component, represent the heterogeneous hybrid product of the mixing process.

Stage 3: Hybrid magma evolution

During ascent of hybrid magmas, further crystallization is testified by the coronitic associations of spinel + cordierite around anhedral crystals of sillimanite, interpreted as the onset of the reaction

Garnet+Sillimanite+Melt=Spinel±Cordierite/K-feldspar±Plagioclase (R4)

Furthermore, the presence of large andalusite crystals could result from late-stage cotectic crystallization, during adiabatic pressure decrease induced by magma ascent ($P < 0.2$ GPa), or from a magmatic peritectic crystallization under water-undersaturated conditions during cooling (Clarke et al. 2005). As underlined by these authors, it is not possible to distinguish peritectic from cotectic crystallization based on textural data from andalusite only; the two suggested reactions are:

Melt=Andalusite+K-feldspar+Plagioclase+Quartz+other magmatic phases (R5)

for cotectic crystallization and

Melt+Cordierite= Andalusite+Biotite+Plagioclase+Quartz (+H_2O) vapor (R6)

for peritectic crystallization.

Our preference is towards (R5) because the reaction occurred in the ascending magma. The later symplectitic association consisting of spinel + plagioclase are considered to reflect a melt-consuming reaction (Cesare 2008) such as:

Garnet+Andalusite+Melt=Spinel±Cordierite/K-feldspar±Plagioclase. (R7)

Crustal evolution and eruption of the CBL

The inferred P-T conditions of a crustal partial-melting event from 725 to 900°C and 0.4 to 0. 45 GPa (15-17 km) are well constrained by the overlap between the stability field of the garnet-cordierite-orthopyroxene peritectic association (in absence of K-feldspar) and independent geobarometric fluid inclusion estimates (Di Martino et al. 2010). Anatexis of crustal rocks should have been initiated at 725°C by fluid-absent dehydration-melting reactions (R1), but melting reactions proceed at progressively increasing temperatures above 800 °C (R2), and probably reached values close to 900°C.

Melting at 15-17 km depth, occurred by heating of the metapelitic basement rocks (cf., Fig. 7b) which, according to the geophysical imaging of the crust beneath the arc, should be granulitic in composition (Peccerillo et al. 2006; Ventura et al. 1999). In the perspective of

fluid-absent melting models, the critical parameter is temperature (e.g., Touret 2009). We envisage that the high-heat flow required to reach similar high temperatures at crustal depths could have been supplied only by ponding of calc-alkaline basaltic magmas, i.e., contact anatexis (Droops et al. 2003), that were emplaced at depths of 20-22 km close to the geophysical Moho, for about 130 ky, since the onset of volcanic activity at Lipari at 223 ka (Fig. 9a; Di Martino et al. 2010). It is very unlikely that a substantial upward shift in the isotherms in the crust of Lipari might have been induced by a regional process, such as mantle-magma doming beneath the Aeolian arc, since this would require a length of time in the order of tens of My (Thompson and Connolly 1995).

The occurrence of peritectic phase assemblages in the CBL indicate that anatectic liquids did not migrate from their melting site; following crustal anatexis, mixing processes to generate the CBL should have occurred at the boundaries with the deep magma chambers. We explain this evidence by injection of fresh mantle-derived mafic magma in a deep-seated chamber. This mechanism might have led to mixing between resident crystallizing mafic magmas (basalts to basalt-andesites), and the overlying high-T rhyolitic anatectic melts, resulting in the hybrid lavas (Fig. 9b and c).

Textural data, e.g., the preservation of delicate orthopyroxene coronae around clinopyroxene, indicate that magma hybridization occurred shortly before eruption. Mixing or the influence of tectonics might have cause a relatively rapid CBL ascent and eruption (Petford et al. 2000, and references therein). At Lipari, crustal tectonic features played an important role on the internal magma dynamics of the older and younger volcanoes (Di Martino et al. 2010; Gioncada et al. 2003; Ventura et al. 1999) but volcanological field-evidence of tectonic influence are lacking for the Monte S. Angelo volcano. Thus, the mixing processes described above appear the most feasible means to drive ascent and eruption of hybrid magmas. Syn-eruptive mixing triggered the recent rhyolitic explosive events of the

Aeolian Islands (Calanchi et al. 1993; Davì et al. 2009; De Rosa et al. 2003; Gioncada et al. 2005; Piochi et al. 2008) in this proposed scenario.

SUMMARY AND CONCLUSIONS

The present study indicates that cordierite-bearing lavas at Lipari (Monte S. Angelo volcano, 105 ka) consist of a complex crystalline mush developed in the lower crust at 725-900°C and 0.4-0.45 GPa, by mixing and consequent hybridization of: 1) mantle-derived mafic magmas at sub-*liquidus* condition, similar to magmas characterizing the older volcanic activity at Lipari with 2) crustal anatectic melts including peritectic phases (garnet, cordierite, and orthopyroxene III), and metamorphic crustal fragments.

We suggest that prolonged ponding of calcalkaline mafic magmas at lower crustal levels > 100 ka (from 223 to 127 ka) acted as the heat source for the onset of fluid-absent biotite dehydration melting of granulite-facies rocks to generate silicic peraluminous melts. Mafic melts co-mingled and mixed with silicic melts shortly before eruption. Fresh, hot mantle-derived magmas entered the deep magma chamber and interacted with the cooler resident melts, thus likely increasing magmatic and volatile overpressure and promoting the ascent of the cordierite-bearing crystal mush.

Sr- and Nd-isotope data of whole-rock samples and mineral separates, highlight the presence of two different components coexisting in the magmatic system in which the CBL generated. The isotopic signature of these components, represented by the isotopic compositions of the mafic lavas of Eruptive Epoch 2 and the cordierite, indicates that they derive respectively from the mantle and from the metamorphic crust. Petrogenetic modeling based on these isotope data confirms that mixing processes involving mantle-derived and

crustally-derived magmas likely occurred. Magma mixing processes generated hybrid melts having the isotopic composition of the CLB whole-rock samples.

At Lipari, the emplacement of the CBL represents one of the last events of the old mafic volcanism, and is followed by a 40-Ka long volcanic gap. The subsequent volcanic activity is rhyolitic, and marks a migration in the emission points from the central portion to the northern and southern sector of the island. In this respect, anatexis at lower crustal levels might have represented a relevant process, inducing important changes in the physical properties of the crust which may modify the magma ascent pathway within the framework of the deep magmatic feeding system.

ACKNOWLEDGEMENTS

Authors are indebted to B. Goldoff and M. Serracino for assistance during EPM analyses.

References

Acosta-Vigil A, Buick I, Hermann J, Cesare B, Rubatto D, London D, Morgan VI GB (2010) Mechanisms of crustal anatexis: a geochemical study of partially melted metapelitic enclaves and host dacite, SE Spain. J Petrol 51:785-821

Ayuso RA, Schulz KJ (2003) Nd, Pb, Sr isotope geochemistry and origin of the Ordovician Bald Mountain and Mount Chase massive sulfide deposits, northern Maine. In: Goodfellow WD, McCutcheon SR,Peter JM (eds) Volcanogenic Massive Sulfide deposits of the Bathurst District and Northern Maine. Econ Geol Mon 11, pp611-630

Ayuso RA, Haeussler PJ, Bradley DC, Farris DW, Foley NK, Wandless GA (2009) The role of the ridge subduction in determining the geochemistry and Nd, Sr, Pb isotopic evolution of the Kodiak batholith in Southern Alaska. Tectonophysics 464:137-163

Bargossi GM, Campos Venuti M, Gasparotto G, Rossi PL (1989) Petrologia e stratigrafia delle successioni andesitiche l.s. di Lipari, Isole Eolie, Italia. Mineral. et Petrogr. Acta 22:295-326

Barker DS (1987) Rhyolites contaminated with metapelite and gabbro, Lipari Aeolian Islands, Italy: products of lower crustal fusion of assimilation plus fractional crystallization?. Contrib Miner Petrol 97:460-472

Bergeat A (1910) Der Cordierit-andesit von Lipari, seine andaliste-fuhrenden Einschlusse un die genetischen Bezienhungen zwischen dem Andalusit, Sillimanit, Biotit, Cordierite, Orthoklas und Spinell in den lezteren. Neues Jahrb Miner 30:575-627

Caggianelli A, Del Moro A, Paglionico A, Piccarreta G, Pinarelli L, Rottura A (1991) Lower crustal granite genesis connected with chemical fractionation in the continental crust of Calabria (Southern Italy). Eur J Miner 3:159-180

Calanchi N, De Rosa R, Mazzuoli R, Rossi PL, Santacroce R, Ventura G (1993) Silicic magma entering a basaltic magma chamber: eruptive dynamics and magma mixing an example from Salina (Aeolian Islands, Southern Tyrrhenian Sea). Bull Volcanol 55:504-522

Carrington DP, Watt GR (1995) A geochemical and experimental study of the role of K-feldspar during water-undersaturated melting of metapelites. Chem Geol 122:59-76

Cesare B, Ferrero S, Salvioli-Mariani E, Pedron D, Cavallo A (2009) "Nanogranites" and glassy inclusions: The anatectic melt in migmatites and granulites. Geology 37:627-630

Cesare B, Marchesi C, Hermann J, Gomez-Pugnaire MT (2003) Primary melt inclusions in andalusite from anatectic graphitic metapelites: implications for the position of the Al_2SiO_5 triple point. Geol Soc Am 31:573-576

Clarke DB, Dorais M, Barbarin B, Barker D, Cesare B, Clarke G, El-Baghdadi M, Erdmann S, Forster HG, Gaeta M, Gottesmann B, Jamieson AR, Kontak D, Koller F, Gomes L, London D, Morgan GB, Neves JPFL, Pattison DRM, Pereira AJSC, Pichavant M, Rapela CW, Renno AD, Richards S, Roberts M, Rottura A, Saavedra J, Sial AN, Toselli AJ, Ugidos JM, Uher P, Villaseca C, Visonà D, Whitney DL, Williamson B, Woodard H (2005) Occurrence and origin of andalusite in peraluminous felsic rocks. J Petrol 46:442-472

Crisci GM, De Rosa R, Esperança S, Mazzuoli R, Sonnino M (1991) Temporal evolution of a three component system: the Island of Lipari (Aeolian Arc, southern Italy). Bull Volcanol 53:207-221

Davì M, De Rosa R, Barca D (2009) A LA-ICP-MS study of minerals in the Rocche Rosse magmatic enclaves: evidence of a mafic input triggering the latest silicic eruption of Lipari island (aeolian arc, Italy). J Volcanol Geother Res 182: 45-56

De Rosa R, Donato P, Gioncada A, Masetti M, Santacroce R (2003) The M. Guardia eruption (Lipari, aeolian islands): an example of reversely zoned magma mixing sequence. Bull Volcanol 65:530-543.

De Vivo B, Maiorani A, Trigilia R (1987) On the origin of the cordierite bearing rhyolites from M. S.Angelo (Lipari, Italy): fluid inclusions and petrological studies. Per Miner 56:71-84

Droop GTR, Clemens JD, Dalrymple DJ (2003) Processes and Conditions during contact anatexis, melt escape and restitic formation the huntly gabbro complex, NE Scotland. J Petrol 44:995-1029

Ebadi A, Johannes W (1991) Beginning of melting and composition of first melts in the system Qz-Ab-Or-H_2O-CO_2. Contrib Miner Petrol 106:286-295

Erdmann S, Clarke DB, MacDonald MA (2004) Origin of chemically zoned and unzoned cordierites from South mountain and Musquodboit Batholiths, Nova Scotia. Geol Soc Am Sp Papers 389, 99-110.

Esperança S, Crisci GM, De Rosa R, Mazzuoli R (1992) The role of the crust in the magmatic evolution of the Island of Lipari (Aeolian Islands, Italy). Contrib Miner Petrol 112:450-562.

Frezzotti ML (2001) Silicate-melt inclusions in magmatic rocks: applications to petrology. Lithos 55: 273-299

Frezzotti ML, Peccerillo A, Zanon V, Nikogosian I (2004) Silica-rich melts in quartz xenoliths from Vulcano Island and their bearing on processes of crustal anatexis and crust-magma interaction beneath the Aeolian Arc, southern Italy. J Petrol 45:3-26

Ginibre C, Kronz A, Wörner G (2002) High-resolution quantitative imaging of plagioclase composition using accumulated backscattered electron images: new constraints on oscillatory zoning. Contrib Miner and Petrol 142:436-448

Ginibre C, Corner G, Keonz A (2007) Crystal zoning as an archive for magma evolution. Elements 3:267-272

Gioncada A, Mazzuoli R, Bisson M, Pareschi MT (2003) Petrology of volcanic products younger than 42ka on lipari-vulcano complex (aeolian islands, Italy): An example of volcanism controlled by tectonics. Journal Volcanol Geother Res 122:191-220

Gioncada A, Mazzuoli R, Milton AJ (2005) Magma mixing at Lipari (aeolian islands, Italy). Insights from textural and compositional features of phenocrysts. Journal Volcanol Geother Res 145:97-118

Grant JA (1985) Phase equilibria in partial melting of pelitic rocks. In: Ashworth JR (ed) Migmatites. Blackie, Glasgow, pp86-144

Hawkesworth CJ, van Calsteren PWC (1984) Radiogenic isotopes – some geological applications. In: Henderson P (ed) Rare earth element geochemistry. Elsevier, Amsterdam, pp375-421

Honnorez J, Keller J (1968) Xenolithe in vulkanischen Gesteiner der Aolischen Inseln (Sizilien). Geol Rundschau 57:719-736

Holdaway MJ, Lee SM (1977) Fe-Mg cordierite in high grade politic rocks based on experimental, theoretical and natural observations. Contrib Miner Petrol 63:175-198

Jerram DA, Kent AJR (2006) An overview of modern trends in petrography: textural and microanalysis of igneous rocks. J Volcanol Geother Res 154:7-9

Kretz R (1983) Symbols for rock forming minerals. Am Miner 68:277-279

Le Breton N, Thompson AB (1988) Fluid-absent (dehydration) melting of biotite in metapelites in the early stages of crustal anatexis. Contrib Miner Petrol 99:226–237

Lucchi F, Tranne C, Rossi PL (2010) Stratigraphic approach to geological mapping of the late-Quaternary volcanic island of Lipari (Aeolian archipelago, Southern Italy). Tn: Groppelli G, Viereck-Goette L (eds) Stratigraphy and Geology of Volcanic Areas. Geol Soc Am Sp Papers 464, pp1-32

Maccarrone E (1963) Aspetti geochimici di alcuni esemplari di andesite granato-cordieritifero dell'isola di Lipari. *Per Miner* 32:277-302

O'Connor J (1965) A classification for quartz-rich igneous rock based on feldspar ratios. US Geol Survey Prof Paper 525:B79-B84

Peccerillo A, Frezzotti ML, De Astis G, Ventura G (2006) Modeling the magma plumbing system of Vulcano (aeolian islands, Italy) by integrated fluid-inclusion geobarometry, petrology, and geophysics. Geology 34:17-20

Perini G, Cesare, Gomez-Pugnaire MT, Grezzi L, Tommasini S (2008) Armouring effect on Sr-Nd isotopes during disequilibrium crustal melting: the case study of frozen migmatites from El Hoyazo and Mazarròn, SE, Spain. Eur J Miner 21:117-131

Petford N, Cruden AR, McCaffrey KJW, Vigneresse JL (2000) Granite magma formation, transport and emplacement in the Earth's crust. Nature 408:669-73

Pichler H (1980) The island of Lipari. Soc It Miner Petrol 36:415-440

Piochi M, De Astis G, Ventura G, Sulpizio R, Zanetti A (2008) Constraining the recent plumbing sistem of Vulcano (Aeolian Arc, Italy) by textural, petrological, and fractal analysis: The 1739 A.D. Pietre Cotte lava flow. Geochem Geophys Geosyst 10, Q01009, doi:10.1029/2008GC002176

Piromallo C, Morelli A (2003) P wave tomography of the mantle under the Alpine-Mediterranean area. *J Geophys Res* 108, B2, 2065, doi:10.1029/2002JB001757

Richardson SW, Gilbert MC, Bell PM (1969). Experimental determination of kyanite-andalusite and

andalusite-sillimanite equilibria; the aluminum silicate triple point. *Am J Science* 207:259-272

Riesco M, Stuwe K, Reche J, Martinez J (2004). Silica depleted melting of pelites. Petrogenetic grid and application to the Susqueda Aureole, Spain. J Metam Geol 22:475-494

Sparks RSJ, Marshall LA (1986) Thermal and mechanical constraints on mixing between mafic and silicic magmas. J Volcanol Geother Res 29:99-124

Spear FS, Kohn MJ, Cheney JT (1999) P-T paths from anatectic pelites. Contrib Miner Petrol 134:17-32

Stevens G, Clemens JD, Droop G (1997) Melt production during granulite-facies anatexis: experimental data from primitive metasedimentary protoliths. Contrib Mineral Petrol 128:352-370

Thompson AB, Connolly JAD (1995) Melting of the continental crust: some thermal and petrological constraints on anatexis in continental collision zones and other tectonic settings. J Geophys Res 100:15565-15579

Touret JLR (2009) Mantle to lower-crust fluid/melt transfer through granulite metamorphism. Russian Geol Geophys 50:1052-1062.

Tranne CA, Lucchi F, Calanchi N, Lanzafame G, Rossi PL (2002) Geological map of the Island of Lipari. (Aeolian Islands), Scale 1:10.000. University of Bologna and INGV, LAC, Firenze

Ventura G, Vilardo G, Milano G, Pino N. (1999) Relationships among crustal structure, volcanism and strike-slip tectonics in the Lipari-Vulcano volcanic complex (Aeolian Islands, Southern Tyrrhenian Sea, Italy). Phys Earth Planet Interior 116:31-52

Vielzeuf D, Clemens JD (1992) The fluid-absent melting of phlogopite+quartz: experiments and models. Am Miner 77:1206-1222

Vielzeuf D, Holloway JR (1988) Experimental determination of the fluid-absent melting relations in the pelitic system. Contrib Miner Petrol 98:257-276

Vielzeuf D, Schmidt MW (2001) Melting relations hydrous systems revisited: application to metapleties, metagreywackes and metabasalts. Contrib Miner Petrol 141:251-267

White R, Powel R, Holland T (2001) Calculation of partial melting equilibria in the system Na_2O-CaO-K_2O-FeO-MgO-$Al_2O_3SiO_2$-H_2O (NCKFMASH). J Metamorph Geol 19:139-153.

Figure legends

Fig. 1. Sketch geological map of Lipari Island showing its eruptive history in terms of successive Eruptive Epochs, according to Lucchi et al. (2010). The area covered by the cordierite-bearing lavas (CBL) is also displayed. The black square indicates the sampling area.

Fig. 2. Main mineral textures in CBL from Lipari. a) Photomicrograph showing porphyritic texture of the CBL, with phenocrysts of plagioclase (Pl) and associated large euhedral cordierite (Crd), which is also present as microcrysts in the groundmass, crossed polars (CP). b) Photomicrograph of a phenocryst of clinopyroxene (Cpx) surrounded by a delicate intergrowth of orthopyroxene II (Opx II) and glass, CP. c) Backscattered electron image of a resorbed clinopyroxene surrounded by orthopyroxene II (Opx II) and glass corona. d) Backscattered electron image of a skeletal microphenocryst of orthopyroxene I (Opx I). e) backscattered electron image of a microphenocryst of orthopyroxene III (Opx III) containing inclusions of cordierite (Crd). f) Backscattered electron image of garnet (Grt) and cordierite (Crd) association; garnet contains inclusions of quartz, biotite, Fe-oxides, and glass (melt); one relatively large inclusion of chlorite (Chl) after biotite is present in cordierite. g) Photomicrograph showing melt inclusion distribution in cordierite. Most inclusions contain clear glass and a shrinkage bubble, CP. h) Backscattered electron image of resorbed garnet (Grt) associated with orthopyroxene III (Opx III). Minerals symbols according to Kretz (1983)

Fig. 3. Backscattered electron images of aluminosilicates in the CBL from Lipari. a) sillimanite relics (Sil) surrounded by a corona consisting of cordierite (Crd) + spinel (Spl); b)

megacryst of andalusite (And) surrounded by a corona consisting of plagioclase (Pl) + spinel (Spl).

Fig. 4. Mg# ($Mg/Mg+Fe^{2+}$) versus MnO (wt%) plot showing the relationships between recognized chemical groups and phenocrysts (early) and microcrysts (late) cordierite (Crd) in rocks of the CBL from Lipari. c=core; r=rim.

Fig. 5. Ca-(Fe+Mg)-Mn (a) and Mg-Fe-(Mn+Ca) (b) triangular diagrams for both euhedral and anhedral crystals of garnet in rocks of the CBL from Lipari. c=core; r=rim.

Fig. 6. Qz-Ab-Or and An-Ab-Or normative triangular plots of glass composition in melt inclusions in cordierite (open circles) and in orthopyroxene I (filled circles) in rocks of the CBL from Lipari. Silicate glass in cordierite has a distinct composition from glass in orthopyroxene I, and resembles experimental melts obtained from fluid absent biotite breakdown at 900° C and 0.5 GPa (Stevens 1995; Droops et al. 2003), see text. The groundmass glass (grey field) and the whole-rock (open triangle) compositions are plotted for comparison. Feldspar triangle from O'Connor (1965).

Fig. 7. (a) Sr *vs.* Nd isotope variations of whole-rock samples and mineral separates (cord=cordierite; pl=plagioclase; cpx=clinopyroxene; opx=orthopyroxene) in rocks of the CBL (Eruptive Epoch 3) and basaltic-andesitic lava of Eruptive Epoch 2. The field of Lipari isotopic compositions is from Esperança et al. (1992) and Gioncada et al. (2003). Isotopic compositions of the Calabrian Basement rocks (metaigneous rocks =layered metagabbroic rocks and pyriclasites; meta-arenite=felsic granulite; metapelites=migmatitic paragneisses, Stefanaconi paragneisses, grt-cord-rich rocks and grt-sill-rich rocks) are from Caggianelli et

al. (1991). (b) Mixing model for the CBL based on Sr- and Nd-isotope compositions of whole-rock samples and mineral separates. Numbers indicate the percentage of crustal end-member in the mixing model. For further explanations, see text.

Fig. 8. P-T grid for the NaKFMASH system showing some dehydration-melting reactions involving muscovite or biotite as reactants and garnet, cordierite, K-feldspar, and orthopyroxene as products (modified after Spear et al. 1999). The shadowed grey area represents the P-T field in which peritectic and cotectic anatexis occurs. *Solidi* at aH_2O=1 and 0.5 from Ebadi and Johannes (1999), and the graphitic *solidus* from Cesare et al. (2003). Grt+Als+Qtz=Crd with Mg# Crd = 0 (Fe-Crd) and Mg#=60 from Holdaway and Lee (1977). Grt+Als=Spl+Crd+Qtz from Riesco et al. (2004). Aluminosilicate phase relations are from Richardson et al. (1969). The P -T estimates from isochoric bands that are independently derived from fluid inclusion studies in metamorphic xenoliths are also reported (Di Martino et al. 2010). Mineral symbols after Kretz (1983).

Fig. 9. Model of the plumbing system beneath Monte S. Angelo, Lipari, at 105 Ka: a) crustal melting (i.e., contact anatexis) of the lower crust induced by prolonged mafic magma ponding since at least 223 ka; b) A batch of mantle-derived magma is injected into the deep-seated magma chamber and subsequently mixed with the resident magmas including the crustal-derived rhyolitic melts; c) mixing mainly generated convection and degassing and thus, induced crystal-mush uprising.

Table 1
Click here to download table: Table1.doc

Table 1 Mineral and melt inclusions and their host phases

Host mineral	m.i.	qtz	opx	ap	ilm	pl	chl	bt	crd	grt	sil	Fe-oxides
Cordierite (early)	●	●	●	●	●		●	●			●	●
Cordierite (late)	●				●							
Garnet (euhedral-crystal)	●	●		●	●	●	●	●	●			●
Garnet (anhedral-crystal)				●	●			●				
Plagioclase (phenocryst)	●			●								
Orthopyroxene (I)	●			●		●						
Orthopyroxene (III)						●			●	●		
Andalusite (megacryst)						●			●			●

m.i.: melt inclusions; qtz: quartz; pl: plagioclase; opx: orthopyroxene; ap: apatite; ilm: ilmenite; chl: chlorite; bt: biotite; crd: cordierite, grt: garnet; sil: sillimanite; sp: spinel.

Table 2
Click here to download table: Table2.doc

Table 2 Selected compositions of plagioclase phenocrysts

Crystal	L1C1	L1C1	L1C1	L1C1	L1C2	L1C2	L1C2	L2bC	L2bC	L2bC	L2bC	L2bA1	L2bA1	L2bA2	L2bA2	L2bA2	L2bA3*	L2bA3	L2bA3
ID	§42	§41	§40	§39	§47	§46	§45	§-55	§-54	§-53	§-51	§-84	§-83	§-89	§-90	§-88	-	§-99	§-102
Domain	core	interm	interm	rim	core	interm	rim	core	interm	interm	rim	core	rim	core	interm	rim	core	interm	rim
SiO_2	49.03	52.33	53.62	53.02	53.33	50.22	53.70	51.11	54.90	55.89	53.46	53.97	50.33	52.17	52.08	53.02	52.55	53.68	52.30
Al_2O_3	31.96	29.77	29.17	29.30	28.77	30.50	29.08	30.67	28.48	27.68	29.42	27.84	30.14	27.84	27.19	27.42	27.30	28.87	29.30
CaO	15.43	12.79	11.89	12.10	11.65	13.96	11.79	13.76	10.97	10.27	12.09	11.67	14.01	12.07	11.67	11.10	11.38	11.85	12.47
FeO	0.56	0.39	0.41	0.55	0.67	0.24	0.57	0.48	0.45	0.39	0.60	0.39	0.73	0.13	0.27	0.16	0.22	0.60	0.50
Na_2O	2.45	3.81	4.30	4.43	4.56	3.38	4.31	3.56	4.67	5.05	4.14	3.86	3.25	4.08	4.16	4.21	4.18	4.31	4.28
K_2O	0.21	0.46	0.59	0.58	0.56	0.31	0.52	0.40	0.58	0.69	0.49	1.74	0.45	0.58	0.60	0.76	0.68	0.62	0.46
Total	99.64	99.55	99.99	99.97	99.54	98.59	99.98	99.97	100.05	99.97	100.20	99.46	98.91	96.89	95.97	96.67	96.32	99.92	99.29
Si	2.25	2.40	2.43	2.41	2.43	2.32	2.43	2.33	2.47	2.52	2.41	2.46	2.32	2.44	2.46	2.48	2.47	2.43	2.39
Al	1.73	1.58	1.56	1.57	1.54	1.66	1.55	1.65	1.51	1.47	1.57	1.50	1.64	1.53	1.51	1.51	1.51	1.54	1.58
Fe^{2+}	0.00	0.00	0.00	0.00	0.00	0.00	0.00	0.00	0.00	0.00	0.00	0.00	0.00	0.00	0.00	0.00	0.00	0.00	0.00
Fe^{3+}	0.02	0.01	0.02	0.02	0.03	0.01	0.02	0.02	0.02	0.01	0.02	0.01	0.03	0.01	0.01	0.01	0.01	0.02	0.02
Ca	0.76	0.62	0.58	0.59	0.57	0.69	0.57	0.67	0.53	0.50	0.59	0.57	0.69	0.60	0.59	0.56	0.57	0.58	0.61
Na	0.22	0.33	0.38	0.39	0.40	0.30	0.38	0.31	0.41	0.44	0.36	0.34	0.29	0.37	0.38	0.38	0.38	0.38	0.38
K	0.01	0.03	0.03	0.03	0.03	0.02	0.03	0.02	0.03	0.04	0.03	0.10	0.03	0.03	0.04	0.05	0.04	0.04	0.03
Total	4.98	4.97	4.98	5.00	5.00	5.00	4.98	5.00	4.97	4.97	4.98	4.99	4.99	4.99	4.98	4.97	4.98	4.98	5.00
Or	0.03	0.01	0.00	0.03	0.01	0.01	0.08	0.02	0.03	0.04	0.03	0.10	0.02	0.00	0.00	0.00	0.00	0.00	0.00
Ab	0.19	0.31	0.26	0.43	0.29	0.22	0.26	0.29	0.40	0.43	0.35	0.33	0.28	0.38	0.49	0.41	0.31	0.48	0.38
An	0.77	0.67	0.72	0.53	0.69	0.76	0.72	0.68	0.55	0.52	0.61	0.55	0.69	0.61	0.50	0.58	0.68	0.51	0.61
	Oscillatory zoning				Oscillatory zoning			Oscillatory zoning				Reverse zoning		Oscillatory zoning			Oscillatory zoning		

compositions as in weight percent *: average of 2 analysis

table 3
Click here to download table: Table3.doc

Table 3 Selected compositions of pyroxene

Crystal	L1cB1	L1cB1	L1cB2	L1cB2	L1cB2	L2bC	L2bC	L2aA	L2aA	L2bA*	L2bA*	L2aB1*
ID	#7	#8	#12	#13	#14	#34	#35	#79	#80	-	-	-
Type of px	opxI	opxI	opxIII	cpx	cpx	opxII	opxII	cpx	opxIII	opxI	opxI	opxI
SiO_2	52.80	52.67	53.06	51.16	51.74	53.62	53.21	52.04	52.24	52.09	51.91	52.65
TiO_2	0.22	0.24	0.33	0.48	0.44	0.29	0.17	0.44	0.27	0.21	0.19	0.25
Al_2O_3	0.96	0.89	0.96	1.36	1.36	0.86	0.87	1.65	1.24	0.81	1.05	0.81
MgO	22.38	22.91	18.23	14.14	13.37	22.59	22.41	14.06	17.29	21.97	22.49	22.32
CaO	1.46	1.51	1.21	19.88	19.65	1.59	1.49	20.33	1.01	1.46	1.45	1.53
MnO	0.77	0.80	0.84	0.35	0.47	0.80	0.83	0.42	0.89	0.65	0.63	0.69
FeO	21.11	21.08	25.74	12.13	12.97	21.68	21.86	11.45	26.06	21.61	20.8	21.07
Na_2O	0.03	0.02	0.11	0.28	0.28	0.03	0.03	0.29	0.09	0.02	0.08	0.04
Tot	99.72	100.19	100.63	99.79	100.31	101.47	100.86	100.84	99.49	98.85	98.59	99.37
Si	1.97	1.95	2.00	1.92	1.94	1.97	1.96	1.94	2.00	1.97	1.95	1.97
Ti	0.01	0.01	0.01	0.01	0.01	0.01	0.00	0.01	0.01	0.01	0.01	0.01
Al	0.04	0.04	0.04	0.06	0.06	0.04	0.04	0.07	0.06	0.04	0.05	0.04
Fe^{2+}	0.64	0.60	0.81	0.29	0.36	0.65	0.65	0.3	0.83	0.65	0.61	0.64
Fe^{3+}	0.01	0.05	0.00	0.09	0.05	0.02	0.03	0.05	0.00	0.01	0.05	0.02
Mn	0.02	0.03	0.03	0.01	0.01	0.02	0.03	0.01	0.03	0.02	0.02	0.02
Mg	1.24	1.26	1.02	0.79	0.75	1.23	1.23	0.78	0.99	1.24	1.26	1.24
Ca	0.06	0.06	0.05	0.80	0.79	0.06	0.06	0.81	0.04	0.06	0.06	0.06
Na	0.00	0.00	0.01	0.02	0.02	0.00	0.00	0.02	0.01	0.00	0.01	0.00
Total	4.00	3.99	3.97	4.00	3.99	4.00	3.99	4.00	3.97	4.00	3.99	4.00
Mg#	0.66	0.68	0.56	0.73	0.68	0.65	0.65	0.72	0.54	0.66	0.67	0.66
Wo	0.03	0.03	0.02	0.42	0.42	0.03	0.03	0.43	0.02	0.03	0.03	0.03
En	0.64	0.66	0.54	0.42	0.39	0.63	0.64	0.41	0.53	0.64	0.65	0.64
Fs	0.33	0.31	0.43	0.15	0.19	0.33	0.33	0.16	0.45	0.33	0.32	0.33

Compositions as in weight percent; Mg#: $Mg/Mg+Fe^{2+}$ atomic percent; Cations recalculated on the basis of 6 oxygen number
*: average of two analyses

table 4
Click here to download table: Table4.doc

Table 4 Selected compositions of cordierite

Sample	L1cB	L1cB	L2aA	L2aA	L2bA1	L1C*	L1bB1	L1bB1	L1bB1	L1bB2	L1bB2	L1cB2	L1cB2	L2aB*	L2bC1*
ID	#6[a]	#2[a]	#51[b]	#52[b]	§25[b]	-[b]	§85[a]	§84[a]	§83[a]	§86[a]	§87[a]	§88[a]	§89[a]	-[b]	-[b]
Domain	core	rim	core	rim	-	-	core	int	rim	rim	core	core	rim	-	-
SiO_2	48.39	48.33	48.50	48.14	47.89	48.56	47.98	48.47	48.90	48.10	48.26	48.22	48.17	48.72	48.64
TiO_2	0.01	0.00	0.01	0.02	0.01	0.00	0.00	0.01	0.04	0.00	0.03	0.03	0.00	0.01	0.02
Al_2O_3	32.22	32.33	32.50	32.73	33.42	33.18	32.18	32.88	32.88	32.56	32.60	32.66	32.84	33.32	32.90
MgO	7.96	7.97	7.89	8.01	6.30	7.34	6.63	7.40	7.56	6.52	6.18	6.40	7.29	7.85	6.88
MnO	0.40	0.33	0.60	0.51	0.49	0.38	0.68	0.35	0.26	0.64	0.73	0.71	0.28	0.26	0.47
FeO	9.59	9.35	9.12	9.04	11.96	10.63	10.82	9.66	10.33	11.24	12.08	11.3	10.49	9.51	10.81
Na_2O	0.04	0.06	0.02	0.01	0.01	0.07	0.00	0.00	0.01	0.05	0.00	0.00	0.03	0.00	0.00
K_2O	0.25	0.27	0.09	0.12	0.26	0.18	0.37	0.25	0.20	0.29	0.16	0.15	0.12	0.21	0.20
Tot	98.91	98.67	98.76	98.59	100.39	100.45	98.74	99.12	100.20	99.64	100.09	99.54	99.26	99.91	99.98
Si	4.98	4.98	4.99	4.96	4.91	4.94	4.98	4.98	4.98	4.96	4.97	4.98	4.95	4.96	4.98
Ti	0.00	0.00	0.00	0.00	0.00	0.00	0.00	0.00	0.00	0.00	0.00	0.00	0.00	0.00	0.00
Al	3.91	3.93	3.94	3.97	4.04	3.98	3.94	3.99	3.94	3.96	3.96	3.98	3.98	4.00	3.97
Fe^{2+}	0.70	0.68	0.69	0.66	0.87	0.77	0.80	0.75	0.75	0.82	0.91	0.89	0.77	0.70	0.84
Fe^{3+}	0.12	0.12	0.09	0.12	0.15	0.14	0.14	0.08	0.13	0.15	0.13	0.08	0.14	0.11	0.09
Mn	0.03	0.03	0.05	0.04	0.04	0.03	0.06	0.03	0.02	0.06	0.06	0.06	0.02	0.02	0.04
Mg	1.22	1.22	1.21	1.23	0.96	1.11	1.03	1.13	1.15	1.00	0.95	0.98	1.12	1.19	1.05
Na	0.01	0.01	0.00	0.00	0.00	0.01	0.00	0.00	0.00	0.01	0.00	0.00	0.01	0.00	0.00
K	0.00	0.04	0.01	0.02	0.03	0.02	0.05	0.03	0.03	0.04	0.02	0.02	0.02	0.03	0.03
Total	10.98	11.01	11.99	11.01	11.01	11.01	11.01	11.01	11.01	11.01	11.01	11.01	11.01	11.01	11.01
Mg#	0.64	0.64	0.64	0.65	0.52	0.59	0.56	0.60	0.61	0.55	0.51	0.52	0.59	0.63	0.56

Compositions as in weight percent; Mg#: $Mg/Mg+Fe^{2+}$ atomic percent; Cations recalculated on the basis of 18 oxygen number;
average of 2 (*) and 4 (*) analyses; a: late cordierite; b: early cordierite

table 5
Click here to download table: Table5.doc

Table 5 Selected compositions of garnet

Sampe	L2bC3	L2bC3	L1bB1	L1bB1	L2bC	L2bC	L2bC	L2bC2*	L2bC2*	L1bB3	L1bB3
ID	#38	#39	#60	#61	§51	§49	§48	-	-	#73[a]	#74[a]
Domain	core	rim	interm.	rim	core	interm.	rim	core	rim	core	rim
SiO_2	38.46	36.85	37.14	37.69	37.58	37.86	37.32	37.52	37.01	37.76	36.16
TiO_2	0.09	0.07	0.14	0.05	0.11	0.17	0.16	0.01	0.00	0.21	0.02
Al_2O_3	21.48	21.24	21.10	20.90	21.58	21.52	21.51	21.07	21.11	20.77	20.94
MgO	6.02	5.90	4.87	5.74	5.80	5.23	5.35	2.78	3.97	3.89	4.62
CaO	1.50	1.50	1.62	1.59	1.51	1.53	1.53	1.64	1.56	1.59	1.77
MnO	2.74	2.71	2.01	2.76	2.70	2.77	2.65	9.13	4.80	8.25	6.13
FeO	31.54	31.67	33.26	30.91	32.06	31.99	31.81	30.10	32.05	28.19	28.85
Tot	101.83	99.94	100.16	99.64	100.8	101.10	100.60	102.26	100.54	100.66	98.49
Si	2.99	2.93	2.96	2.99	2.94	2.97	2.95	2.97	2.96	3.00	2.93
Ti	0.01	0.00	0.01	0.00	0.01	0.01	0.01	0.00	0.00	0.01	0.00
Al	1.96	1.99	1.98	1.96	1.99	1.99	2.01	1.97	1.99	1.95	2.00
Fe^{2+}	2.00	2.03	2.16	2.00	2.04	2.08	2.08	1.93	2.09	1.83	1.89
Fe^{3+}	0.04	0.08	0.05	0.05	0.06	0.02	0.03	0.06	0.05	0.04	0.06
Mn	0.18	0.18	0.14	0.19	0.18	0.18	0.18	0.61	0.32	0.56	0.42
Mg	0.70	0.70	0.58	0.68	0.68	0.61	0.63	0.33	0.47	0.46	0.56
Ca	0.13	0.13	0.14	0.14	0.13	0.13	0.13	0.14	0.13	0.14	0.15
Total	8.00	8.03	8.02	8.00	8.03	8.01	8.02	8.01	8.02	7.99	8.03
Alm	0.67	0.67	0.72	0.67	0.68	0.69	0.69	0.64	0.69	0.61	0.63
Pyr	0.23	0.23	0.19	0.23	0.22	0.20	0.21	0.11	0.16	0.15	0.18
Sps	0.06	0.06	0.04	0.06	0.06	0.06	0.06	0.20	0.11	0.19	0.14
Grs	0.02	0.00	0.02	0.02	0.01	0.03	0.03	0.02	0.02	0.02	0.02
Adr	0.02	0.04	0.03	0.03	0.03	0.01	0.01	0.03	0.03	0.02	0.03

Compositions as in weight percent; Mg#: Mg/Mg+Fe^{2+} atomic percent;
Cations recalculated on the basis of 12 oxygen number; a: anhedral crystrals;*: average of two analyses.

table 6
Click here to download table: Table6.doc

Table 6 Selected melt inclusion, groundmass, whole-rock and experimental melt compositions

Sample	L1C	L1c	L1C	L1bB	L1cB	L1cB	L2bC	A✶	A✶✶		L2bC	L1cB	L1bB11	L1bB3D	L1bB1A	B★	C★★
ID	§30	§32	§36	§81	#9	#10	#36	-	C112	B1	#32	#11	#21	#6	#25	-	-
Analysis	Melt inclusions							Experimental melts			Groundmass					Whole-rock	
	crd				opxI				(n=14)	(n=10)						n=8	
SiO_2	71.93	70.29	70.94	74.06	70.99	70.51	72.04	74.48	72.28	72.35	70.51	70.69	71.61	73.70	69.52	63.33	59.30
TiO_2	0.27	0.34	0.43	0.06	0.25	0.23	0.22	0.00	0.39	0.56	0.29	0.44	0.44	0.15	0.32	0.63	0.60
Al_2O_3	13.68	14.54	14.6	13.28	14.98	14.89	15.30	14.29	13.75	14.51	14.74	14.44	12.38	13.33	17.12	16.57	16.50
MgO	0.04	0.08	0.08	0.06	0.06	0.25	0.03	0.25	0.55	0.47	0.02	0.01	0.05	0.05	0.02	1.06	2.20
CaO	1.35	1.34	1.31	1.00	1.37	1.60	1.05	0.64	0.69	1.23	1.13	2.04	0.82	1.10	3.61	4.66	5.30
MnO	0.10	0.18	0.07	0.10	0.09	0.01	0.07	0.00	0.00	0.00	0.00	0.00	0.00	0.09	0.01	0.10	0.10
FeO	1.79	3.30	3.04	2.28	0.86	1.08	1.03	1.65	3.80	3.38	0.67	1.12	1.24	1.60	0.85	6.26	7.80
Na_2O	1.90	2.33	2.25	2.06	3.46	3.30	3.32	2.30	0.81	1.47	2.31	2.48	1.22	1.76	3.52	2.23	2.00
K_2O	5.92	6.04	5.99	5.91	5.34	5.37	5.77	6.39	7.73	6.03	7.28	5.04	5.87	5.91	3.48	3.89	3.50
F	0.26	0.20	0.47	0.17	0.01	0.08	0.05	-	-	-	0.16	0.06	0.03	0.19	0.15	-	-
Cl	0.18	0.23	0.20	0.16	0.30	0.22	0.28	-	-	-	0.09	0.14	0.11	0.13	0.07	-	-
P_2O_5	0.31	0.42	0.28	0.01	-	-	-	-	-	-	-	-	-	-	-	0.22	0.20
Total	97.73	99.29	99.66	99.15	97.71	97.54	99.16	100.00	100.00	100.00	97.20	96.46	93.79	98.01	98.67	98.95	96.50
CIPW (%)																	
Q	35.73	29.50	30.83	35.73	27.51	26.97	27.93	33.52	32.80	34.98	27.25	33.23	42.17	37.97	27.91	19.89	14.40
C	2.50	2.77	2.73	1.72	1.04	0.76	1.71	2.43	2.80	3.33	1.04	1.24	2.70	2.08	1.01	0.75	0.27
Or	35.96	36.11	35.76	35.35	32.40	32.63	34.50	37.76	45.68	35.64	44.38	30.94	37.07	35.78	20.90	23.23	21.22
Ab	16.53	19.94	19.23	17.64	30.06	28.72	28.42	19.46	6.85	12.44	20.16	21.80	11.03	15.26	30.24	19.07	17.36
An	4.80	3.95	4.72	4.96	6.98	8.16	5.27	3.18	3.42	6.10	5.79	10.51	4.35	5.57	18.20	21.91	25.63
Hy	3.21	6.10	5.26	4.48	1.52	2.31	1.75	3.65	7.70	6.45	0.83	1.41	1.80	3.05	1.12	13.42	19.49
Il	0.53	0.65	0.82	0.12	0.49	0.45	0.42	0.00	0.74	1.06	0.57	0.87	0.90	0.30	0.61	1.21	1.17
Ap	0.74	0.99	0.66	0.02	0.00	0.00	0.00	0.00	0.00	0.00	0.00	0.00	0.00	0.00	0.00	0.51	0.48
A.S.I.	1.14	1.13	1.16	1.14	1.07	1.05	1.12	1.20	1.25	1.30	1.01	1.09	1.26	1.18	1.06	1.01	0.99
Na_2O/K_2O	0.32	0.39	0.38	0.35	0.65	0.61	0.58	0.36	0.10	0.24	0.32	0.49	0.21	0.30	1.01	0.57	0.57

Compositions as in weight percent; A.S.I.: Alumina saturation index (molar Al_2O_3/Na_2O+K_2O+CaO); Crisci et al. 1991 (★) and Pichler 1981 (★★);
A: experimental melt from dehydration melting of biotite (T=900°C; P=0.5 GPa) obtained by Stevens, 1995 (✶) and Droop et al., 2003 (✶✶);

table 7
Click here to download table: Table 7.doc

Table 7 Sr and Nd isotope compositions of whole-rock samples and mineral separates

Sample	A16	T3	LS90-13	cord	pl	cpx	opx
Type	wr	wr	wr	ms	ms	ms	ms
Description	BA	CBL	CBL	CBL	CBL	CBL	CBL
$^{87}Sr/^{86}Sr$	0.706073±15	0.706133±18	0.706850±16	0.710228±22	0.707650±19	0.705848±25	0.706562±27
$^{143}Nd/^{144}Nd$	0.512523±8	0.512431±10	0.512176±12	0.511999±10	0.512064±19	0.512320±8	0.512458±17
Sr ppm	531	406	403	-	-	-	-
Nd ppm	22.7	25.9	35.3	-	-	-	-

Analytical errors on $^{143}Nd/^{144}Nd$ and $^{87}Sr/^{86}Sr$ measurements represent 2σ.
wr:whole-rock sample; ms: mineral separates; BA: basaltic andesite; CBL: cordierite-bearing lavas.

line figure 1

Click here to download high resolution image

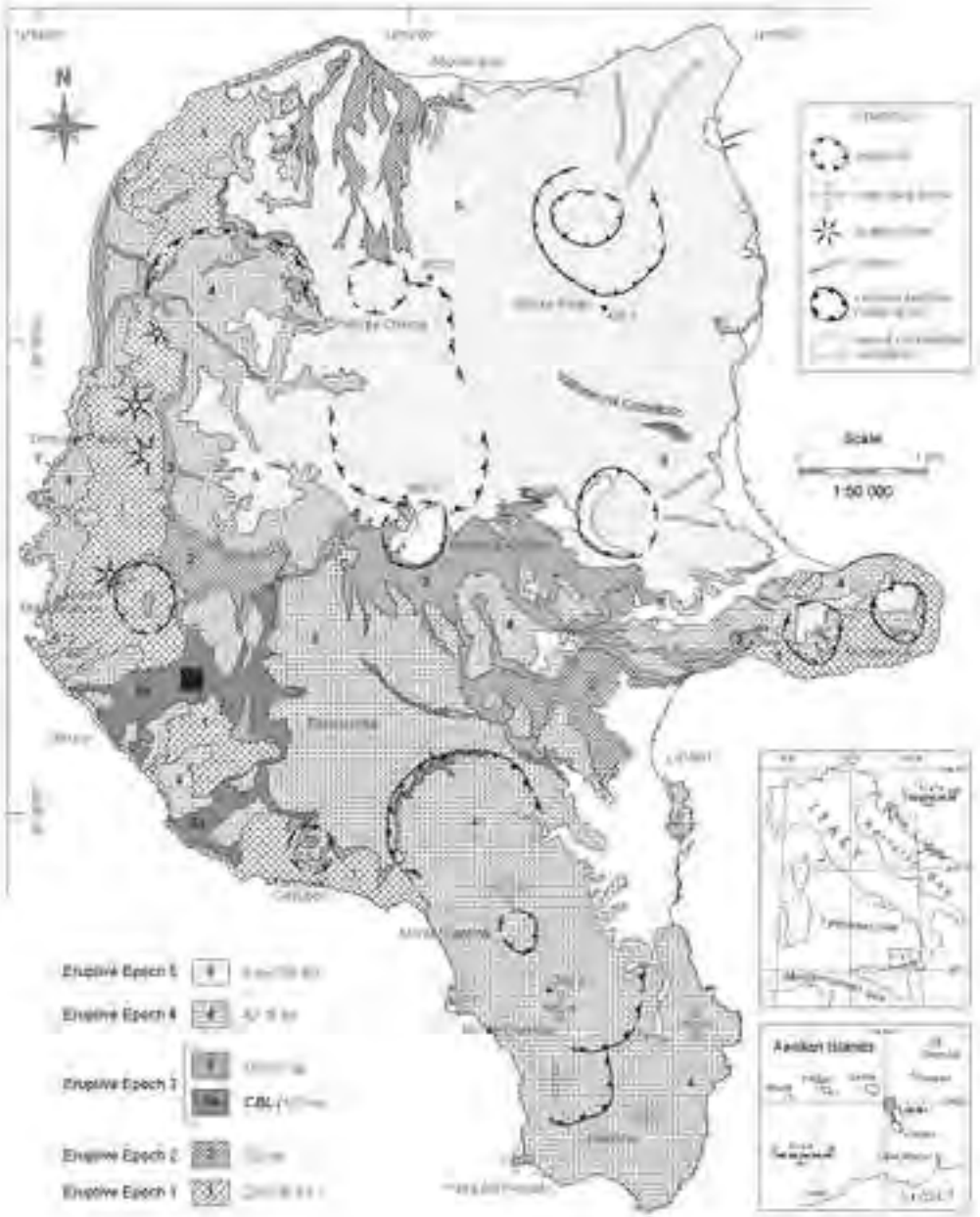

line figure 2

Click here to download high resolution image

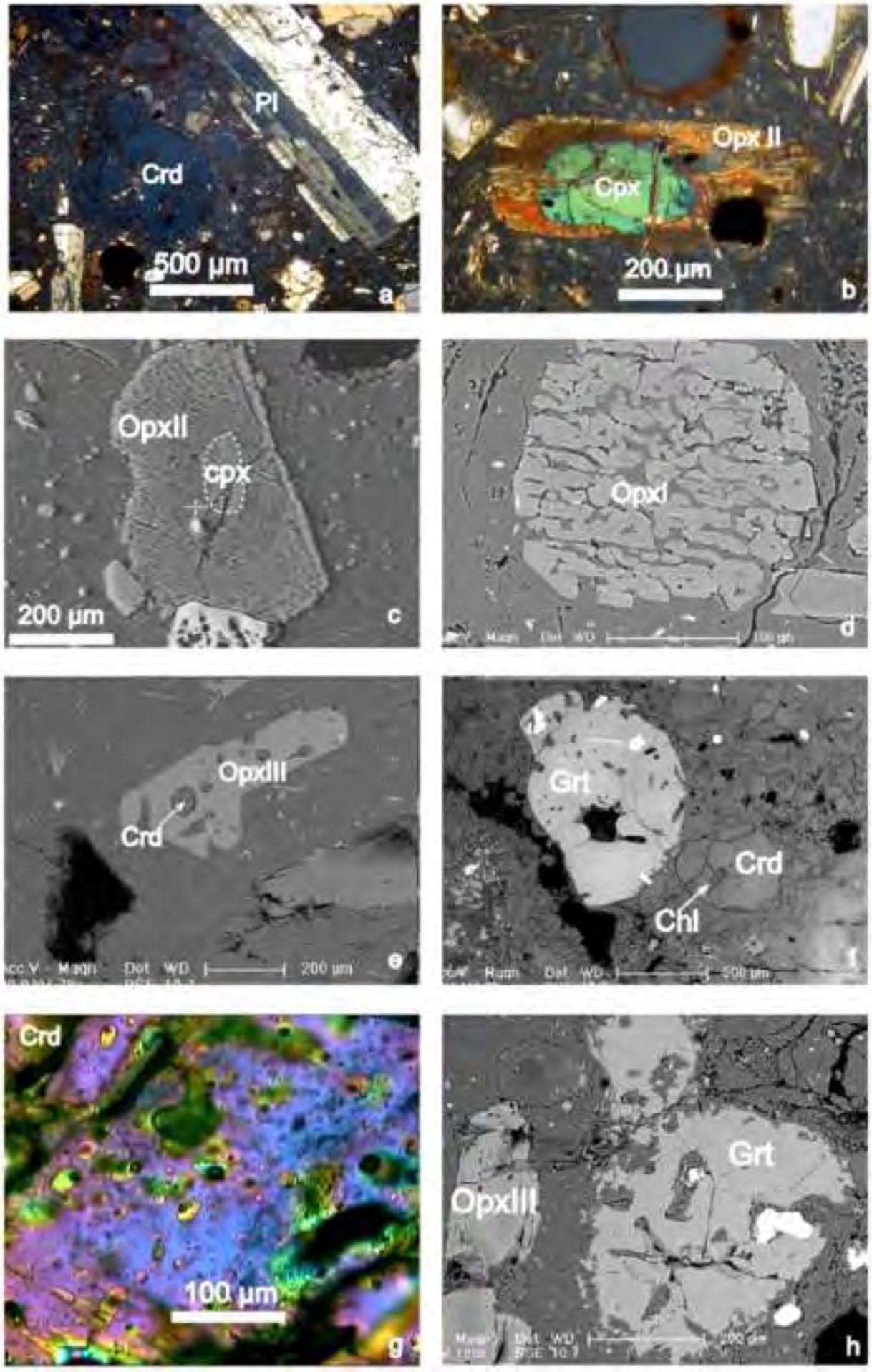

line figure 3

Click here to download high resolution image

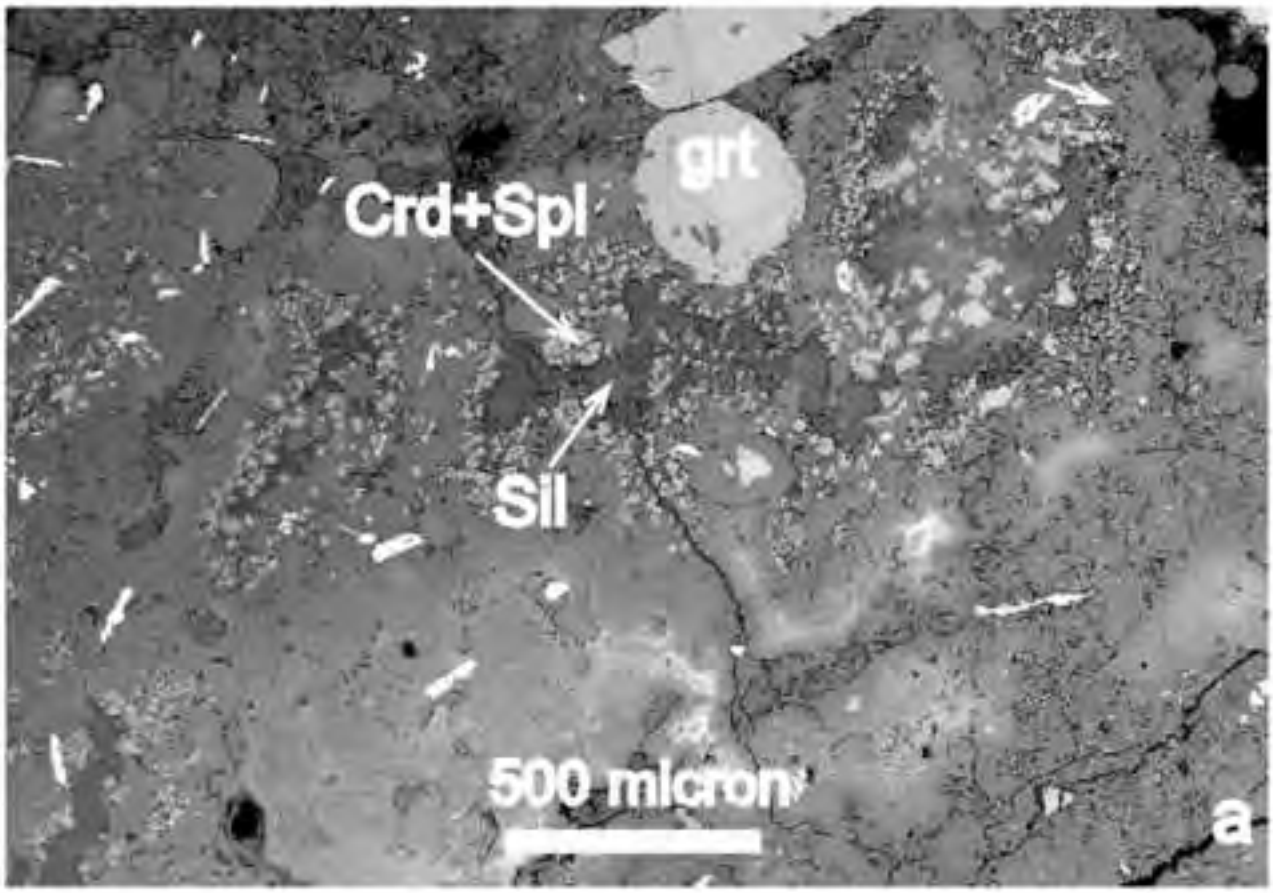

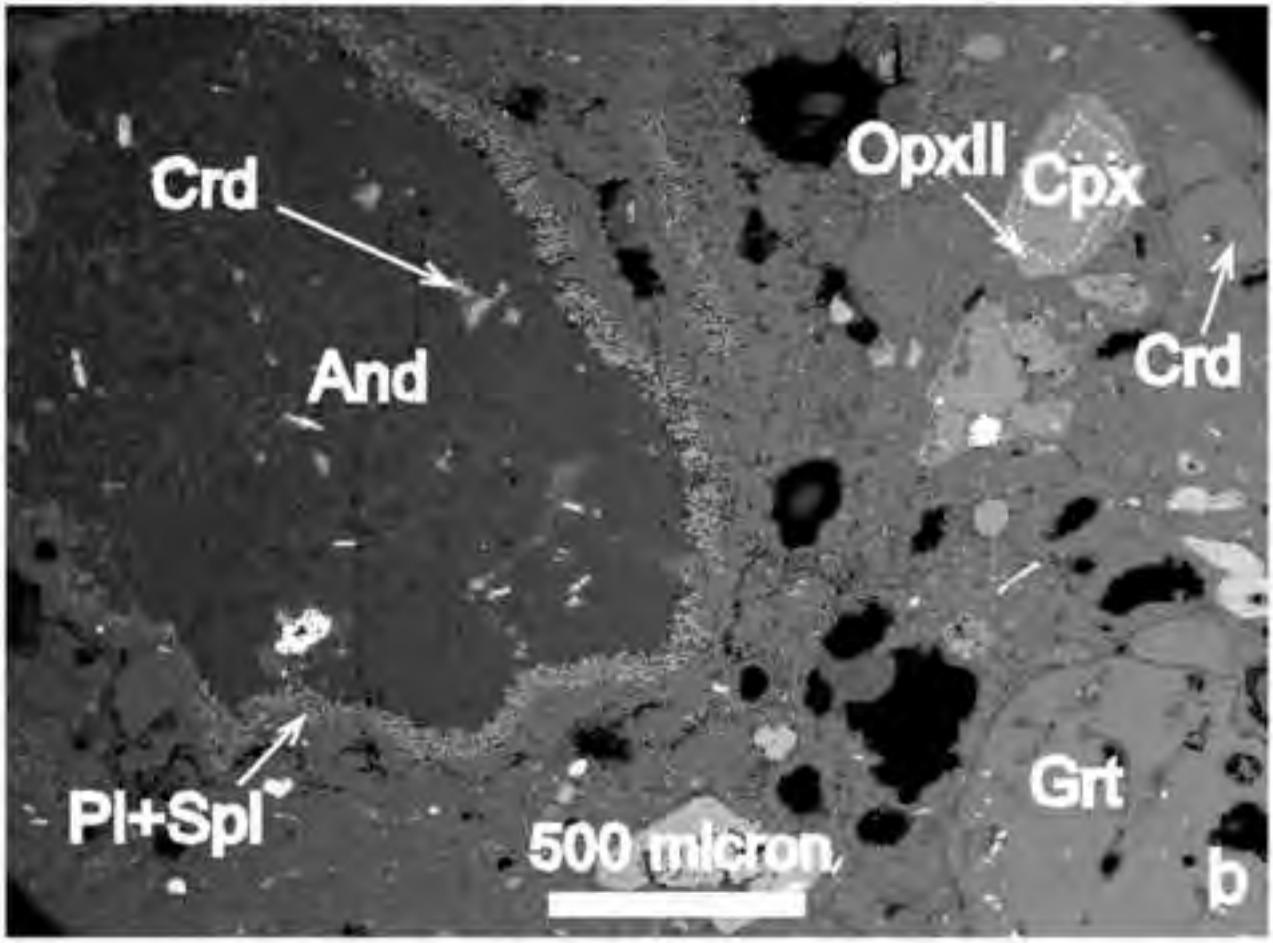

line figure 4
Click here to download high resolution image

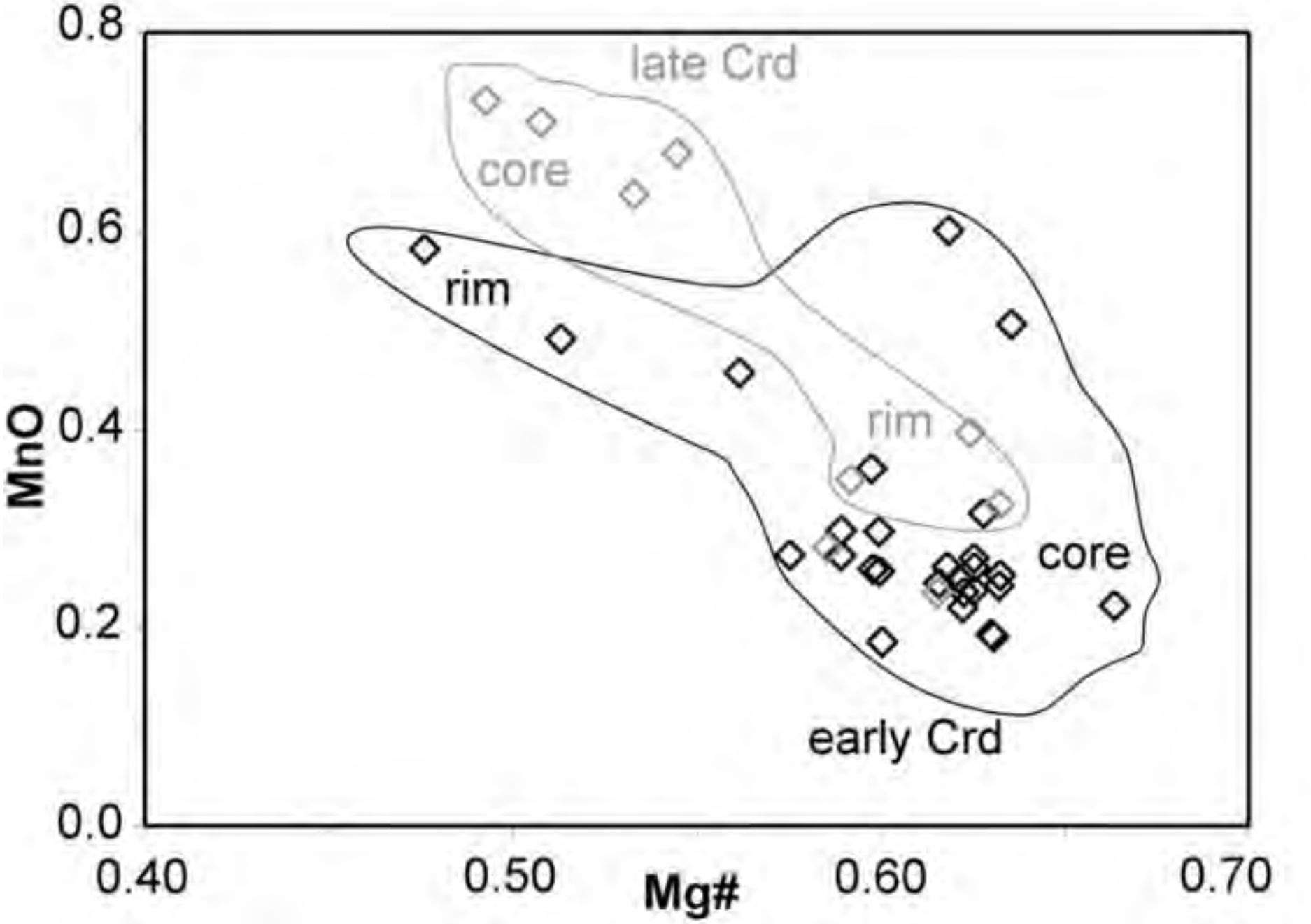

line figure 5

Click here to download high resolution image

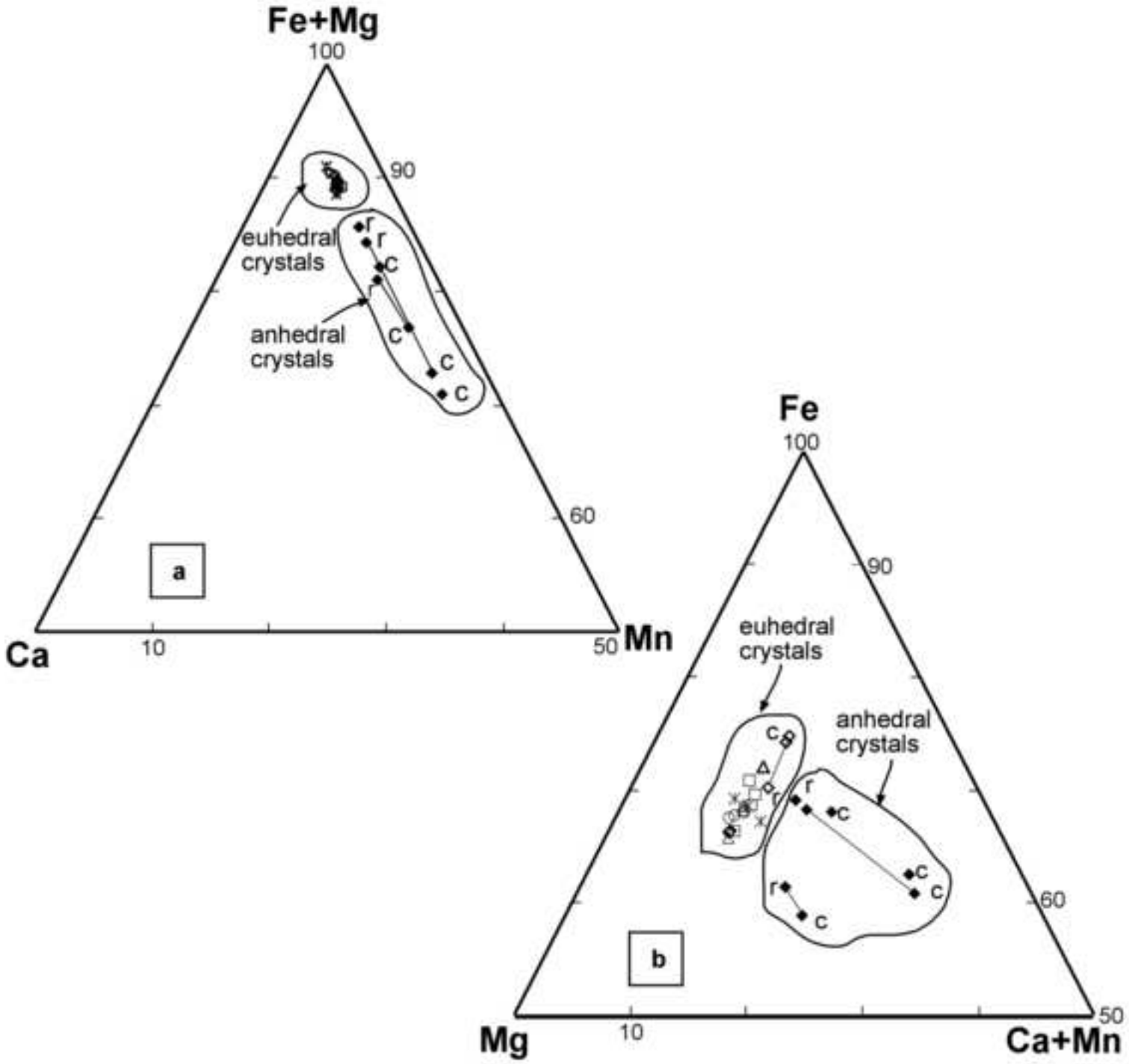

line figure 6
Click here to download high resolution image

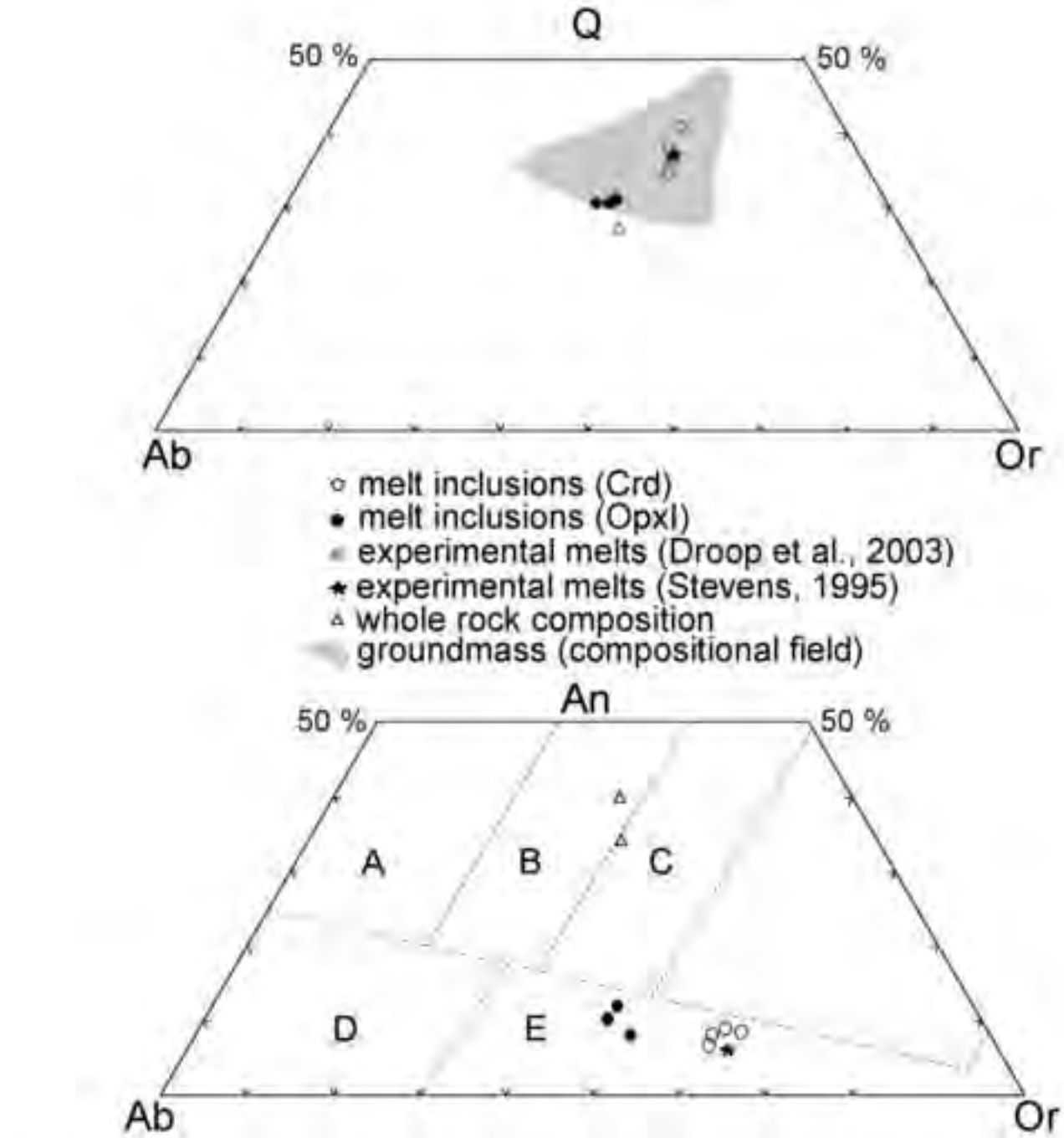

A: tonalite; B: granodiorite; C: monzogranite; D: trondhjemite; E: leucogranite.

line figure 7

Click here to download high resolution image

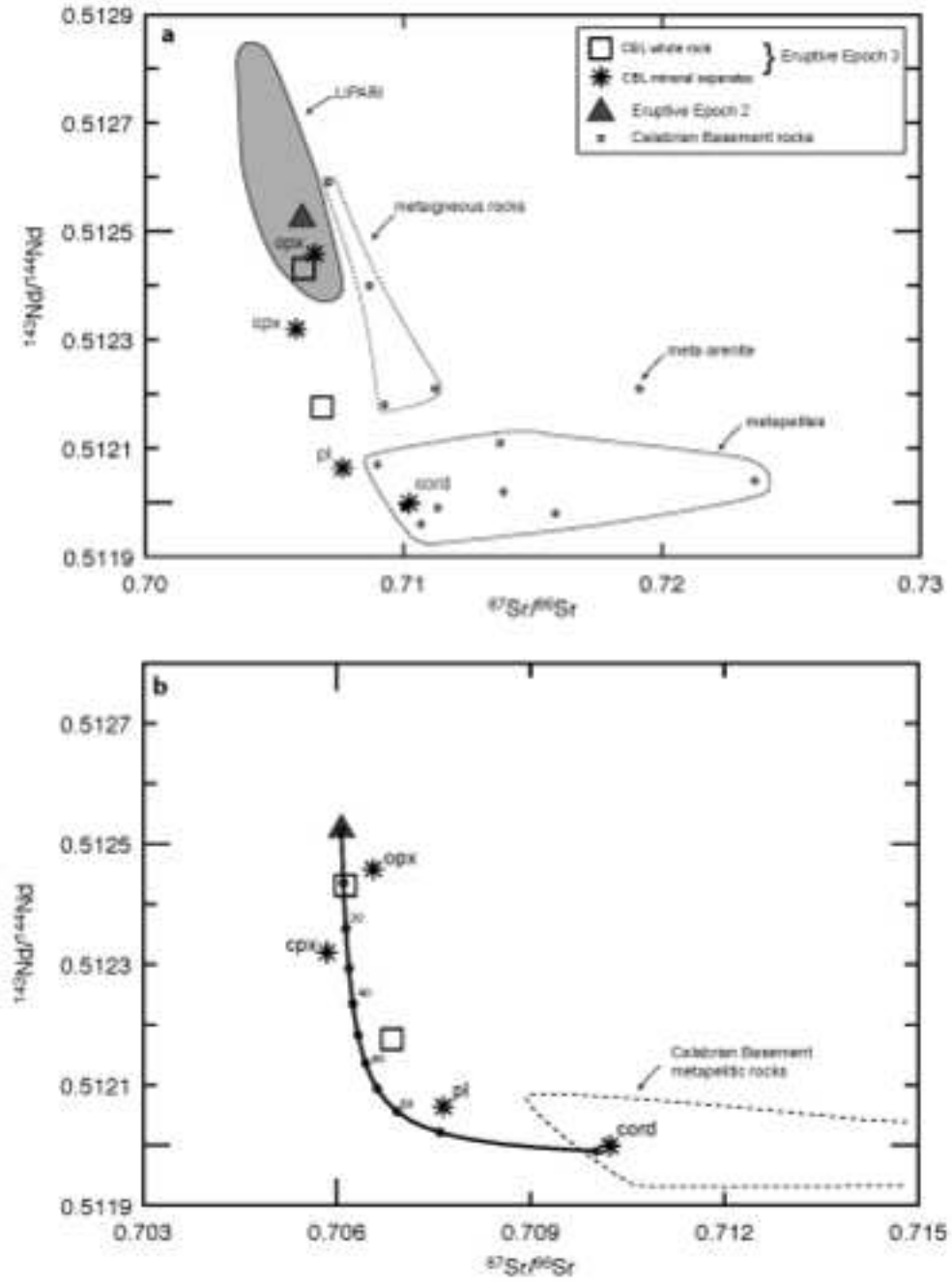

line figure 8

Click here to download high resolution image

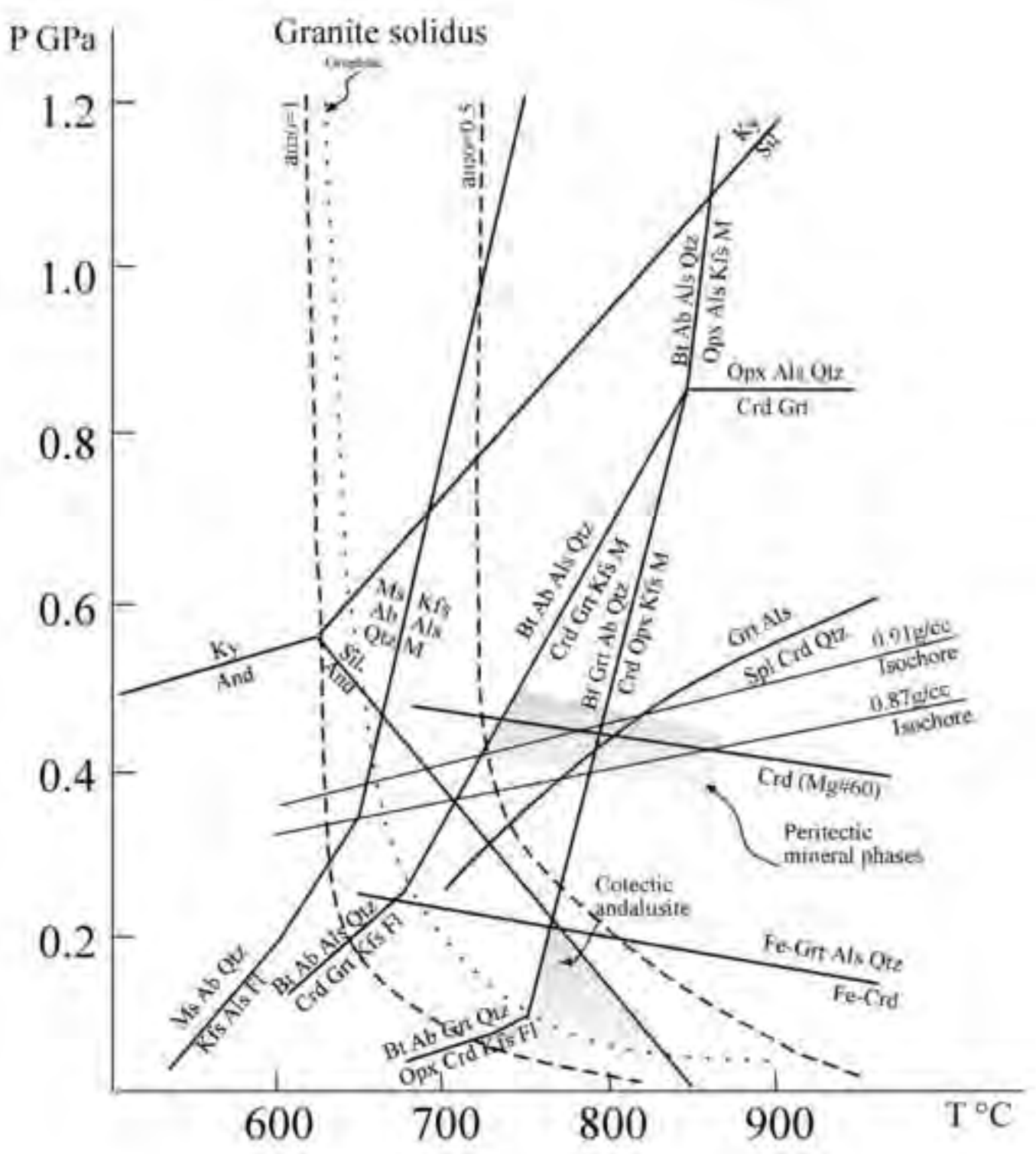

line figure 9
Click here to download high resolution image

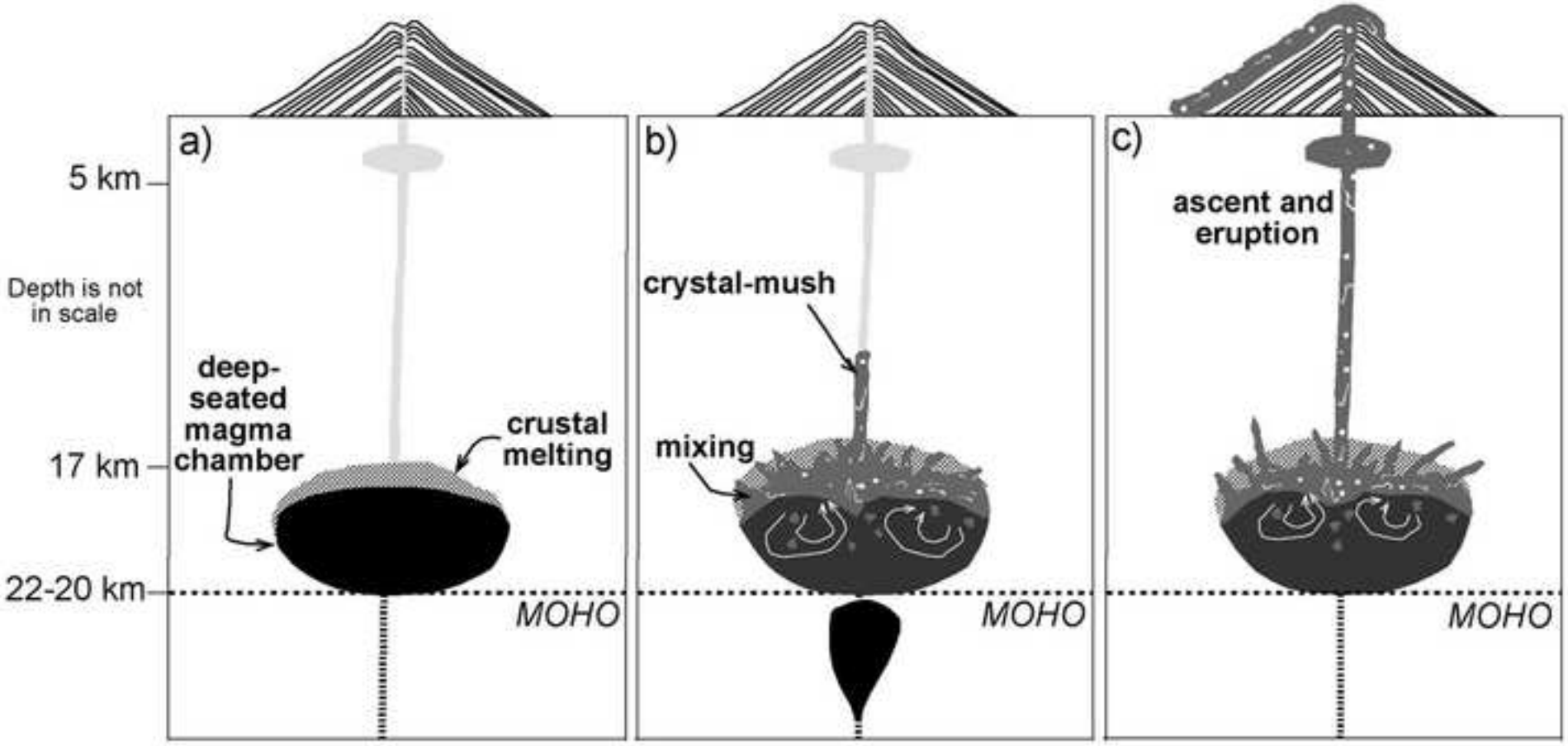

CHAPTER 4

Petrogenesis of the rhyolitic rocks referred to the Eruptive Epochs 7-9 (40 ka-historical times)

4.1 – Introduction

The rhyolitic magmatism at Lipari occurs from 42 ka to historical times, after a 40 ka-long period of quiescence of volcanic activity that follows the end of the mafic to intermediate magmatism on the island (270-80 ka). The eruptive history of Lipari, from 42 ka to historical times, is described by three Eruptive Epochs (7, 8 and 9) that are fully detailed in Chapter 1 (Forni et al., accepted for publication). The renewal of volcanic activity, under the control of the main tectonic trend (NNW-SSE), initially took place in the southern sector of the island (42-21 ka) with the emplacement of endogenous lava domes (P.ta del Perciato, Falcone and M. Giardina formations) and pumiceous pyroclastics (M. Guardia formation) (Eruptive Epoch 7 and 8). During the late phases of Eruptive Epoch 8 (16-8 ka), the volcanic activity controlled by the N-S tectonic trend, progressively moves toward the northeast leading to the emplacement of a series of lava domes cropping out in the eastern sector of the island (P.ta S.Giuseppe, Castello, V.ne Canneto Dentro and Capo Rosso formations). Eruptive Epoch 9 (8 ka-historical times) is characterized by the emplacement of pumiceous pyroclastics and viscous lava coulees, constructing the north-eastern sector of Lipari Island (V.ne del Gabellotto, Pomiciazzo, Forgia Vecchia, Lami and Fossa delle Rocche Rosse formations). The composition of volcanic products ranges from HKCA dacites to rhyolites (Fig.1).

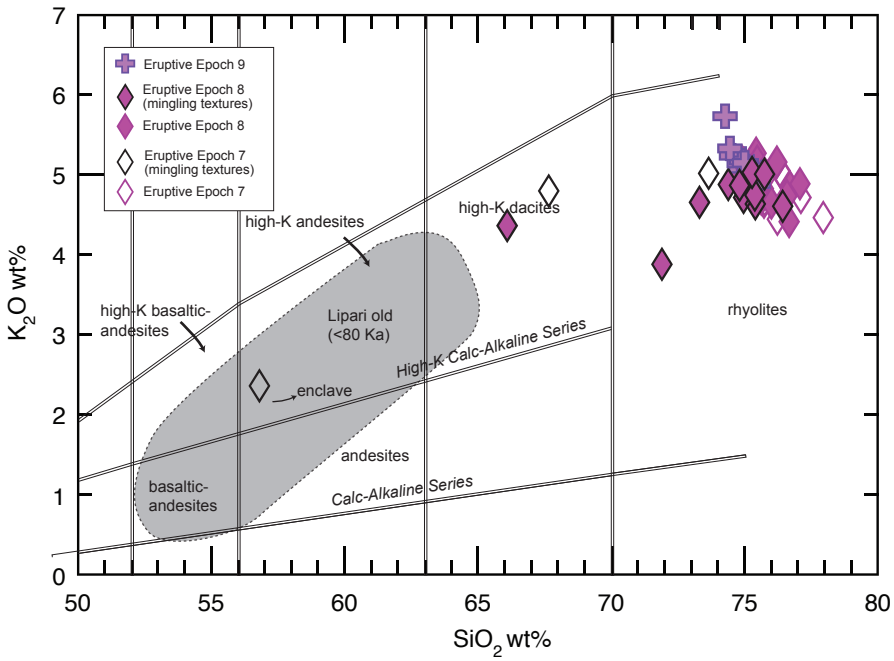

Fig.1 - K_2O vs. SiO_2 classification diagram (Peccerillo & Taylor, 1976) for the rocks from Lipari younger than 40 ka. The compositional field of Lipari mafic to intermediate rocks (270-80 ka) is reported for comparison.

The origin of the sialic melts, the relationships with the mafic rock of Eruptive Epochs 1 to 6, the role of the continental crust and the lack of intermediate compositions in Lipari suite, still represent a matter of debate. A summary of the previous studies carried out by Crisci et al. (1991), Esperanca et al. (1992), De Rosa et al. (2002), Gioncada et al. (2003, 2005) and Davì et al. (2009, 2010), is given in Forni et al. (accepted for publication; cf. Chapter 1). In this Chapter new geochemical, mineral chemistry and isotope data are presented and discussed.

4.2 - Petrographic features

A detailed petrographic description of the rhyolitic rocks of Lipari is reported in Chapter 1 (Forni et al., accepted for publication). In this section a brief summary of the petrographic features with new mineral chemistry data (Tables 2, 3, 4 and 5; cf. Appendix) is presented.

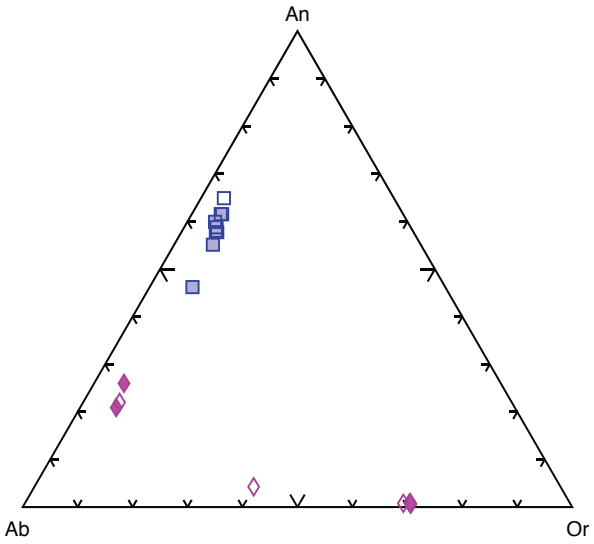

Fig.2 - Composition of feldspars in the rocks of Eruptive Epochs 7 and 8. Full diamonds: cores of phenocrysts in rhyolites; empty diamonds: rims of phenocrysts in rhyolites; full squares: cores of xenocrysts or phenocrysts in the enclaves; emplty squares: rims of xenocrysts or phenocrysts in the enclaves.

Most volcanic products of Eruptive Epochs 7 and 8 (P.ta del Perciato, Falcone and M. Giardina formations) are scarcely porphyritic with less than 5 vol% phenocrysts of K-feldspar, plagioclase (An_{26-22}; Fig.2) and hornblende. Biotite, Ti-magnetite, zircon and apatite are the main accessories (Gioncada et al., 2005).

The pyroclastic rocks of M. Guardia formation (Eruptive Epoch 8) are characterized by white pumices showing the same paragenesis described above for the rhyolitic rocks, and grey pumices, latitic in composition, containing clinopyroxene, plagioclase (An_{76}), minor olivine, Ti- magnetite and apatite (De Rosa et al., 2003). White rhyolitic and dark latite pumices occur both as separated clasts and banded samples, indicating intermingling between felsic and intermediate magmas. The lava domes of P. S.Giuseppe formation (Eruptive Epoch 8) are almost

aphyric, with some phenocrysts of K-feldspar, plagioclase (Fig.2) and Fe-Ti oxides (Fig.4).

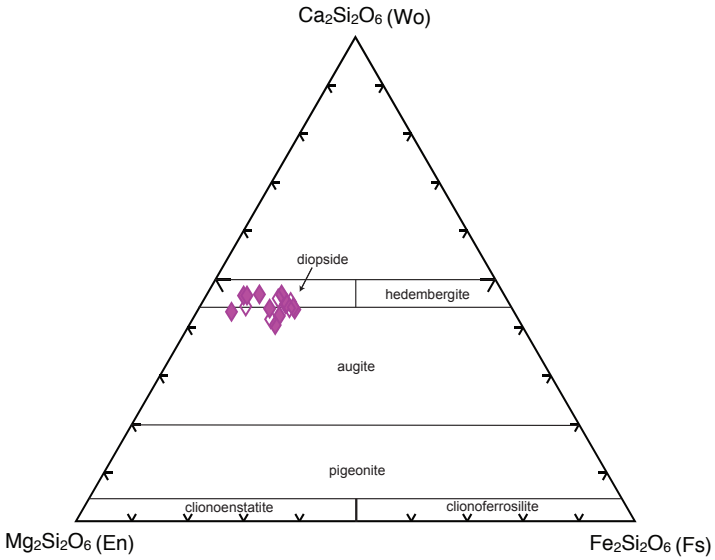

Fig.3 - Composition of clinopyroxenes in the rocks of Eruptive Epochs 7 and 8. Empty diamonds: clinopyroxene in rhyolites; full diamonds: clinopyroxenes from the mafic enclaves.

The pyroclastic rocks and lavas of Eruptive Epoch 8 (Castello, V.ne Canneto Dentro and Capo Rosso formations) and 9 (V.ne del Gabellotto, Pomiciazzo, Pirrera, Serra dell'Arena and Fossa delle Rocche Rosse formations) are aphyric to subaphyric, with eutaxitic texture.

A large amount of mafic enclaves and xenocrysts of clinopyorxene and plagioclase has been detected in the lavas of Falcone formation (fa3 member) and P. S.Giuseppe formation (Fig.5). The mafic enclaves are andesitic (Fig.1) to latitic (Gioncada et al., 2003) in composition and display a highly porphyritic texture (16-28 vol.%) with phenocrysts of plagioclase (An_{65-55}; Fig.2), diopsidic to augitic clinopyroxene (Fig.3), forsteritic olivine and Ti-magnetite (Fig.4).

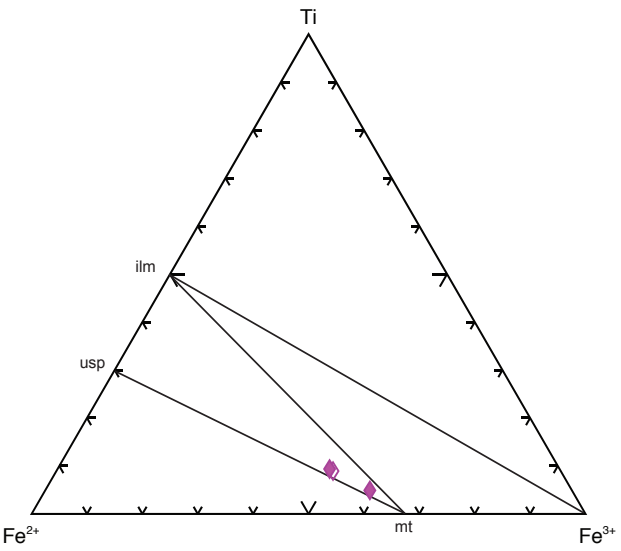

Fig.4 - Composition of Fe-Ti oxides from the rocks of Eruptive Epochs 7 and 8. Empty diamonds: Fe-Ti oxides in rhyolites; full diamonds: Fe-Ti oxides from the mafic enclaves.

Magmatic enclaves have been recently found by Davì et al. (2009) in the Rocche Rosse lava coulee (Fossa delle Rocche Rosse formation; Eruptive Epoch 9). These enclaves have latitic to trachytic composition and contain diopsidic to augitic clinopyroxene, plagioclase (An_{30-18}), sanidine, olivine (Fo_{70-90}), biotite and magnetite. However, no enclaves have been detected in the samples referred to Rocche Rosse formation analyzed in this work.

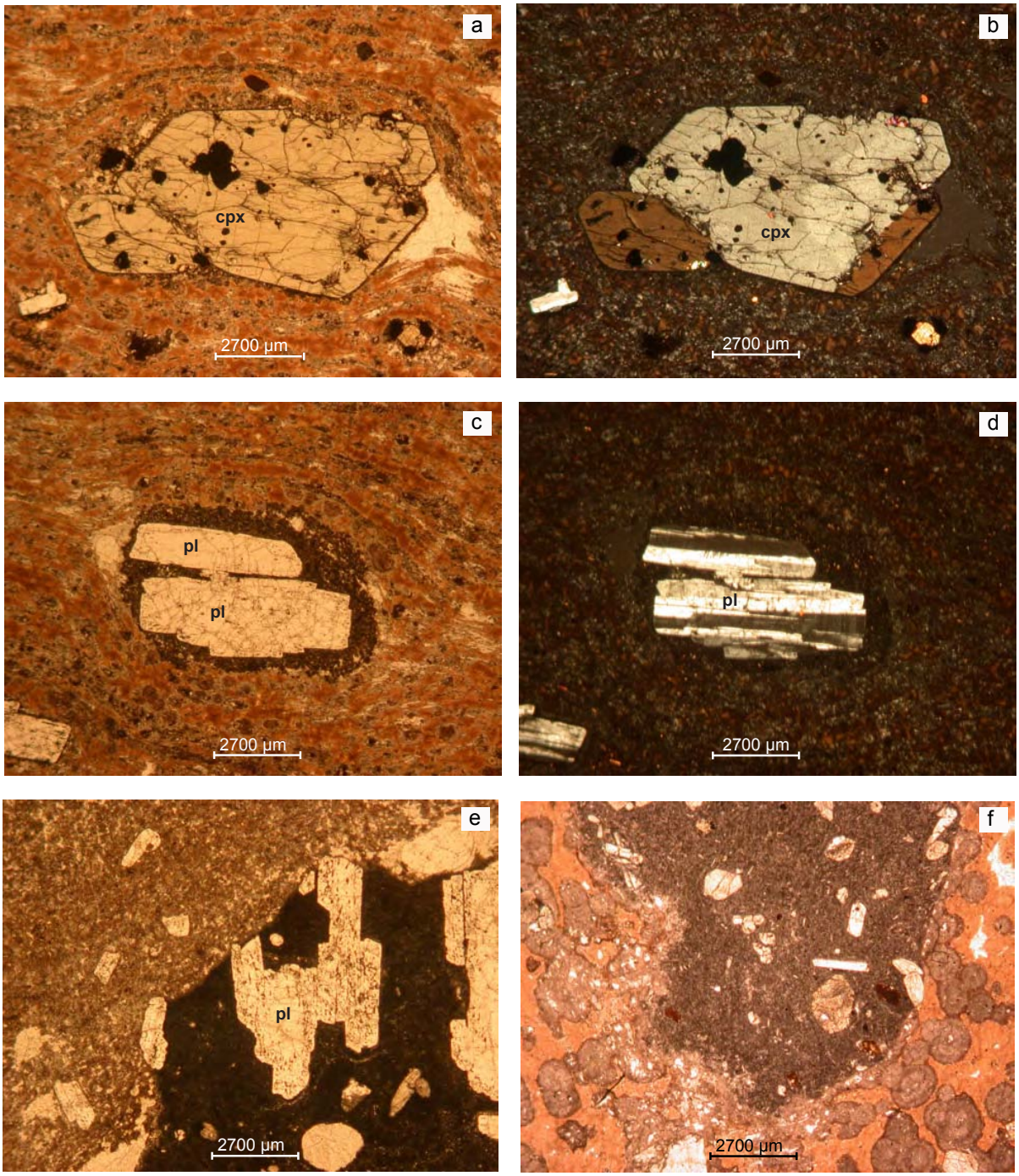

Fig.5 - Examples of mingling textures in the rhyolitic rocks from Lipari: xenocrysts of clinopyroxene (=cpx) (a-b) enbedded within aphiric groundmass; mafic enclave containing plagioclase phenocrysts (=pl) (c-d); Details of contact surfaces between mafic enclaves containing phenocrysts of plagioclase and pyroxene, and the host rhyolitic rock (e-f).

4.3 - Analytical methods

A number of 53 samples, representative of the volcanic products of Eruptive Epochs 7, 8 and 9 (40 ka to historical times), were analyzed for major and trace elements by X-ray fluorescence at Dipartimento di Scienze della Terra (University of Bologna). Data were corrected for matrix effect using the method described by Franzini et al. (1975) and Leoni & Saitta (1976). Loss of ignition (LOI) was determined by heating at 950°C.

A subset of these samples (n=20) was analyzed for trace and rare earth elements (REE), by ICP-AES and ICP-MS at SGS Laboratory (Toronto, Canada). Precision is better than 10% for Cr, 5% for Sc, 1% for V, Co, Ni, Rb, Sr, Zr, Nb, Cs, Ba, La, Ce, Nd, Ta, Hf and Pb and 0.1% for the other trace elements.

Mineral chemistry analyses were performed using a Philips 515b scanning electron microscope (SEM), equipped with Edax dx4 microprobe (EDS) at University of Bologna. Operating conditions were: acceleration voltage 15 kv and beam current 2 nA.

Representative whole-rock samples (n=15) and mafic enclaves (n=2) were selected and prepared for radiogenic isotope analysis. Sr, Nd and Pb isotopic ratios were determined using a multicollector automated Finnigan-MAT 262 mass spectrometer at the U.S. Geological Survey, Reston, VA. Detailed analytical technique for Pb, Nd and Sr are given in Ayuso & Schulz (2003) and Ayuso et al. (2009). Sr and Nd isotope data were reported relative to international standards: La Jolla standard ($^{143}Nd/^{144}Nd$ average value =0.511850±5) and NIST-SRM 987 standard ($^{87}Sr/^{86}Sr$ average value =0.710250±6). Pb isotope ratios were corrected for mass fractionation by 0.08%, 0.12% and 0.16% amu-1 at 2sigma for $^{206}Pb/^{204}Pb$, $^{207}Pb/^{204}Pb$ and $^{208}Pb/^{204}Pb$ respectively, according to replicate measurement of NBS 981.

4.4 - Major and trace elements

Major and trace element data for representative samples from Lipari are reported in Table 1 (cf. Appendix).

The rocks referred to the volcanic activity during Eruptive Epochs 7, 8 and 9, have an almost homogeneous rhyolitic composition (Fig.1). Few samples, showing macroscopic evidences of mingling processes, plot in the HKCA dacitic field and in the rhyolitic field at lower values of SiO_2 wt% (rhyodacites) (Fig.1). The mafic enclave, sampled from the lavas of Falcone formation (fa3 member; Eruptive Epoch 7), displays a HKCA andesitic composition, thus plotting in the field of the old rocks from Lipari (<80 Ka, Eruptive Epochs 1-6) (Fig.1).

A selection of major and trace elements vs. SiO_2 variation diagrams is reported in Figs.6 and 7. Among major elements, MgO, Al_2O_3, TiO_2 (Fig.6 a-b-c), Fe_2O_3 and CaO (not shown), generally show negative correlations with SiO_2 with small variations in the rhyolitic terms. K_2O and Na_2O (Fig.6 a), instead, display larger variations among the rhyolites and are enriched in the volcanic rocks of Eruptive Epoch 9.

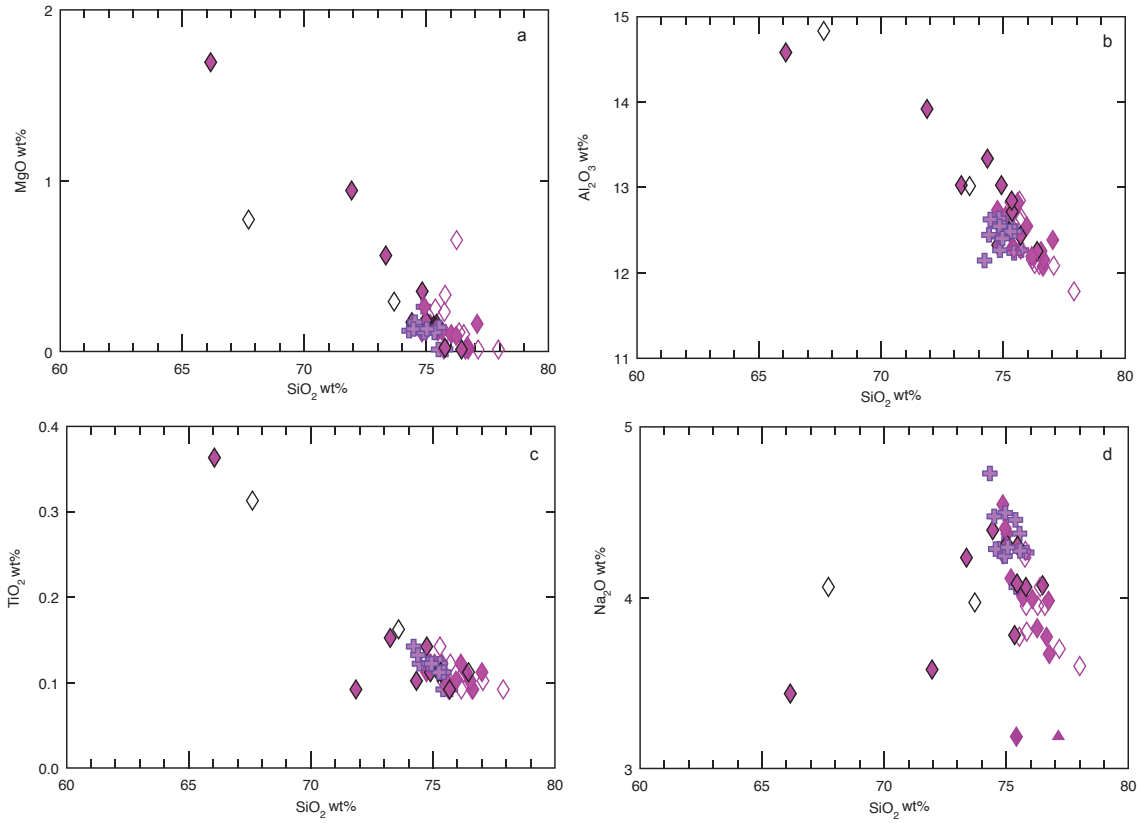

Fig.6 - Variation diagrams of major elements vs. SiO_2 for Lipari rocks younger than 40 ka. Symbols as in Fig.1.

Among trace elements, Rb and Nb increase from HKCA dacites to rhyolites (Fig.7 b-c), while Sr (Fig.7 a) and Ba (not shown) decrease, but they do not display significant variations in the rhyolitic rocks. On the contrary, La and Th show steep trends in the rhyolites, leading to a general enrichment of these elements with time from Eruptive Epochs 7 to 9 (Fig.7 e-f). Zr describes a curvilinear trend typical of fractional crystallization processes involving zircon, which is diffusely present as accessory phase in the rhyolites (Fig.7 d). The contents of ferromagnesian trace elements (Cr, Ni, Co, V) in these samples are mostly below detection limits.

The spider diagram of the Rare Earth Elements (REE) normalized to chondrites (Sun & McDonaugh, 1989) displays a moderate fractionation between HREE and LREE and a marked Eu negative anomaly (less pronounced in the mingled samples; Fig.8). The enrichment in REE generally increases from Eruptive Epochs 7 and 8 to Eruptive Epoch 9.

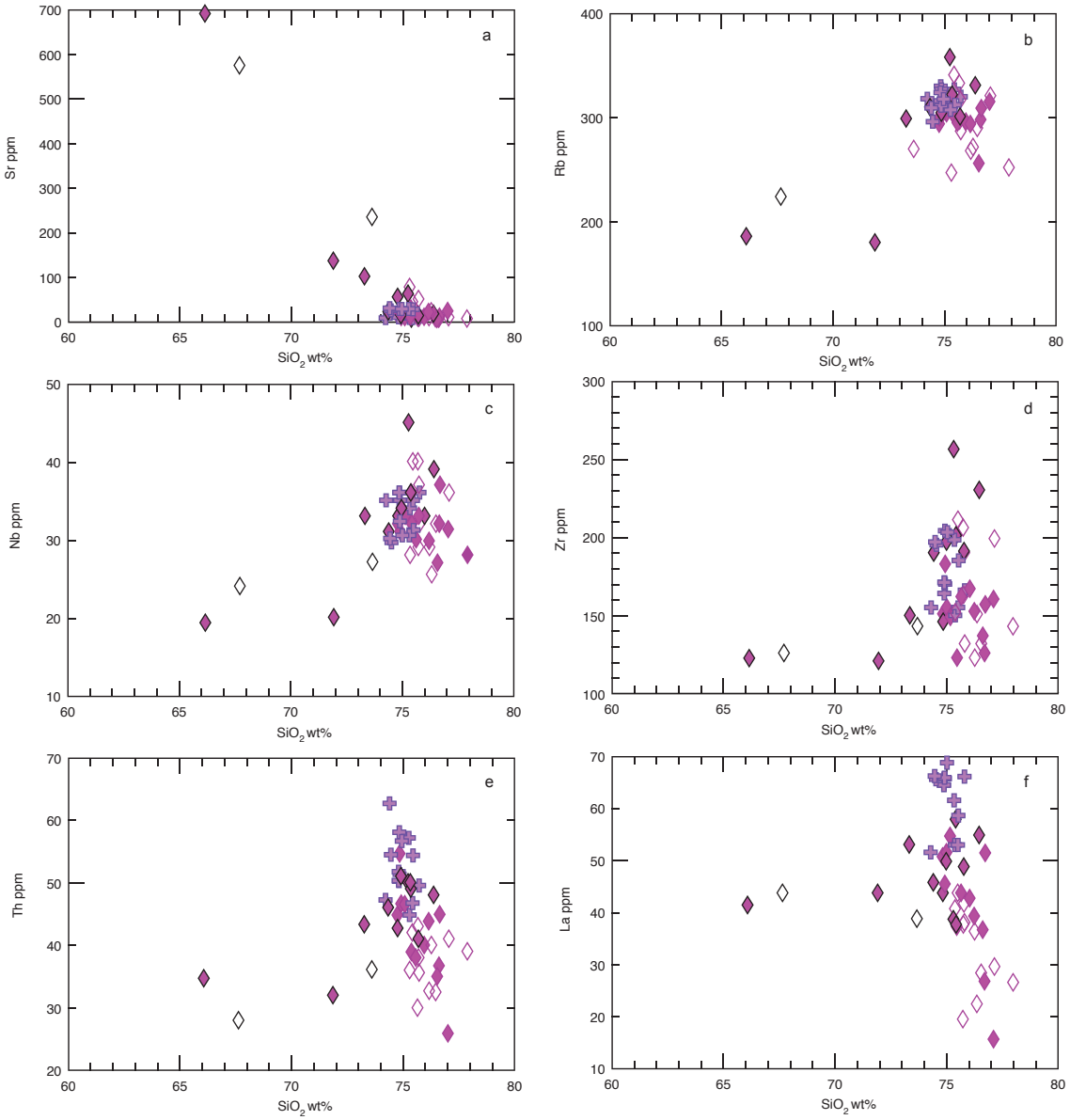

Fig.7 - Variation diagrams of trace elements vs. SiO_2 for Lipari rocks younger than 40 ka. Symbols as in Fig.1.

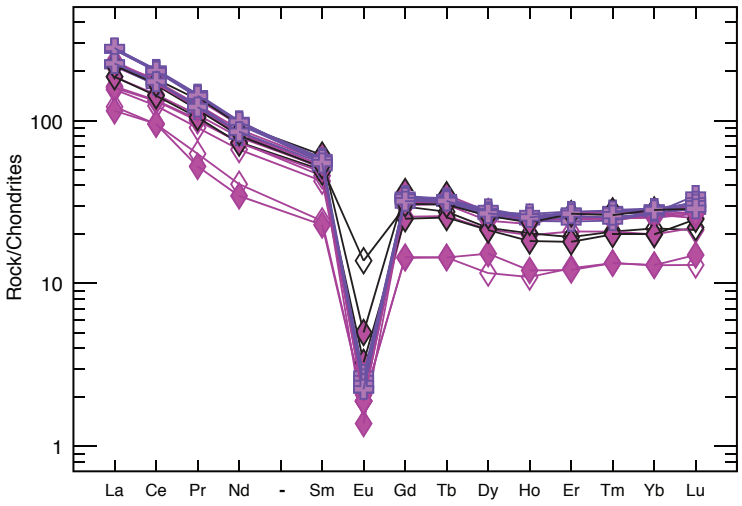

Fig.8 - REE patterns normalized to chondrite values (Sun & Mc Donough, 1989) for the rocks from Lipari younger than 40 ka. Symbols as in Fig.1.

4.5 - Sr, Nd and Pb isotopes

Sr, Nd and Pb isotope data for Lipari samples, referred to Eruptive Epochs 7, 8 and 9, are reported in Table 1 (cf. Appendix).

The samples mostly plot within the range of Sr and Nd isotopic compositions described by the magmatic rocks relative to the oldest activity of Lipari (<40 Ka), but show lower ranges of Nd and higher ranges of Sr isotope ratios ($^{144}Nd/^{143}Nd$ =0.512292-0.512634; $^{87}Sr/^{86}Sr$ =0.705005-0.707538) (Fig.9). Notably, distinct groups of samples showing the same $^{144}Nd/^{143}Nd$ ratios and increasing values of $^{87}Sr/^{86}Sr$ ratios may be recognized (Fig.9). The mingled samples and the mafic enclaves display the lowest values of $^{87}Sr/^{86}Sr$ in each group.

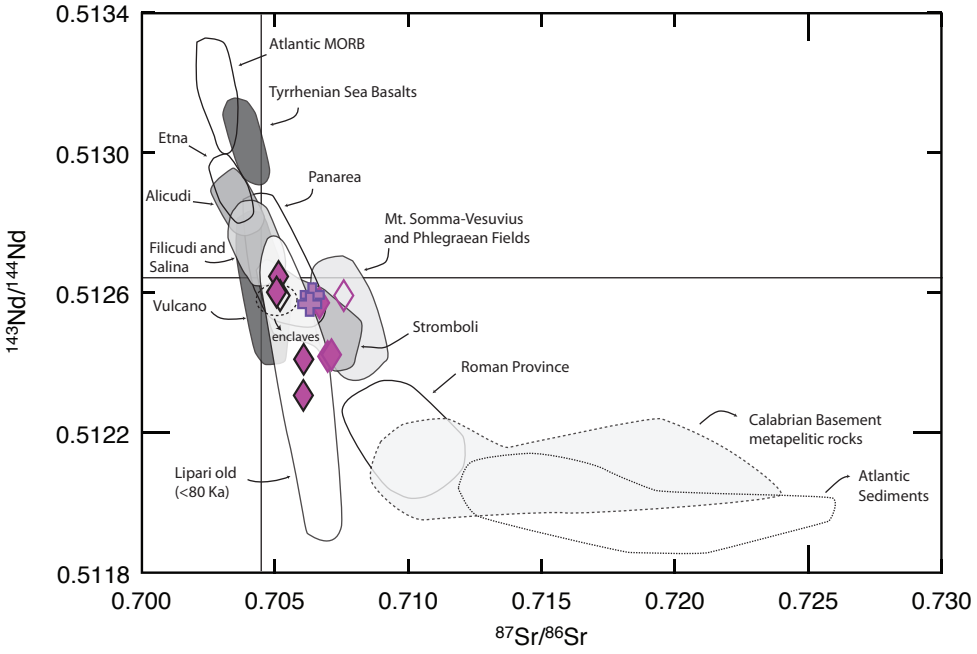

Fig.9 - Nd vs. Sr isotope variations for the rocks from Lipari younger than 40 ka. Symbols as in Fig.1. Compositional fields of the mafic to intermediate rocks from Lipari (cf. Chapter 2), Calabrian basement rocks (Caggianelli et al., 1991), Alicudi (Peccerillo & Wu, 1992; Peccerillo et al., 1993; Peccerillo et al. 2004), Filicudi (Santo et al., 2004), Salina (Ellam et al., 1989; Francalanci et al., 1993;Gertisser & Keller, 2000), Panarea (Calanchi et al., 2002), Vulcano (De Astis et al., 1997, 2000; Gioncada et al., 2003), Stromboli (Ellam et al., 1989; Francalanci et al., 1993) , Atlantic Sediments (Plank & Langmuir,1998), Roman Province (Hawkesworth & Vollmer, 1979; Rogers et al., 1985; D'Antonio et al., 1996; Conticelli et al., 1997; Di Battistini et al., 2001; Gasperini et al., 2002; Perini et al., 2004), Mt. Somma-Vesuvius and Phlegraean Fields (Hawkesworth & Vollmer, 1979; Civetta et al., 1991; Ayuso et al., 1998; D'Antonio et al., 1999; Pappalardo et al., 2002) , Tyrrhenian Sea Basalts ODP site (Beccaluva et al., 1990) Atlantic MORB (Cohen et al., 1980; Ito et al., 1987) and Etna (Tonarini et al., 1995; D'Orazio, 1997; Armienti et al., 2004) are reported for comparison.

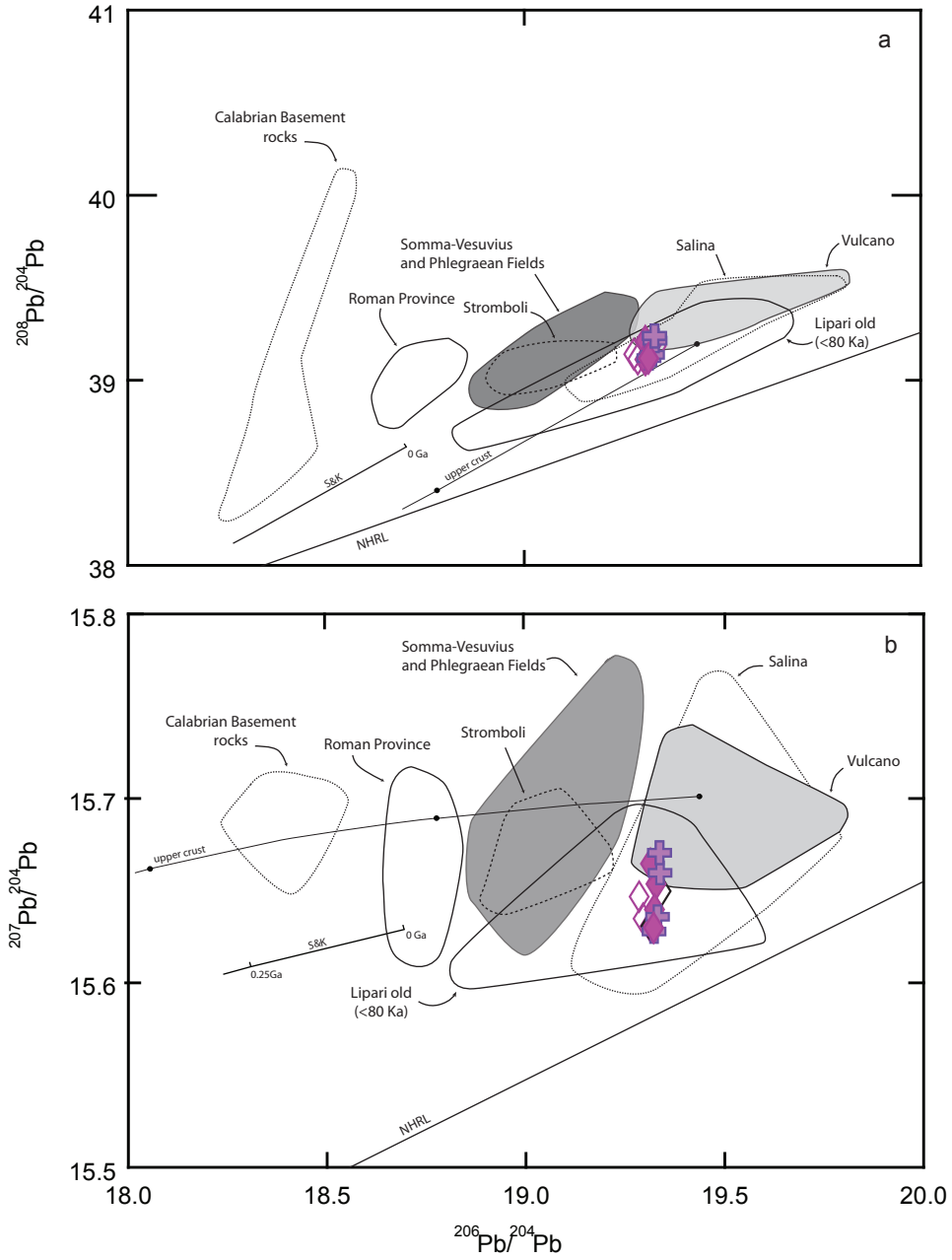

Fig.10 - Pb isotope variations for the rocks of Lipari younger than 40 ka. Symbols as in Fig.1. Compositional fields of Lipari mafic to intermediate rocks (270-81 ka; cf. Chapter 2), Calabrian Basement rocks (Caggianelli et al., 1991), Alicudi (Peccerillo & Wu, 1992; Peccerillo et al., 1993; Peccerillo et al. 2004), Filicudi (Santo et al., 2004), Salina (Ellam et al., 1989; Francalanci et al., 1993;Gertisser & Keller, 2000), Panarea (Calanchi et al., 2002), Vulcano (De Astis et al., 1997, 2000; Gioncada et al., 2003), Stromboli (Ellam et al., 1989; Francalanci et al., 1993), Roman Province (Hawkesworth & Vollmer, 1979; D'Antonio et al., 1996; Conticelli et al., 1997; Di Battistini et al., 2001; Gasperini et al., 2002; Perini et al., 2004), Somma-Vesuvius and Phlegraean Fields (Civetta et al., 1991; Ayuso et al., 1998; D'Antonio et al., 1999; Pappalardo et al., 2002) are reported for comparison. Northern Hemispher Reference Line (NHRL) from Hart (1984). Pb isotope evolution curve for the upper crust from Zartman & Haines (1988). Model growth for the average crust from Stacey & Kramers (1975; S&K).

Pb isotope ratios display very small ranges of variation and plot within the field of Lipari oldest rocks (Fig.10). In particular, $^{206}Pb/^{204}Pb$ and $^{208}Pb/^{204}Pb$ ratios range from 19.277 to 19.333, and from 39.101 to 39.229 respectively, while $^{207}Pb/^{204}Pb$ ratios show the widest range of variation (15.627-15.670).

4.6 - Discussions

4.6.1 - Petrogenetic modelling

In most major and incompatible trace elements variation diagrams the rhyodacitic and rhyolitic rocks of Eruptive Epochs 7, 8 and 9 and the mafic to intermediate rocks of Eruptive Epochs 1 to 6 describe continuous linear trends (cf. Chapter 1, Figs.17, 18).

Inter-elemental plots display both continuous linear trends (e.g. La vs. Ce; Nd vs. Sm, not shown) and distinct parallel trends, in which the younger rocks are shifted towards higher contents of incompatible trace elements ("step-like" trend) (e.g. Rb vs. Zr cf. Chapter 1, Fig.19 a). Moreover, the rocks of Eruptive Epochs 1-6 display wider variations of trace element ratios (e.g. Zr/Nb, Ba/Rb, La/Th) with respect to the rocks of Eruptive Epochs 7-9, which appear almost homogeneous (Fig.11). Conversely, the isotope data do not outline such a clear subdivision (Figs.9, 10).

As a whole, geochemical and isotopic data suggest a possible derivation of the silicic liquids from the mafic melts through fractional crystallization, as already hypothesized in Gioncada et al. (2003). Therefore assimilation and fractional crystallization (AFC; De Paolo, 1981) modeling has been tested. AFC models carried out using incompatible trace element ratios and isotopic ratios are reported in Fig.12. In these models the sample A1 (CA basaltic andesite of Eruptive Epoch 2) has been used as parent (Co), whereas two different compositions of the Calabrian Basement rocks have been used as assimilants (Ca). Geochemical and isotopic compositions of the Calabrain Basement rocks (Caggianelli et al., 1991) and of the mafic to intermediate rocks from Lipari (Eruptive Epochs 1-6; cf. Chapter 2) have been indicated in the plots (Fig.12). Moreover two different rates of assimilation vs. fractional crystallization (r=0.2 and r=0.3) have been tested. Relatively low rates of assimilation vs. fractional crystallization are suggested by the small differences of isotopic variations observed between the mafic and the sialic rocks of Lipari. Partition coefficients have been estimated based on the different behaviour of trace elements in the variation diagrams (Fig.7) and compared to the ones reported in literature for sialic rocks (Rollingson, 1993). For example the compatible behaviour of Sr strongly suggests that plagioclase played a fundamental role as fractionating phase in the evolutionary processes (Fig.7). Zr/Nb and Ba/La vs.

$^{87}Sr/^{86}Sr$ AFC models (Figs.12 a, 13 a) show that it is possible to obtain rhyolitic melts with relatively high $^{87}Sr/^{86}Sr$ and low Zr/Nb and Ba/La starting from a liquid, which is compositionally similar to Lipari oldest products (CA basaltic andesites: Eruptive Epoch 2). The same results have been obtained with least-square major element calculations (Table 8, cf. Appendix), through fractionation of plagioclase, pyroxenes and minor Ti-magnatite and apatite. The $^{87}Sr/^{86}Sr$ vs. $^{143}Nd/^{144}Nd$ model (Fig.14 a) evidences that high $^{87}Sr/^{86}Sr$ rhyolitic compositions, with slightly different $^{143}Nd/^{144}Nd$ ratios, may be obtained both through AFC processes, starting from the same mafic composition, and through mixing with a crustal melt (Fig.14 a).

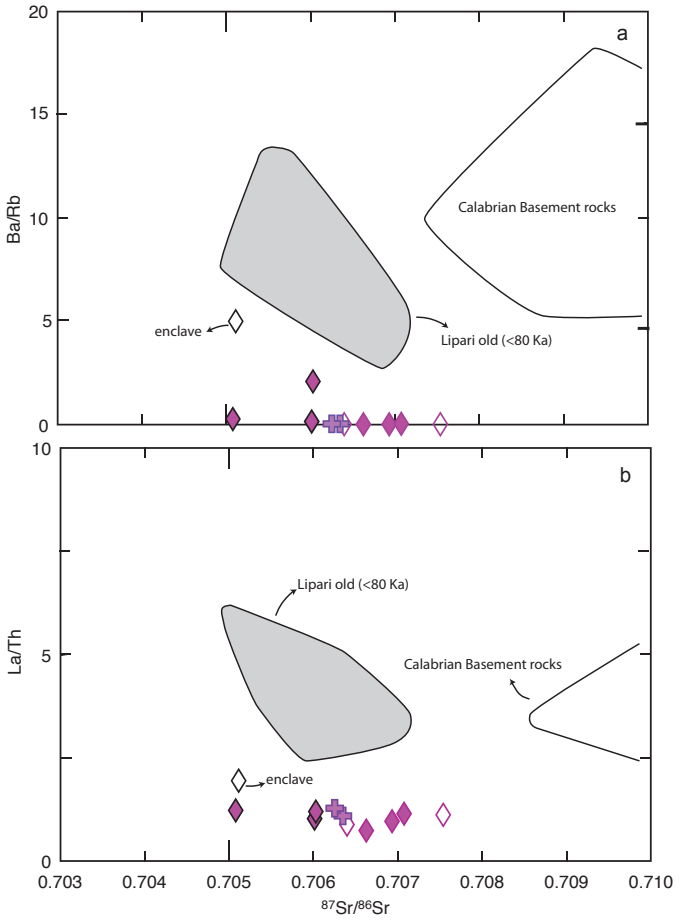

Fig.11 - Plots of trace element ratios vs. Sr isotope ratio for Lipari rocks younger than 40 ka. Symbols as in Fig.1. Compositional fields of mafic to intermediate rocks of Lipari (270-80 ka; cf. Chapter 2) and Calabrian Basement rocks (Caggianelli et al., 1991) are reported for comparison.

The sialic melts obtained through AFC and/or mixing processes, display the highest values of $^{87}Sr/^{86}Sr$ ratios (Fig.14 a) and do not show mixing/mingling textures, therefore they might be considered “pure” rhyolitic terms.

On the contrary, clear evidences of mixing/mingling textures have been widely observed in the rhyolitic rocks of Falcone (f3 member; Eruptive Epoch 7), P.ta S.Giuseppe and M.te Guardia formations (Eruptive Epoch 8) (Fig.5) and recently in the

rhyolitic lavas of Fossa delle Rocche Rosse formation (Eruptive Epoch 9) by Davì et al. (2009). Therefore these rocks may likely represent the product of mixing processes (back-mixing) between the “pure” rhyolitic terms and fresh mafic melts, compositionally similar to the enclave and to the oldest rocks of Lipari (< 80Ka). Mixing models, carried out using trace element and isotope ratios, are shown in Figs.12b, 13b and 14b.

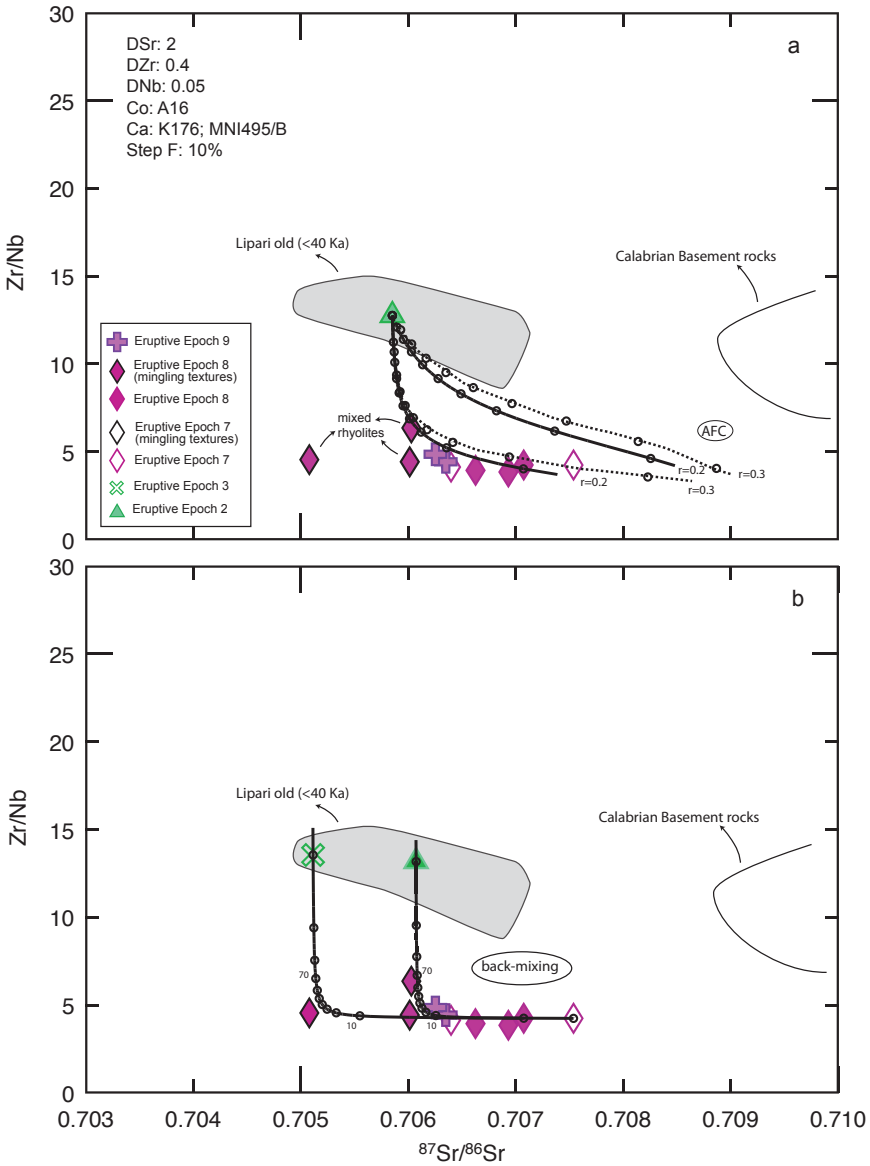

Fig.12 - AFC (a) and back-mixing (b) models for the rocks of Lipari younger than 40 ka. Compositional fields of the mafic to intermediate rocks of Lipari (270-80 ka; cf. Chapter 2) and Calabrian Basement rocks (Caggianelli et al., 1991) are reported for comparison.

The “pure” rhyolitic samples that show the highest $^{87}Sr/^{86}Sr$ ratios and plot at different $^{143}Nd/^{144}Nd$ (Lip97 and Lip259, referred to Eruptive Epochs 7 and 8 respectively) have been used as rhyolitic end-members. These samples are representative of the lava domes of P.ta del Perciato and Vallone Canneto Dentro formations, whose emplacement corresponds respectively to the first episode of volcanic activity on Lipari and to the beginning of the northward shifting of the rhyolic magmatism on the island.

Two CA basaltic-andesitic samples relative to the oldest activity of Lipari (Eruptive Epochs 2 and 3) have been used as mafic end-members in the mixing models.

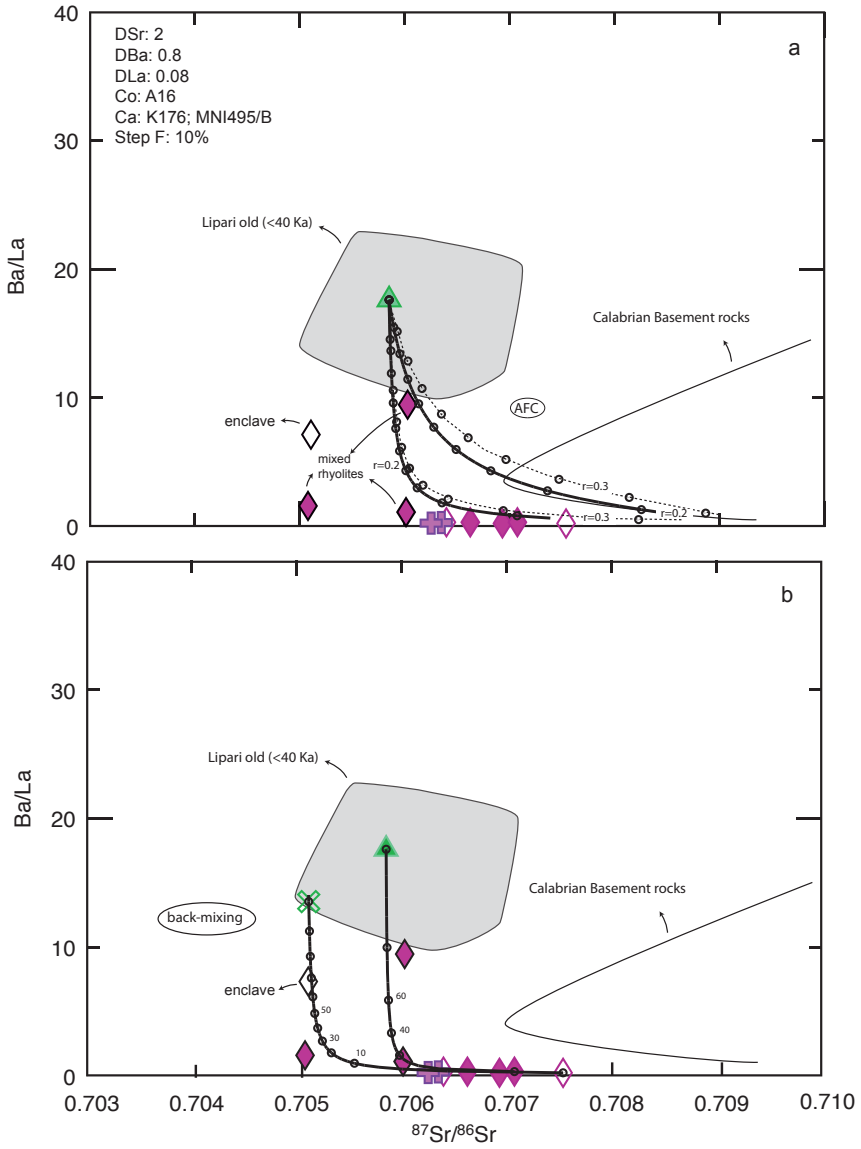

Fig.13 - AFC (a) and back-mixing (a) models for the rocks of Lipari younger than 40 ka. Symbols as in Fig.12. Compositional fields of the mafic to intermediate rocks of Lipari (270-80 ka; cf. Chapter 2) and Calabrian Basement rocks (Caggianelli et al., 1991) are reported for comparison.

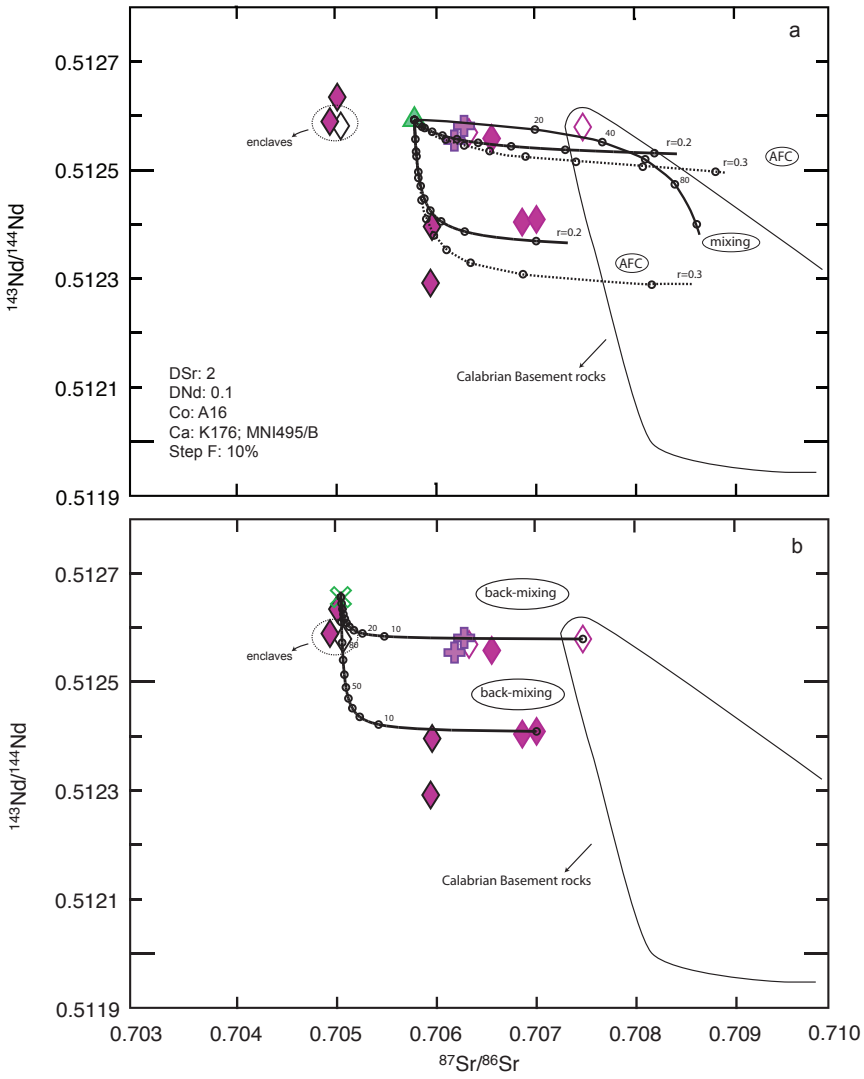

Fig.14 - AFC (a) and back-mixing (b) models for the rocks of Lipari younger than 40 ka. Symbols as in Fig.12. Compositional fields of the mafic to intermediate rocks of Lipari (270-80 ka; cf. Chapter 2) and Calabrian Basement rocks (Caggianelli et al., 1991) are reported for comparison.

All the mingled samples and the enclaves fit the mixing lines, except for sample Lip301 in the $^{87}Sr/^{86}Sr$ vs. $^{143}Nd/^{144}Nd$ model, which plots at lower $^{143}Nd/^{144}Nd$ ratio (=0.512292) (Fig.14). Nevertheless, as already shown in the previous models, “pure” rhyolitic compositions showing different $^{143}Nd/^{144}Nd$ ratios may derive from mafic melts through AFC processes (Fig.12 a, 13 a, 14 a). Therefore, the presence of another “pure” rhyolitic melt (with $^{143}Nd/^{144}Nd$ ratio similar to sample Lip301) in the system is very likely. This rhyolitic melt may have then mixed with the mafic end-members, giving the hybrid composition of sample Lip301.

4.6.2. The role of low-pressure evolutionary processes

Geochemical modeling based on trace element and isotope ratios suggests that the rhyolitic rocks of Eruptive Epochs 7 to 9 derive from mafic melts though AFC processes with relatively low rates of assimilation vs. fractional crystallization (r=0.2-0.3). The compositions of the mafic parents might be similar to the ones of the rocks related to Lipari oldest activity (Eruptive Epochs 1-6). Mixing processes involving mafic and crustal melts have been also suggested, but they are not supported by trace elements vs. $^{87}Sr/^{86}Sr$ models, therefore they might be considered less effective.

One of the most important petrogenetic problem linked to the genesis of the rhyolitic magmas at Lipari is the absence of intermediate compositions (dacites), which should likely generate during the differentiation processes from basaltic andesites to rhyolites. However, the mafic to intermerdiate volcanic activity at Lipari was followed by a 40 ka-long period of dormancy, which started soon after the eruption of the cordierite-bearing lavas (Eruptive Epoch 5; 105 ka) and the HKCA andesitic lavas of M. S.Angelo and M. Chirica volcanoes (Eruptive Epoch 6; 92-81 ka). Following Di Martino et al. (accepted for publication; cf. Chapter 3), the occurrence at mid-crustal levels of the silicic anatectic melts involved in the genesis of the cordierite-bearing lavas, might have acted as a density barrier, preventing the ascent of mafic magmas to the surface during the 40-ka long period of quiescence of the volcanic activity. The proposed scenario is consistent with the time required for the generation of silicic magmas though AFC processes (104-105 years; Reagan et al., 2003). Moreover it well explains the lack of volcanic products with intermediate compositions (dacitic) in the stratigraphic record of Lipari. The reactivation of volcanic activity probably occurred when slightly evolved magmas were able to bypass the density barrier and migrated towards shallow level reservoirs (<10 Km; De Rosa et al., 1993). This hypothesis may likely represent a key interpretation to understand the still controversial genesis of the rhyolitic melts and their relationships with the previous volcanic activity at Lipari, therefore it hints at further investigations.

Notably, the rhyolitc melts obtained though AFC processes (“pure” rhyolites) are characterized by non-homogenous trace element (i.e. Th and La) and isotopic compositions (i.e. $^{87}Sr/^{86}Sr$ and $^{143}Nd/^{144}Nd$). This might be traced back to the occurrence of distinct batches of rhyolitc magmas, deriving from different mafic parents, variably interacting with the crustal rocks during fractionation, as suggested by Gioncada et al. (2003). This hypothesis is consistent with the stratigraphic reconstructions, which indicate the occurrence at Lipari of different pulses of volcanic activity from 42 ka to historical times.

Moreover, petrographic observations (i.e. the presence of mingling textures such as

banded pumices, mafic enclaves and xenocrysts) evidence that interactions of the rhyolitic magmas with new batches of fresh mafic magmas (back-mixing) have clearly occurred. The analyzed mafic enclave displays a HKCA andesitic composition thus resembling the mafic rocks referred to Lipari oldest activity. However, in some inter-elemental plots (e.g. Rb vs. Zr) the dacitic and rhyolitic products and the mafic to intermediate rocks of Lipari describe two distinct linear trends (Fig.19 a, cf. Chapter 1). This is not compatible with magma mixing processes that would generate single linear correlations in the element-element plots (Langmuir et al., 1978). Detailed chemical analyses on rock samples affected by mixing processes (Perugini & Poli, 2004; Perugini et al., 2006) demonstrate that trace elements with similar values of diffusion coefficients (e.g. La and Ce; Nd and Sm) display good correlations in inter-elemental plots. On the contrary, as the difference between diffusion coefficients increases the correlation is progressively lost, producing scattered trends and sometimes “step-like” variations, which closely resemble those described by the rocks from Lipari (e.g. Rb vs. Zr; cf. Chapter 1, Fig.19 a).

Besides, mafic enclaves showing more potassic compositions (trachitic and latititc), akin to the mafic rocks of Vulcano, have been also reported in literature by De Rosa et al. (2003), Gioncada et al. (2003) and Davì et al. (2009, 2010). Therefore, it is very likely that different batches of mafic magmas have interacted with the silicic magmas. Following Davì et al. (2009), multiple injections of mafic magmas in the shallow reservoir might have triggered the eruptions of the different rhyolites.

References

Ayuso R.A., De Vivo B., Rolandi G., Seal II R.R. & Paone A. 1998. Geochemical and isotopic (Nd-Pb-Sr-O) variations bearing on the genesis of volcanic rocks from Vesuvius, Italy. J. Volcanol. Geotherm. Res., 82, 53-78.

Ayuso R.A. & Schulz K.J. 2003. Nd, Pb, Sr isotope geochemistry and origin of the Ordovician Bald Mountain and Mount Chase massive sulfide deposits, northern Maine. In: Goodfellow W.D., McCutcheon S.R., Peter J.M. (Eds.), Volcanogenic Massive Sulfide deposits of the Bathurst District and Northern Maine. Economic Geology Monograph, 11, 611-630.

Ayuso R.A., Haeussler P.J., Bradley D.C., Farris D.W., Foley N.K. & Wandless G.A. 2009. The role of the ridge subduction in determining the geochemistry and Nd, Sr, Pb isotopic evolution of the Kodiak batholith in Southern Alaska. Tectonophysics, 464, 137-163.

Armienti P., Tonarini S., D'Orazio M. & Innocenti F. 2004. Genesis and evolution of Mt. Etna alkaline lavas: petrological and Sr-Nd-B isotope constraints. Per Mineral., 73, 29-52.

Beccaluva L., Bonatti E., Dupuy C., Ferrara G., Innocenti F., Lucchini F., Macera P., Petrini R., Rossi P.L., Serri G., Seyler M. & Siena F. 1990. Geochemistry and mineralogy of the volcanic rocks from ODP sites 650, 651, 655 and 654 in the Tyrrhenian Sea. In: Kastens K.A., Mascle J. et al. (Eds.). Proc. Ocean Drilling Program, Scientific Results, 107, 49-74.

Calanchi N., Peccerillo A., Tranne C.A., Lucchini F., Rossi P.M., Kempton P.D., Barbieri M. & Wu T.W. 2002. Petrology and geochemistry of the Island of Panarea: implications for mantle evolution beneath the Aeolian island arc (Southern Tyrrhenian Sea, Italy). J. Volcanol. Geotherm. Res., 115, 367-395

Caggianelli A., Del Moro A., Paglionico A., Piccarreta G., Pinarelli L. & Rottura A. 1991. Lower crustal granite genesis connected with chemical fractionation in the continental

crust of Calabria (Southern Italy). European Journal of Mineralogy, 3, 159-180.

Cohen R.S., Evensen M.S., Hamilton P.J. & O'Nions R.K. 1980. U-Pb, Sm-Nd and Rb-Sr systematic sod mid-ocean ridge basalts glasses. Nature, 283, 149-153.

Civetta L., Carluccio E., Innocenti F., Sbrana A. & Taddeucci G. 1991. Magma chamber evolution under Phlegraean Field during the last 10 ka: trace element and isotope

data. Eur. J. Mineral., 3 , 415-428.

Conticelli S., Francalanci L., Manetti P., Cioni R. & Sbrana A. 1997. Petrology and geochemistry of the ultrapotassic rocks from the Sabatini volcanic district, central Italy: the role of evolutionary processes in the genesis of variably enriched alkaline magmas. J. Volcanol. Geotherm. Res., 75, 107-136.

Crisci G.M., De Rosa R., Esperanca S., Mazzuoli R. & Sonnino M. 1991. Temporal

evolution of three component system: the island of Lipari (Aeolian Arc, southern Italy). Bull. Volcanol., 53, 207-221.

D'Antonio M., Civetta L. & Di Girolamo P. 1999. Mantle source heterogeneity in the Campanian Region (south Italy) as inferred from geochemical and isotopic features of mafic volcanic rocks with shoshonitic affinity. Mineral. Petrol., 67, 163-192.

D'Antonio M., Tilton G.R. & Civetta L. 1996. Petrogenesis of Italian alkaline lavas deduced from Pb-Sr-Nd isotope relationships. In: Basu A. & Hart S.R. (Eds.) Isotopic Studies of Crust-Mantle Evolution. Am. Geophys. Un. Mon., 95, 253-267.

Davì M., De Rosa R. & Barca D. 2009. A LA-ICP-MS study of minerals in the Rocche Rosse magmatic enclaves: Evidence of a ma!c input triggering the latest silicic eruption of Lipari Island (Aeolian Arc, Italy). Journal of Volcanology and Geothermal Research, 182, 45–56.

Davì M., De Rosa R. & Holtz F. 2010. Mafic enclaves in the rhyolitic products of Lipari historical eruptions; relationships with the coeval Vulcano magmas (Aeolian Islands, Italy). Bull Volcanology, DOI 10.1007/s00445-010-0376-5.

De Astis G., La Volpe L., Peccerillo A. & Civetta L. 1997. Volcanologic and petrological evolution of Vulcano Island (Aeolian Arc, Southern Tyrrhenian Sea). J. Geophisical Res., 102, 8021-8050.

De Astis G., Peccerillo A., Kempton P.D., La Volpe L. & Wu T.W. 2000. Transition from calcalkaline to potassium-rich magmatism in subduction environments: geochemical and Sr, Nd, Pb isotopic constraints from the Island of Vulcano (Aeolian arc). Contributions of Mineralogy and Petrology, 139, 684-703.

D'Orazio M., Tonarini S., Innocenti F. & Pompilio M. 1997. Northern Valle del Bove volcanic succession (Mt. Etna, Siciliy): petrography, geochemistry and Sr-Nd isotope data. Acta Vulcanol., 9, 73-86.

De Rosa R., Donato P., Gioncada A., Masetti M. & Santacroce R. 2003. The Monte Guardia eruption (Lipari, Aeolian Islands): an example of a reversely zoned magma mixing sequence. Bulletin of Volcanology, 65, 530-543.

De Paolo D.J. 1981. Trace element and isotopic effects of combined wallrock assimilation and fractional crystallization. Earth Planet. Sci. Lett., 53, 189-202.

Di Battistini G., Montanini A., Vernia L., Venturelli G. & Tonarini S. 2001. Petrology of melilite-bearing rocks from the Montefiascone volcanic complex (Roman Magmatic Province): new insights into the ultrapotassic volcanism of Central Italy. Lithos, 59, 1-24.

Di Martino C., Frezzotti M.L., Palmeri R., Lucchi F., Peccerillo A., Tranne C.A. & Diamond L.W. 2010. Magma storage and ascent at Lipari Island (Aeolian archipelago, Southern Italy) at 223–81 ka: the role of crustal processes and tectonic influence. Bull. of Volcanology, DOI 10.1007/s00445-010-0383-6.

Ellam R.M., Hawkeswort C.J., Menzies M.A & Rogers N.W.1989. The volcanism of Southern Italy: role of subducion and the relationships between potassic and sodic alkaline magmatism. Journal of Geophysical Research, 94, 4589-4601.

Esperanca S., Crisci G.M:, De Rosa R. & Mazzuoli R. 1992. The role of the crust in the magmatic evolution of the island of Lipari (Aeolian Islands, Italy). Contr. Mineral. Petrol., 112, 450-462.

Forni F., Lucchi F., Peccerillo A., Tranne C.A., Rossi P.L., Di Martino C., Frezzotti M.L. & Ayuso R.A. Lipari. In: Lucchi, F., Peccerillo A., Keller J., Tranne C.A. & Rossi P.L. (Eds.), Geology of the Aeolian Islands (Italy). Geological Society of London, accepted for publication.

Francalanci L., Tayolor S.R., McCulloch M.T. & Woodhead J.D. 1993. Geochemical and isotopic variations in the calc-alkaline rocks of Aeolian arc, southern Tyrrhenian Sea, Italy: constraints on magma genesis. Contributions of Mineralogy and Petrology, 113, 300-313.

Franzini M., Leoni L. & Saitta M., 1975. Revisione di una metodologia analitica per la fluorescenza-X, basata sulla correzione completa degli effetti di matrice. Rend. Soc. Ital. Mineral. Petrol. 31, 2, 36-378.

Gasperini D., Blichert-Toft J., Bosch D., Del Moro A., Macera P. & Albarede F. 2002 Upwelling of deep mantle material through a plate window: evidence from

the geochemisty of Italian basaltic volcanics. J. Geophys. Res. 107(B12), 2367, DOI10.1029/2001JB000418.

Gertisser R. & Keller J. 2000. From basalt to dacite: origin and evolution of the calcalkaline series of Salina, Aeolain Arc, Itlay. Contrib. Mineral. Petrol., 139, 607-626.

Gioncada A., Mazzuoli R., Bisson M. & Pareschi M.T. 2003. Petrology of volcanic products younger than 42 ka on the Lipari-Vulcano complex (Aeolian Island, Italy): an example of volcanism controlled by tectonics. J. Volcanol. Geotherm. Res., 122, 191-220.

Gioncada A., Mazzuoli R. & Milton A.J. 2005. Magma mixing at Lipari (Aeolian Islands, Italy): insights from textural and compositional features of phenocrysts. Journal of Volcanology and Geothermal Research, 145, 97-118.

Hart S.R. 1984. A large-scale isotope anomaly in the southern hemisphere mantle. Nature, 309, 753-757.

Hawkesworth C.J. & Vollmer R. 1979. Crustal contamination vs. enriched mantle: 143Nd/144Nd and 87Sr/86Sr evidence from the Italian volcanics. Contrib. Mineral. Petrol., 69, 151-165.

Ito E., White W.M. & Gopel C. 1987. The O, Sr, Nd and Pb isotope geochemistry of MORB. Chem. Geol., 62, 157-176.

Langmuir C.H., Vocke R.D., Hanson G.N. & Hart S.R. 1978. A general mixing equation with applications to icelandic basalts. Earth Planet. Sci. Lett., 37, 380-392.

Leoni L. & Saitta M. 1976. X-ray fluorescence analysis of 29 trace elements in rock and mineral standard. Rend. Soc. Mineral. Petrol., 32, 479-510.

Pappalardo L., Piochi M., D'Antonio M., Civetta L. & Petrini R. 2002. Evidence for multistage magmatic evolution during the past 60 kyr at Campi Flegrei (Italy) deduced from Sr, Nd and Pb isotope data. J. Petrol., 43, 1415-1434.

Peccerillo A., Dallai L., Frezzotti M.L. & Kempton P.D. 2004. Sr-Nd-Pb-O isotopic evidence for decreasing crustal contamination with ongoing magma evolution at Alicudi volcano (Aeolian Arc, Italy): implication for style of magma-crust interaction and for mantle soure compositions. Lithos, 78, 217-233.

Peccerillo A., Kempton P.D., Harmon R.S., Wu T.W., Santo A.P., Boyce A.J. & Tripodo A. 1993. Petrological and geochemical characteristics of the Alicudi Volcano, Aeolian

Island, Italy: implications for magma genesis and evolution. Acta Vulcanol. 3, 235-249.

Peccerillo A. & Taylor S.R. 1976. Geochemistry of the Eocene calc-alkaline volcanic rocks from the Kastamonu area, northern Turkey. Contrib. Mineral.Petrol., 58, 63-81.

Peccerillo A. & Wu T.W. 1992. Evolution of calc-alkaline magmas in continental arc volcanoes: evidence from Alicudi, Aeolian Arc (Southern Tyrrhenian Sea, Italy). J. Petrol., 33, 1295-1315.

Perini G., Francalanci L., Davidson J.P. & Conticelli S. 2004. The petrogenesis of Vico Volcano, Central Italy: an example of low scale mantle heterogeneity. J. Petrol., 45, 139-182.

Perugini D., Petrelli M. & Poli G. 2006. Diffusive fractionation of trace elements by chaotic mixing of magmas. Earth Planet. Sci. Lett., 243, 669-680.

Perugini D. & Poli G. 2004. Analysis and numerical simulation of chaotic advection and chemical diffusion during magma mixing: petrological implications. Lithos, 78, 43-66.

Plank T. & Langmuir C. H. 1998. The chemical composition of subducting sediment and its consequences for the crust and mantle. Chem. Geol., 145, 325–394.

Reagan M. K., Sims K. W. W., Erich J., Thomas R.B., Cheng H., Edwards R. L., Layne G. & Ball L. 2003. Time-scales of Differentiation from Mafic Parents to Rhyolite in North American Continental Arcs J. Petrology. 44, 9, 1703-1726.

Rogers N.W., Hawkesworth C.J, Parker R.J. & Marsh J.S. 1985. Geochemistry of potassic lavas from Vulsini, central Italy, and implications for the mantle enrichment processes beneath the Roman region. Contrib. Mineral. Petrol., 90, 244-257.

Rollinson H. 1993. Using geochemical data: evaluation, presentation, interpretation (Longman Geochemistry). Pearson, Edinburg Gate, 352 pp.

Santo A.P., Jacobsen S.B. & Barker J. 2004. Evolution and genesis of calc-alkaline magmas at Filicudi volcano, Aeolian Arc (Southern Tyrrhenian Sea, Italy). Lithos, 72, 73-96.

Stacey J.S. & Kramers J.D. 1975. Approximation of terrestial lead isotope evolution by a two-stage model. Earth and Planetary Science Letters, 26, 207-221.

Sun S.S. & MC Donough W.F. 1989. Chemical and isotopic systematics of oceanic basalts: implications fort he mantle composition and processes. In: Saunders A.D. and Norry M.J. (eds.), Magmatism in ocean basins. Geol. Soc. London. Spec. Pub., 42,

313-345.

Tonarini S., Armienti P., D'Orazio M., Innocenti F., Pompilio M. & Petrini R. 1995. Geochemical and isotopic monitoring of Mt. Etna 1989-93 eruptive activity: bearing on the shallow feeding system. J. Volcanol. Geotherm. Res., 64, 95-155.

Zartman R.E. & Haines S.M. 1988. The plumbotectonic model fro Pb isotopic systematics among major terrestrial reservoirs – a case for bidirectional transport. Geochimica et Cosmochimica Acta, 52, 1327-1339.

CHAPTER 5

Summary and conclusions

The recentmost stratigraphic studies, combined with petrochemical investigations, available radiometric ages and correlation of tephra layers and marine terrace deposits, allow reconstruction of the geological and magmatic history of Lipari Island, developing between 271 ka and historical times (Forni et al., 2010; Lucchi et al., accepted for publication; cf. Chapter 1). This results from the emplacement of a large variety of lava flows, scoriaceous deposits, lava domes, coulees and pyroclastics, varying in composition from CA and HKCA basaltic andesites to rhyolites with a steep increase of K_2O with SiO_2 through time. These products are related to the volcanic activity of different eruptive vents, partially overlapping in space and time and variably controlled by the main regional tectonic trends (NNW-SSE, N-S and minor E-W). The eruptive history of Lipari is described by nine successive Eruptive Epochs, interrupted by periods of volcanic quiescence, volcano-tectonic events and episodes of marine terrace formation during the last interglacial.

Based on this stratigraphic and volcanologic framework, geochemical and isotopic investigations, combined with available melt and fluid inclusions data (Di Martino, 2010; Di Martino et al., 2010), give insights on the petrogenesis and evolution of magmas during the whole magmatic history of Lipari.

Mafic to intermediate magmatism dominate from 270 to 116 ka (Eruptive Epochs 1-4) and is linked to the activity of a series of monogenic and polygenic scattered volcanic centres mainly located in the western and central sector of the Island (M. Chirica, Chiesa Vecchia, Pietrovito, M. Mazzacaruso, and M. S.Angelo volcanoes, Fuori del Pertuso and Timpone Ospedale spatter cones) and secondarily in the eastern sector (Monterosa scoria cones). The associated products vary in composition from CA and HKCA basaltic andesites to HKCA dacites and consist of variably porphiritic pyroclastic rocks and lavas containing plagioclase, pyroxenes and minor olivine and Fe-Ti oxides. Although these rocks represent the most primitive rocks on the island, their geochemical and isotopic features (such as relatively low Ni and Cr contents and high $^{87}Sr/^{86}Sr$ ratios) suggest that they have suffered some pre-emplacement evolution involving fractionation of mafic phases at depth and interaction with the crustal rocks. Moreover, they are characterized by wide variations of trace element ratios (especially LILE/HSFE and HFSE/HFSE) and isotopic compositions. Petrogenetic models based on geochemical and isotope data, combined with petrographic observations, suggest that the evolution from CA basaltic andesites to dacites has been ruled mainly by AFC and RAFC processes (with high rates of assimilation vs. fractional crystallization, r=0.5) involving fractionation of mafic phases (mostly olivine and clinopyroxene, with a minor role of plagioclase), assimilation of wall rocks and mixing with newly injected mafic magma. Extensive interactions of the mantle-derived magmas with the crustal rocks,

both within the deep magma chamber (15-22 km; Di Martino et al., 2010) and during the ascents to the surface of different magma batches, are deemed to be responsible for the large spectrum of isotopic and geochemical variations (cf. Chapter 2).

It is noteworthy that, on the basis of the geochemical and isotope data presented in this study, possible genetic connections between the mafic to intermediate rocks of Lipari (Eruptive Epochs 1-4; 270-116 ka) and the HKCA and SHO basalts to shoshonites of Vulcano (120-30 ka), have been suggested. With respect to Lipari, the rocks from Vulcano display higher contents of incompatible trace elements and K_2O, together with higher Nd, lower Sr and higher Pb isotope ratios. However, the two suites of rocks show very similar incompatible trace element ratios. All these features have been traced back to different degrees of partial melting of the same mantle source, producing both CA magmas (higher degrees of partial melting) and HKCA to SHO magmas (lower degrees of partial melting). Differences in isotopic signature instead, have been attributed to variable extents of crustal assimilation (cf. Chapter 2).

A comparison between the mafic rocks from Lipari (SiO_2<56%, MgO>3.5%) and from the other islands of the Aeolian archipelago reveals that the mafic rocks from Salina, Lipari, Vulcano and Filicudi likely derive from a similar mantle source (MORB-like source), variably metasomatized by aqueous fluids coming from the slab (and to a lesser degree by the additions of sediments). A more extensive contribution of crustal assimilation is responsible for the higher $^{87}Sr/^{86}Sr$ and lower $^{143}Nd/^{144}Nd$ ratios observed in the mafic rocks from Lipari with respect to Salina, Vulcano and Filicudi.

Interaction of mantle-derived magmas with the crust, which represents an essential process in the whole magmatic history of Lipari, culminate with the generation of the cordierite-bearing lavas, erupted from the M. S.Angelo volcano during Eruptive Epoch 5 (105 ka). These HKCA andesites to dacites (whole-rock composition) look like a heterogeneous crystal mash characterized by the coexistence of typical igneous minerals (plagioclase and pyroxenes) along with phenocrysts of cordierite and garnet and a large amount of gabbroic and metamorphic xenoliths (up to 20-30%), set in a rhyodacitic to rhyolitic groundmass. These rocks have been interpreted as the products of mixing and subsequent hybridization of mantle-derived magmas, akin to the ones characterizing the older phases of activity of Lipari (Eruptive Epochs 1-4), and crustal anatectic melts deriving from dehydration-melting reactions of metapelites in the lower crust of Lipari (Di Martino et al., 2010, accepted for publication; cf. Chapter 3). Prolonged ponding (>100 ka) of mafic magmas in the deep magma chamber (15-22 km) has been suggested to provide the heat source for the crustal melting at the roof of the magma chamber. Magma hybridization and eruption are deemed to be the consequence of the entrance of fresh mafic mantle-derived magmas into the deep magma chamber.

These magmas might have interacted with the resident melts increasing magmatic and volatile overpressure and favouring the ascent of the cordierite-bearing crystal mash. Sr and Nd isotope data on both whole-rock and mineral samples, confirm the presence of two distinct component (mantle-derived and crustally-derived) coexisting in the magmatic system in which the cordierite-bearing lavas generated. Petrogenetic modeling indicates that magma mixing between mafic magmas and crustal anatectic melts has generated hybrid melts having the same isotopic signature of the cordierite-bearing lavas.

Following the cordierite-bearing lavas, the magmatic history of Lipari is characterized by the emission of HKCA andesitic lavas constructing the upper portions of the M. S.Angelo stratocone and M. Chirica volcano (Eruptive Epoch 6). These rocks have been genetically connected to the volcanic activity preceding the eruption of the cordierite-bearing lavas, because of their textural, geochemical and isotopic similarities with the andesitic to dacitic rocks of Eruptive Epoch 4 (cf. Chapter 2). AFC petrogenetic modeling indicates that they may likely represent the fractionated products of the AFC paths. The eruption of the HKCA andesitic lavas of M. S.Angelo and M. Chirica volcanoes signs the interruption of mafic to intermediate magmatism at Lipari.

Renewal of volcanism occurred after a 40 ka-long period of quiescence with the emplacement of pumiceous pyroclastics and viscous lava domes and coulees, initially taking place in the southern and eastern sector of Lipari (Eruptive Epoch 7 and 8; 42-8 ka) and progressively moving to the north-eastern areas (Eruptive Epoch 9; 8 ka-historical times). This signs the appearance of rhyolitic magmas in the history of Lipari. The rhyolitic products are scarcely porphyritic and contain K-feldspar, plagioclase and minor horneblende, biotite, Ti-magnetite, zircon and apatite. Some of them (HKCA dacites to low-SiO_2 rhyolites) are particularly rich in mafic enclaves, which range in composition from HKCA andesites to trachites and latites and contain clinopyroxene, plagioclase, olivine and Ti-magnetite. Because of their isotopic similarities with the mafic to intermediate rocks of Lipari (Eruptive Epochs 1-4), the rhyolitic products are interpreted to derive from the previous mafic melts through AFC processes with relatively low rates of assimilation vs. fractional crystallization (r=0.2-0.3). The presence of mafic enclaves in some hybrid rocks indicates that mixing processes between new batches of mafic magmas and the fractionated sialic melts have likely occurred (cf. Chapter 4).

References

Forni F., Lucchi F., Peccerillo A., Tranne C.A., Rossi P.L., Di Martino C., Frezzotti M.L. & Ayuso R.A. Lipari. In: Lucchi, F., Peccerillo A., Keller J., Tranne C.A. & Rossi P.L. (Eds.), Geology of the Aeolian Islands (Italy). Geological Society of London, accepted for publication.

Lucchi F., Tranne C.A., Forni, F. & Rossi, P.L. Geological map of Lipari Island, scale 1:10,000 (Aeolian archipelago), in: Lucchi F., Peccerillo A., Keller J., Tranne C.A. & Rossi P.L. (Eds.), Geology of the Aeolian Islands (Italy), Geological Society of London, Memoirs, accepted for publication.

Di Martino C. 2010. Evoluzione del sistema di alimentazione magmatica dell'Isola di Lipari (Isole Eolie, Italia). Unpublished PhD Thesis, University of Bologna, Italy, 155 pp.

Di Martino C., Forni F., Frezzotti M.L., Palmeri R., Webster J.D., Ayuso R.A., Lucchi F. & Tranne C.A. Anatexis and magma-hybridization in the lower-crust: petrogenesis of cordierite-bearing lavas from Lipari, Aeolian Arc, Italy. Contribution to Mineralogy and Petrology, accepted for publication.

Di Martino C., Frezzotti M.L., Palmeri R., Lucchi F., Peccerillo A., Tranne C.A. & Diamond L.W. 2010. Magma storage and ascent at Lipari Island (Aeolian archipelago, Southern Italy) at 223–81 ka: the role of crustal processes and tectonic influence. Bull. of Volcanology, DOI 10.1007/s00445-010-0383-6.

APPENDIX

Table 1 - Major, trace element and Sr, Nd and Pb isotope data for Lipari samples

Eruptive Epoch 1

Synthem	PALEO-LIPARI									
Lithosome	Timpone Carrubbo (lower portion)					Timpone Croci				
Formation	Scoglio Bianco					Timpone Croci	Fossa di Faurdo			
	sb1	sb1	sb1	sb1	sb1	tcr	ff	ff	ff	ff
Sample	Lip92	Lip102	A2**	A3*	A6**	T17*	A11**	A13**	A18**	Lip118
SiO_2	53.20	52.54	52.35	53.84	54.00	53.59	53.40	52.42	53.74	54.64
TiO_2	0.65	0.63	0.65	0.68	0.69	0.77	0.71	0.64	0.63	0.62
Al_2O_3	15.46	16.65	15.45	16.75	16.94	16.99	16.62	16.87	17.19	16.57
Fe_2O_3	9.57	8.92	9.10	9.36	9.51	9.60	9.09	9.23	8.42	8.97
MnO	0.17	0.16	0.17	0.16	0.16	0.16	0.16	0.16	0.16	0.16
MgO	6.02	5.09	6.83	5.25	5.23	4.74	6.24	5.78	4.76	5.16
CaO	9.33	9.35	10.61	8.89	8.36	9.42	9.57	10.77	10.20	9.49
Na_2O	2.46	2.66	2.08	2.36	2.58	2.10	1.93	2.18	2.34	2.18
K_2O	1.71	1.85	1.04	1.65	1.59	1.54	1.02	0.89	1.26	1.23
P_2O_5	0.14	0.20	0.19	0.23	0.14	0.18	0.20	0.17	0.17	0.14
LOI	1.29	1.95	1.54	0.83	0.80	0.91	1.06	0.89	1.13	0.85
Sc	-	-	-	30	-	31	-	-	-	-
V	267	255	274	305	228	264	270	293	281	263
Cr	46	23	117	40	36	52	100	76	54	48
Co	31	26	37	27.8	36	32	31	32	32	26
Ni	31	21	38	33	28	26	39	34	28	32
Rb	46	42	36	44	46	53.9	35	33	27	36
Sr	755	754	720	531	820	567	600	559	640	590
Y	18	16	19	19.1	21	19.3	21	17	17	16
Zr	78	63	99	66.8	109	77.1	95	87	92	59
Nb	b.d.l.	7	b.d.l.	6	b.d.l.	7	b.d.l.	b.d.l.	b.d.l.	b.d.l.
Cs	1.6	-	-	1.6	-	1.8	-	-	-	-
Ba	402	500	412	372	431	342	464	245	292	339
La	22	20	26	18.3	30	21.8	26	22	24	21
Ce	47	42	47	36.2	50	44.3	47	44	40	29
Pr	-	-	-	4.47	-	5.42	-	-	-	-
Nd	17	-	-	18.1	-	21.8	-	-	-	-
Sm	3.4	-	-	3.8	-	4.9	-	-	-	-
Eu	1.2	-	-	1.12	-	1.32	-	-	-	-
Gd	-	-	-	3.54	-	4.31	-	-	-	-
Tb	0.56	-	-	0.6	-	0.64	-	-	-	-
Dy	-	-	-	3.44	-	3.67	-	-	-	-
Ho	-	-	-	0.7	-	0.72	-	-	-	-
Er	-	-	-	2.01	-	2.27	-	-	-	-
Tm	-	-	-	0.3	-	0.31	-	-	-	-
Yb	1.9	-	-	2	-	2	-	-	-	-
Lu	0.29	-	-	0.29	-	0.31	-	-	-	-
Ta	-	-	-	b.d.l.	-	b.d.l.	-	-	-	-
Hf	2	-	-	b.d.l.	-	3	-	-	-	-
Pb	-	-	-	b.d.l.	-	b.d.l.	-	-	-	-
Th	b.d.l.	b.d.l.	b.d.l.	3.8	b.d.l.	6.3	b.d.l.	b.d.l.	b.d.l.	b.d.l.
U	1.5	-	-	1.22	-	1.54	-	-	-	-
$^{87}Sr/^{86}Sr$	-	-	-	-	-	0.706752	-	-	-	-
$^{143}Nd/^{144}Nd$	-	-	-	0.512468	-	0.512412	-	-	-	-
$^{206}Pb/^{204}Pb$	-	-	-	19.378	-	19.308	-	-	-	-
$^{207}Pb/^{204}Pb$	-	-	-	15.620	-	15.658	-	-	-	-
$^{208}Pb/^{204}Pb$	-	-	-	39.102	-	39.208	-	-	-	-

Table 1 (continued) - Major, trace element and Sr, Nd and Pb isotope data for Lipari samples

Eruptive Epoch	**1**			**2**						
Synthem	PALEO-LIPARI			PIANO GRANDE						
Lithosome	M. Mazzacaruso									
Formation	Vallone dei Lacci			M. Mazzacaruso						
	vla	vla	vla	maz	maz	maz	maz	maz	maz	maz
Sample	A26*	A38**	Lip127	A16*	Lip75	Lip77	Lip78	Lip79	Lip80	Lip81
SiO_2	54.94	54.28	53.20	54.10	53.62	53.87	54.62	53.60	55.58	54.73
TiO_2	0.67	0.75	0.56	0.81	0.69	0.75	0.70	0.71	0.82	0.69
Al_2O_3	16.19	16.44	15.86	17.26	17.45	17.62	18.63	19.49	16.81	16.61
Fe_2O_3	8.84	8.24	8.77	8.67	7.69	8.08	6.80	7.15	8.38	7.57
MnO	0.16	0.16	0.20	0.14	0.10	0.11	0.12	0.10	0.12	0.12
MgO	5.61	5.72	6.97	4.42	4.39	3.50	2.94	2.57	3.76	4.09
CaO	8.88	9.42	10.53	8.89	9.34	8.87	9.46	9.52	8.27	9.65
Na_2O	2.22	2.25	2.00	2.49	2.97	3.11	3.01	3.23	3.06	2.85
K_2O	1.62	1.70	0.77	1.56	1.89	1.87	1.83	1.71	2.27	1.66
P_2O_5	0.20	0.22	0.10	0.23	0.21	0.24	0.19	0.21	0.29	0.21
LOI	0.67	0.82	0.64	1.43	1.65	1.98	1.70	1.71	0.64	1.82
Sc	32	-	-	27	-	-	-	-	-	-
V	259	241	244	250	237	241	224	220	189	260
Cr	70	114	153	80	62	24	22	b.d.l.	32	62
Co	28.6	28	34	31.3	23	20	17	18	21	23
Ni	42	38	47	48	29	22	20	16	20	32
Rb	50.4	55	19	55.2	51	45	49	49	56	47
Sr	580	492	469	531	620	586	656	697	509	605
Y	17.9	23	17	20.1	19	18	18	18	21	17
Zr	63.8	107	54	79	86	83	86	90	100	82
Nb	5	b.d.l.	b.d.l.	6	b.d.l.	b.d.l.	8	b.d.l.	9	b.d.l.
Cs	1.1	-	-	2.2	-	1.6	-	-	-	2
Ba	403	362	226	478	455	429	408	393	480	445
La	20.8	25	5	24	30	24	18	20	28	24
Ce	40.7	54	19	47.2	44	52	39	38	57	50
Pr	4.88	-	-	5.75	-	-	-	-	-	-
Nd	20	-	-	22.7	-	16	-	-	-	15
Sm	4	-	-	4.8	-	3.6	-	-	-	3.5
Eu	1.14	-	-	1.2	-	1.4	-	-	-	1.4
Gd	3.81	-	-	4.12	-	-	-	-	-	-
Tb	0.59	-	-	0.64	-	0.62	-	-	-	0.6
Dy	3.4	-	-	3.57	-	-	-	-	-	-
Ho	0.66	-	-	0.72	-	-	-	-	-	-
Er	1.99	-	-	2.21	-	-	-	-	-	-
Tm	0.28	-	-	0.32	-	-	-	-	-	-
Yb	1.7	-	-	2.1	-	2.3	-	-	-	2.1
Lu	0.29	-	-	0.3	-	0.35	-	-	-	0.32
Ta	b.d.l.	-	-	b.d.l.	-	-	-	-	-	-
Hf	b.d.l.	-	-	3	-	2	-	-	-	2
Pb	b.d.l.	-	-	11	-	-	-	-	-	-
Th	4.6	b.d.l.	b.d.l.	5.3	b.d.l.	b.d.l.	b.d.l.	b.d.l.	b.d.l.	b.d.l.
U	1.62	-	-	1.67	-	1.4	-	-	-	-
$^{87}Sr/^{86}Sr$	-	-	-	0.706073	-	-	-	-	-	-
$^{143}Nd/^{144}Nd$	-	-	-	0.512523	-	-	-	-	-	-
$^{206}Pb/^{204}Pb$	-	-	-	19.232	-	-	-	-	-	-
$^{207}Pb/^{204}Pb$	-	-	-	15.644	-	-	-	-	-	-
$^{208}Pb/^{204}Pb$	-	-	-	39.098	-	-	-	-	-	-

Table 1 (continued) - Major, trace element and Sr, Nd and Pb isotope data for Lipari samples

Eruptive Epoch	**2**									
Synthem	PIANO GRANDE									
Lithosome	M. Mazzacaruso								Timpone Ospedale	
Formation	M. Mazzacaruso								Timpone Ospedale	
	maz	maz	maz	maz1	maz1	maz1	maz1	maz1	to	to
Sample	Lip84	Lip90	Lip122	Lip82	Lip86	Lip88	Lip109	A28**	Lip105	Lip130
SiO_2	53.58	52.83	55.18	53.38	52.41	53.13	54.98	54.27	51.87	54.77
TiO_2	0.72	0.68	0.83	0.67	0.62	0.72	0.70	0.63	0.55	0.66
Al_2O_3	16.94	16.92	16.27	16.28	15.25	16.28	16.18	17.45	14.85	16.12
Fe_2O_3	8.99	8.65	9.35	8.72	8.99	9.12	8.45	9.01	8.75	8.78
MnO	0.14	0.15	0.15	0.14	0.15	0.15	0.14	0.16	0.14	0.19
MgO	4.71	4.75	4.17	4.91	5.56	5.64	5.08	4.86	7.63	4.92
CaO	9.85	10.08	8.84	10.39	11.01	9.77	8.58	9.53	10.95	9.28
Na_2O	2.90	2.80	2.01	2.87	2.57	2.70	2.49	2.35	2.41	2.04
K_2O	1.95	1.37	1.61	1.62	1.47	1.85	2.07	1.27	0.95	1.29
P_2O_5	0.22	0.20	0.21	0.23	0.16	0.20	0.20	0.14	0.16	0.14
LOI	1.54	1.57	1.38	0.79	1.81	0.44	1.13	0.33	1.74	1.81
Sc	27	-	29	-	-	-	-	-	43	-
V	261	231	286	265	243	247	237	258	261	236
Cr	40	48	80	64	85	52	52	37	170	71
Co	24	25	26.1	23	28	27	25	29	33.2	30
Ni	37	27	37	23	31	28	31	25	68	28
Rb	51.7	42	55.3	29	32	50	58	38	26	47
Sr	753	640	545	528	590	793	613	634	458	636
Y	18.5	16	21.3	15	16	17	21	20	14.4	22
Zr	76.4	75	76.7	59	62	100	110	97	41.7	83
Nb	7	b.d.l.	6	b.d.l.	b.d.l.	9	8	b.d.l.	3	7
Cs	2.1	-	1.8	-	-	2	-	-	0.9	-
Ba	474	337	410	389	400	497	429	302	266	461
La	24.7	15	24.3	18	21	26	34	23	12.5	25
Ce	48	40	46.7	29	35	46	58	40	24.7	38
Pr	5.7	-	5.66	-	-	-	-	-	3.19	-
Nd	23.7	-	22.3	-	-	19	-	-	12.9	-
Sm	4.7	-	4.6	-	-	3.7	-	-	3	-
Eu	1.32	-	1.2	-	-	1.4	-	-	0.86	-
Gd	4.2	-	4.1	-	-	-	-	-	2.76	-
Tb	0.67	-	0.66	-	-	0.56	-	-	0.45	-
Dy	3.41	-	3.75	-	-	-	-	-	2.57	-
Ho	0.71	-	0.8	-	-	-	-	-	0.54	-
Er	2.07	-	2.2	-	-	-	-	-	1.63	-
Tm	0.32	-	0.31	-	-	-	-	-	0.25	-
Yb	1.9	-	2	-	-	1.9	-	-	1.5	-
Lu	0.3	-	0.34	-	-	0.29	-	-	0.3	-
Ta	b.d.l.	-	b.d.l.	-	-	-	-	-	b.d.l.	-
Hf	3	-	3	-	-	2	-	-	b.d.l.	-
Pb	b.d.l.	-	11	-	-	-	-	-	b.d.l.	-
Th	b.d.l.	b.d.l.	5.1	b.d.l.	b.d.l.	b.d.l.	b.d.l.	b.d.l.	2.5	b.d.l.
U	1.84	-	1.6	-	-	1.3	-	-	0.85	-
$^{87}Sr/^{86}Sr$	0.706149	-	0.705507	-	-	-	-	-	0.705587	-
$^{143}Nd/^{144}Nd$	0.512526	-	0.512417	-	-	-	-	-	0.512624	-
$^{206}Pb/^{204}Pb$	19.355	-	19.422	-	-	-	-	-	19.599	-
$^{207}Pb/^{204}Pb$	15.632	-	15.680	-	-	-	-	-	15.625	-
$^{208}Pb/^{204}Pb$	39.094	-	39.323	-	-	-	-	-	39.268	-

Table 1 (continued) - Major, trace element and Sr, Nd and Pb isotope data for Lipari samples

Eruptive Epoch **2**

Synthem PIANO GRANDE

Lithosome Timpone Ospedale

Formation Timpone Ospedale

	to	to	to	to (dike)	to (dike)	to (dike)	to (dike)	to	to1	to1
Sample	Lip131	Lip134	A30**	D1**	D2**	A23**	A24**	A25**	A22**	Lip104
SiO_2	54.70	54.06	52.29	52.16	54.88	54.40	51.75	52.91	55.36	53.43
TiO_2	0.63	0.64	0.65	0.67	0.89	0.71	0.83	0.66	0.68	0.67
Al_2O_3	16.97	16.93	16.11	16.27	17.10	16.56	16.61	16.70	16.27	15.94
Fe_2O_3	8.51	9.06	8.69	9.14	8.72	8.80	9.71	8.74	8.28	8.63
MnO	0.15	0.25	0.16	0.16	0.15	0.17	0.18	0.15	0.15	0.15
MgO	4.78	4.91	7.16	6.84	3.87	4.74	6.47	6.50	5.96	5.30
CaO	9.36	9.96	10.68	10.74	9.18	9.42	9.93	9.85	8.52	9.11
Na_2O	2.12	2.23	2.16	2.21	2.51	2.32	2.31	2.07	2.26	2.62
K_2O	1.04	1.15	0.99	1.14	1.45	1.41	1.09	0.95	1.60	2.00
P_2O_5	0.14	0.14	0.17	0.16	0.24	0.18	0.23	0.18	0.21	0.20
LOI	1.60	0.67	0.95	0.51	1.01	1.29	0.89	1.29	0.71	1.95
Sc	-	38	-	-	-	-	-	-	-	-
V	265	269	278	290	297	270	310	292	257	224
Cr	119	80	178	134	56	61	97	90	90	52
Co	29	30.3	33	27	34	25	31	29	33	25
Ni	36	48	48	25	42	27	37	38	36	27
Rb	30	35.1	22	31	33	40	32	31	52	55
Sr	551	595	454	518	608	627	567	576	606	593
Y	20	16.8	18	17	21	21	21	18	23	16
Zr	66	49.4	82	84	107	101	91	85	105	78
Nb	b.d.l.	4	b.d.l.	b.d.l.	b.d.l.	b.d.l.	b.d.l.	9	7	b.d.l.
Cs	-	0.7	-	-	-	-	-	-	-	2
Ba	314	318	278	301	416	401	323	273	361	388
La	10	16.3	13	18	36	25	24	17	28	26
Ce	31	31.3	44	48	52	49	45	47	46	45
Pr	-	3.82	-	-	-	-	-	-	-	-
Nd	-	15.5	-	-	-	-	-	-	-	20
Sm	-	3.5	-	-	-	-	-	-	-	3.7
Eu	-	0.97	-	-	-	-	-	-	-	1.4
Gd	-	3.04	-	-	-	-	-	-	-	-
Tb	-	0.53	-	-	-	-	-	-	-	0.61
Dy	-	2.9	-	-	-	-	-	-	-	-
Ho	-	0.62	-	-	-	-	-	-	-	-
Er	-	1.91	-	-	-	-	-	-	-	-
Tm	-	0.27	-	-	-	-	-	-	-	-
Yb	-	1.7	-	-	-	-	-	-	-	2.2
Lu	-	0.32	-	-	-	-	-	-	-	0.33
Ta	-	b.d.l.	-	-	-	-	-	-	-	-
Hf	-	b.d.l.	-	-	-	-	-	-	-	2
Pb	-	b.d.l.	-	-	-	-	-	-	-	-
Th	b.d.l.	3.1	b.d.l.	b.d.l.	b.d.l.	b.d.l.	b.d.l.	b.d.l.	b.d.l.	b.d.l.
U	-	1.02	-	-	-	-	-	-	-	1.4
$^{87}Sr/^{86}Sr$	-	0.705876	-	-	-	-	-	-	-	0.706428
$^{143}Nd/^{144}Nd$	-	0.512418	-	-	-	-	-	-	-	0.512484
$^{206}Pb/^{204}Pb$	-	19.399	-	-	-	-	-	-	-	19.283
$^{207}Pb/^{204}Pb$	-	15.615	-	-	-	-	-	-	-	15.639
$^{208}Pb/^{204}Pb$	-	39.055	-	-	-	-	-	-	-	39.128

Table 1 (continued) - Major, trace element and Sr, Nd and Pb isotope data for Lipari samples

Eruptive Epoch 2

Synthem	PIANO GRANDE			
Lithosome	Timpone Ospedale	T.Carrubbo (upper p.)	M.Chirica (lower portion)	
Formation	Timpone Ospedale	Belvedere	Vallone Malopasso	

	to1	to1	bel2	vma	vma	vma	vma	vma	vma	vma
Sample	Lip108	Lip115	Lip282	Lip146	Lip213	Lip241	A1*	A4**	A32**	A33**
SiO_2	54.83	52.83	55.38	54.68	53.18	54.88	52.12	53.89	52.72	53.28
TiO_2	0.69	0.62	0.67	0.61	0.65	0.62	0.68	0.65	0.71	0.73
Al_2O_3	16.51	15.58	16.05	17.08	16.12	16.66	17.29	15.80	16.53	16.54
Fe_2O_3	8.36	8.82	7.37	8.81	8.67	6.92	9.57	8.70	8.63	8.28
MnO	0.14	0.15	0.15	0.16	0.16	0.10	0.17	0.15	0.16	0.16
MgO	4.36	6.56	2.85	5.23	6.71	6.25	5.84	6.96	5.36	5.34
CaO	9.14	10.74	8.60	9.73	10.19	10.21	10.11	8.98	10.66	10.78
Na_2O	2.45	2.41	2.87	2.19	2.47	2.26	2.22	2.44	2.22	1.87
K_2O	2.18	0.97	3.01	1.05	1.13	1.54	1.22	1.53	1.36	1.66
P_2O_5	0.19	0.15	0.28	0.14	0.14	0.21	0.15	0.22	0.20	0.23
LOI	1.15	1.17	2.78	0.32	0.57	1.05	0.63	0.69	1.45	1.13
Sc	-	-	26	33	43	40	33	-	-	-
V	254	270	179	242	268	248	250	260	255	260
Cr	43	23	38	80	107	175	80	69	124	119
Co	29	31	25	34.2	40	29	30.3	30	31	27
Ni	27	41	20	54	35	41	42	29	36	40
Rb	55	31	96	38.4	35	51	41.6	45	49	56
Sr	559	537	1016	541	556	583	456	719	603	624
Y	16	16	21	17	17	16	17.8	19	21	19
Zr	80	57	109	53.6	60	60	63.8	105	115	102
Nb	7	b.d.l.	7	4	b.d.l.	b.d.l.	5	b.d.l.	9	8
Cs	2	-	-	1.3	-	-	1.6	-	-	-
Ba	397	293	643	293	332	372	287	445	311	291
La	25	15	29	18.3	10	24	16.3	27	24	30
Ce	47	39	76	34	28	47	31.8	46	56	56
Pr	-	-	-	4.35	-	-	3.98	-	-	-
Nd	17	-	-	18	-	-	16.1	-	-	-
Sm	3.7	-	-	3.7	-	-	3.5	-	-	-
Eu	1.4	-	-	1	-	-	0.97	-	-	-
Gd	-	-	-	3.41	-	-	3.06	-	-	-
Tb	0.63	-	-	0.5	-	-	0.56	-	-	-
Dy	-	-	-	3.07	-	-	2.99	-	-	-
Ho	-	-	-	0.61	-	-	0.63	-	-	-
Er	-	-	-	1.9	-	-	1.8	-	-	-
Tm	-	-	-	0.26	-	-	0.25	-	-	-
Yb	2.2	-	-	1.6	-	-	1.8	-	-	-
Lu	0.33	-	-	0.27	-	-	0.36	-	-	-
Ta	-	-	b.d.l.	b.d.l.	-	-	b.d.l.	-	-	-
Hf	2	-	b.d.l.	b.d.l.	-	-	b.d.l.	-	-	-
Pb	-	-	9	b.d.l.	-	6	b.d.l.	-	-	-
Th	b.d.l.	b.d.l.	b.d.l.	3	b.d.l.	b.d.l.	6.2	b.d.l.	b.d.l.	b.d.l.
U	1.7	-	-	1.1	-	-	1.2	-	-	-
$^{87}Sr/^{86}Sr$	-	-	-	-	-	-	0.705852	-	-	-
$^{143}Nd/^{144}Nd$	-	-	-	-	-	-	0.512592	-	-	-
$^{206}Pb/^{204}Pb$	-	-	-	-	-	-	19.173	-	-	-
$^{207}Pb/^{204}Pb$	-	-	-	-	-	-	15.638	-	-	-
$^{208}Pb/^{204}Pb$	-	-	-	-	-	-	38.985	-	-	-

Table 1 (continued) - Major, trace element and Sr, Nd and Pb isotope data for Lipari samples

Eruptive Epoch 2

Synthem PIANO GRANDE

Lithosome M. Chirica (lower portion)

Formation Vallone Malopasso

	vma (dike)	vma	vma	vma	vma	vma	vma	vma	vma	vma
Sample	A34**	B3*	B5*	B6**	B7**	B8**	B9**	B14*	B15**	B16*
SiO_2	53.73	54.83	52.93	54.25	53.49	52.68	53.19	53.04	53.36	52.80
TiO_2	0.78	0.68	0.59	0.70	0.64	0.62	0.73	0.61	0.71	0.61
Al_2O_3	16.33	17.21	15.74	17.68	15.32	15.81	17.10	14.83	16.17	16.25
Fe_2O_3	8.14	8.50	7.73	8.94	8.25	8.29	9.01	8.72	9.24	8.71
MnO	0.15	0.14	0.14	0.15	0.16	0.16	0.15	0.15	0.16	0.17
MgO	5.21	4.43	7.70	4.61	8.16	7.88	5.71	7.41	6.21	7.03
CaO	10.44	8.93	10.31	9.09	10.32	10.68	9.25	9.64	9.46	10.49
Na_2O	2.22	2.98	2.43	2.72	2.09	2.17	2.81	2.90	2.31	2.26
K_2O	1.72	1.10	0.93	1.24	1.09	1.03	1.32	1.01	1.28	0.98
P_2O_5	0.25	0.14	0.14	0.16	0.15	0.15	0.18	0.17	0.18	0.13
LOI	1.03	1.06	1.36	0.46	0.35	0.53	0.55	1.52	0.92	0.57
Sc	-	30	-	-	-	-	-	-	-	-
V	256	305	257	270	256	239	275	229	260	260
Cr	148	40	281	22	271	266	103	162	125	142
Co	27	27.8	34	28	30	36	33	43	33	36
Ni	39	33	51	20	61	60	29	45	36	41
Rb	56	44	37	42	30	35	46	44	44	29
Sr	616	531	556	594	464	499	560	594	523	554
Y	22	19.1	21	20	18	19	22	21	21	19
Zr	100	66.8	92	97	88	88	104	97	100	73
Nb	b.d.l.	6	9	b.d.l.	b.d.l.	b.d.l.	7	8	b.d.l.	7
Cs	-	1.6	-	-	-	-	-	-	-	-
Ba	302	372	286	321	254	267	351	299	336	250
La	18	18.3	23	23	20	18	27	22	20	23
Ce	55	36.2	31	42	38	41	50	33	50	43
Pr	-	4.47	-	-	-	-	-	-	-	-
Nd	-	18.1	16	-	-	-	-	15	-	12
Sm	-	3.8	3.5	-	-	-	-	3.4	-	2.7
Eu	-	1.12	1	-	-	-	-	0.9	-	0.8
Gd	-	3.54	-	-	-	-	-	-	-	-
Tb	-	0.6	0.5	-	-	-	-	0.5	-	0.4
Dy	-	3.44	-	-	-	-	-	-	-	-
Ho	-	0.7	-	-	-	-	-	-	-	-
Er	-	2.01	-	-	-	-	-	-	-	-
Tm	-	0.3	-	-	-	-	-	-	-	-
Yb	-	2	1.8	-	-	-	-	1.9	-	1.6
Lu	-	0.29	0.27	-	-	-	-	0.27	-	0.25
Ta	-	b.d.l.	-	-	-	-	-	-	-	-
Hf	-	b.d.l.	3	-	-	-	-	2	-	b.d.l.
Pb	-	b.d.l.	-	-	-	-	-	-	-	b.d.l.
Th	b.d.l.	3.8	b.d.l.	b.d.l.	b.d.l.	b.d.l.	b.d.l.	b.d.l.	b.d.l.	b.d.l.
U	-	1.22	0.5	-	-	-	-	1.7	-	0.5
$^{87}Sr/^{86}Sr$	-	0.706261	-	-	-	-	-	-	-	-
$^{143}Nd/^{144}Nd$	-	0.512568	-	-	-	-	-	-	-	-
$^{206}Pb/^{204}Pb$	-	19.314	-	-	-	-	-	-	-	-
$^{207}Pb/^{204}Pb$	-	15.649	-	-	-	-	-	-	-	-
$^{208}Pb/^{204}Pb$	-	39.175	-	-	-	-	-	-	-	-

Table 1 (continued) - Major, trace element and Sr, Nd and Pb isotope data for Lipari samples

Eruptive Epoch 2

Synthem PIANO GRANDE

Lithosome M. Chirica (lower portion)

Formation Vallone Malopasso

	vma	vma	vma	vma	vma	vma	vma	vma	vma	vma
Sample	B18*	B20**	B22**	B23**	B24**	T11**	T13**	T14**	T15**	T16**
SiO_2	53.21	52.39	52.64	52.01	53.77	54.45	53.66	53.17	53.03	55.65
TiO_2	0.57	0.60	0.60	0.61	0.71	0.71	0.65	0.63	0.67	0.72
Al_2O_3	16.41	16.74	15.52	15.29	17.21	15.81	16.25	16.07	15.55	17.15
Fe_2O_3	8.23	8.44	7.96	8.12	8.76	8.79	8.84	8.82	8.94	8.81
MnO	0.15	0.15	0.14	0.15	0.15	0.15	0.16	0.16	0.16	0.15
MgO	7.13	6.89	7.92	7.92	5.27	6.54	7.11	7.71	7.99	4.56
CaO	10.19	10.03	10.27	10.90	9.17	9.51	10.57	10.75	10.68	8.96
Na_2O	2.56	2.48	2.27	2.10	2.73	1.81	1.87	1.56	1.43	2.19
K_2O	0.92	0.81	0.87	0.97	1.29	0.83	0.52	0.42	1.06	1.06
P_2O_5	0.13	0.12	0.15	0.14	0.18	0.25	0.22	0.23	0.26	0.20
LOI	0.51	1.36	1.66	1.79	0.76	1.15	0.15	0.48	0.23	0.55
Sc	-	-	-	-	-	-	-	-	-	-
V	257	287	246	261	263	262	262	256	235	254
Cr	140	112	278	268	102	99	107	133	249	25
Co	40	35	40	35	33	33	33	33	30	24
Ni	37	31	61	60	24	37	40	44	57	20
Rb	28	25	31	34	50	43	34	32	54	46
Sr	542	590	548	554	616	567	542	502	572	642
Y	17	17	18	21	25	22	21	19	23	24
Zr	74	75	89	88	108	97	79	70	96	102
Nb	b.d.l.	7	8	b.d.l.	8	8	7	b.d.l.	7	b.d.l.
Cs	-	-	-	-	-	-	-	-	-	-
Ba	250	244	269	309	361	485	220	216	259	329
La	22	18	21	23	24	22	18	16	11	17
Ce	30	37	31	36	41	42	29	30	36	35
Pr	-	-	-	-	-	-	-	-	-	-
Nd	12	-	-	-	-	-	-	-	-	-
Sm	2.7	-	-	-	-	-	-	-	-	-
Eu	0.8	-	-	-	-	-	-	-	-	-
Gd	-	-	-	-	-	-	-	-	-	-
Tb	0.4	-	-	-	-	-	-	-	-	-
Dy	-	-	-	-	-	-	-	-	-	-
Ho	-	-	-	-	-	-	-	-	-	-
Er	-	-	-	-	-	-	-	-	-	-
Tm	-	-	-	-	-	-	-	-	-	-
Yb	1.4	-	-	-	-	-	-	-	-	-
Lu	0.23	-	-	-	-	-	-	-	-	-
Ta	-	-	-	-	-	-	-	-	-	-
Hf	2	-	-	-	-	-	-	-	-	-
Pb	b.d.l.	-	-	-	-	-	-	-	-	-
Th	b.d.l.	b.d.l.	b.d.l.	b.d.l.	b.d.l.	b.d.l.	b.d.l.	b.d.l.	b.d.l.	b.d.l.
U	0.5	-	-	-	-	-	-	-	-	-
$^{87}Sr/^{86}Sr$	-	-	-	-	-	-	-	-	-	-
$^{143}Nd/^{144}Nd$	-	-	-	-	-	-	-	-	-	-
$^{206}Pb/^{204}Pb$	-	-	-	-	-	-	-	-	-	-
$^{207}Pb/^{204}Pb$	-	-	-	-	-	-	-	-	-	-
$^{208}Pb/^{204}Pb$	-	-	-	-	-	-	-	-	-	-

Table 1 (continued) - Major, trace element and Sr, Nd and Pb isotope data for Lipari samples

Eruptive Epoch 2

Synthem	PIANO GRANDE									
Lithosome	Fuori del Pertuso			Chiesa Vecchia						
Formation	Fuori del Pertuso			Bonanno		Puddino				
	fp	fp	fp	bo	bo	pd	pd	pd	pd	pd
Sample	Lip114	Lip106	Lip107	Lip111	Lip113	T6**	T8**	T9*	TI2**	Lip143
SiO_2	53.96	52.11	52.49	56.92	52.55	56.20	59.43	54.83	59.80	57.03
TiO_2	0.69	0.62	0.63	0.67	0.67	0.73	0.79	0.68	0.78	0.62
Al_2O_3	15.13	14.53	14.49	15.69	14.94	16.31	16.49	17.21	16.37	17.41
Fe_2O_3	9.23	8.85	9.12	7.66	9.10	8.25	7.97	8.50	7.95	8.33
MnO	0.32	0.15	0.17	0.15	0.19	0.16	0.14	0.14	0.14	0.17
MgO	5.86	6.57	6.80	4.66	6.43	4.63	3.14	4.43	3.24	3.79
CaO	10.14	11.08	10.92	8.19	10.47	7.85	6.64	8.93	6.51	7.62
Na_2O	2.28	2.36	2.35	2.55	2.23	2.56	2.50	2.98	2.02	2.27
K_2O	1.37	1.26	1.37	2.30	1.40	2.03	2.45	1.10	2.43	1.54
P_2O_5	0.18	0.18	0.19	0.17	0.16	0.20	0.19	0.14	0.22	0.13
LOI	0.84	2.29	1.47	1.04	1.86	1.08	0.26	1.06	0.54	1.08
Sc	34	-	-	-	36	35	-	23	-	-
V	278	276	267	228	228	230	210	217	202	235
Cr	110	112	112	62	110	77	48	80	54	86
Co	39	30	30	23	31.7	31	23	23.9	21	35
Ni	50	47	47	28	51	26	27	63	28	38
Rb	33	35	36	77	44.8	63	99	102	101	33
Sr	512	560	505	519	514	457	454	417	520	567
Y	17.4	19	16	22	18.1	18	26	23.9	32	18
Zr	58.1	66	62	112	58.3	84	135	121	163	63
Nb	4	b.d.l.	b.d.l.	9	4	b.d.l.	8	10	b.d.l.	b.d.l.
Cs	0.9	-	-	-	0.9	-	-	4.4	-	1.6
Ba	296	291	285	412	303	485	424	600	467	297
La	17.9	18	22	25	17.2	37	34	30.3	27	24
Ce	35.5	39	34	44	34.7	65	72	59.4	59	41
Pr	4.35	-	-	-	4.38	-	-	7.13	-	-
Nd	17.6	-	-	-	18.1	-	-	27.6	-	22
Sm	3.9	-	-	-	3.8	-	-	5.6	-	4.2
Eu	1.03	-	-	-	1.18	-	-	1.13	-	1.4
Gd	3.43	-	-	-	3.64	-	-	4.75	-	-
Tb	0.57	-	-	-	0.57	-	-	0.78	-	0.75
Dy	3.21	-	-	-	3.4	-	-	4.58	-	-
Ho	0.68	-	-	-	0.7	-	-	0.87	-	-
Er	1.88	-	-	-	1.99	-	-	2.5	-	-
Tm	0.26	-	-	-	0.27	-	-	0.35	-	-
Yb	1.8	-	-	-	1.9	-	-	2.5	-	3
Lu	0.34	-	-	-	0.33	-	-	0.38	-	0.48
Ta	b.d.l.	-	-	-	b.d.l.	-	-	b.d.l.	-	-
Hf	b.d.l.	-	-	-	b.d.l.	-	-	4	-	2
Pb	b.d.l.	-	-	-	b.d.l.	11	b.d.l.	19	-	-
Th	4.5	b.d.l.	b.d.l.	b.d.l.	3.7	b.d.l.	b.d.l.	8.3	b.d.l.	b.d.l.
U	1.27	-	-	-	1.06	-	-	2.66	-	1.3
$^{87}Sr/^{86}Sr$	0.705339	-	-	-	0.705278	-	-	0.706991	-	0.706539
$^{143}Nd/^{144}Nd$	0.512644	-	-	-	0.512714	-	-	0.511937	-	0.512415
$^{206}Pb/^{204}Pb$	19.399	-	-	-	19.297	-	-	18.865	-	19.268
$^{207}Pb/^{204}Pb$	15.648	-	-	-	15.688	-	-	15.608	-	15.642
$^{208}Pb/^{204}Pb$	39.216	-	-	-	39.245	-	-	38.724	-	39.095

Table 1 (continued) - Major, trace element and Sr, Nd and Pb isotope data for Lipari samples

Eruptive Epoch	**2**	**3**		**4**						
Synthem	PIANO GRANDE			SC.O LE TORRICELLE						
Lithosome	Chiesa Vecchia	M.Chirica (upper portion)		Monterosa						
Formation	Bertaccia	Vallone di Bezzotti		Sciarra di Monterosa			Pignataro di Fuori			
	ber2	vb2	vb2	sci1	sci2	sci2	pf	pf	pf	pf
Sample	Lip271	Lip110	Lip211	Lip180	Lip101	MR6	Lip182	Lip183	Lip186	Lip140
SiO_2	56.81	53.08	52.35	53.82	54.26	54.92	53.54	54.67	55.28	55.97
TiO_2	0.65	0.67	0.61	0.67	0.69	0.71	0.69	0.65	0.69	0.76
Al_2O_3	17.57	14.94	16.69	17.80	17.32	17.81	17.19	18.23	17.63	17.41
Fe_2O_3	8.36	8.80	8.82	8.59	8.70	9.01	8.99	8.15	8.35	9.20
MnO	0.16	0.14	0.16	0.15	0.16	0.16	0.17	0.15	0.15	0.16
MgO	3.10	5.65	6.38	4.50	4.79	4.03	4.58	4.46	4.37	3.53
CaO	6.81	10.60	9.71	8.12	8.66	8.48	8.87	7.60	7.74	8.26
Na_2O	2.50	2.52	2.32	2.45	2.77	2.88	2.65	2.98	2.82	2.40
K_2O	1.71	1.56	1.05	1.90	2.02	1.79	2.07	2.01	1.74	1.58
P_2O_5	0.15	0.19	0.14	0.21	0.21	0.19	0.26	0.22	0.17	0.19
LOI	2.18	1.85	1.76	1.82	0.41	0.01	0.99	0.91	1.07	0.54
Sc	34	-	35	38	34	33	37	37	33	-
V	146	258	251	254	239	259	264	252	253	296
Cr	43	102	100	b.d.l.	26	b.d.l.	b.d.l.	24	b.d.l.	b.d.l.
Co	31	29	33.2	32	33	32	35	32	28	29
Ni	21	36	53	18	19	15	14	15	12	12
Rb	53	46	35.4	38	60	48	64	31	59	46
Sr	679	566	501	492	804	774	796	361	754	682
Y	22	18	18.3	13	20	20	20	11	22	25
Zr	78	84	54.2	45	93	84	87	33	104	97
Nb	b.d.l.	7	4	b.d.l.	7	b.d.l.	b.d.l.	b.d.l.	7	7
Cs	-	-	1.3	2	1.6	1.6	1.6	3	3	0
Ba	360	358	264	486	572	518	478	542	510	505
La	29	24	19.5	30	29	31	45	36	29	25
Ce	38	44	33.8	50	53	62	49	48	54	29
Pr	-	-	4.81	-	-	-	-	-	-	-
Nd	-	-	19.3	19	19	17	20	25	20	-
Sm	-	-	4.1	5.5	4	3.7	4.5	4.8	3.8	-
Eu	-	-	1.08	1.6	1.4	1.4	1.3	1.4	2.5	-
Gd	-	-	3.62	-	-	-	-	-	-	-
Tb	-	-	0.62	0.67	0.61	0.53	0.6	0.7	0.66	-
Dy	-	-	3.14	-	-	-	-	-	-	-
Ho	-	-	0.64	-	-	-	-	-	-	-
Er	-	-	1.98	-	-	-	-	-	-	-
Tm	-	-	0.28	-	-	-	-	-	-	-
Yb	-	-	1.8	2.5	2.2	2	1.8	2.1	2.2	-
Lu	-	-	0.27	0.39	0.34	0.3	0.27	0.31	0.33	-
Ta	-	-	-	-	-	-	-	-	-	-
Hf	-	-	-	2	2	3	3	3	2	-
Pb	7	b.d.l.	-	8	7	10	10	6	2	b.d.l.
Th	b.d.l.	b.d.l.	3.3	b.d.l.	b.d.l.	b.d.l.	b.d.l.	b.d.l.	b.d.l.	b.d.l.
U	-	-	1.22	1.9	2	1.4	1.3	1.1	1.7	-
$^{87}Sr/^{86}Sr$	-	-	0.705115	0.705597	-	-	0.706207	-	-	-
$^{143}Nd/^{144}Nd$	-	-	0.512656	0.512580	-	0.512479	0.512405	-	-	-
$^{206}Pb/^{204}Pb$	-	-	19.362	19.314	-	19.368	19.251	-	-	-
$^{207}Pb/^{204}Pb$	-	-	15.654	15.638	-	15.645	15.634	-	-	-
$^{208}Pb/^{204}Pb$	-	-	39.120	39.107	-	39.166	39.048	-	-	-

Table 1 (continued) - Major, trace element and Sr, Nd and Pb isotope data for Lipari samples

Eruptive Epoch 4

Synthem	SC.O LE TORRICELLE									
Lithosome	Monterosa				M. S.Angelo (lower portion)					
Formation	Pignataro di Fuori		U'Mazzuni		Timpone del Corvo					
	pf1	pf2	ma2	ma2	ma2	tc	tc	tc	tc	tc
Sample	Lip184	Lip302	Lip138	Lip139	Lip171	Lip148	Lip151	Lip157	Lip303	T18**
SiO_2	54.06	54.38	56.81	55.31	54.15	64.05	63.51	60.53	61.49	55.07
TiO_2	0.74	0.71	0.68	0.70	0.70	0.59	0.60	0.56	0.59	0.76
Al_2O_3	17.50	18.02	17.91	17.66	17.94	17.91	18.62	19.36	17.96	16.66
Fe_2O_3	8.77	9.02	8.78	8.69	8.87	4.38	4.34	4.39	4.62	9.00
MnO	0.14	0.15	0.16	0.16	0.16	0.07	0.08	0.09	0.12	0.15
MgO	4.28	3.24	3.05	4.24	3.97	1.41	0.93	0.86	0.73	4.23
CaO	8.48	7.02	8.07	8.20	8.50	5.38	5.75	5.59	5.64	8.02
Na_2O	2.65	2.37	2.54	2.84	2.84	2.86	2.69	3.34	3.35	2.45
K_2O	2.13	1.60	1.63	1.70	1.74	3.15	3.28	3.56	3.75	1.81
P_2O_5	0.19	0.16	0.17	0.17	0.17	0.20	0.20	0.20	0.22	0.20
LOI	1.06	3.32	0.20	0.33	0.95	0.00	0.00	1.52	1.52	1.65
Sc	34	32	-	27	35	-	-	-	-	-
V	243	252	246	275	237	64	63	56	61	257
Cr	25	15	b.d.l.	-	b.d.l.	b.d.l.	b.d.l.	10	b.d.l.	39
Co	33	31	28	27.8	33	6	6	7.5	7	34
Ni	13	14	13	29	b.d.l.	b.d.l.	b.d.l.	13	b.d.l.	25
Rb	43	50	52	56.9	56	131	128	125	118	56
Sr	513	851	790	649	828	726	793	674	1012	650
Y	15	24	23	19.5	24	23	26	22.3	42	26
Zr	51	73	95	80.3	96	170	169	151	130	120
Nb	b.d.l.	b.d.l.	7	7	7	11	14	12	9	9
Cs	-	-	-	2.1	-	-	-	4.7	-	-
Ba	542	467	486	452	520	772	783	718	696	459
La	32	28	23	23.3	32	42	44	40.8	48	37
Ce	73	69	45	45.9	49	76	75	76.6	90	58
Pr	-	-	-	5.56	-	-	-	9.07	-	-
Nd	-	-	-	22.3	-	-	-	32.6	-	-
Sm	-	-	-	4.9	-	-	-	6.3	-	-
Eu	-	-	-	1.3	-	-	-	1.41	-	-
Gd	-	-	-	3.92	-	-	-	5.03	-	-
Tb	-	-	-	0.66	-	-	-	0.8	-	-
Dy	-	-	-	3.34	-	-	-	3.98	-	-
Ho	-	-	-	0.72	-	-	-	0.82	-	-
Er	-	-	-	2.01	-	-	-	2.27	-	-
Tm	-	-	-	0.3	-	-	-	0.34	-	-
Yb	-	-	-	1.9	-	-	-	2.2	-	-
Lu	-	-	-	0.32	-	-	-	0.35	-	-
Ta	-	-	-	-	-	-	-	-	-	-
Hf	-	-	-	3	-	-	-	5	-	-
Pb	9	10	b.d.l.	11	5	b.d.l.	b.d.l.	18	20	b.d.l.
Th	b.d.l.	b.d.l.	b.d.l.	4.8	b.d.l.	b.d.l.	b.d.l.	11.1	11	b.d.l.
U	-	-	-	1.68	-	-	-	3.68	-	-
$^{87}Sr/^{86}Sr$	-	-	-	-	-	-	-	0.706409	-	-
$^{143}Nd/^{144}Nd$	-	-	-	-	-	-	-	0.512311	-	-
$^{206}Pb/^{204}Pb$	-	-	-	-	-	-	-	19.305	-	-
$^{207}Pb/^{204}Pb$	-	-	-	-	-	-	-	15.654	-	-
$^{208}Pb/^{204}Pb$	-	-	-	-	-	-	-	39.167	-	-

Table 1 (continued) - Major, trace element and Sr, Nd and Pb isotope data for Lipari samples

Eruptive Epoch	**4**	**5**								
Synthem	S. LE TORR.	BRUCA								
Lithosome	M. S.Angelo (lower p.)	M. S.Angelo (intermediate portion)								
Formation	T. del Corvo	Pulera								
	tc	pu	pu	pu	pu	pu	pu	pu	pu	pu
Sample	MSA3	LS9004	LS9006	LS9007	LS9008	LS9009	LS90010	LS90011	LS90012	LS90013
SiO_2	62.66	64.19	63.28	64.13	63.56	63.51	63.82	64.48	63.79	64.47
TiO_2	0.60	0.56	0.54	0.55	0.55	0.53	0.52	0.50	0.66	0.67
Al_2O_3	17.26	18.29	18.54	18.37	18.46	18.30	18.92	18.63	16.33	16.43
Fe_2O_3	4.66	4.33	4.17	4.51	4.05	4.01	3.47	4.04	6.48	6.66
MnO	0.13	0.11	0.11	0.11	0.11	0.12	0.12	0.12	0.11	0.12
MgO	0.88	0.96	1.32	1.52	1.25	0.94	1.37	1.47	2.69	1.36
CaO	5.64	5.30	5.23	4.95	5.19	5.58	4.89	4.22	4.08	4.19
Na_2O	3.34	2.80	3.19	2.27	3.20	3.41	3.50	2.76	2.03	2.20
K_2O	3.48	3.23	3.41	3.35	3.40	3.37	3.17	3.50	3.62	3.69
P_2O_5	0.22	0.23	0.21	0.24	0.23	0.23	0.22	0.28	0.21	0.21
LOI	1.13	0.00	0.00	0.00	0.00	0.00	0.00	0.00	0.00	0.00
Sc	-	13	16	-	16	16	15	11	19	15
V	57	59	55	57	57	57	49	48	138	136
Cr	b.d.l.	b.d.l.	b.d.l.	b.d.l.	b.d.l.	b.d.l.	b.d.l.	b.d.l.	41	40
Co	6	8	10	14	9	8	10	7	19	15.3
Ni	b.d.l.	b.d.l.	b.d.l.	b.d.l.	b.d.l.	b.d.l.	b.d.l.	b.d.l.	19	40
Rb	104	111	84	123	89	111	119	122	140	163
Sr	782	715	609	806	611	791	857	785	450	403
Y	28	24	22	28	22	26	29	27	27	25.4
Zr	172	165	119	166	120	155	169	155	157	151
Nb	13	13	12	14	14	12	15	13	16	16
Cs	-	-	-	-	-	-	-	-	-	6.1
Ba	685	743	737	732	740	753	630	891	519	559
La	49	44	40	41	39	37	38	37	41	43.2
Ce	88	71	75	83	70	79	58	73	70	82.5
Pr	-	-	-	-	-	-	-	-	-	9.66
Nd	-	28	37	27	31	31	b.d.l.	b.d.l.	b.d.l.	35.3
Sm	-	4.9	5.9	5.5	5	5.2	b.d.l.	b.d.l.	b.d.l.	6.5
Eu	-	1.6	1.5	1.6	1.6	1.7	b.d.l.	b.d.l.	b.d.l.	1.27
Gd	-	-	-	-	-	-	-	-	-	5.29
Tb	-	0.72	0.7	0.71	0.74	0.75	b.d.l.	b.d.l.	b.d.l.	0.88
Dy	-	-	-	-	-	-	-	-	-	4.46
Ho	-	-	-	-	-	-	-	-	-	0.91
Er	-	-	-	-	-	-	-	-	-	2.51
Tm	-	-	-	-	-	-	-	-	-	0.37
Yb	-	2.5	2.2	2.5	2.5	2.5	b.d.l.	b.d.l.	b.d.l.	2.5
Lu	-	0.38	0.34	0.38	0.39	0.39	b.d.l.	b.d.l.	b.d.l.	0.39
Ta	-	-	-	-	-	-	-	-	-	b.d.l.
Hf	-	4	4	4	5	5	b.d.l.	b.d.l.	b.d.l.	5
Pb	b.d.l.	b.d.l.	b.d.l.	b.d.l.	b.d.l.	b.d.l.	b.d.l.	b.d.l.	b.d.l.	21
Th	b.d.l.	b.d.l.	b.d.l.	b.d.l.	b.d.l.	b.d.l.	b.d.l.	b.d.l.	b.d.l.	13.2
U	-	2.6	3.8	2.7	3.2	3.3	b.d.l.	b.d.l.	b.d.l.	3.77
$^{87}Sr/^{86}Sr$	-	-	-	-	-	-	-	-	-	0.706850
$^{143}Nd/^{144}Nd$	-	-	-	-	-	-	-	-	-	0.512176
$^{206}Pb/^{204}Pb$	-	-	-	-	-	-	-	-	-	19.136
$^{207}Pb/^{204}Pb$	-	-	-	-	-	-	-	-	-	15.645
$^{208}Pb/^{204}Pb$	-	-	-	-	-	-	-	-	-	39.015

Table 1 (continued) - Major, trace element and Sr, Nd and Pb isotope data for Lipari samples

Eruptive Epoch 5

Synthem BRUCA

Lithosome M. S.Angelo (intermediate portion)

Formation Pulera

	pu	pu	pu	pu	pu	pu	pu	pu	pu	pu
Sample	LS90039	LS90040	Lcord	LS8802	LS8803	LS8804	LS8805	LS8806	T3*	Lip212
SiO_2	60.91	62.23	62.36	63.95	63.31	60.03	63.19	63.06	59.12	60.96
TiO_2	0.72	0.67	0.62	0.67	0.67	0.63	0.67	0.67	0.76	0.55
Al_2O_3	18.33	16.76	16.36	16.81	17.45	17.00	18.37	17.92	16.08	19.73
Fe_2O_3	7.24	6.88	6.54	6.31	6.22	6.22	6.34	6.34	7.91	4.45
MnO	0.13	0.11	0.07	0.13	0.13	0.14	0.13	0.13	0.15	0.08
MgO	2.32	2.25	2.38	2.38	2.20	2.58	2.13	2.34	4.26	0.85
CaO	4.34	4.37	5.07	4.11	4.17	8.27	3.63	3.79	7.30	5.96
Na_2O	2.14	2.35	2.49	2.07	2.35	1.71	2.05	2.29	1.92	3.50
K_2O	3.66	4.18	3.94	3.34	3.28	3.19	3.29	3.25	2.30	3.44
P_2O_5	1.74	0.74	0.17	0.23	0.22	0.23	0.20	0.21	0.20	0.20
LOI	1.74	0.74	0.00	0.00	0.00	0.00	0.00	0.00	1.59	0.26
Sc	-	-	-	23	22	18	17	20	25	19
V	136	139	110	133	127	128	133	143	213	62
Cr	50	32	30	40	40	43	38	36	70	b.d.l.
Co	20	17	20	19	19	22	12	14	26.4	5
Ni	21	17	b.d.l.	27	21	29	13	14	41	b.d.l.
Rb	143	143	160	144	139	101	114	135	103	108
Sr	517	582	499	496	480	397	360	444	406	768
Y	37	36	b.d.l.	30	27	24	23	26	22.9	23
Zr	211	197	190	171	165	119	132	159	105	159
Nb	20	18	b.d.l.	18	16	12	14	15	9	11
Cs	0	0	-	-	-	-	-	-	2.9	-
Ba	632	660	800	532	534	506	509	567	455	818
La	43	45	-	43	44	45	47	47	27.6	39
Ce	126	67	-	70	70	57	70	70	55.7	80
Pr	-	-	-	-	-	-	-	-	6.77	-
Nd	-	-	-	-	-	-	-	-	25.9	-
Sm	-	-	-	-	-	-	-	-	5.9	-
Eu	-	-	-	-	-	-	-	-	1.19	-
Gd	-	-	-	-	-	-	-	-	4.81	-
Tb	-	-	-	-	-	-	-	-	0.8	-
Dy	-	-	-	-	-	-	-	-	4.19	-
Ho	-	-	-	-	-	-	-	-	0.87	-
Er	-	-	-	-	-	-	-	-	2.34	-
Tm	-	-	-	-	-	-	-	-	0.37	-
Yb	-	-	-	-	-	-	-	-	2.4	-
Lu	-	-	-	-	-	-	-	-	0.37	-
Ta	-	-	-	-	-	-	-	-	b.d.l.	-
Hf	-	-	-	-	-	-	-	-	3	-
Pb	b.d.l.	b.d.l.	b.d.l.	b.d.l.	b.d.l.	b.d.l.	b.d.l.	b.d.l.	15	14
Th	b.d.l.	b.d.l.	b.d.l.	b.d.l.	b.d.l.	b.d.l.	b.d.l.	b.d.l.	7.9	b.d.l.
U	-	-	-	-	-	-	-	-	2.61	-
$^{87}Sr/^{86}Sr$	-	-	-	-	-	-	-	-	0.706133	-
$^{143}Nd/^{144}Nd$	-	-	-	-	-	-	-	-	0.512431	-
$^{206}Pb/^{204}Pb$	-	-	-	-	-	-	-	-	19.212	-
$^{207}Pb/^{204}Pb$	-	-	-	-	-	-	-	-	15.642	-
$^{208}Pb/^{204}Pb$	-	-	-	-	-	-	-	-	39.077	-

Table 1 (continued) - Major, trace element and Sr, Nd and Pb isotope data for Lipari samples

Eruptive Epoch	**5**	**6**								
Synthem	BRUCA	FONTANELLE								
Lithosome	M. S.Angelo (interm. p.)	M. S.Angelo (upper portion)			M.Chirica-Costa d'Agosto					
Formation	Pulera	Chiappe Lisce			M.Chirica- Costa d'Agosto					
	pu	ch2	ch2	ch2	cc	cc	cc	cc	cc	cc
Sample	Lip275	Lip283	MSA1	LS9005	Lip144	Lip281	MSA2	LS9001	LS9002	LS9003
SiO_2	62.75	59.12	60.38	61.55	60.73	60.31	58.96	60.49	60.73	59.19
TiO_2	0.67	0.73	0.70	0.63	0.71	0.71	0.72	0.63	0.62	0.60
Al_2O_3	16.94	16.66	16.18	17.36	17.44	16.60	16.46	17.46	17.44	16.88
Fe_2O_3	6.76	7.11	6.69	5.83	6.88	6.95	7.14	6.03	5.88	5.86
MnO	0.15	0.15	0.14	0.12	0.12	0.14	0.14	0.12	0.12	0.12
MgO	1.62	2.27	2.86	2.40	2.37	2.19	2.88	3.34	3.27	6.11
CaO	4.21	6.76	6.34	5.98	6.22	6.65	6.75	5.95	5.77	5.85
Na_2O	2.53	3.01	2.96	2.87	2.62	3.08	2.65	2.85	2.97	2.41
K_2O	3.52	3.35	3.02	3.00	2.71	3.16	3.00	2.89	2.98	2.75
P_2O_5	0.24	0.22	0.25	0.26	0.20	0.22	0.25	0.24	0.25	0.23
LOI	0.60	0.63	0.48	0.00	0.00	0.00	1.05	0.00	0.00	0.00
Sc	22	23	-	19	-	17	-	19	18	19
V	137	158	164	154	158	152	175	158	154	169
Cr	38	-	25	b.d.l.	29	b.d.l.	25	b.d.l.	b.d.l.	27
Co	21	20	20	14	21	16.9	19	16	18	20
Ni	27	13	17	11	11	22	17	15	b.d.l.	11
Rb	136	110	89	94	109	111	88	80	114	122
Sr	655	898	653	661	636	586	642	529	688	783
Y	32	25	28	23	26	22	26	22	26	28
Zr	182	149	154	137	169	131	150	117	158	170
Nb	12	8	9	10	11	11	11	13	14	17
Cs	-	-	-	-	-	2.4	-	-	-	-
Ba	613	659	651	640	747	622	592	675	645	628
La	54	46	43	38	47	36.2	44	38	37	35
Ce	91	82	81	66	88	69.4	71	69	67	69
Pr	-	-	-	-	-	7.98	-	-	-	-
Nd	-	-	35	-	-	30.9	-	27	26	-
Sm	-	-	6.3	-	-	6.1	-	4.7	4.9	-
Eu	-	-	1.7	-	-	1.34	-	1.4	1.4	-
Gd	-	-	-	-	-	4.8	-	-	-	-
Tb	-	-	0.75	-	-	0.75	-	0.7	0.7	-
Dy	-	-	-	-	-	4.19	-	-	-	-
Ho	-	-	-	-	-	0.79	-	-	-	-
Er	-	-	-	-	-	2.36	-	-	-	-
Tm	-	-	-	-	-	0.34	-	-	-	-
Yb	-	-	2.4	-	-	2.1	-	2.4	2.4	-
Lu	-	-	0.35	-	-	0.36	-	0.37	0.36	-
Ta	-	-	-	-	-	b.d.l.	-	-	-	-
Hf	-	-	5	-	-	4	-	4	4	-
Pb	19	17	b.d.l.	b.d.l.	b.d.l.	13	b.d.l.	b.d.l.	b.d.l.	b.d.l.
Th	19	11	b.d.l.	b.d.l.	b.d.l.	10.7	b.d.l.	b.d.l.	b.d.l.	b.d.l.
U	-	-	4.2	-	-	3.19	-	2.4	2.4	-
$^{87}Sr/^{86}Sr$	-	0.706162	-	-	-	0.706286	-	-	-	-
$^{143}Nd/^{144}Nd$	-	0.512430	-	-	-	0.512355	-	-	-	-
$^{206}Pb/^{204}Pb$	-	19.315	-	-	-	19.323	-	-	-	-
$^{207}Pb/^{204}Pb$	-	15.644	-	-	-	15.640	-	-	-	-
$^{208}Pb/^{204}Pb$	-	39.143	-	-	-	39.131	-	-	-	-

Table 1 (continued) - Major, trace element and Sr, Nd and Pb isotope data for Lipari samples

Eruptive Epoch	**6**	**7**								
Synthem	FONTAN.	SCOGLIERA SOTTO IL MONTE								
Lithosome	M.Chirica-C. d'Agosto	Punta del Perciato			Falcone					
Formation	M.Chirica-C. d'Agosto	Punta del Perciato			Falcone					
	cc1	pe1	pe1	pe1	fa1	fa2	fa2	fa2	fa2	fa2
Sample	Lip284	Lip95	Lip97	Lip99	Lip220	Lip38	Lip38A	Lip64	Lip65	Lip239
SiO_2	58.98	75.88	75.12	73.84	72.00	74.18	73.52	75.51	76.79	77.64
TiO_2	0.79	0.09	0.09	0.08	0.13	0.10	0.09	0.09	0.10	0.09
Al_2O_3	16.47	12.36	11.99	12.30	12.26	12.08	11.92	12.82	12.04	11.75
Fe_2O_3	8.21	1.46	1.53	1.34	2.17	1.82	1.65	1.56	1.64	1.47
MnO	0.16	0.00	0.07	0.00	0.00	0.00	0.00	0.00	0.00	0.00
MgO	2.56	0.06	0.64	0.07	0.08	0.09	0.08	0.06	0.07	0.06
CaO	6.60	0.38	0.86	0.09	0.24	0.12	0.32	0.00	0.00	0.00
Na_2O	2.49	0.71	3.89	0.76	1.15	1.11	1.10	0.66	0.57	0.58
K_2O	2.65	4.21	4.37	4.53	3.05	3.71	3.83	4.22	3.69	3.59
P_2O_5	0.19	4.44	0.01	4.36	4.45	5.06	4.53	4.80	4.68	4.43
LOI	0.90	0.02	1.43	0.02	0.04	0.03	0.03	0.03	0.02	0.02
Sc	24	b.d.l.	b.d.l.	b.d.l.	b.d.l.	b.d.l.	b.d.l.	b.d.l.	b.d.l.	b.d.l.
V	191	b.d.l.	b.d.l.	b.d.l.	15	b.d.l.	b.d.l.	b.d.l.	b.d.l.	b.d.l.
Cr	52	b.d.l.	b.d.l.	b.d.l.	b.d.l.	b.d.l.	b.d.l.	b.d.l.	b.d.l.	b.d.l.
Co	27	b.d.l.	b.d.l.	b.d.l.	b.d.l.	b.d.l.	b.d.l.	b.d.l.	b.d.l.	b.d.l.
Ni	23	b.d.l.	b.d.l.	b.d.l.	b.d.l.	b.d.l.	b.d.l.	b.d.l.	64	b.d.l.
Rb	95	209	270	313	249	343	319	335	323	254
Sr	609	18	12.2	13	80	47	53	20	12	9
Y	28	139	32.8	53	45	67	58	21	27	22
Zr	124	185	123	187	152	211	190	206	199	143
Nb	7	34	29	36	28	40	37	40	36	28
Cs	-	-	9.5	-	-	-	-	-	-	-
Ba	482	14	8	21	51	16	16	11	5	12
La	34	32	36.7	40	41	44	42	20	30	27
Ce	61	254	75.4	66	83	79	90	47	57	57
Pr	-	-	8.59	-	-	-	-	-	-	-
Nd	-	-	31	-	12	-	-	-	-	-
Sm	-	-	6.5	-	2.9	-	-	-	-	-
Eu	-	-	0.14	-	1	-	-	-	-	-
Gd	-	-	5.28	-	-	-	-	-	-	-
Tb	-	-	0.97	-	0.52	-	-	-	-	-
Dy	-	-	5.45	-	-	-	-	-	-	-
Ho	-	-	1.12	-	-	-	-	-	-	-
Er	-	-	3.45	-	-	-	-	-	-	-
Tm	-	-	0.53	-	-	-	-	-	-	-
Yb	-	-	3.7	-	1.9	-	-	-	-	-
Lu	-	-	0.54	-	0.28	-	-	-	-	-
Ta	-	-	2	-	-	-	-	-	-	-
Hf	-	-	6	-	2	-	-	-	-	-
Pb	22	b.d.l.	26	b.d.l.	-	b.d.l.	b.d.l.	b.d.l.	b.d.l.	b.d.l.
Th	b.d.l.	39	32.7	31	36	42	38	30	41	39
U	-	-	11.8	-	1.3	-	-	-	-	-
$^{87}Sr/^{86}Sr$	-	-	0.707538	-	-	-	-	-	-	-
$^{143}Nd/^{144}Nd$	-	-	0.512579	-	-	-	-	-	-	-
$^{206}Pb/^{204}Pb$	-	-	19.277	-	-	-	-	-	-	-
$^{207}Pb/^{204}Pb$	-	-	15.646	-	-	-	-	-	-	-
$^{208}Pb/^{204}Pb$	-	-	39.130	-	-	-	-	-	-	-

Table 1 (continued) - Major, trace element and Sr, Nd and Pb isotope data for Lipari samples

Eruptive Epoch	**7**							**8**		
Synthem	SCOGLIERA SOTTO IL MONTE							VALLE MURIA		
Lithosome	Falcone							M.Guardia-M.Giardina		
Formation	Falcone							M.Guardia		
	fa2	fa2	fa2	fa2	fa3	fa3	fa3	gu	gu	gu
Sample	Lip248	Lip292	Lip287	Lip290	Lip288A	Lip288A-E	Lip288B	Lip167	Lip237	Lip238
SiO_2	73.88	76.13	73.34	75.73	66.92	56.91	73.05	69.55	75.91	75.32
TiO_2	0.10	0.11	0.12	0.11	0.31	0.66	0.16	0.23	0.09	0.09
Al_2O_3	12.30	12.08	12.25	11.98	14.66	12.67	12.91	13.46	11.96	12.06
Fe_2O_3	1.56	1.56	1.74	1.60	3.96	9.54	2.43	3.13	2.05	1.70
MnO	0.00	0.08	0.09	0.07	0.12	0.19	0.10	0.00	0.00	0.00
MgO	0.07	0.11	0.10	0.10	0.76	4.94	0.29	0.09	0.06	0.08
CaO	0.22	0.61	0.69	0.58	3.22	9.37	1.30	0.91	0.03	0.00
Na_2O	0.74	4.05	3.68	3.91	4.01	3.18	3.94	2.09	0.61	0.74
K_2O	4.17	5.02	4.79	4.87	4.73	2.36	4.96	3.46	3.94	3.71
P_2O_5	4.53	0.02	0.01	0.04	0.17	0.18	0.05	3.74	4.36	4.64
LOI	0.00	0.23	3.20	1.00	1.14	2.23	0.80	0.06	0.02	0.02
Sc	b.d.l.	b.d.l.	b.d.l.	b.d.l.	b.d.l.	14	b.d.l.	11	b.d.l.	b.d.l.
V	b.d.l.	b.d.l.	b.d.l.	b.d.l.	53	111	12	41	b.d.l.	b.d.l.
Cr	b.d.l.	b.d.l.	b.d.l.	b.d.l.	40	49	b.d.l.	24	b.d.l.	b.d.l.
Co	b.d.l.	b.d.l.	b.d.l.	b.d.l.	8.4	12	b.d.l.	4	b.d.l.	b.d.l.
Ni	b.d.l.	b.d.l.	14	11	12	16	b.d.l.	b.d.l.	b.d.l.	b.d.l.
Rb	299	273.7	289	292	226	31	271.8	182	300	258
Sr	11	25.3	10.9	9.6	578	366	237.4	139	8.5	8
Y	52	30.5	39.9	16.3	33.3	22	45.6	29	19.1	43
Zr	163	150.8	132	132	126	49	143.1	121	126	137
Nb	29	25.5	32	32	24	-	27.1	20	32	27
Cs	-	-	14.9	12.3	10.8	-	-	-	11.4	-
Ba	17	5.7	6.2	9	398	166	97.6	164	8.4	13
La	38	22.9	38.4	28.8	44	20	39.1	44	27.2	37
Ce	78	67.5	81.4	58.2	88.5	61	87.9	65	58.4	70
Pr	-	-	9.68	5.94	10.3	-	-	-	4.97	-
Nd	-	-	34.4	19	36.9	-	-	-	16.1	-
Sm	-	-	7	3.7	7.9	-	-	-	3.5	-
Eu	-	-	0.13	0.11	0.8	-	-	-	0.11	-
Gd	-	-	6.21	2.95	6.09	-	-	-	2.98	-
Tb	-	-	1.15	0.54	1.03	-	-	-	0.54	-
Dy	-	-	6.61	2.94	5.57	-	-	-	3.87	-
Ho	-	-	1.37	0.62	1.15	-	-	-	0.68	-
Er	-	-	4.19	2.05	3.19	-	-	-	2	-
Tm	-	-	0.64	0.34	0.53	-	-	-	0.34	-
Yb	-	-	4.3	2.2	3.4	-	-	-	2.2	-
Lu	-	-	0.68	0.33	0.56	-	-	-	0.38	-
Ta	-	-	2.2	2.2	1.5	-	-	-	2.1	-
Hf	-	-	6	6	5	-	-	-	5	-
Pb	b.d.l.	18.3	29	45	26	7	29.7	b.d.l.	25	b.d.l.
Th	43	40	35.6	32.5	28	10	36.1	32	36.7	35
U	-	-	11.9	10.6	9.3	-	-	-	10.4	-
$^{87}Sr/^{86}Sr$	-	-	-	0.706398	-	0.705136	-	-	0.706626	-
$^{143}Nd/^{144}Nd$	-	-	-	0.512569	0.512374	0.512579	-	-	0.512558	-
$^{206}Pb/^{204}Pb$	-	-	-	19.287	19.333	-	-	-	19.306	-
$^{207}Pb/^{204}Pb$	-	-	-	15.634	15.649	-	-	-	15.664	-
$^{208}Pb/^{204}Pb$	-	-	-	39.104	39.174	-	-	-	39.200	-

Table 1 (continued) - Major, trace element and Sr, Nd and Pb isotope data for Lipari samples

Eruptive Epoch 8

Synthem	VALLE MURIA									
Lithosome	M.Guardia-M.Giardina						P. S. Giuseppe			
Formation	M.Guardia				M. Giardina			P. S. Giuseppe		
	gu	gu	gu	gu	gi	gi	gi	sg	sg	sg
Sample	Lip249	Lip252	Lip276	Lip277	Lip293	Lip294	Lip295	Lip60	Lip62	Lip72
SiO_2	73.33	73.26	64.10	72.77	73.77	73.56	75.59	74.99	76.08	73.71
TiO_2	0.10	0.10	0.35	0.11	0.12	0.12	0.11	0.09	0.09	0.11
Al_2O_3	12.44	12.10	14.13	12.40	11.81	12.01	12.15	12.32	12.20	12.23
Fe_2O_3	1.66	1.65	5.01	1.86	1.56	1.81	1.82	1.78	1.72	2.00
MnO	0.00	0.00	0.12	0.10	0.09	0.09	0.08	0.00	0.00	0.00
MgO	0.08	0.08	1.64	0.11	0.09	0.12	0.16	0.08	0.08	0.08
CaO	0.12	0.10	3.86	0.70	0.69	0.74	0.29	0.02	0.00	0.15
Na_2O	0.80	0.80	3.33	4.42	3.70	3.95	3.10	0.76	0.71	1.01
K_2O	3.88	3.85	4.22	4.82	4.98	5.12	4.75	4.02	4.05	3.70
P_2O_5	4.54	4.46	0.15	0.01	0.01	0.02	0.01	4.94	4.57	4.91
LOI	0.03	0.00	3.08	2.70	3.19	2.47	1.94	0.02	0.05	0.03
Sc	b.d.l.	b.d.l.	11	b.d.l.	b.d.l.	b.d.l.	b.d.l.	b.d.l.	b.d.l.	b.d.l.
V	b.d.l.	b.d.l.	81	b.d.l.	b.d.l.	b.d.l.	b.d.l.	b.d.l.	b.d.l.	11
Cr	b.d.l.	b.d.l.	43	30	b.d.l.	b.d.l.	b.d.l.	b.d.l.	b.d.l.	b.d.l.
Co	b.d.l.	b.d.l.	14	1.2	b.d.l.	b.d.l.	b.d.l.	b.d.l.	b.d.l.	b.d.l.
Ni	b.d.l.	b.d.l.	17	22	b.d.l.	15	b.d.l.	b.d.l.	b.d.l.	b.d.l.
Rb	297	298	187.9	296	317.3	305	295.8	303	333	360
Sr	b.d.l.	13	694.5	18	26.1	8.8	23.7	16	20	65
Y	52	46	39	40.6	17.4	41.3	49.7	49	43	67
Zr	162	167	122.7	151	160.4	123	152.6	191	230	256
Nb	30	33	19.3	32	31.3	32	29.8	33	39	45
Cs	-	-	-	15.8	-	16	-	-	-	-
Ba	21	21	394.5	21.3	9	8.5	7.9	19	24	42
La	44	43	41.7	50.9	16.2	37.6	39.6	49	55	39
Ce	84	84	82.9	102	29.9	80.7	81.6	106	111	81
Pr	-	-	-	11.1	-	9.48	-	-	-	-
Nd	-	-	-	38.1	-	34.4	-	-	-	-
Sm	-	-	-	7.8	-	7.6	-	-	-	-
Eu	-	-	-	b.d.l.	-	0.12	-	-	-	-
Gd	-	-	-	6.51	-	6.34	-	-	-	-
Tb	-	-	-	1.14	-	1.16	-	-	-	-
Dy	-	-	-	6.16	-	6.73	-	-	-	-
Ho	-	-	-	1.31	-	1.39	-	-	-	-
Er	-	-	-	4.37	-	4.07	-	-	-	-
Tm	-	-	-	0.62	-	0.64	-	-	-	-
Yb	-	-	-	4.5	-	4.5	-	-	-	-
Lu	-	-	-	0.64	-	0.7	-	-	-	-
Ta	-	-	-	2.2	-	2.2	-	-	-	-
Hf	-	-	-	6	-	5	-	-	-	-
Pb	b.d.l.	b.d.l.	21.8	30	84.7	31	30.5	b.d.l.	b.d.l.	b.d.l.
Th	38	40	34.7	44.8	25.9	38.9	43.8	41	48	50
U	-	-	-	14.3	-	13	-	-	-	-
$^{87}Sr/^{86}Sr$	-	-	0.706029	-	-	0.706932	-	-	-	-
$^{143}Nd/^{144}Nd$	-	-	0.512396	-	-	0.512404	-	-	-	-
$^{206}Pb/^{204}Pb$	-	-	-	-	-	19.320	-	-	-	-
$^{207}Pb/^{204}Pb$	-	-	-	-	-	15.653	-	-	-	-
$^{208}Pb/^{204}Pb$	-	-	-	-	-	39.178	-	-	-	-

Table 1 (continued) - Major, trace element and Sr, Nd and Pb isotope data for Lipari samples

Eruptive Epoch	**8**									
Synthem	VALLE MURIA									
Lithosome	P. S.Giuseppe							Castello		V. Canneto Dentro
Formation	P. S.Giuseppe							Castello		V.ne Canneto
	sg	sg	sg	sg	sg	sg	sg	cas	cas	cd2
Sample	Lip250	Lip251	Lip254	Lip255	Lip289	Lip289-E	Lip301	Lip285	Lip286	Lip259
SiO_2	75.02	72.84	72.43	73.67	72.75	-	74.67	74.34	74.18	74.19
TiO_2	0.11	0.11	0.10	0.11	0.15	-	0.14	0.12	0.12	0.09
Al_2O_3	12.66	13.06	12.35	12.81	12.93	-	12.31	12.41	12.32	11.76
Fe_2O_3	1.78	1.84	1.75	1.80	2.34	-	2.03	1.92	1.90	1.69
MnO	0.00	0.00	0.00	0.00	0.10	-	0.09	0.11	0.10	0.08
MgO	0.08	0.08	0.08	0.08	0.56	-	0.35	0.12	0.26	0.01
CaO	0.16	0.17	0.13	0.18	1.56	-	1.11	0.73	0.71	0.70
Na_2O	0.81	0.75	0.78	0.76	4.20	-	4.24	4.33	4.36	3.55
K_2O	4.28	4.30	3.92	4.24	4.60	-	4.84	5.07	5.10	4.67
P_2O_5	4.60	4.76	4.55	4.62	0.04	-	0.04	0.03	0.00	0.01
LOI	0.01	0.00	0.01	0.02	0.76	-	0.17	0.82	0.95	3.25
Sc	b.d.l.	b.d.l.	b.d.l.	b.d.l.	b.d.l.	-	b.d.l.	b.d.l.	b.d.l.	b.d.l.
V	b.d.l.	b.d.l.	b.d.l.	b.d.l.	22	-	11	b.d.l.	b.d.l.	b.d.l.
Cr	b.d.l.	b.d.l.	b.d.l.	b.d.l.	b.d.l.	-	b.d.l.	b.d.l.	b.d.l.	b.d.l.
Co	b.d.l.	b.d.l.	b.d.l.	24	3.8	-	2.7	b.d.l.	b.d.l.	b.d.l.
Ni	b.d.l.	b.d.l.	b.d.l.	b.d.l.	20	-	12	b.d.l.	b.d.l.	b.d.l.
Rb	322	312	324	306	301	-	302	315	306.6	311
Sr	32	25	14	17	104	-	57.8	12.5	25.3	13.3
Y	36	35	48	50	41.6	-	30.1	41	51.2	41.5
Zr	201	190	201	197	150	-	146	155	182.8	157
Nb	36	31	36	34	33	-	33	34	31	37
Cs	-	-	-	-	16	-	11.2	16.5	-	16.7
Ba	41	34	26	28	84.3	-	48.4	14.6	10.3	16.1
La	38	46	58	50	53.2	-	44	51.7	45.7	51.6
Ce	74	84	99	100	110	-	86.9	103	102.3	103
Pr	-	-	-	-	12.8	-	9.93	11.4	-	11.4
Nd	-	-	-	-	44	-	34	38.7	-	39.5
Sm	-	-	-	-	9.4	-	7.4	7.8	-	8.1
Eu	-	-	-	-	0.29	-	0.19	0.11	-	0.11
Gd	-	-	-	-	7.54	-	5.13	6.39	-	6.34
Tb	-	-	-	-	1.31	-	0.95	1.17	-	1.14
Dy	-	-	-	-	7.01	-	5.4	6.78	-	6.6
Ho	-	-	-	-	1.44	-	1.03	1.41	-	1.34
Er	-	-	-	-	4.22	-	2.98	4.41	-	4.43
Tm	-	-	-	-	0.63	-	0.51	0.71	-	0.71
Yb	-	-	-	-	4.4	-	3.4	4.6	-	4.6
Lu	-	-	-	-	0.7	-	0.63	0.73	-	0.68
Ta	-	-	-	-	2.1	-	2.2	2.3	-	2.2
Hf	-	-	-	-	6	-	6	6	-	6
Pb	b.d.l.	b.d.l.	b.d.l.	b.d.l.	28	-	24	30	29.9	30
Th	49	46	50	51	43.3	-	42.7	46.6	54.6	44.9
U	-	-	-	-	13.6	-	12.5	14.8	-	14.6
$^{87}Sr/^{86}Sr$	-	-	-	-	0.705080	0.705005	0.706014	-	-	0.707075
$^{143}Nd/^{144}Nd$	-	-	-	-	0.512634	0.512589	0.512292	-	-	0.512409
$^{206}Pb/^{204}Pb$	-	-	-	-	19.305	-	19.307	-	-	19.314
$^{207}Pb/^{204}Pb$	-	-	-	-	15.630	-	15.630	-	-	15.629
$^{208}Pb/^{204}Pb$	-	-	-	-	39.102	-	39.101	-	-	39.108

Table 1 (continued) - Major, trace element and Sr, Nd and Pb isotope data for Lipari samples

Eruptive Epoch	**8**		**9**							
Synthem	V. MURIA	VALLONE FIUME BIANCO								
Lithosome	Capo Rosso	V.ne del Gabellotto-M.Pilato				Forgia Vecchia	M.Pilato			
Formation	Capo Rosso	V.ne del Gabellotto	Pomiciazzo			Forgia Vecchia	Lami		Fossa delle Rocche Rosse	
	cr	vg	po	po	po	fv2	lm	lm	ffr1	ffr2
Sample	Lip297	Lip278	Lip296	Lip265	Lip300	Lip272	Lip299	Lip268	Lip298	Lip273A
SiO_2	74.77	73.87	73.29	74.93	73.66	74.20	72.66	73.82	71.65	74.50
TiO_2	0.12	0.12	0.14	0.09	0.11	0.12	0.12	0.09	0.12	0.12
Al_2O_3	12.61	12.31	11.99	12.15	12.19	12.48	12.27	11.97	12.15	12.21
Fe_2O_3	1.92	1.89	1.93	1.95	1.76	2.01	1.98	1.82	2.06	2.02
MnO	0.10	0.10	0.11	0.09	0.09	0.10	0.10	0.08	0.10	0.11
MgO	0.16	0.11	0.12	0.01	0.14	0.11	0.15	0.01	0.16	0.13
CaO	0.75	0.72	0.82	0.76	0.70	0.75	0.76	0.69	0.77	0.77
Na_2O	4.09	3.98	4.66	4.34	4.17	4.26	4.12	4.16	4.12	4.47
K_2O	5.02	4.93	5.64	4.94	4.75	5.07	4.91	4.89	5.02	5.15
P_2O_5	0.01	0.02	0.00	0.02	0.01	0.02	0.01	0.01	0.02	0.00
LOI	0.45	1.97	1.29	0.72	2.42	0.88	2.92	2.46	3.84	0.52
Sc	b.d.l.	b.d.l.	b.d.l.	b.d.l.	b.d.l.	b.d.l.	b.d.l.	b.d.l.	b.d.l.	b.d.l.
V	b.d.l.	b.d.l.	b.d.l.	b.d.l.	b.d.l.	b.d.l.	b.d.l.	b.d.l.	b.d.l.	b.d.l.
Cr	b.d.l.	b.d.l.	b.d.l.	b.d.l.	b.d.l.	b.d.l.	b.d.l.	b.d.l.	b.d.l.	b.d.l.
Co	b.d.l.	1.1	1.1	b.d.l.	b.d.l.	b.d.l.	b.d.l.	b.d.l.	b.d.l.	b.d.l.
Ni	b.d.l.	b.d.l.	b.d.l.	b.d.l.	b.d.l.	b.d.l.	13	b.d.l.	b.d.l.	b.d.l.
Rb	306	313	320	329	314.2	332	318	322	298	329
Sr	12.3	10.4	10.2	10.1	29.7	12.8	12.9	13.1	27.5	13.1
Y	42.5	41.3	39.8	42.6	53.9	43.2	41.9	42.5	53.1	43.9
Zr	149	150	155	155	185	171	164	166	195	170
Nb	33	34	35	35	31.2	36	35	36	29.6	35
Cs	14.9	16.6	15.2	17	-	17.9	17.2	17.7	-	17.5
Ba	16.2	12.7	15	14.8	8.5	16.7	17.9	18.9	6.7	16.3
La	54.8	53.1	51.7	53.1	58.7	65.7	64.5	66.1	65.6	65.7
Ce	107	104	101	106	119.2	125	123	123	120.7	126
Pr	11.9	11.8	11.1	11.5	-	13.6	13.3	13.5	-	13.8
Nd	41.2	39.5	37.7	39.9	-	45.4	45.1	45.9	-	46.5
Sm	8.6	8.1	7.9	8.4	-	9	8.5	8.8	-	8.5
Eu	0.14	0.13	0.16	0.13	-	0.15	0.13	0.14	-	0.14
Gd	6.59	6.7	6.26	6.57	-	6.97	6.81	6.92	-	7.11
Tb	1.18	1.21	1.17	1.2	-	1.25	1.2	1.21	-	1.22
Dy	6.9	6.71	6.58	6.83	-	7.14	7.28	6.98	-	6.93
Ho	1.44	1.36	1.37	1.44	-	1.43	1.46	1.51	-	1.45
Er	4.39	4.27	3.97	4.44	-	4.47	4.51	4.58	-	4.49
Tm	0.68	0.65	0.62	0.67	-	0.7	0.69	0.71	-	0.72
Yb	4.8	4.6	4.6	4.8	-	4.9	4.6	4.7	-	4.9
Lu	0.75	0.74	0.73	0.73	-	0.79	0.88	0.78	-	0.71
Ta	2.2	2.3	2.3	2.3	-	2.5	2.3	2.5	-	2.5
Hf	6	6	7	6	-	7	7	7	-	7
Pb	34	32	30	30	36.4	33	33	33	36	32
Th	46.5	44.8	47.2	46.7	54.3	50.2	50.3	49.5	54.4	51.3
U	14.8	14.8	14.8	15.1	-	16	15.8	16.3	-	16
$^{87}Sr/^{86}Sr$		-	0.706349	-	-	-	-	-	-	0.706253
$^{143}Nd/^{144}Nd$	0.512561	-	0.512581	0.512539	-	-	-	0.512563	-	0.512554
$^{206}Pb/^{204}Pb$	19.316	-	19.315	19.329	-	-	-	19.329	-	19.324
$^{207}Pb/^{204}Pb$	15.639	-	15.627	15.670	-	-	-	15.670	-	15.635
$^{208}Pb/^{204}Pb$	39.136	-	39.109	39.229	-	-	-	39.229	-	39.127

Table 1 (continued) - Major, trace element and Sr, Nd and Pb isotope data for Lipari samples

Eruptive Epoch 9

Synthem VALLONE FIUME BIANCO
Lithosome M. Pilato

Formation Fossa delle Rocche Rosse

	ffr2	ffr2	ffr2	ffr2	ffr2
Sample	Lip274C	Lip274A	Lip273B	Lip274B	Lip273C
SiO_2	74.10	74.77	73.83	73.62	74.59
TiO_2	0.12	0.11	0.12	0.13	0.12
Al_2O_3	12.31	12.40	12.37	12.31	12.34
Fe_2O_3	1.98	1.86	2.04	2.11	2.03
MnO	0.10	0.10	0.10	0.11	0.10
MgO	0.26	0.11	0.11	0.13	0.13
CaO	0.76	0.70	0.76	0.79	0.78
Na_2O	4.27	4.42	4.18	4.42	4.27
K_2O	5.08	4.82	5.09	5.25	5.10
P_2O_5	0.02	0.01	0.00	0.03	0.00
LOI	0.99	0.70	1.39	1.11	0.54
Sc	b.d.l.	b.d.l.	b.d.l.	b.d.l.	b.d.l.
V	b.d.l.	b.d.l.	b.d.l.	b.d.l.	b.d.l.
Cr	b.d.l.	b.d.l.	b.d.l.	b.d.l.	b.d.l.
Co	b.d.l.	b.d.l.	b.d.l.	b.d.l.	b.d.l.
Ni	b.d.l.	b.d.l.	b.d.l.	b.d.l.	b.d.l.
Rb	326	309.4	313.3	311.2	319.6
Sr	12.2	30.8	30.6	32.3	30.6
Y	43	52.5	54.9	54.9	53.9
Zr	171	198.2	204	196.8	203
Nb	36	30.5	32.3	30.1	30.5
Cs	18	-	-	-	-
Ba	17.7	17.7	14.9	24.1	16.7
La	64.5	61.6	65.9	66.2	68.9
Ce	123	122.6	126	116.2	124.2
Pr	13.2	-	-	-	-
Nd	44	-	-	-	-
Sm	8.6	-	-	-	-
Eu	0.13	-	-	-	-
Gd	6.88	-	-	-	-
Tb	1.21	-	-	-	-
Dy	6.6	-	-	-	-
Ho	1.39	-	-	-	-
Er	4.42	-	-	-	-
Tm	0.71	-	-	-	-
Yb	4.7	-	-	-	-
Lu	0.81	-	-	-	-
Ta	2.5	-	-	-	-
Hf	7	-	-	-	-
Pb	32	28.7	29.9	33.7	27.1
Th	51.7	57.1	58	62.6	56.6
U	16	-	-	-	-
$^{87}Sr/^{86}Sr$	-	-	-	-	-
$^{143}Nd/^{144}Nd$	0.512581	-	-	-	-
$^{206}Pb/^{204}Pb$	19.330	-	-	-	-
$^{207}Pb/^{204}Pb$	15.659	-	-	-	-
$^{208}Pb/^{204}Pb$	39.203	-	-	-	-

b.d.l.= below detection limit

* Major element data from Bargossi et al. (1989)

** Major and trace element data from Bargossi et al., (1989)

Grey boxes indicate the samples analyzed for trace elements by ICP-AES and ICP-MS.

All the Sr and Nd isotope data have errors at 2σ of better than ±3 and ±2 in the fifth decimal place respectively.

All the Pb isotope data have external precisions of better than ±5 in the third decimal place for each ratio.

Table 2 - Composition of feldspars from selected rocks of Lipari

Eruptive Epoch	**1**									**2**					
Sample/Phenocryst	A3/1	A3/1	A3/2	A3/2	A3/3	A3/3	A3/4	A3/5	A3/6	Lip105/1	Lip105/1	Lip105/2	Lip105/3	Lip105/4	Lip105/5
Rock Composition	ba	ba	ba	ba	ba	ba	ba	ba	ba	ba	ba	ba	ba	ba	ba
Mineral	pl core	pl rim	pl core	pl rim	pl core	pl rim	pl gm	pl gm	pl gm	pl core	pl rim	pl core	pl rim	pl gm	pl (gx)
SiO2	47.79	46.95	48.77	51.42	48.03	49.35	51.83	52.47	53.23	51.58	51.18	51.58	50.98	52.18	51.51
Al2O3	32.36	32.49	31.92	29.57	32.48	31.17	28.65	29.14	28.84	29.75	29.98	29.77	29.59	30.24	29.64
FeO	0.77	0.9	0.78	1.25	0.9	0.99	1.11	1.15	1.25	1.06	0.85	1.02	1.06	0.87	0.93
CaO	15.85	16.08	15.62	13.14	16.08	14.45	11.85	12.57	11.76	13.47	13.6	13.38	13.31	13.86	13.35
Na2O	2.37	1.89	2.16	3.54	2.3	2.77	4.32	3.92	4.72	3.24	3.15	3.34	3.35	3.15	3.3
K2O	0.21	0.19	0.24	0.34	0.24	0.3	0.47	0.33	0.4	0.34	0.38	0.41	0.42	0.39	0.4
-----	-------	-------	-------	-------	-------	-------	-------	-------	-------	-------	-------	-------	-------	-------	-------
Tot.	99.35	98.5	99.49	99.26	100.03	99.03	98.23	99.58	100.2	99.44	99.14	99.5	98.71	100.69	99.13
Si	8.83	8.75	8.97	9.43	8.82	9.11	9.59	9.57	9.65	9.44	9.40	9.44	9.41	9.43	9.45
Al	7.05	7.14	6.92	6.39	7.03	6.78	6.25	6.27	6.17	6.42	6.49	6.42	6.44	6.44	6.41
Fe(3+)	0.12	0.14	0.12	0.19	0.14	0.15	0.17	0.18	0.19	0.16	0.13	0.16	0.16	0.13	0.14
Ca	3.14	3.21	3.08	2.58	3.16	2.86	2.35	2.46	2.29	2.64	2.68	2.62	2.63	2.68	2.63
Na	0.85	0.68	0.77	1.26	0.82	0.99	1.55	1.39	1.66	1.15	1.12	1.19	1.20	1.10	1.17
K	0.05	0.05	0.06	0.08	0.06	0.07	0.11	0.08	0.09	0.08	0.09	0.10	0.10	0.09	0.09
-----	-----	-----	-----	-----	-----	-----	-----	-----	-----	-----	-----	-----	-----	-----	-----
Tot.	20.04	19.97	19.92	19.94	20.03	19.96	20.03	19.94	20.05	19.89	19.90	19.92	19.94	19.88	19.90
An	77.7	81.5	78.8	65.9	78.3	72.9	58.6	62.7	56.6	68.2	68.9	67.2	67.0	69.2	67.4
Ab	21.0	17.3	19.7	32.1	20.3	25.3	38.6	35.4	41.1	29.7	28.9	30.4	30.5	28.5	30.2
Or	1.2	1.1	1.4	2.0	1.4	1.8	2.8	2.0	2.3	2.0	2.3	2.5	2.5	2.3	2.4

Table 2 (continued) - Composition of feldspars from selected rocks of Lipari

Eruptive Epoch	**2**									**3**			4		
Sample/Phenocryst	T9/1	T9/2	T9/3	T9/3	T9/4	T9/5	T9/5	T9/6	T9/7	Lip211/1	Lip211/1	Lip211/2	Lip157/3	Lip157/3	Lip157/4
Rock Composition	a	a	a	a	a	a	a	a	a	ba	ba	ba	a	a	a
Mineral	pl	pl	pl core	pl rim	pl gm	pl (xeno) core	pl (xeno) rim	pl (xeno)	pl (xeno)	pl core	pl rim	pl gm	pl core	pl rim	pl core
SiO2	49.39	49.44	52.95	51.22	48.31	51.73	52.58	46.32	49.16	46.61	49.23	46.66	53.03	48.62	48.6
Al2O3	31.93	31.33	30.2	30.61	31.69	30.41	29.46	34.5	32.22	33.26	29.51	33.46	30.28	32.95	32.71
FeO	0.91	0.6	0.46	0.59	2.02	0.62	0.68	0.93	0.57	0.73	2.91	0.6	0.52	0.5	0.46
CaO	15.34	14.61	12.75	13.47	15.26	13.63	12.63	17.25	15.02	16.92	15.08	17.24	12.46	15.8	15.53
Na2O	2.31	2.59	3.76	3.4	1.99	3.33	3.99	1.36	2.66	1.66	2.01	1.72	3.95	2.45	2.44
K2O	0.43	0.47	0.52	0.54	0.36	0.52	0.63	0.2	0.37	0.19	0.46	0.22	0.56	0.36	0.31
-----	-------	-------	-------	-------	-------	-------	-------	-------	-------	-------	-------	-------	-------	-------	-------
Tot.	100.31	99.04	100.64	99.83	99.63	100.24	99.97	100.56	100	99.37	99.2	99.9	100.8	100.68	100.05
Si	9.02	9.12	9.55	9.35	8.90	9.40	9.57	8.48	8.99	8.63	9.12	8.61	9.55	8.86	8.90
Al	6.87	6.81	6.42	6.58	6.88	6.51	6.32	7.45	6.95	7.26	6.45	7.27	6.42	7.08	7.06
Fe(3+)	0.14	0.09	0.07	0.09	0.31	0.09	0.10	0.14	0.09	0.11	0.45	0.09	0.08	0.08	0.07
Ca	3.00	2.89	2.46	2.63	3.01	2.65	2.46	3.39	2.94	3.36	2.99	3.41	2.40	3.08	3.05
Na	0.82	0.93	1.31	1.20	0.71	1.17	1.41	0.48	0.94	0.60	0.72	0.62	1.38	0.87	0.87
K	0.10	0.11	0.12	0.13	0.09	0.12	0.15	0.05	0.09	0.05	0.11	0.05	0.13	0.08	0.07
-----	-----	-----	-----	-----	-----	-----	-----	-----	-----	-----	-----	-----	-----	-----	-----
Tot.	19.94	19.95	19.93	19.98	19.90	19.95	20.00	19.99	20.00	20.00	19.84	20.05	19.96	20.04	20.01
An	76.6	73.6	63.2	66.5	79.1	67.2	61.3	86.5	74.1	84.0	78.3	83.6	61.4	76.5	76.5
Ab	20.9	23.6	33.7	30.4	18.7	29.7	35.0	12.3	23.8	14.9	18.9	15.1	35.3	21.4	21.7
Or	2.6	2.8	3.1	3.2	2.2	3.0	3.6	1.2	2.2	1.1	2.9	1.3	3.3	2.1	1.8

Table 2 (continued) - Composition of feldspars from selected rocks of Lipari

Eruptive Epoch	**4**					**5**		**6**					**7**		
Sample/Phenocryst	Lip157/4	Lip157/4	Lip157/4	Lip157/5	Lip157/6	T3/1	T3/2	Lip281/1	Lip281/1	Lip281/2	Lip281/2	Lip281/3	Lip288A/1	Lip288A/1	Lip288A/2
Rock Composition	a	a	a	a	a	a	a	a	a	a	a	a	d	d	d
Mineral	pl core	pl rim	pl rim	pl (mt)	pl gm	pl	pl	pl core	pl rim	pl core	pl rim	pl gm	pl (xeno) core	pl (xeno) rim	pl (xeno) core
SiO2	47.23	49.34	47.72	51.58	49.71	51.91	48.42	54.6	54.04	52.77	53.49	50.74	54.15	52.7	52.49
Al2O3	33.65	32.23	33.59	30.24	32.37	30.11	32.74	28.01	28.67	28.98	29.83	30.21	28.57	30.03	29.36
FeO	0.45	0.33	0.43	1.42	0.38	0.69	0.4	0.43	0.39	0.43	0.4	0.47	0.64	0.58	0.5
CaO	16.79	15.25	16.4	12.67	15.22	13.46	15.49	10.53	10.94	11.53	12.12	13.25	10.89	12.39	11.79
Na2O	1.94	2.66	2.01	3.6	2.7	3.39	2.16	4.59	4.56	4.12	4.01	3.35	4.13	3.69	4.02
K2O	0.22	0.26	0.24	0.65	0.32	0.59	0.31	0.88	0.78	0.66	0.7	0.44	1.17	0.89	1.05
-----	-------	-------	-------	-------	-------	-------	-------	-------	-------	-------	-------	-------	-------	-------	-------
Tot.	100.28	100.07	100.39	100.16	100.7	100.15	99.52	99.04	99.38	98.49	100.55	98.46	99.55	100.28	99.21
Si	8.66	9.01	8.72	9.39	9.03	9.44	8.90	9.95	9.83	9.70	9.64	9.38	9.84	9.55	9.61
Al	7.27	6.94	7.24	6.49	6.93	6.45	7.09	6.02	6.15	6.28	6.34	6.58	6.12	6.41	6.34
Fe(3+)	0.07	0.05	0.07	0.22	0.06	0.11	0.06	0.07	0.06	0.07	0.06	0.07	0.10	0.09	0.08
Ca	3.30	2.99	3.21	2.47	2.96	2.62	3.05	2.06	2.13	2.27	2.34	2.62	2.12	2.41	2.31
Na	0.69	0.94	0.71	1.27	0.95	1.20	0.77	1.62	1.61	1.47	1.40	1.20	1.46	1.30	1.43
K	0.05	0.06	0.06	0.15	0.07	0.14	0.07	0.21	0.18	0.16	0.16	0.10	0.27	0.21	0.25
-----	-----	-----	-----	-----	-----	-----	-----	-----	-----	-----	-----	-----	-----	-----	-----
Tot.	20.04	19.99	20.01	19.98	20.00	19.95	19.95	19.92	19.96	19.94	19.94	19.95	19.91	19.95	20.02
An	81.7	74.9	80.7	63.5	74.3	66.3	78.3	53.0	54.4	58.3	60.0	66.8	55.1	61.6	58.0
Ab	17.1	23.6	17.9	32.6	23.8	30.2	19.8	41.8	41.0	37.7	35.9	30.6	37.8	33.2	35.8
Or	1.3	1.5	1.4	3.9	1.9	3.5	1.9	5.3	4.6	4.0	4.1	2.6	7.0	5.3	6.1

Table 2 (continued) - Composition of feldspars from selected rocks of Lipari

Eruptive Epoch	**7**											**8**			
Sample/Phenocryst	Lip288A/2	Lip288A/3	Lip288A/3	Lip288A/4	Lip288A/4	Lip288A/5	Lip288A/5	Lip288A/5	Lip288A/6	Lip288A/6	Lip288A/6	Lip237/1	Lip237/1	Lip237/2	Lip237/2
Rock Composition	d	d	d	d	d	d	d	d	d	d	d	r	r	r	r
Mineral	pl (xeno) rim	pl (enclave) core	pl (enclave) rim	pl (enclave) core	pl (enclave) rim	kfeld core	kfeld rim	pl (kfeld)	kfeld core	kfeld rim	pl (kfeld)	pl core	kfeld rim	kfeld core	kfeld rim
SiO2	53.41	52.79	52.88	52.46	51.27	65.34	65.09	61.79	65.48	65.31	62.88	62.97	78.01	66.21	65.19
Al2O3	29.17	29.78	29.44	29.47	30.41	18.84	18.73	23.96	18.81	18.92	23.22	22.95	12.68	19.07	18.87
FeO	0.56	0.53	0.58	0.75	0.52	0	0	0.12	0	0	0	0.16	0.3	0	0.09
CaO	11.52	12.16	12.01	11.89	13.21	0.18	0.14	5.18	0.12	0	4.58	4.28	0.55	0.18	0.16
Na2O	3.94	3.6	3.99	3.84	3.48	3.15	3.2	7.55	3.2	3.19	8.21	8.2	3.97	3.23	3.38
K2O	1.09	0.92	1.01	0.84	0.71	11.54	11.77	0.91	11.76	11.77	1.16	1.13	4.31	11.78	11.66
-----	-------	-------	-------	-------	-------	-------	-------	-------	-------	-------	-------	-------	-------	-------	-------
Tot.	99.69	99.78	99.91	99.25	99.6	99.05	98.93	99.51	99.37	99.19	100.05	99.69	99.82	100.47	99.35
Si	9.71	9.60	9.62	9.60	9.38	11.98	11.97	11.01	11.98	11.97	11.15	11.197	13.421	11.97	11.94
Al	6.25	6.38	6.31	6.35	6.56	4.07	4.06	5.03	4.06	4.09	4.85	4.81	2.571	4.06	4.07
Fe(3+)	0.09	0.08	0.09	0.12	0.08	0.00	0.00	0.02	0.00	0.00	0.00	0.024	0.043	0.00	0.01
Ca	2.25	2.37	2.34	2.33	2.59	0.04	0.03	0.99	0.02	0.00	0.87	0.815	0.101	0.04	0.03
Na	1.39	1.27	1.41	1.36	1.23	1.12	1.14	2.61	1.14	1.13	2.82	2.827	1.324	1.13	1.20
K	0.25	0.21	0.23	0.20	0.17	2.70	2.76	0.21	2.74	2.75	0.26	0.256	0.946	2.72	2.72
-----	-----	-----	-----	-----	-----	-----	-----	-----	-----	-----	-----	-----	-----	-----	-----
Tot.	19.94	19.91	20.00	19.95	20.00	19.90	19.96	19.87	19.94	19.93	19.96	19.929	18.406	19.92	19.98
An	57.8	61.5	58.8	59.9	64.9	0.9	0.7	26.0	0.6	0.0	22.0	20.91	4.26	0.9	0.8
Ab	35.7	33.0	35.3	35.0	30.9	29.1	29.0	68.6	29.1	29.2	71.4	72.52	55.84	29.1	30.3
Or	6.5	5.5	5.9	5.0	4.2	70.0	70.3	5.4	70.3	70.8	6.6	6.57	39.90	70.0	68.9

Table 2 (continued) - Composition of feldspars from selected rocks of Lipari

Eruptive Epoch	
Sample/Phenocryst	Lip289/1
Rock Composition	r
Mineral	pl (enclave)
SiO2	56
Al2O3	27.09
FeO	0.81
CaO	9.33
Na2O	5.13
K2O	1.32
-----	-------
Tot.	99.68
Si	10.14
Al	5.78
Fe(3+)	0.12
Ca	1.81
Na	1.80
K	0.31
-----	-----
Tot.	19.96
An	46.2
Ab	46.0
Or	7.8

Notes: ba= basaltic andesite; a=andesite; d=dacite; r=rhyolite; gm= ground mass; kfeld= alcali feldspar; pl= plagioclase; pl (gx)= plagioclase within gabbroic xenoliths; pl (xeno)= plagioclase xenocrysts or plagiocalse within metamorphic xenoliths; pl (enclave)= plagioclase within mafic enclaves; pl (kfeld)= plagioclase within kfeld phenocryst; pl (mt)= plagioclase within Ti-magnetite phenocryst.

Table 3 - Composition of pyroxenes from selected rocks of Lipari

Eruptive Epoch	**1**								**2**						
Sample/Phenocryst	A3/1	A3/1	A3/1	A3/1	A3/2	A3/2	A3/2	A3/3	Lip105/1	Lip105/2	Lip105/3	Lip105/4	Lip105/5	Lip105/5	Lip105/6
Rock Composition	ba	ba	ba	ba	ba	ba	ba	ba	ba	ba	ba	ba	ba	ba	ba
Mineral	cpx core	cpx core	cpx rim	cpx rim	cpx core	cpx interm	cpx rim	cpx gm	cpx	cpx	cpx (gx)	cpx (gx)	opx core	opx rim	opx
SiO2	51.37	51.35	51.79	52.27	51.5	51.51	51.39	51.2	52.29	53.36	53.21	50.98	54.74	54.3	52.76
TiO2	0.39	0.4	0.44	0.21	0.29	0.22	0.27	0.47	0.16	0.13	0	0.37	0.14	0.23	0.18
Al2O3	3.63	3.45	2.67	2.55	3.36	2.51	2.56	3.45	2.42	2.26	1.8	3.15	1.4	1.32	2.12
Cr2O3	0	0	0	0	0.22	0	0	0	0	0.45	0.39	0.17	0	0	0
FeO	9.44	9.87	15.82	10.44	8.37	9.07	8.2	8.92	9.51	4.8	3.5	8.87	13.95	13.75	13.73
MnO	0.35	0.19	0.2	0.27	0.26	0.39	0.22	0.41	0.27	0	0	0.21	0.35	0.39	0.39
MgO	15.93	16.15	14.52	15.8	15.52	17.27	17.53	15.88	18.07	17.78	17.88	17.21	27.77	27.41	26.93
CaO	19.45	18.54	14.67	16.92	18.95	17.93	18.48	18.73	16.39	21.16	22.43	17.54	2.18	2.09	2.26
Na2O	0.39	0.52	0.47	0.44	0.52	0.6	0.45	0.61	0.47	0.49	0.21	0.56	0	0	0.71
-----	---------	---------	---------	---------	---------	---------	---------	---------	---------	---------	---------	---------	---------	---------	---------
Tot.	101	100.5	100.6	98.9	99	99.5	99.1	99.7	99.6	100.4	99.4	99.1	100.5	99.5	99.1
Si	1.88	1.88	1.94	1.96	1.92	1.9	1.9	1.89	1.92	1.93	1.94	1.88	1.95	1.96	1.9
Al(z)	0.12	0.12	0.06	0.04	0.08	0.1	0.1	0.11	0.08	0.07	0.06	0.12	0.05	0.04	0.09
Al(vi)	0.04	0.03	0.06	0.07	0.07	0.01	0.01	0.04	0.03	0.03	0.02	0.02	0.01	0.02	0
Ti	0.01	0.01	0.01	0.01	0.01	0.01	0.01	0.01	0	0	0	0.01	0	0.01	0
Cr	0	0	0	0	0.01	0	0	0	0	0.01	0.01	0	0	0	0
Fe3+	0.1	0.1	0.02	0	0.04	0.13	0.12	0.09	0.08	0.06	0.05	0.11	0.03	0.02	0.15
Fe2+	0.19	0.2	0.48	0.33	0.22	0.15	0.14	0.19	0.22	0.09	0.06	0.17	0.39	0.4	0.26
Mn	0.01	0.01	0.01	0.01	0.01	0.01	0.01	0.01	0.01	0	0	0.01	0.01	0.01	0.01
Mg	0.87	0.88	0.81	0.88	0.86	0.95	0.96	0.87	0.99	0.96	0.97	0.95	1.48	1.47	1.44
Ca	0.76	0.73	0.59	0.68	0.76	0.71	0.73	0.74	0.65	0.82	0.88	0.69	0.08	0.08	0.09
Na	0.03	0.04	0.03	0.03	0.04	0.04	0.03	0.04	0.03	0.03	0.01	0.04	0	0	0.05
-------	---------	---------	---------	---------	---------	---------	---------	---------	---------	---------	---------	---------	---------	---------	---------
Tot.	4.01	4	4.01	4.01	4.02	4.01	4.01	3.99	4.01	4	4	4	4	4.01	3.99
Q	1.82	1.81	1.88	1.89	1.84	1.81	1.83	1.8	1.86	1.87	1.91	1.81	1.95	1.95	1.79
J	0.06	0.08	0.06	0.06	0.08	0.08	0.06	0.08	0.06	0.06	0.02	0.08	0	0	0.1
J/(Q+J)	0.03	0.04	0.03	0.03	0.04	0.04	0.03	0.04	0.03	0.03	0.01	0.04	0	0	0.05
Ca	39.4	38	30.9	35.8	40.2	36.4	37.2	38.9	33.3	42.5	44.9	35.8	4	4	4.6
Mg	45.1	45.8	42.4	46.3	45.5	48.7	49	45.8	50.8	49.7	49.5	49.2	74.4	74.2	73.8
Fe*	15.5	16.1	26.7	17.9	14.3	14.9	13.8	15.3	15.9	7.8	5.6	15	21.6	21.7	21.5
Q	96.8	95.8	96.9	96.9	95.8	95.8	96.8	95.7	96.9	96.9	99	95.8	100	100	94.7
Ae	2.3	3.3	0.8	0	1.5	3.9	2.9	2.9	2.3	2.1	0.7	3.6	0	0	5.3
Jd	0.9	1	2.3	0	2.7	0.3	0.2	1.3	0.9	1	0.3	0.7	0	0	0
Mg#	0.75	0.75	0.62	0.73	0.77	0.77	0.79	0.76	0.77	0.86	0.9	0.77	0.78	0.78	0.78

Table 3 (continued) - Composition of pyroxenes from selected rocks of Lipari

Eruptive Epoch	**2**											**3**			
Sample/Phenocryst	Lip105/7	T9/1	T9/1	T9/2	T9/2	T9/3	T9/4	T9/4	T9/5	T9/6	T9/7	Lip211/1	Lip211/1	Lip211/2	Lip211/2
Rock Composition	ba	a	a	a	a	a	a	a	a	a	a	ba	ba	ba	ba
Mineral	opx gm	cpx core	cpx rim	opx core	opx rim	opx gm	opx core	opx rim	opx	opx (xenolith)	opx (xenolith)	cpx core	cpx rim	cpx core	cpx rim
SiO2	53.83	51.78	51.15	53.4	52.53	51.99	53.3	53.37	52.42	51.77	52.17	52.81	52.73	51.98	52.73
TiO2	0.11	0.28	0.4	0	0	0.5	0.18	0.18	0.4	0.38	0.33	0.27	0.23	0.26	0.22
Al2O3	1.54	2.81	3.44	1.48	1.71	1.55	1.74	2.08	2.26	1.49	1.41	2.48	2.55	2.69	2.28
Cr2O3	0	0.1	0.12	0	0	0	0	0	0	0	0	0.14	0.26	0.34	0.13
FeO	13.67	11.54	10.69	19.83	20.21	23.26	18.89	19.13	20.23	24.3	23.04	10.34	6.63	6.7	6.86
MnO	0.31	0.29	0.21	0.45	0.49	0.57	0.45	0.39	0.56	0.64	0.64	0.35	0.2	0.12	0.12
MgO	27.63	15.08	14.94	23.37	22.61	20.98	23.88	23.96	19.63	19.97	20.72	17.8	17.31	16.8	17.62
CaO	2.16	17.51	18.92	1.91	2.01	1.84	2.06	1.99	4.43	1.81	1.93	17.01	20.3	20.07	19.73
Na2O	0	0.53	0.45	0	0	0	0	0	0	0	0	0.34	0.42	0.39	0.47
-----	---	---	---	---	---	---	---	---	---	---	---	---	---	---	---
Tot.	99.3	99.9	100.3	100.4	99.6	100.7	100.5	101.1	99.9	100.4	100.2	101.5	100.6	99.4	100.2
Si	1.94	1.93	1.89	1.96	1.95	1.94	1.95	1.94	1.96	1.95	1.95	1.91	1.91	1.91	1.92
Al(z)	0.06	0.07	0.11	0.04	0.05	0.06	0.05	0.06	0.04	0.05	0.05	0.09	0.09	0.09	0.08
Al(vi)	0.01	0.05	0.04	0.02	0.03	0.01	0.03	0.03	0.06	0.02	0.01	0.02	0.02	0.03	0.02
Ti	0	0.01	0.01	0	0	0.01	0	0	0.01	0.01	0.01	0.01	0.01	0.01	0.01
Cr	0	0	0	0	0	0	0	0	0	0	0	0	0.01	0.01	0
Fe3+	0.05	0.05	0.07	0.02	0.02	0.03	0.02	0.03	0	0.02	0.01	0.07	0.07	0.06	0.08
Fe2+	0.37	0.31	0.26	0.59	0.6	0.69	0.56	0.56	0.63	0.74	0.71	0.24	0.13	0.15	0.13
Mn	0.01	0.01	0.01	0.01	0.02	0.02	0.01	0.01	0.02	0.02	0.02	0.01	0.01	0	0
Mg	1.49	0.84	0.82	1.28	1.25	1.17	1.3	1.3	1.1	1.12	1.16	0.96	0.94	0.92	0.96
Ca	0.08	0.7	0.75	0.08	0.08	0.07	0.08	0.08	0.18	0.07	0.08	0.66	0.79	0.79	0.77
Na	0	0.04	0.03	0	0	0	0	0	0	0	0	0.02	0.03	0.03	0.03
-------	---	---	---	---	---	---	---	---	---	---	---	---	---	---	---
Tot.	4.01	4.01	3.99	4	4	4	4	4.01	4	4	4	3.99	4.01	4	4
Q	1.94	1.85	1.83	1.95	1.93	1.93	1.94	1.94	1.91	1.93	1.95	1.86	1.86	1.86	1.86
J	0	0.08	0.06	0	0	0	0	0	0	0	0	0.04	0.06	0.06	0.06
J/(Q+J)	0	0.04	0.03	0	0	0	0	0	0	0	0	0.02	0.03	0.03	0.03
Ca	4	36.6	39.3	4	4.1	3.5	4.1	4	9.3	3.6	4	34	40.7	41.1	39.7
Mg	74.5	44	42.9	64.6	63.5	59.1	66	65.7	57	56.9	58.6	49.5	48.5	47.9	49.5
Fe*	21.5	19.4	17.8	31.3	32.5	37.4	29.9	30.3	33.7	39.6	37.4	16.5	10.8	10.9	10.8
Q	100	95.9	96.8	100	100	100	100	100	100	100	100	97.9	96.9	96.9	96.9
Ae	0	2.1	2	0	0	0	0	0	0	0	0	1.6	2.4	2.1	2.5
Jd	0	2.1	1.2	0	0	0	0	0	0	0	0	0.5	0.7	1	0.6
Mg#	0.78	0.7	0.71	0.68	0.67	0.62	0.69	0.69	0.64	0.6	0.62	0.76	0.82	0.81	0.82

Table 3 (continued) - Composition of pyroxenes from selected rocks of Lipari

Eruptive Epoch	**3**	**4**							**5**						
Sample/Phenocryst	Lip211/3	Lip157/1	Lip157/1	Lip157/1	Lip157/2	Lip157/3	Lip157/4	Lip157/5	T3/1	T3/2	T3/2	T3/3	T3/3	T3/3	T3/3
Rock Composition	ba	a	a	a	a	a	a	a	a	a	a	a	a	a	a
Mineral	opx gm	cpx core	cpx interm	cpx rim	opx	opx gm	opx (xenolith)	opx (xenolith)	cpx	cpx core	cpx rim	opx core	opx core	opx interm	cpx rim
SiO2	37.16	50.35	51.45	51.56	52.81	52.76	51.51	51.71	53.37	51.42	51.66	52.2	51.59	50.99	51.5
TiO2	0.1	0.56	0.52	0.38	0.19	0.18	0.29	0.32	0.2	0.46	0.34	0.3	0.27	0.24	0.52
Al2O3	0.59	3.3	2.81	2.28	1.38	1.72	2.55	1.65	1.71	2.67	3.46	2.23	2.26	2.17	3.56
Cr2O3	0	0.35	0.2	0	0	0	0	0	0	0.16	0	0	0	0	0
FeO	28.04	12.41	12.49	12.4	20.91	20.84	23.08	23.07	10.56	11.97	7.62	20.81	21.72	24.51	9.22
MnO	0.62	0.45	0.35	0.36	0.63	0.6	0.64	0.64	0.36	0.3	0.16	0.52	0.4	0.45	0.3
MgO	32.48	14.47	14.57	13.93	22.95	22.55	20.96	21.45	17.37	15.61	16.69	22.47	21.49	19.68	15.98
CaO	0.31	17.9	17.85	18.88	1.49	1.63	1.35	1.32	16.99	17.48	19.78	2.12	2.19	2.11	19.88
Na2O	0	1.17	0.49	0.53	0	0	0.56	0	0	0.44	0.33	0	0	0	0
-----	---------	---------	---------	---------	---------	---------	---------	---------	---------	---------	---------	---------	---------	---------	---------
Tot.	99.3	101	100.7	100.3	100.4	100.3	100.9	100.2	100.6	100.5	100	100.7	99.9	100.2	101
Si	1.34	1.85	1.91	1.92	1.95	1.95	1.9	1.93	1.96	1.9	1.89	1.92	1.92	1.92	1.89
Al(z)	0.03	0.14	0.09	0.08	0.05	0.05	0.1	0.07	0.04	0.1	0.11	0.08	0.08	0.08	0.11
Al(vi)	0	0	0.03	0.02	0.01	0.03	0.01	0	0.03	0.02	0.04	0.02	0.02	0.02	0.04
Ti	0	0.02	0.01	0.01	0.01	0.01	0.01	0.01	0.01	0.01	0.01	0.01	0.01	0.01	0.01
Cr	0	0.01	0.01	0	0	0	0	0	0	0	0	0	0	0	0
Fe3+	0.85	0.19	0.06	0.07	0.03	0.02	0.11	0.05	0	0.08	0.07	0.04	0.04	0.05	0.04
Fe2+	0	0.19	0.33	0.32	0.61	0.63	0.6	0.67	0.33	0.29	0.16	0.6	0.64	0.72	0.24
Mn	0.02	0.01	0.01	0.01	0.02	0.02	0.02	0.02	0.01	0.01	0	0.02	0.01	0.01	0.01
Mg	1.75	0.79	0.81	0.77	1.26	1.24	1.15	1.19	0.95	0.86	0.91	1.23	1.19	1.1	0.87
Ca	0.01	0.71	0.71	0.75	0.06	0.06	0.05	0.05	0.67	0.69	0.78	0.08	0.09	0.09	0.78
Na	0	0.08	0.04	0.04	0	0	0.04	0	0	0.03	0.02	0	0	0	0
-------	---------	---------	---------	---------	---------	---------	---------	---------	---------	---------	---------	---------	---------	---------	---------
Tot.	4	3.99	4.01	3.99	4	4.01	3.99	3.99	4	3.99	3.99	4	4	4	3.99
Q	1.76	1.69	1.85	1.84	1.93	1.93	1.8	1.91	1.95	1.84	1.85	1.91	1.92	1.91	1.89
J	0	0.16	0.08	0.08	0	0	0.08	0	0	0.06	0.04	0	0	0	0
J/(Q+J)	0	0.09	0.04	0.04	0	0	0.04	0	0	0.03	0.02	0	0	0	0
Ca	0.4	37.6	37	39.1	3	3	2.6	2.5	34.2	35.8	40.6	4.1	4.6	4.6	40.2
Mg	66.5	41.8	42.2	40.1	63.6	62.9	59.6	60.1	48.5	44.6	47.4	62.4	60.4	55.8	44.8
Fe*	33.1	20.6	20.8	20.8	33.3	34	37.8	37.4	17.3	19.7	12	33.5	35	39.6	14.9
Q	100	91.4	95.9	95.8	100	100	95.7	100	100	96.8	97.9	100	100	100	100
Ae	0	8.6	2.8	3.2	0	0	3.9	0	0	2.5	1.3	0	0	0	0
Jd	0	0	1.4	0.9	0	0	0.4	0	0	0.6	0.8	0	0	0	0
Mg#	0.67	0.68	0.68	0.66	0.66	0.66	0.62	0.62	0.74	0.7	0.8	0.66	0.64	0.59	0.76

Table 3 (continued) - Composition of pyroxenes from selected rocks of Lipari

Eruptive Epoch	**5**		**6**							**7**					
Sample/Phenocryst	T3/3	T3/4	Lip281/1	Lip281/1	Lip281/2	Lip281/3	Lip281/4	Lip281/5	Lip281/6	Lip288A/1	Lip288A/1	Lip288A/2	Lip288A/2	Lip288A/3	Lip288A/3
Rock Composition	a	a	a	a	a	a	a	a	a	d	d	d	d	d	d
Mineral	cpx rim	opx	cpx core	cpx rim	cpx gm	cpx (gx)	opx	opx	opx (gx)	cpx (xeno) core	cpx (xeno) rim	cpx (xeno) core	cpx (xeno) rim	cpx (enclave) core	cpx (enclave) rim
SiO2	51.11	50.99	50.93	52.03	51.46	50.86	50.69	52.67	50.11	50.47	49.72	49.8	50.81	50.73	50.56
TiO2	0.36	0.27	0.77	0.4	0.31	0.38	0.4	0.27	0.28	0.59	0.5	0.6	0.4	0.35	0.5
Al2O3	3.86	1.11	4.52	2.03	2.57	2.49	1.82	1.45	1.95	3.75	5.21	4.29	3.76	3.56	4.02
Cr2O3	0	0	0.18	0	0.11	0	0	0	0	0.2	0.13	0	0	0	0
FeO	6.17	28.35	12.35	11.21	10.31	12.54	24.81	21.64	22.77	8.64	7.76	9.17	9.37	8.48	9.78
MnO	0	0.68	0.41	0.31	0.2	0.24	0.77	0.73	0.42	0.25	0	0.11	0.21	0.18	0.21
MgO	16.86	17.49	12.02	14.49	14.62	14.13	19.2	21.91	20.64	14.05	14.29	13.52	13.82	14.06	13.45
CaO	20.2	1.15	17.79	19.76	19.74	18.32	2.06	1.49	2.33	21.83	22.14	21.63	21	21.68	20.83
Na2O	0	0	0.69	0.56	0.59	0.48	0	0	0	0.56	0.71	0.6	0.54	0.43	0.6
-----	---------	---------	---------	---------	---------	---------	---------	---------	---------	---------	---------	---------	---------	---------	---------
Tot.	98.6	100	99.7	100.8	99.9	99.4	99.8	100.2	98.5	100.3	100.5	99.7	99.9	99.5	100
Si	1.9	1.96	1.92	1.92	1.91	1.91	1.92	1.96	1.9	1.86	1.82	1.85	1.89	1.89	1.88
Al(z)	0.1	0.04	0.08	0.08	0.09	0.09	0.08	0.04	0.09	0.14	0.18	0.15	0.11	0.11	0.12
Al(vi)	0.07	0.01	0.12	0.01	0.02	0.02	0	0.02	0	0.02	0.05	0.04	0.06	0.05	0.06
Ti	0.01	0.01	0.02	0.01	0.01	0.01	0.01	0.01	0.01	0.02	0.01	0.02	0.01	0.01	0.01
Cr	0	0	0.01	0	0	0	0	0	0	0.01	0	0	0	0	0
Fe3+	0.02	0.02	0	0.08	0.09	0.08	0.05	0	0.09	0.11	0.15	0.12	0.08	0.08	0.08
Fe2+	0.17	0.9	0.39	0.26	0.23	0.32	0.74	0.67	0.63	0.16	0.09	0.17	0.21	0.19	0.23
Mn	0	0.02	0.01	0.01	0.01	0.01	0.02	0.02	0.01	0.01	0	0	0.01	0.01	0.01
Mg	0.93	1	0.68	0.8	0.81	0.79	1.09	1.21	1.17	0.77	0.78	0.75	0.77	0.78	0.75
Ca	0.8	0.05	0.72	0.78	0.79	0.74	0.08	0.06	0.09	0.86	0.87	0.86	0.84	0.86	0.83
Na	0	0	0.05	0.04	0.04	0.03	0	0	0	0.04	0.05	0.04	0.04	0.03	0.04
-------	---------	---------	---------	---------	---------	---------	---------	---------	---------	---------	---------	---------	---------	---------	---------
Tot.	4	4.01	4	3.99	4	4	3.99	3.99	3.99	4	4	4	4.02	4.01	4.01
Q	1.9	1.95	1.79	1.84	1.83	1.85	1.91	1.94	1.89	1.79	1.74	1.78	1.82	1.83	1.81
J	0	0	0.1	0.08	0.08	0.06	0	0	0	0.08	0.1	0.08	0.08	0.06	0.08
J/(Q+J)	0	0	0.05	0.04	0.04	0.03	0	0	0	0.04	0.05	0.04	0.04	0.03	0.04
Ca	41.7	2.5	40	40.4	40.9	38.1	4	3.1	4.5	45	46	45.3	44	44.8	43.7
Mg	48.4	50.3	37.8	41.5	42	40.7	55.1	61.7	58.8	40.3	41.3	39.5	40.3	40.6	39.5
Fe*	9.9	47.2	22.2	18.1	17.1	21.1	40.9	35.2	36.7	14.7	12.7	15.3	15.7	14.6	16.8
Q	100	100	94.7	95.8	95.8	96.9	100	100	100	95.7	94.6	95.7	95.8	96.8	95.8
Ae	0	0	0	3.7	3.4	2.5	0	0	0	3.6	4.1	3.2	2.4	2	2.4
Jd	0	0	0	0.5	0.8	0.6	0	0	0	0.7	1.4	1.1	1.8	1.2	1.8
Mg#	0.83	0.52	0.64	0.7	0.72	0.66	0.58	0.64	0.62	0.74	0.76	0.72	0.73	0.74	0.71

Table 3 (continued) - Composition of pyroxenes from selected rocks of Lipari

Eruptive Epoch	**7**						**8**					
Sample/Phenocryst	Lip288A/4	Lip288A/4	Lip288A/5	Lip288A/5	Lip288A/6	Lip288A/7	Lip289/1	Lip289/1	Lip289/2	Lip289/2	Lip289/3	Lip289/4
Rock Composition	d	d	d	d	d	d	r	r	r	r	r	r
Mineral	cpx (enclave) core	cpx (enclave) rim	cpx (enclave) core	cpx (enclave) rim	cpx (enclave) gm	cpx (enclave)	cpx (xeno) core	cpx (xeno) rim	cpx (enclave) core	cpx (enclave) rim	cpx (enclave) gm	cpx (enclave)
SiO2	50.42	49.96	50.87	48.28	51.49	51.7	52.9	51.19	50.89	51.02	53.04	52.07
TiO2	0.51	0.53	0.41	0.65	0.3	0.28	0.11	0.36	0.32	0.26	0.15	0.26
Al2O3	4.02	4.57	4.04	6.36	3.17	2.89	2.17	3	3.93	3.87	2.09	2.66
Cr2O3	0.09	0.12	0.3	0.22	0.86	0.18	0.35	0.08	0.1	0.16	0.92	0.09
FeO	8.55	9.5	5.54	7.88	4.23	4.1	4.65	8.12	8.63	7.51	3.7	8.94
MnO	0.28	0.19	0.13	0.11	0	0.11	0.09	0.26	0.24	0.08	0.05	0.2
MgO	14.06	13.55	15.49	13.62	16.32	16.61	17.05	15.68	15.01	15.11	18.22	15.62
CaO	21.83	21.07	22.82	22.1	22.76	22.98	21.98	20.23	20.56	21.13	21.49	19.83
Na2O	0.71	0.61	0.56	0.73	0.56	0.46	0.54	0.56	0.59	0.63	0.51	0
-----	---------	---------	---------	---------	---------	---------	---------	---------	---------	---------	---------	---------
Tot.	100.5	100.1	100.2	100	99.7	99.3	99.8	99.5	100.3	99.8	100.2	99.7
Si	1.85	1.85	1.86	1.78	1.88	1.89	1.93	1.89	1.87	1.88	1.92	1.93
Al(z)	0.15	0.15	0.14	0.22	0.12	0.11	0.07	0.11	0.13	0.12	0.08	0.07
Al(vi)	0.02	0.05	0.03	0.06	0.02	0.02	0.02	0.02	0.04	0.05	0.01	0.05
Ti	0.01	0.01	0.01	0.02	0.01	0.01	0	0.01	0.01	0.01	0	0.01
Cr	0	0	0.01	0.01	0.02	0.01	0.01	0	0	0	0.03	0
Fe3+	0.14	0.11	0.12	0.17	0.1	0.1	0.08	0.1	0.11	0.1	0.08	0
Fe2+	0.13	0.19	0.05	0.07	0.03	0.02	0.07	0.15	0.16	0.13	0.03	0.28
Mn	0.01	0.01	0	0	0	0	0	0.01	0.01	0	0	0.01
Mg	0.77	0.75	0.84	0.75	0.89	0.91	0.93	0.86	0.82	0.83	0.98	0.87
Ca	0.86	0.84	0.89	0.87	0.89	0.9	0.86	0.8	0.81	0.83	0.83	0.79
Na	0.05	0.04	0.04	0.05	0.04	0.03	0.04	0.04	0.04	0.04	0.04	0
-------	---------	---------	---------	---------	---------	---------	---------	---------	---------	---------	---------	---------
Tot.	3.99	4	3.99	4	4	4	4.01	3.99	4	3.99	4	4.01
Q	1.76	1.78	1.78	1.69	1.81	1.83	1.86	1.81	1.79	1.79	1.84	1.94
J	0.1	0.08	0.08	0.1	0.08	0.06	0.08	0.08	0.08	0.08	0.08	0
J/(Q+J)	0.05	0.04	0.04	0.06	0.04	0.03	0.04	0.04	0.04	0.04	0.04	0
Ca	45	44.2	46.8	46.8	46.6	46.6	44.3	41.7	42.4	43.9	43.2	40.5
Mg	40.3	39.5	44.2	40.3	46.6	47.2	47.9	44.8	42.9	43.9	51	44.6
Fe*	14.7	16.3	8.9	12.9	6.8	6.2	7.7	13.5	14.7	12.2	5.7	14.9
Q	94.6	95.7	95.7	94.4	95.8	96.8	95.9	95.8	95.7	95.7	95.8	100
Ae	4.7	3	3.4	4.1	3.5	2.6	3.3	3.5	3.1	2.9	3.7	0
Jd	0.7	1.3	0.9	1.5	0.7	0.5	0.8	0.7	1.1	1.4	0.5	0
Mg#	0.74	0.71	0.83	0.76	0.87	0.88	0.86	0.77	0.75	0.78	0.9	0.76

Notes: ba= basaltic andesite; a=andesite; d=dacite; r=rhyolite; gm= ground mass; cpx= clinopyroxene; opx=ortopyroxene; cpx (gx)= clinopyroxene within gabbroic xenoliths; opx (xenolith)= ortopyroxene within metamorphic xenoliths; cpx (xeno)= clinopyroxene xenocrysts ; cpx (enclave)= clinopyroxene within mafic enclaves.

Table 4 - Composition of olivines from selected rocks of Lipari

Eruptive Epoch	**2**	**3**		**8**
Sample/Phenocryst	Lip105/1	Lip211/1	Lip211/2	Lip289/1
Rock Composition	ba	ba	ba	r
Mineral	ol (gx)	ol	ol	ol (enclave)
SiO2	40.65	38.75	38.71	38.09
FeO	12.88	19.91	19.63	21.25
MnO	0.19	0.41	0.38	0.36
MgO	47.19	40.59	40.29	39.19
CaO	0.2	0.16	0.18	0.29
NiO	0	0	0	0
-----	--------	--------	--------	--------
Total	101.11	99.82	99.19	99.18
Si	1	1	1	1
Fe	0.26	0.43	0.43	0.46
Mn	0	0.01	0.01	0.01
Mg	1.73	1.56	1.56	1.53
Ca	0.01	0	0	0.01
Ni	0	0	0	0
---	---------	---------	---------	---------
Total	3	3	3	3.01
X_Mg	0.87	0.78	0.78	0.76
X_Fe	0.13	0.22	0.22	0.23
X_Mn	0	0.01	0.01	0
X_Ca	0.01	0	0	0
X_Ni	0	0	0	0
%Fo	87	78	78	76.8

Notes: ba= basaltic andesite; r=rhyolite; ol= olivine; ol (gx)= olivine within gabbroic xenoliths; ol (enclave)= olivine within mafic enclaves.

Table 5 - Composition of Fe-Ti oxides from selected rocks of Lipari

Eruptive Epoch	**1**		**2**		**4**			**5**			**6**				**7**
Sample/Phenocryst	A3/1	A3/2	T9/1	T9/2	Lip157/1	Lip157/2	Lip157/3	T3/1	T3/2	T3/3	Lip281/1	Lip281/2	Lip281/3	Lip281/4	Lip288A/1
Rock Composition	ba	ba	a	a	a	a	a	a	a	a	a	a	a	a	d
Mineral	mt	mt	her (xenolith)	ilm	mt	mt	mt (xenolith)	her (xenolith)	ilm	ilm	mt	mt	mt	her (gx)	mt
SiO2	0.74	0.43	0.36	0.47	1.91	0.48	0.67	0.42	0.43	0.28	0.61	0.49	0.54	48.62	0.6
TiO2	5.14	7.85	1.26	48.92	18.1	16.91	17.39	0.56	49.98	49.46	10.91	14.1	10.3	0	8.29
Al2O3	0.92	0.58	48.35	0.36	2.63	3.07	2.99	54.38	0.21	0.25	3.72	3.01	4.06	31.67	6.9
Cr2O3	0	0.14	0.35	0.29	0	0.18	0	0	0	0	0.13	0.09	0.14	0	0
FeO	82.05	77.92	37.01	46.95	70.46	73.8	73.09	33.86	48.06	41.1	77.28	74.49	76.24	0.55	73.57
MnO	0.19	0.36	0.13	0.44	0.76	0.55	0.41	0.37	0.23	0.9	0.47	0.38	0.36	0	0.45
MgO	1.76	2.33	9.69	2.24	1.42	1.79	2.02	7.83	0.67	3.37	1.93	1.41	1.93	0.38	4.11
CaO	0	0	0	0.2	0	0	0	0	0	0	0	0	0	14.96	0
-----	---------	---------	---------	---------	---------	---------	---------	---------	---------	---------	---------	---------	---------	---------	---------
Tot.	90.8	89.61	97.15	99.87	95.28	96.78	96.57	97.42	99.58	95.36	95.05	93.97	93.57	96.18	93.92
Fe2O3*	54.6	49.5	12.63	7.87	25.79	32.4	31.22	5.83	4.5	3.57	42.55	36.06	42.45	0	44.56
FeO*	32.91	33.38	25.64	39.86	47.25	44.64	45	28.61	44	37.88	39	42.04	38.04	0.53	33.48
-----	---------	---------	---------	---------	---------	---------	---------	---------	---------	---------	---------	---------	---------	---------	---------
Tot.	96.26	94.57	98.41	100.65	97.86	100.02	99.7	98	100.02	95.71	99.32	97.58	97.82	96.16	98.39
Si	0.029	0.017	0.01	0.012	0.071	0.018	0.025	0.012	0.011	0.007	0.023	0.019	0.02	1.416	0.022
Al	0.042	0.027	1.643	0.01	0.116	0.133	0.129	1.827	0.006	0.008	0.162	0.134	0.179	1.087	0.294
Ti	0.15	0.233	0.027	0.907	0.508	0.466	0.48	0.012	0.944	0.955	0.303	0.4	0.29	0	0.225
Cr	0	0.004	0.008	0.006	0	0.005	0	0	0	0	0.004	0.003	0.004	0	0
Fe3+	1.599	1.469	0.274	0.146	0.725	0.894	0.862	0.125	0.085	0.069	1.183	1.025	1.196	0	1.212
Fe2+	1.071	1.101	0.618	0.822	1.476	1.369	1.381	0.682	0.924	0.813	1.205	1.328	1.191	0.013	1.012
Mn	0.006	0.012	0.003	0.009	0.024	0.017	0.013	0.009	0.005	0.02	0.015	0.012	0.011	0	0.014
Mg	0.102	0.137	0.416	0.082	0.079	0.098	0.111	0.333	0.025	0.129	0.106	0.079	0.108	0.016	0.221
Ca	0	0	0	0.005	0	0	0	0	0	0	0	0	0	0.467	0
-------	---------	---------	---------	---------	---------	---------	---------	---------	---------	---------	---------	---------	---------	---------	---------
Tot.	2.999	3	2.999	1.999	2.999	3	3.001	3	2	2.001	3.001	3	2.999	2.999	3
Usp	17.9	25	3.7		57.9	48.4	50.5	2.4			32.6	41.9	31	141.6	24.7

Table 5 (continued) - Composition of Fe-Ti oxides from selected rocks of Lipari

Eruptive Epoch	**7**	**8**
Sample/Phenocryst	Lip288A/2	Lip289/1
Rock Composition	d	r
Mineral	mt (enclave)	mt (enclave)
SiO2	0.63	0.79
TiO2	8.77	4.63
Al2O3	6.54	5.84
Cr2O3	0.08	0.69
FeO	74.22	76.31
MnO	0.46	0.36
MgO	4.02	4.58
CaO	0	0
-----	---------	---------
Tot.	94.72	93.2
Fe2O3*	44.39	51.99
FeO*	34.26	29.52
-----	---------	---------
Tot.	99.15	98.4
Si	0.023	0.029
Al	0.277	0.25
Ti	0.237	0.126
Cr	0.002	0.02
Fe3+	1.201	1.42
Fe2+	1.03	0.896
Mn	0.014	0.011
Mg	0.215	0.248
Ca	0	0
-------	---------	---------
Tot.	2.999	3
Usp	26	15.5

Notes: ba= basaltic andesite; a=andesite; d= dacite; r= rhyolite; mt= magnetite; mt (xenoliths)= magnetite within metamorphic xenoliths; mt (enclave)= magnetite within mafic enclaves; ilm=ilmenite; her= hercinite; her (gx)=hercinite within gabbroic xenoliths; her (xenoliths)= hercinite within metamorphic xenoliths

Table 6 - Least-squares major element mass-balance models of fractional crystallization

Differentiation from Lip113 (CA basaltic andesite, Eruptive Epoch 2) to Lip157 (HKCA andesite, Eruptive Epoch 4)

	Bulk composition of		Obs diff between magmas	Calc diff between magmas	Obs-Calc (Residuals)
	Add	Subt			
SiO_2	0.00	49.06	7.704	7.663	0.041
TiO_2	0.00	0.45	-0.114	0.077	-0.191
Al_2O_3	0.00	12.50	4.402	4.356	0.046
Fe_2O_3	0.00	0.00	0.000	0.000	0.000
FeO	0.00	11.55	-4.439	-4.493	0.054
MnO	0.00	0.17	-0.102	0.170	-0.054
MgO	0.00	10.60	-5.787	-5.820	0.033
CaO	0.00	14.07	-4.959	-4.996	0.037
Na_2O	0.00	1.48	1.107	1.158	-0.050
K_2O	0.00	0.13	2.188	2.104	0.084

Sum of squares of residuals= 0.058

Sum of squares of residuals/(M-N)= 0.010

Phase	*Amount as wt% of initial magma	Amount as wt% of all phases	Amount as wt% of added phases	Amount as wt% of subt phases
Cpx (Lip113)	-32.77	54.77	0.00	54.77
Pl (Lip113)	-22.12	36.97	0.00	36.97
Ti-mt (Lip113)	-3.74	6.25	0.00	6.25
Opx (Lip113)	-1.20	2.00	0.00	2.00

*Calculated amounts of the phenocryst phases fractionated from Lip113 that best satisfy the least-squares approximation to the final composition (Lip157)

Table 7 - Least-squares major element mass-balance models of fractional crystallization

Differentiation from Lip113 (CA basaltic andesite, Eruptive Epoch 2) to Lip281 (HKCA andesite, Eruptive Epoch 6)

	Bulk composition of		Obs diff between magmas	Calc diff between magmas	Obs-Calc (Residuals)
	Add	Subt			
SiO_2	0.00	49.65	6.695	7.663	0.090
TiO_2	0.00	0.37	0.029	0.077	-0.176
Al_2O_3	0.00	14.51	1.375	4.356	0.054
Fe_2O_3	0.00	0.00	0.000	0.000	0.000
FeO	0.00	10.13	-2.167	-4.493	0.086
MnO	0.00	0.16	-0.051	0.170	-0.043
MgO	0.00	9.81	-4.453	-5.820	0.028
CaO	0.00	13.52	-3.965	-4.996	0.046
Na_2O	0.00	1.70	0.803	1.158	-0.029
K_2O	0.00	0.15	1.733	2.104	-0.057

Sum of squares of residuals= 0.058

Sum of squares of residuals/(M-N)= 0.010

Phase	*Amount as wt% of initial magma	Amount as wt% of all phases	Amount as wt% of added phases	Amount as wt% of subt phases
Cpx (Lip113)	-26.46	44.89	0.00	44.89
Pl (Lip113)	-26.10	44.28	0.00	44.28
Opx (Lip113)	-3.40	5.77	0.00	5.77
Ti-mt (Lip113)	-2.98	5.06	0.00	5.06

*Calculated amounts of the phenocryst phases fractionated from Lip113 that best satisfy the least-squares approximation to the final composition (Lip281)

Table 8 - Least-squares major element mass-balance models of fractional crystallization

Differentiation from A16 (CA basaltic andesite, Eruptive Epoch 2) to Lip97 (rhyolite, Eruptive Epoch 7)

	Bulk composition of		Obs diff between magmas	Calc diff between magmas	Obs-Calc (Residuals)
	Add	Subt			
SiO_2	0.00	48.32	20.993	20.865	0.128
TiO_2	0.00	0.89	-0.737	-0.598	-0.139
Al_2O_3	0.00	19.63	-5.477	-5.547	0.069
Fe_2O_3	0.00	0.00	0.000	0.000	0.000
FeO	0.00	10.42	-6.583	-6.717	0.134
MnO	0.00	0.15	-0.071	-0.057	-0.014
MgO	0.00	5.83	-3.869	-3.859	-0.010
CaO	0.00	12.00	-8.230	-8.289	0.059
Na_2O	0.00	1.96	1.404	1.488	-0.084
K_2O	0.00	0.31	2.793	3.070	-0.277
P_2O_5	0.00	0.49	-0.222	-0.356	0.134

Sum of squares of residuals= 0.164

Sum of squares of residuals/(M-N)= 0.027

Phase	*Amount as wt% of initial magma	Amount as wt% of all phases	Amount as wt% of added phases	Amount as wt% of subt phases
Pl (A16)	-46.53	62.49	0.00	62.49
Cpx (A16)	-14.21	19.08	0.00	19.08
Opx (A16)	-7.85	10.54	0.00	10.54
Ti-mt (A16)	-5.06	6.79	0.00	6.79
Ap (A16)	-0.82	1.10	0.00	1.10

*Calculated amounts of the phenocryst phases fractionated from A16 that best satisfy the least-squares approximation to the final composition (Lip97)